STUDIES OF LIPID-LIPID INTERACTIONS IN PHOSPHOLIPID BILAYER MEMBRANES

Thesis by

Nils Overgaard Petersen

In Partial Fulfillment of the Requirements

for the Degree of

Doctor of Philosophy

California Institute of Technology

Pasadena, California 91125

1978

(submitted June 20, 1977)

The road to wisdom? — Well, it's plain
  and simple to express:
Err and err and err again
  but less and less and less.

Piet Hein
Short Grooks I

ACKNOWLEDGEMENTS

Sincere thanks go to Professor Sunney Chan for providing perspective, guidance and stimulation throughout this work. Our numerous discussions were always fruitful and enjoyable including those not related to science. It has been a pleasure and a privilege to work with a man I will always respect.

I am indebted to Florence Trentacosti for her critical reading of the manuscript. Her helpful suggestions on language greatly improved this thesis.

I am grateful to all the people associated with the Chan group during my stay for displaying interest in my work and for listening patiently to the many problems encountered along the way. In particular I thank Dr. Dov Lichtenberg with whom we initiated the absorbance studies; Ron Blackman, who helped with some of the absorbance measurements; K.P. Lo, for his synthetic work; Paul K.L. Yu, who helped with some computer calculations; and Pat Hagan, with whom the theoretical FID calculations were done.

In my five years at Caltech I have made many friends. Their contribution to this thesis is found between the lines.

My wife, Pat, has shared the good and the bad and provided the moral support when needed. Her enormous effort in typing this thesis is greatly appreciated.

I thank Caltech and Sunney Chan for financial support, which included GRA's, GTA's and the Earl C. Anthony Fellowship.

ABSTRACT

Lipid-lipid interactions in bilayer membranes are studied in relation to their influence on (i) the state of motion of phospholipid molecules in the liquid crystalline phase, (ii) the miscibility of different lipids in the various bilayer phases, and (iii) the aggregation and fusion of sonicated bilayer vesicles.

Proton and deuterium order parameters measured for the liquid crystalline phase of unsonicated lipid bilayer membranes are interpreted in terms of two types of acyl chain motions, rapid isomerization and slower reorientations. The observed order parameters are compatible with 50° angular deflections of the chain with respect to the bilayer normal, coupled with a probability of a trans orientation of a methylene segment in the upper two-thirds of the chain of about 0.8 - 0.9. The motional model can be shown to account for the dynamic properties of the membrane system as measured by nuclear magnetic relaxation measurements, assuming that the chain isomerization occurs at a rate of $\sim 10^{10}\ s^{-1}$ while chain reorientation occurs at $\sim 10^{7}\ s^{-1}$. Analysis of proton and deuterium linewidth data in terms of this model shows that a bilayer curvature, as induced by sonication, causes an increase in the rate and amplitude of chain reorientation without substantially affecting the isomerization motion along the acyl chain.

Phase diagrams for lecithin mixtures are inferred from Differential Thermal Analysis measurements. In the liquid crystalline phase all the lecithins form ideal solutions whereas in the gel phases immis-

cibility occurs when the lecithin acyl chains differ by four or more methylene groups in length.

Cholesterol-lecithin interactions are discussed in terms of the motional model for the lecithin bilayer. A phase diagram for cholesterol-lecithin-water mixtures is proposed and discussed in relation to the currently available data on these mixtures. The condensing effect of cholesterol is interpreted as a decrease in lecithin chain fluctuations.

Changes in light scattering properites of DPL vesicles at their phase transition are interpreted using the above model of chain motion. The results are compatible with the conclusions derived from the NMR data.

Time dependent absorbance measurements of DPL vesicles are explained by the colloidal properties of the suspension. It is shown that aggregation consists of both coagulation and flocculation, the latter of which is abolished with di- or trivalent cations. The possibility of controlling vesicle-vesicle fusion by coagulation is discussed.

TABLE OF CONTENTS

I. INTRODUCTION

A large number of physiological, biochemical and physico-chemical studies of membranes in cells have demonstrated that the cellular membrane is more than just a structural assembly designed to confine a cell's cytoplasm (1). In fact, the cellular functions presently known or suspected to be associated with membrane structures are so numerous and diverse that a detailed account of them in this thesis would be inappropriate. However, a general description of the structure of the cell membrane seems necessary. The concept of cell membrane structure has developed from one of a phospholipid bilayer with protein sheets associated with the polar bilayer surface (2) (Figure 1a) to one of a dynamic lipid bilayer with integral proteins embedded in and frequently spanning the bilayer (3) (Figure 1b).

Cell membranes are asymmetric because membrane proteins have specific orientations and the lipid composition in each half of the bilayer, that is each monolayer, differs. Some protein components are mobile (4) and translate along the surface or inside the bilayer, while other immobile proteins are often closely associated to form extensive arrays (5,6,7). Most, if not all, of the lipid components are mobile and appear to diffuse several orders of magnitude faster than do the proteins (4) but they still move considerably more slowly than when free in solution. Many other peripheral proteins are only loosely bound to the membrane surface. In some systems the peripheral proteins apparently serve important structural functions (3). The concept of a cell membrane as a steady state rather than an equilibrium system is

FIGURE 1

Schematic illustrations of two membrane models:
(a) Davson-Danielli model of a bilayer of phospholipids with extended proteins covering the surface.
(b) Fluid mosaic model of a bilayer of phospholipids with proteins embedded in it. 1 and 2 are integral proteins and 3 is a peripheral protein.

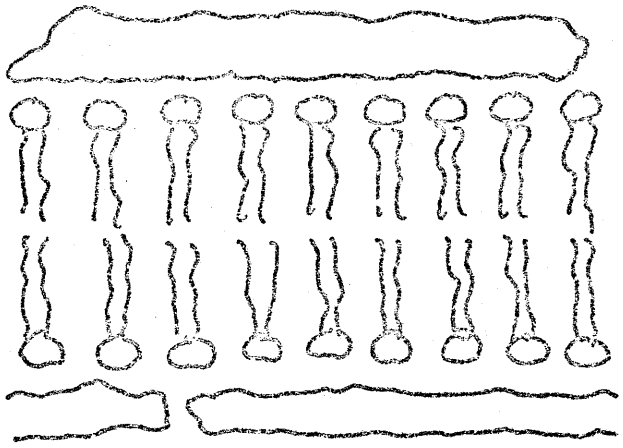

a

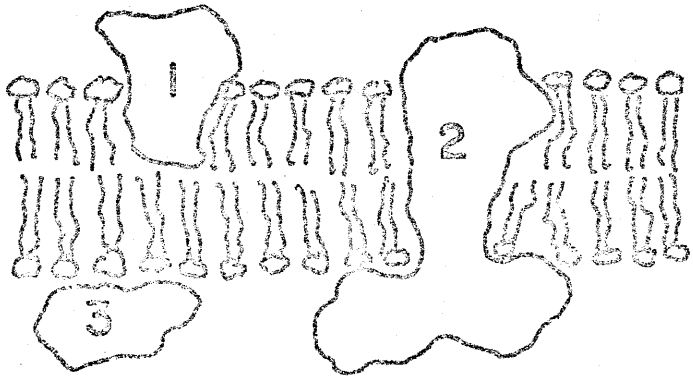

b

perhaps the most important aspect of the current membrane model. This is supported by observations that several events may occur at different sites in a membrane, which requires localization of membrane components (1,5,6). The dynamic and multifunctional membrane model has promoted speculation about the control of the membrane functions. Of particular interest is the relation between the structural organization of a membrane component and its specific function in that membrane. The diversity of a membrane rests in its protein composition whereas the expression of a given function under particular conditions depends on its structural organization.

In order to deal effectively with questions concerning structure-function relationships in a cell membrane, it is essential to understand the nature and effect of the interactions among the various membrane components. It is particularly important to study these interactions in the membrane environment because of the unique features of a membrane. For example, the chemical and physical properties of the membrane should reflect the fact that it is only two molecules thick. Indeed, it has been suggested that diffusion of molecules in the membrane should depend on properties of both the membrane and the surrounding aqueous environment (8). Similarly, the dimensions of a membrane might well be important in determining other properties such as solubility or activity which are generally interpreted in the context of bulk solutions. Even if the membrane is thought of as a hydrophobic solvent, it must be viewed as an anisotropic fluid. The anisotropy is illustrated by the observation that the time to transfer lipids from one monolayer to the other is on the order of days (9) whereas the time of

mixing of lipids within a monolayer is measured in microseconds (4). The anisotropy in the bilayer may also have more subtle effects on molecular properties. For example, small antibiotics such as X537A are known to complex divalent cations in a bulk hydrocarbon solution by attaining a near circular conformation and forming dimers which enclose the ion (10). However, it has been suggested that in the anisotropic medium of the bilayer membrane, X537A might be more stable in its linear conformation. Dimers or oligomers of the antibiotic could then form pores in the membrane through which ions could pass (11). Extrapolation of conclusions derived from bulk solution properties to behavior in membranes could be misleading and underscores the importance of studying the molecular interaction directly in the membrane.

The intermolecular interactions which could be important in membrane function are those of (i) proteins with proteins, (ii) proteins with lipids, (iii) lipids with proteins and (iv) lipids with lipids. It is evident that most membrane proteins have multiple subunits (12, 13,14) and that there are very specific and strong complexes formed between them. It is also possible that large multi-protein complexes form between groups of proteins which are functionally interdependent as illustrated by the proteins involved in oxidative phosphorylation (15). Further, there is much evidence for the existence of extensive arrays or aggregates of protein complexes (5,6,7,16). The function of these is not known, nor is it yet established how these nearly crystalline arrays are formed. The intermolecular forces may arise from direct protein-protein interactions, or may be mediated by the interspersed lipid. In some membrane proteins certain special lipids have been

found to be essential for their integrity, function and activity. For example cytochrome-c-oxidase protein subunits dissociate without at least 2 wt % cardiolipin (14). These lipids are not covalently bound to the protein, but may be important for the protein's quarternary structure. In addition, there is some evidence (17) that there is a monolayer of tightly bound and highly immobile lipids in an annulus around the protein. However, the lipids in the annulus may be of many types indicating that the protein-lipid interactions are not very specific. At this point it is useful to elaborate on our distinction between protein-lipid and lipid-protein interactions. Protein-lipid interactions refer to the effects upon lipid organization by the presence of a protein and are primarily due to the shape, size and charge of the protein rather than specific binding effects. The resulting changes in lipid properties may then in some ways be compared with the familiar colligative effects of solutes on solution properties such as freezing point depression. In contrast, lipid-protein interactions are those between specific proteins and special lipids (e.g. cytochrome-c-oxidase and cardiolipin) which are necessary for the function of the protein. Lipid-lipid interactions, comprising hydrophobic, electrostatic and van der Waals interactions, are responsible for the formation of the lamellar rather than for example a micellar phase of the lipids. Certain lipid-lipid interactions might result in phase or species separation in the plane of the bilayer and, if present, would affect the membrane function. Clearly, all anisotropic properties of the membrane are consequences of the intermolecular forces in the bilayer.

In the present study three general questions dealing with lipid-

lipid interactions have been addressed. First, how does the packing of lipid molecules into a bilayer array affect the extent and rate of each type of molecular motion? Answers to this question have been derived from careful analysis of existing magnetic resonance data by means of a general motional model which will be presented. Some of the implications of this model are discussed specifically for the phospholipid-cholesterol interactions. This leads to the second question addressed here: what is the nature of the interactions among different types of lipid components? Although this is a most difficult question to answer completely, some insight may be gained from studying the phase equilibria of mixtures of lipids. This is the approach we have taken here. Constructing the phase diagram has enabled us to gain some understanding of the consequences of having multiple components in the membrane. The third question deals not with interactions within a membrane, but rather with interactions between membranes. Specifically, how does the motional state of the lipids affect the surface properties of the membrane, and what are the subsequent consequences for intermembrane interactions? This problem was addressed by studying the aggregation behavior of small phospholipid vesicles in aqueous dispersions. The temperature and time dependence of aggregation phenomena as monitored by light scattering yielded information about some of the motional changes occurring at the thermal phase transitions of the model lipid.

References

1. G. Weissman and R. Claiborne, eds., "Cell Membranes, Biochemistry, and Pathology", H.P. Publishing Co. Inc., 1975.
2. H. Davson and J.F. Danielli, in "The Permeability of Natural Membranes" (2nd ed.), London, Cambridge University Press, 1952.
3. S.J. Singer and G.L. Nicholson, Science, 175, 720 (1972).
4. M. Edidin, Annu. Rev. Biophys. Bioengineer., 3, 179 (1974).
5. D. Axelrod, P. Ravden, D.E. Koppel, J. Schlessinger, W.W. Webb, E.L. Elson and T.R. Podleski, Proc. Nat. Acad. Sci., 73, 4594 (1976).
6. A.E. Blaurock, J. Mol. Biol., 93, 159 (1975).
7. H.A. Lester, Sci. American, 236, 107 (1977).
8. P.G. Saffman and M. Delbrück, Proc. Nat. Acad. Sci. (U.S.), 72, 3111 (1975).
9. J.E. Rothman and E.A. Dawidowicz, Biochemistry, 14, 2809 (1975).
10. H. Degani and H.L. Friedman, Biochemistry, 14, 3755 (1975).
11. C.S. Springer, private communication (1977).
12. M.M. Briggs and R.A. Capaldi, Biochemistry, 16, 73 (1977).
13. M.A. Raftery, R.L. Vandlen, K.L. Reed and T. Lee, Cold Spring Harbor Symposium on Quantitative Biology, Volume XL, 193 (1976).
14. J.F. Hare and F.L. Crane, Sub-Cell. Biochem., 3, 1 (1974).
15. E. Racker, in "Cell Membranes, Biochemistry, Cell Biology and Pathology", H.P. Publishing Co. Inc., 1975, Chapter 14.
16. H. Hayashi, G. Vanderkooi and R.A. Capaldi, Biochem. Biophys. Res. Commun., 49, 92 (1972).
17. P. Jost, O.H. Griffith, R.A. Capaldi, and G. Vanderkooi, Biochim, Biophys. Acta, 311, 141 (1973).

II. MATERIALS AND METHODS

1. Materials

The principal phospholipids employed in these studies were L-α-dilauroyl lecithin (DLL), L-α-dimyristoyl lecithin (DML), L-α-dipalmitoyl lecithin (DPL) and L-α-distearoyl lecithin (DSL). They are all characterized by the same general structure, shown in Figure 2, but differ in the length of the fatty acid chain as indicated in the figure. These lipids were obtained from Calbiochem and usually used without purification. Other lipids used were: The enantiomeric form of DPL, D-α-dipalmitoyl lecithin (D-α-DPL); the racemic mixture, DL-α-dipalmitoyl lecithin (DL-DPL); and β-dipalmitoyl lecithin (β-DPL). This differs from the α-dipalmitoyl lecithin in that the position of the phosphate ester linkage is at the central carbon in the glycerol segment. These three lipids were obtained from Serdary. Diperdeuteropalmitoyl lecithin (DPL-d_{62}) and diperdeuterostearoyl lecithin (DSL-d_{70}) were synthesized in this laboratory by standard procedures primarily through the efforts of P.A. Kroon and M. Kainosho (1,2).

When necessary the phospholipids were purified by chromatography on silicic acid support either on plates or in a column. The plates were eluted with a mixture of methanol, chloroform and water in the proportion 60:25:4. The columns were prepared from a slurry of the gel in 2% (v/v) methanol in chloroform. After thoroughly rinsing the support with the same solvent, lipid was applied (usually 1 g lipid to about 200 g silicic acid support) in a concentrated solution. The column was eluted with constant volumes of solvent containing increasing

FIGURE 2

Chemical structure of a diacyl lecithin molecule. The number of methylene groups in the acyl chains is the primary distinction between the lipids used in this work

n = 12 : DLL

n = 14 : DML

n = 16 : DPL

n = 18 : DSL

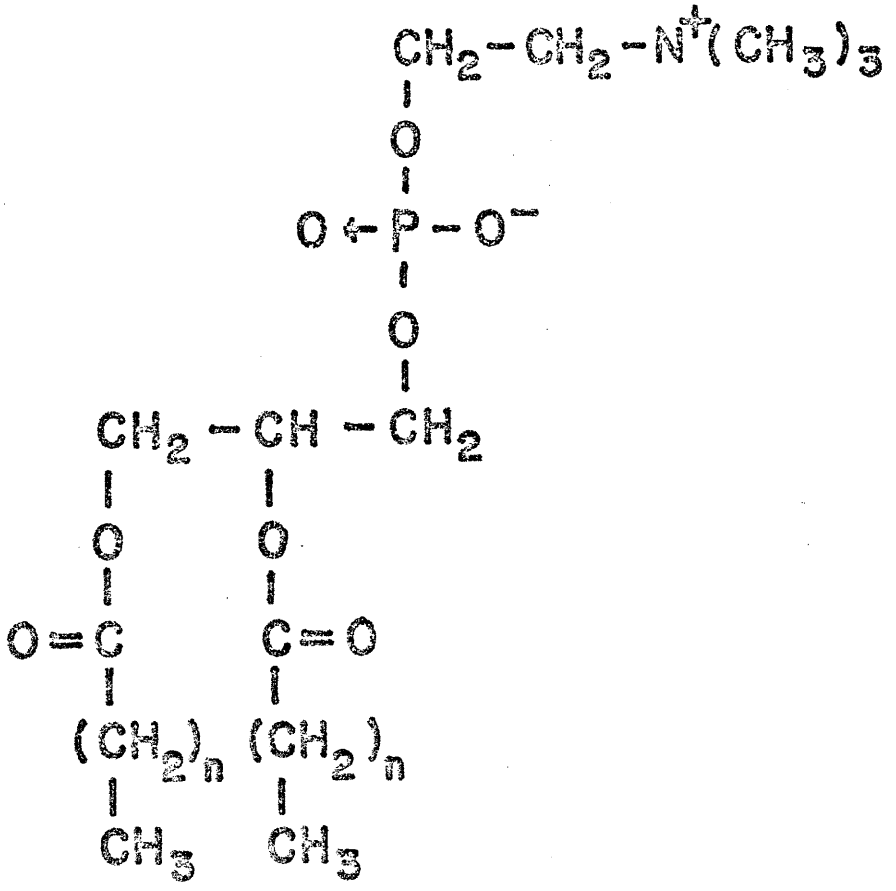

proportions of methanol to chloroform. The phospholipid usually came off the column in the 30-40% (v/v) methanol solvents.

Cholesterol was obtained from Grand Island Biological Co. Standard salts ($NaNO_3$, $Ca(NO_3)_2$, etc.) were from Baker Chemical Co. Lanthanide salts were from Research Organic, Inorganic Chemical Corp. ^2H_2O (99.8%) was obtained from Stohler.

2. Preparation of Samples

Samples of multilamellar lipid dispersions used for differential thermal analysis (DTA) were routinely prepared by adding 5-10 mg phospholipid to a 2 mm outside diameter capillary tube. 10-15 µl aqueous solution was added and the capillary tubes were sealed and incubated for at least one hour in a sandbath kept at 65°C. At the time of the DTA run the capillary tube was broken open, and the sample was agitated to remove air bubbles so that the thermocouple was exposed only to lipid suspension. The reference sample was typically 10 µl H_2O or 10 µl of a 50% (v/v) ethylene glycol solution in water.

The lipid mixtures were prepared at the desired composition by dissolving known amounts of lipids in known volumes of $CHCl_3$ and mixing the solutions in the appropriate proportions. The chloroform, usually 100-200 µl, was allowed to evaporate at room temperature for a day. Occasionally the samples were evacuated for a few hours to remove residual traces of chloroform faster. This mixing technique left less chloroform in the sample than could be detected directly by proton magnetic resonance. More importantly, the residual chloroform, if any, had no detectable effect on the DTA of single component lipid samples prepared

in an identical manner.

Samples of dilute multilamellar lipid suspensions used for turbidimetric measurements were prepared by mixing the desired amounts of phospholipid and aqueous solution in a large test tube. The mixture was heated with an air gun and simultaneously agitated vigorously with a vortex mixer for several minutes. The resulting, frequently opaque, suspensions were usually diluted further prior to the turbidity measurements.

Samples of small bilayer vesicles were prepared from multilamellar suspensions obtained as described above. The 1-2 ml suspensions were sonicated with an MSE 150 W probe sonicator using one of the following procedures depending on the experiment. (a) To obtain normal annealed (3,4) vesicles, the samples were placed in a water or glycerol bath and sonicated continuously for 10-15 min. During sonication the sample temperature, monitored with a copper-constantan thermocouple, would rise to about 40°C within a minute and reach a temperature between 55 and 65°C (Figure 3A). (b) To prepare unannealed vesicles (3, 4) it is essential that the sample temperature never exceed the annealing temperature during sonication. This was accomplished for the original experiments (3,4) by placing the samples in an ice-water bath and sonicating in cycles of 30 s on and 30 s off. For some of the experiments with mixed lipids this proved to be unsatisfactory because the temperature became too high (Figure 3B). It was possible to maintain temperatures below 23°C at all times by using a different cycling period and cooling method (Figure 3C). This was the coolest condition attainable with the probe configuration without freezing the sample during

FIGURE 3

The temperature of a 1 ml solution of 20 mM $La(NO_3)_3$ during exposure to sonication. A: Continuous sonication with the sample cooled by a water bath. B: Intervals of sonication with a cycle of 30 s sonication and 30 s off. C: Intervals of sonication with a cycle of 15 s sonication and 45 s off. In both B and C the sample was cooled by an ice-water bath.

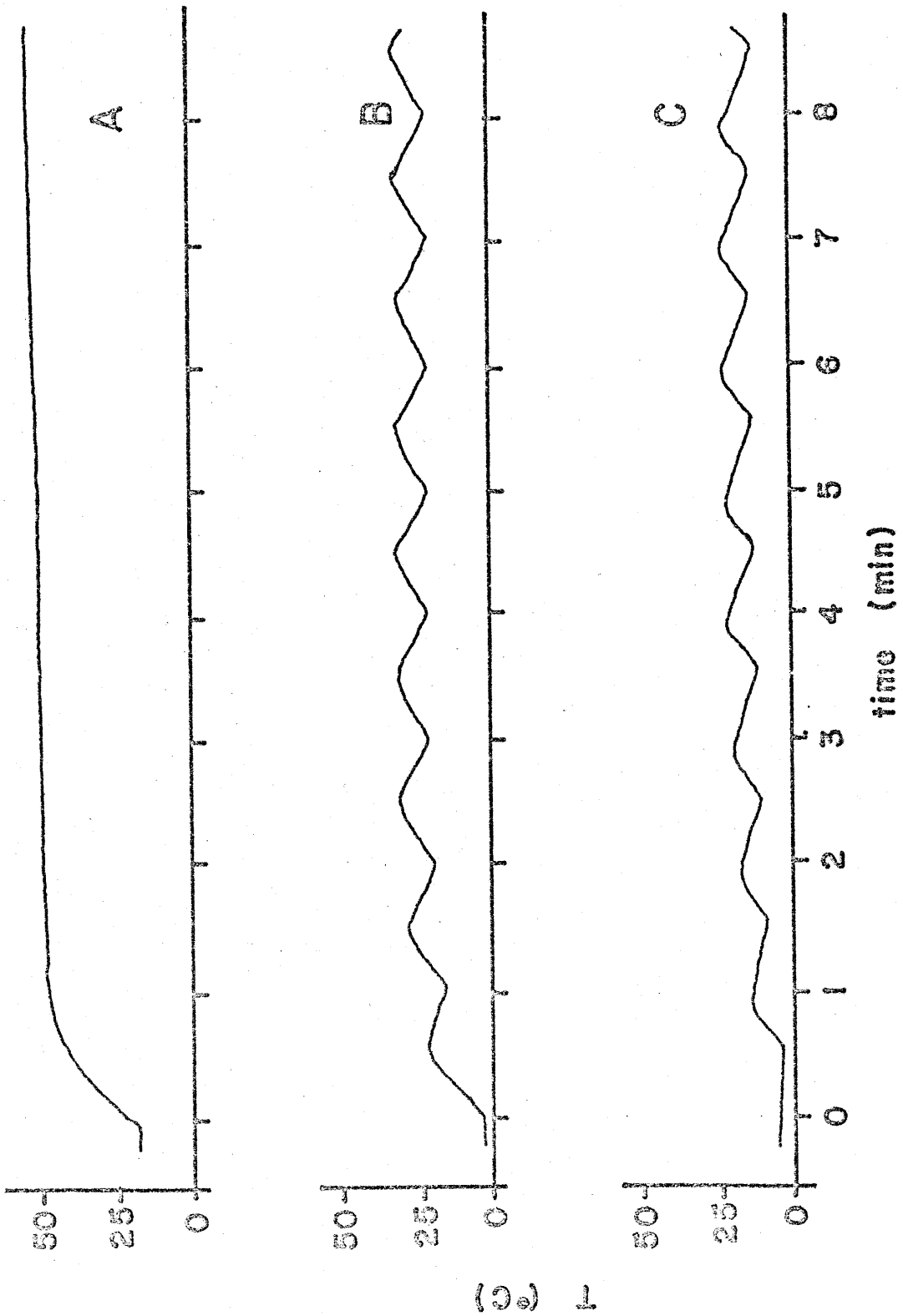
A
B
C
50
25
0
0
1
2
3
4
5
6
7
8
time (min)
T (°C)

the cooling cycles. As will be seen, this was not always cold enough.

3. Instrumentation

Nuclear magnetic resonance (NMR) spectra were obtained either on a Varian HR-220 NMR spectrometer or a Varian XL-100 NMR spectrometer. Both instruments were interfaced with Varian 620/i 16K computers which provided the instrument with Fourier Transform capabilities and allowed for time averaging of free induction decays. Temperature control was achieved with a Varian 4500 temperature controller.

Differential thermal analysis was carried out on a DuPont 900 Differential Thermal Analyzer. It was found that for lipid samples the 2 mm outside diameter capillaries gave sharper melting transitions than the larger tubes available. The reference electrode was usually immersed in water or an ethylene glycol-water mixture since this provided for good heat capacity matching of sample and reference. The heating rate was chosen to be $7^{\circ}C$ per minute. Faster heating led to unacceptable artificial broadening of the transition. Slower heating rates resulted in small differential temperatures causing a poor signal-to-noise ratio. A $7^{\circ}C$ per minute heating rate still led to a slight broadening of the observed transition for pure lipid systems, but the broadening effect was insignificant for mixed lipid samples. Cooling of the samples to subambient temperatures was achieved by cooling the heating block containing the capillary tubes with a stream of cold air or cold N_2 gas. The gas, or air, was cooled as it was passed through a copper coil immersed either in an ice-water bath, an acetone-dry ice slurry or liquid N_2. Occasionally cooling curves were measured, but never at

controlled cooling rates.

Turbidity measurements were made either with a Beckman Acta CIII or a Beckman DU UV-Visible spectrophotometer at the wavelengths specified with the results. The Beckman Acta CIII spectrometer was equipped with a TM temperature programmer which allowed for heating and cooling of the sample at constant rates (0.4-2^{o}C per minute). The sample temperature was measured with a Pt thermistor calibrated to provide an output of 1 mV/^{o}C. Turbidity and temperature measurements recorded on a Hewlett Packard 7035B XY-recorder provided the melting curves. Some melting curves were recorded point-by-point using the Beckman DU which was equipped with a custom-made temperature programmer. This accessory, built in the Caltech electronics shop, heated water which was circulating continuously through the sample compartment at a selected rate. The feedback temperature was, for technical reasons, monitored at the exit of the programmer rather than in the sample compartment, and the sample temperature was measured independently with a copper-constantan thermocouple. As with the DTA measurements, the cooling rates were not well controlled.

References

1. P.A. Kroon, Ph.D. Thesis, California Institute of Technology (1975).

2. N.O. Petersen, P.A. Kroon, M. Kainosho and S.I. Chan, Chem. Phys. Lipids, 14, 343 (1975).

3. R. Lawaczeck, M. Kainosho, J.L. Girardet and S.I. Chan, Nature, 256, 584 (1975).

4. R. Lawaczeck, M. Kainosho and S.I. Chan, Biochim. Biophys. Acta, 443, 313 (1976).

III. A MODEL FOR THE MOLECULAR MOTION OF LIPIDS IN A BILAYER MEMBRANE. ANALYSIS OF MAGNETIC RESONANCE DATA OF MEMBRANES IN TERMS OF THE MODEL.

1. Introduction

When it was first suggested that the cell membrane primarily consisted of a bilayer membrane of phospholipids (1,2) it was hoped that studies of model membrane systems could shed light on the structure and function of the cell membrane itself. As a result, a great deal of interest was generated in studies of the structure of the various phases that phospholipids assumed when dispersed in water (3). X-ray (4,5,6) and differential scanning calorimetry (7,8,9) studies proved extremely useful in characterizing the basic structure of lipid aggregates in these dispersions. Neither technique, however, is capable of yielding information about the detailed molecular order or dynamics of the phospholipids in the bilayer phase. Much of this information was derived from magnetic resonance experiments (10,11,12). Early proton magnetic resonance measurements demonstrated that membrane mobility reflected a state intermediate between a fluid and a solid (13). The first quantitative assessments of the extent of ordering became available through electron spin resonance (ESR) measurements with spin-labelled phospholipids (Figure 4) (14,15,16). Subsequently, similar information about the molecular order was obtained by ^{2}H-NMR measurements on selectively labelled phospholipids (17,18,19). Conclusions derived from the two sets of measurements did not agree (20). The ESR measurements were strongly criticized because the large spin label probably perturbed the local ordering measured by the probe. At the same time, proton NMR

FIGURE 4

Typical geometry of nitroxide spin labels attached to the acyl chains of phospholipids (14).

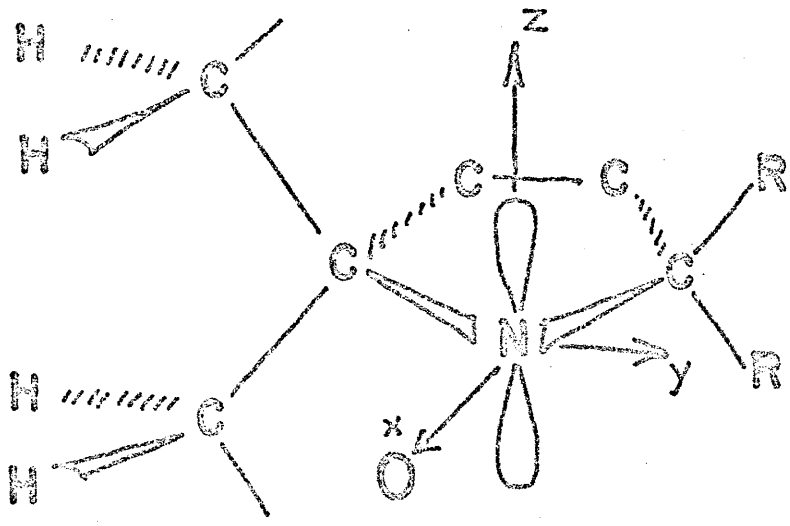
H
H
C
C
C
C
C
R
R
N
Z
y
x
O
H
H
C

relaxation time and linewidth measurements were interpreted in terms of the rates of molecular motions in the bilayer (21,22,23). These measurements were found to be qualitatively consistent with the degree of order measured by ^{2}H-NMR. Yet, none of the motional models employed in the interpretation of data from each of the various magnetic resonance experiments could adequately explain all the data. The purpose of the studies presented in this section is to develop and quantitate a physically reasonable model for the molecular motions which is consistent with all the available magnetic resonance data.

A complicating factor, which has been the source of much controversy, is that there are several physically distinct preparations of the model membrane which have been used in magnetic resonance studies (Figure 5). As we shall see, magnetic resonance measurements on these preparations differ merely with the size and shape of the bilayer superstructure. Moreover, the lipid-lipid interactions in liposomes and in vesicles (Figures 5b and 5c) are distinct as a result of the structural differences.

In the following, we will present the model in detail and proceed to examine its implications for interpretation of magnetic resonance order parameters. This examination allows us to assess the relative importance of the motions on the basis of the measured order parameters. Next, the model is used to analyze the NMR relaxation behavior expected for the lipid system. This makes it possible to interpret experimental linewidth data, and therefore the homogeneous linewidths from small lipid vesicles will be discussed in this light. Finally, one approach to modeling the chain isomerization will be discussed.

FIGURE 5

Typical bilayer membrane preparations. A: Oriented multilamellar system of bilayers. B: Liposomes. C: Vesicles.

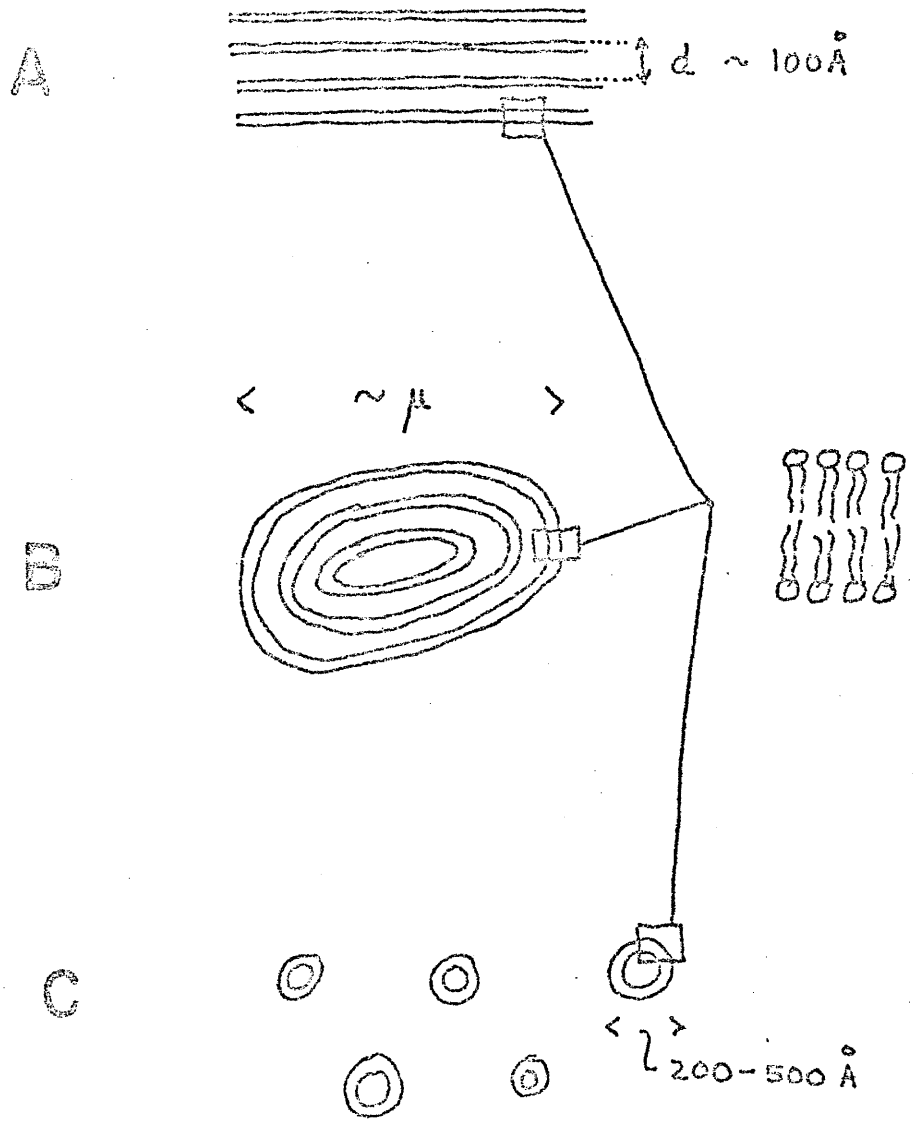
A
d ~ 100Å
B
< ~μ >
C
< l >
200-500 Å

2. The Model

Molecular motions may be characterized by equations of motion of the atoms relative to a molecular coordinate frame of reference plus that of the molecular frame relative to a laboratory fixed frame. For a general case of N atoms in a molecule, there would be 3N parameters to be specified. Most of these are fixed since bond angles and bond lengths are invariant for our purposes, so the number of parameters needed to define the molecular motions are greatly reduced. In the case of a phospholipid molecule in a membrane, the detailed motion of each atom is still complex, but certain simplifying assumptions can, nevertheless, be made.

For the present discussion we restrict our attention to the overall motion of the methylene segments in the fatty acid chain. The reasons for this are twofold. First, the fatty acid chains constitute the more interesting hydrophobic environment in the membrane and many characteristics of the membrane are determined by the intermolecular interactions in this region. Secondly, the polar head group motions are more complicated and have not been as extensively studied with magnetic resonance techniques.

The motional model for the fatty acid chain will be presented in terms of the vectors and angles illustrated in Figure 6. We define a vector, $\vec{r}$, representing each methylene group in the fatty acid chain. Motion of a methylene group is then correlated with the movement of $\vec{r}$. We define $\vec{c}$ as a vector along the instantaneous chain orientation and $\vec{d}$, the director, as a vector along the average orientation of the chain. The vector $\vec{H}_0$, which is fixed in a laboratory frame of reference, cor-

FIGURE 6

Illustration of the vectors and angles relevant to the lipid chain motional model. $\vec{H}_o$ is the direction of the applied magnetic field. The director, $\vec{d}$, is normal to the bilayer surface.

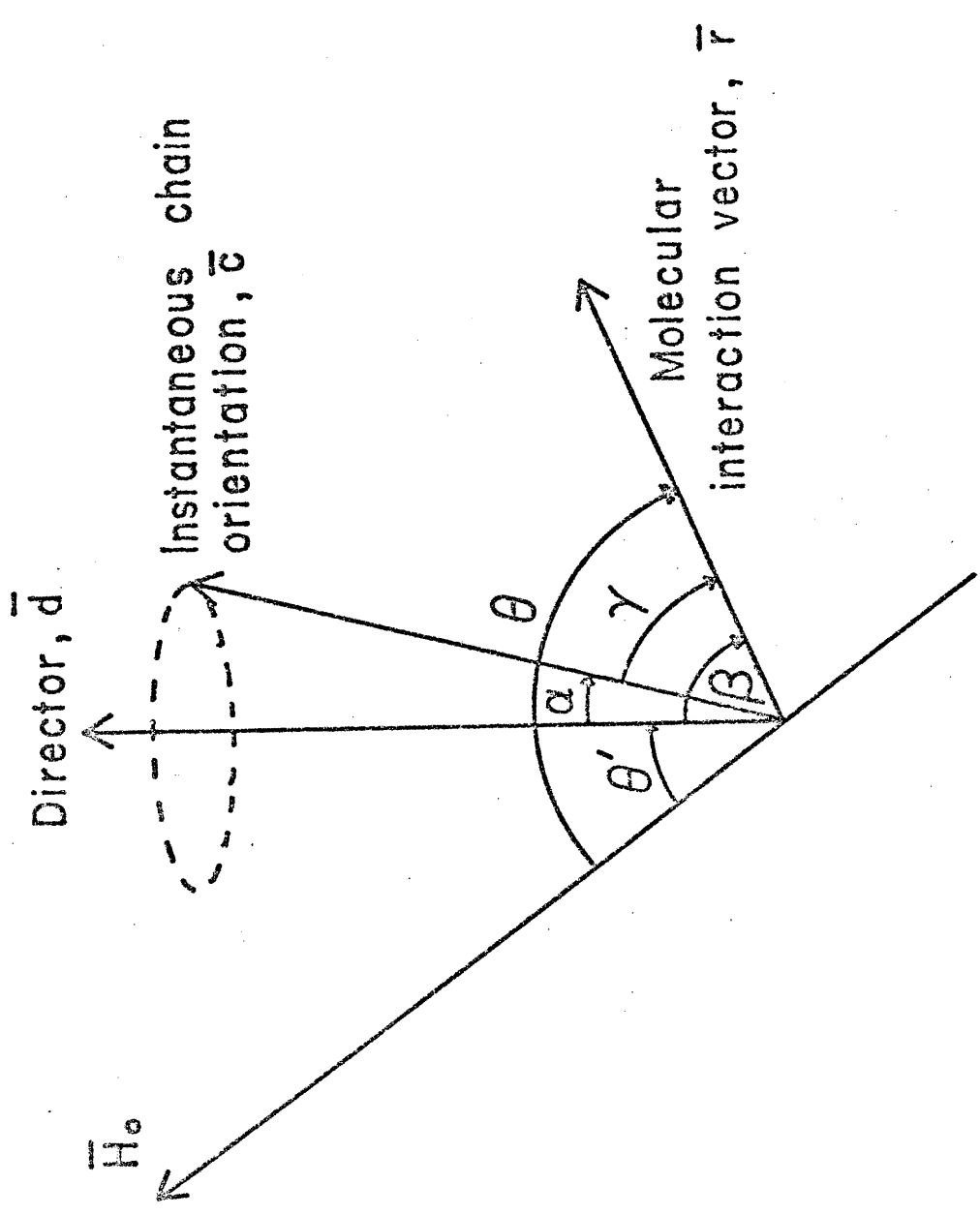
Director, $\bar{d}$
Instantaneous chain orientation, $\bar{c}$
Molecular interaction vector, $\bar{r}$
$\bar{H}_o$
θ
γ
α
β
θ'

responds to the magnetic field direction in the magnetic resonance experiment. The choice of these vectors is particularly convenient because the movement of $\vec{r}$ relative to $\vec{c}$ represents the intramolecular motion of a methylene group relative to the chain. Reorientation of the vector $\vec{c}$ relative to the director in turn corresponds to the motion of the chain (or perhaps the entire lipid molecule) relative to the bilayer membrane. Finally, the change in orientation of $\vec{d}$ with respect to $\vec{H}_0$ describes the motion of the bilayer relative to the laboratory fixed reference coordinates. A full characterization of the motion of a methylene segment in a fatty acid chain is reduced to the description of the following vector reorientations: $\vec{r}$ relative to $\vec{c}$, $\vec{c}$ relative to $\vec{d}$ and $\vec{d}$ relative to $\vec{H}_0$. Specifically, this implies defining the appropriate angular distributions and time scales on which they are observed.

In our model the following assumptions about chain motions are made: (i) intramolecular chain isomerization, affecting γ, is fast and involves only three rotational isomers about any given carbon-carbon bond; trans, gauche - and gauche +, (ii) rotation of $\vec{r}$ about $\vec{c}$ is unrestricted and faster than motions of $\vec{c}$ itself, (iii) $\vec{c}$ rotates about $\vec{d}$ in an unrestricted manner but at a rate comparable to motions of $\vec{c}$ with respect to $\vec{d}$, affecting α, and (iv) this last motion in α is restricted to a specific angular range. For oriented multilayers we assume a single $\vec{d}$ fixed in the laboratory frame, while for liposomes we assume that there is an isotropic but static distribution of directors, i.e. the bilayer does not move fast enough to affect the magnetic resonance data. The motion of $\vec{d}$ is faster and therefore more important for the vesicle system as will be discussed in detail later.

In summary, the proposed motional model for the lipid molecule encompasses a fast chain isomerization and a slower chain reorientation. Both motions are axially symmetric. For certain membrane systems, the bilayer motion must be included in the interpretation of the experimental data.

3. Interpretation of Order Parameters

A general consequence of molecular order or motional restriction is that all interactions governed by second-rank tensors are incompletely averaged. In magnetic resonance this is revealed experimentally by (i) nuclear dipolar broadening in the ^{1}H-NMR spectra (23, 24), (ii) quadrupolar splittings in the ^{2}H-NMR spectra (18,19), (iii) broadening by nuclear dipole interactions and by chemical shift anisotropy in ^{19}F-NMR spectra (25,26), (iv) broadening by chemical shift anisotropy in proton-decoupled ^{13}C-NMR and ^{31}P-NMR spectra (27,28,29), as well as (v) line shape changes in ESR spectra arising from anisotropies in the electonic Zeeman and the nuclear hyperfine interactions (14,15,16). A brief discussion of these second-rank tensor interactions is provided in Appendix I. Because of the incomplete averaging of the tensor interactions, the spectra contain information about the extent of motional averaging or the degree of molecular ordering. This information can, in principle, be extracted.

It has been customary to describe the degree of ordering of motionally restricted systems with respect to a laboratory frame of reference. In general, this requires specifying a matrix of order parameters. However, when the motions lead to tensor interactions with

effective axial symmetry, the motional parameters can be described relative to the symmetry axis. As a result, the motional restriction can be expressed in terms of a single order parameter. In the motional model introduced in the previous section there are two distinct axes of symmetry on different time scales. As we shall see, this allows us to expand the order parameter and obtain more detailed information.

A good illustration of the effects of motional averaging can be obtained by considering the averaging of the nuclear dipolar interactions between a pair of protons in a methylene segment (23,30). For a static methylene group with an interproton vector $\vec{r}$ oriented at an angle θ relative to the applied magnetic field (Figure 7a) the dipolar Hamiltonian

$$\hat{H} = \frac{\gamma^2\hbar^2}{r^3}\left\{\vec{I}^a\cdot\vec{I}^b - \frac{3(\vec{I}^a\cdot\vec{r})\ (\vec{r}\cdot\vec{I}^b)}{r^2}\right\}$$

$$= \frac{\gamma^2\hbar^2}{r^3}\ \vec{I}^a\cdot\underline{\underline{D}}\cdot\vec{I}^b \qquad \text{(III-1)}$$

reduces in the first order perturbation limit to

$$\hat{H} = \frac{\gamma^2\hbar^2}{r^3}\left\{I^aI^b - \frac{1}{4}\left(I_+^aI_-^b + I_-^aI_+^b\right)\right\}\left(1 - 3\cos^2\theta\right) \qquad \text{(III-2)}$$

Here γ is the gyromagnetic ratio, and I, I_+ and I_- represent the usual spin operators. $\underline{\underline{D}}$ is the dipolar interaction tensor and the superscripts denote the proton in question. The dipolar interaction gives rise to a perturbation of the Zeeman energy levels of the spin pair as indicated in Figure 7b. The resulting spectrum (Figure 7c) consists of

FIGURE 7

Illustration of the origin of dipolar splitting of a resonance line. a: The orientation of an inter-proton vector, $\vec{r}_{12}$, relative to the applied magnetic field. Here, 1 and 2 are the protons in a methylene group. b: The first order effect of the dipolar Hamiltonian on the Zeeman energy levels of the pair of protons. The wave functions are shown next to the energy levels. c: The ideal frequency spectra arising from the transitions illustrated in b.

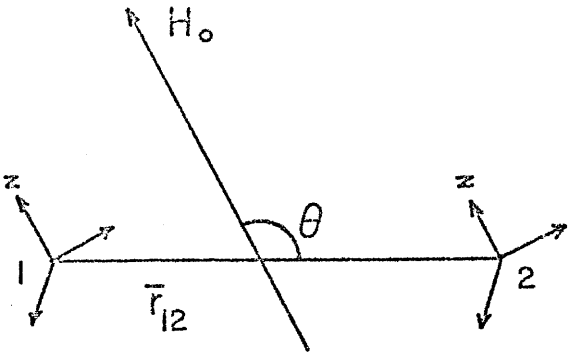
H_o
z
z
θ
1
2
$\bar{r}_{12}$

a.

b.

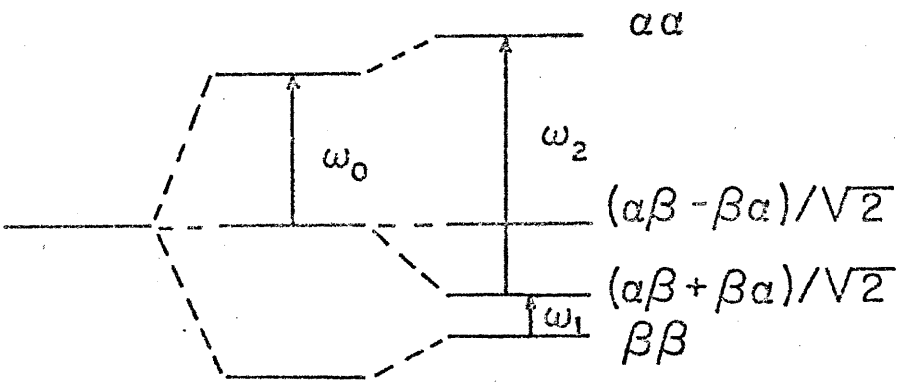
$\alpha\alpha$
ω_0
ω_2
$(\alpha\beta - \beta\alpha)/\sqrt{2}$
$(\alpha\beta + \beta\alpha)/\sqrt{2}$
ω_1
$\beta\beta$

c.

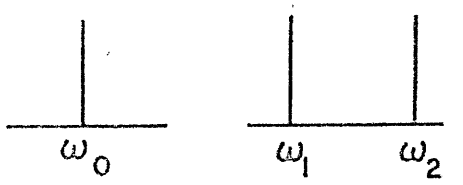
ω_0
ω_1
ω_2

a pair of lines positioned in the frequency domain at

$$\omega = \omega_o \pm \Omega' \ (1 - 3\cos^2\theta) \qquad \text{(III-3)}$$

where $\Omega' = \frac{3}{4} \frac{\gamma^2 \hbar}{r^3}$.

When the methylene group moves, the angle θ changes, and the resonance frequency is affected accordingly. In fact, since $|\vec{r}|$ remains constant, the separation of the pair of lines reduces from

$$\Delta = |2\Omega'(1 - 3\cos^2\theta)| \qquad \text{(III-4)}$$

to

$$\Delta = |2\Omega' \langle 1 - 3\cos^2\theta \rangle| \qquad \text{(III-5)}$$

where $\langle \ \rangle$ denotes the expectation value.

The quantity $\langle 1 - 3\cos^2\theta \rangle$ depends on the extent of motion of the methylene group relative to the applied field. If this motion allows the Hamiltonian to retain axial symmetry relative to a laboratory set of axes and the symmetry axis coincides with $\vec{d}$ of Figure 6, then

$$\langle 3\cos^2\theta - 1 \rangle = \frac{1}{2} \langle 3\cos^2\beta - 1 \rangle (3\cos^2\theta' - 1) \qquad \text{(III-6)}$$

where the angles are defined in Figure 6. The order parameter is defined by

$$S_\beta \equiv \frac{1}{2}\left\langle 3\cos^2\beta - 1 \right\rangle \qquad \text{(III-7)}$$

The effect of the coordinate transformation in equation III-6 is to reduce the nuclear dipolar interaction to a product of a scalar quantity, the order parameter, and a function describing the orientation of the director with respect to the applied magnetic field. Thus, the order parameter reflects the motion of the vector $\vec{r}$ about the director and is independent of the orientation of that director.

Equation III-3 is equally valid for the deuterium quadrupolar splitting except that

$$\Omega' = \frac{3e^2qQ}{16h} \qquad \text{(III-8)}$$

and the vector $\vec{r}$ is along the C—D bond in the methylene group rather than along the interproton vector as for the proton-proton dipolar interaction. The operational definition of the proton order parameter, S^{HH}, and the deuterium order parameter, S^{CD}, is given by eq III-7. Since the vector $\vec{r}$, and hence the angle β, is different, the values for these order parameters must be expected to differ.

Measurements of the proton-proton dipolar interactions and deuterium quadrupolar interactions in oriented lipid bilayer membranes as a function of orientation in the magnetic field (24,31) have shown that, on the nuclear magnetic resonance time scale, effective symmetry exists about the bilayer normal. The order parameters for the membrane system must therefore be understood in terms of a director which is

normal to the bilayer. In fact, the order parameter is a measure of the distribution of orientations of the molecular vector $\vec{r}$ with respect to the director. Because of the axial symmetry the corresponding distribution function, $g(\beta)$, depends only on the angle β between the molecular vector and the director. If this distribution function can be deduced for a given model of the motions, then the order parameter can be calculated for this model by

$$S_\beta = \frac{1}{2}\left\langle 3\cos^2\beta - 1 \right\rangle$$

$$= \frac{1}{2}\frac{\int_0^\pi (3\cos^2\beta - 1)\, g(\beta)\, \sin\beta\, d\beta}{\int_0^\pi g(\beta)\, \sin\beta\, d\beta} \qquad \text{(III-9)}$$

where the $\sin\beta$ factor takes into account a statistical weighting for the number distribution of $\vec{r}$'s about the director for a given β.

As a first approach to interpreting the NMR order parameter in lipid bilayer systems, Chan and coworkers (21,22) have suggested a model in which the interproton vector of a methylene segment is considered to be freely moving by Brownian motion but only within an angular range of $\bar{\beta} \pm \Delta\beta$. As a result of the axial symmetry, the average orientation corresponds to $\bar{\beta} = \pi/2$, and the distribution function for this model is

$$g(\beta) = \text{constant for } \pi/2 - \Delta\beta \leq \beta \leq \pi/2 + \Delta\beta$$

$$= 0 \text{ for } \beta \text{ outside the above range} \qquad \text{(III-10)}$$

Integration of eq III-9 yields the value of the order parameter as a

function of $\Delta\beta$ only, namely

$$S_\beta = -\frac{1}{2}\cos^2\Delta\beta \qquad \text{(III-11)}$$

Although this model can include several types of motion, it does not lend insight into the motional detail and is therefore not entirely satisfactory.

We now consider in detail the motional model outlined in the previous section, in which the distribution of β is governed by two types of motions: (i) chain reorientation and (ii) chain isomerization. If the two motions are independent, that is, if interconversion between trans and gauche methylene orientations does not depend on the instantaneous chain orientation, or vice versa, and if they occur on different timescales, we may describe the distribution functions arising from each motion independently . As discussed previously, the reorientation results in changes in the angle α characterized by a distribution function $g(\alpha)$, whereas chain isomerization effects changes in the angle γ, characterized by a distribution function $g(\gamma)$. The distribution function, $g(\beta)$, appearing in eq III-9 can be replaced by $g(\alpha)g(\gamma)$.

Analogous to the model proposed by Seelig and coworkers (17,18) we assume that the distribution function arising from chain isomerizations is governed by the methylene segment orientation with respect to the instantaneous chain orientation. Therefore, the distribution function is described by discrete values of γ, each with a population fraction $p(\gamma)$, i.e.

$$g(\gamma) = p(\gamma_i)\ \delta(\gamma - \gamma_i) \qquad \text{(III-12)}$$

with $\Sigma p(\gamma_i) = 1$. Chain reorientation may result from reorientation of the molecule possibly through cooperative motions within the bilayer. We consider it as likely, however, to be a result of individual chains tilting with respect to the bilayer as a consequence of motions in the glycerol segments and the ester linkages. Because of steric restrictions from neighboring chains, this tilting is also likely to be locally cooperative. In either case, the chain may reorient through all angles within a certain range, say $\Delta\alpha$, at a rate slow compared with that for chain isomerizations. It is therefore reasonable to approximate this motion to a random walk, and we propose

$$g(\alpha) = \text{constant for } 0 \leq \alpha \leq \Delta\alpha$$

$$g(\alpha) = 0 \text{ for } \alpha > \Delta\alpha \qquad \text{(III-13)}$$

Note again that for this distribution function, the <u>average</u> orientation of the chain is the director.

To evaluate the order parameter, we now express the function $(3\cos^2\beta - 1)$ in terms of α and γ. The relationship is given by the well-known addition theorem for spherical harmonics, namely

$$(3\cos^2\beta - 1) = \frac{1}{2}(3\cos^2\alpha - 1)(3\cos^2\gamma - 1)$$

$$+ \frac{3}{2}\sin^2\alpha \sin^2\gamma \cos 2\psi + \frac{3}{2}\sin 2\alpha \sin 2\gamma \cos\psi \qquad \text{(III-14)}$$

where ψ is a phase angle of $\vec{r}$ about the instantaneous chain orientation. Although chain isomerization cannot average the phase angle over all values, a combination of chain reorientation and rotation of the lipid molecule about its long axis should. The latter motion does not affect α or γ and therefore not the distribution functions proposed above. An effective averaging of the phase angle as assumed in the model does, however, simplify eq III-14 to

$$(3\cos^2\beta - 1) = \frac{1}{2}(3\cos^2\alpha - 1)(3\cos^2\gamma - 1) \qquad \text{(III-15)}$$

With this change in variables, the expression for the order parameter may be rewritten as

$$S_\beta = \frac{1}{4}\frac{\int_\alpha\int_\gamma (3\cos^2\alpha - 1)(3\cos^2\gamma - 1)\, g(\alpha)\, g(\gamma) \sin\alpha \sin\gamma \, d\gamma \, d\alpha}{\int_\alpha\int_\gamma g(\alpha)\, g(\gamma) \sin\alpha \sin\gamma \, d\gamma \, d\alpha} \qquad \text{(III-16)}$$

In the present model, chain reorientation and chain isomerization are considered independent motions so that α and γ are independent variables. The integrations can therefore be performed independently, and with the distribution functions proposed in eqs III-12 and III-13, we obtain

$$S_\beta = \frac{1}{2} \frac{\int_0^{\Delta\alpha} (3\cos^2\alpha - 1) \sin\alpha \, d\alpha}{\int_0^{\Delta\alpha} \sin\alpha \, d\alpha} \cdot \frac{1}{2} \sum_i p(\gamma_i) (3\cos^2\gamma_i - 1)$$

$$= S_\alpha \cdot S_\gamma \qquad \text{(III-17)}$$

which is analogous to the expressions previously used by Niederberger and Seelig (32) and by Hubbell and McConnell (14). In eq III-17 we have introduced two new, independent order parameters S_α and S_γ defined by

$$S_\alpha \equiv \frac{1}{2} \left\langle 3\cos^2\alpha - 1 \right\rangle \qquad \text{(III-18)}$$

$$S_\gamma \equiv \frac{1}{2} \left\langle 3\cos^2\gamma - 1 \right\rangle \qquad \text{(III-19)}$$

corresponding to eq III-9. It is important to note that these two order parameters cannot be measured independently by NMR. Eq III-17 expresses the measured order parameter as a simple product of S_α, the chain order parameter, and S_γ, the intramolecular order parameter. By definition, S_α is independent of the vector $\vec{r}$ and its orientation relative to the chain. Thus one should expect that S_α would be the same for the experimental order parameters from proton and deuterium NMR whereas S_γ could be quite different. In principle then, the two accessible experimental order parameters can yield information about the relative importance of S_α and S_γ.

An important consequence of the model leading to eq III-17 is that the order parameter predicted from chain isomerization calculations

is scaled by the factor, S_α, which is assumed to be constant for the whole chain. Thus the relative order parameter for various segments along the chain should be predictable by models for chain isomerization, as has been attempted by several investigators (18,33,34,35,36). Indeed neither Jackson (35) nor Scott (36) can fit their calculations to experimental data without some form of scaling. The key difference between the present model and those proposed by Schindler and Seelig (18) and Marčelja (34) is the manner in which the scaling is performed. The latter workers were forced to invoke a rapid equilibrium among a distribution of orientations of the first methylene segment in order to fit their calculations to the observed order parameter values. As a result, the probabilities obtained for the various orientations of a segment relative to the bilayer normal depend strongly on the orientation of the first segment and their p_t values depend on the choice of the distribution. Although the equilibrium between orientations within the distribution is fast on the NMR timescale, as pointed out by Schindler and Seelig (18), we believe this interconversion must be slow compared with the rate of chain isomerization. Since we also argue that the chain reorientation is locally cooperative and involves a number of lipid molecules, p_t is expected to be essentially independent of the chain orientation. This is the important difference between previous approaches and the model employed here.

4. Assessment of Relative Importance of S_α and S_γ

We now calculate the order parameter expected in various NMR experiments for our model of molecular motion. The chain order param-

eter, S_α, depends only on the magnitude of chain deflection, $\Delta\alpha$, and therefore contributes equally to proton dipolar splitting and deuterium quadrupolar splitting. The intramolecular order parameter, S_γ, depends on the population fraction of a given conformer, $p(\gamma)$, as well as the angle γ which the molecular vector makes with respect to the instantaneous chain direction. Since this angle is different for the C—D bond and the geminal H—H internuclear vector in some of the chain methylene group conformations, S_γ is in general different for the two measurements.

It is readily shown that for the $g(\alpha)$ given by eq III-13

$$S_\alpha = \frac{1}{2}(\cos^2\Delta\alpha + \cos\Delta\alpha) \qquad \text{(III-20)}$$

This function is illustrated in Figure 8. Unrestricted motion of the chain would require $\Delta\alpha = 180^\circ$, and, as expected, S_α vanishes in this limit. In many liquid crystal systems the end-over-end orientation of the molecules is of little consequence because the two ends are similar in size and polarity. When this is the case, unrestricted motion is achieved when $\Delta\alpha \geq 90^\circ$ since the orientation distribution function is symmetric about $\alpha = 90$. This is not true of lipid molecules in bilayers because of the amphiphilic nature of the molecules. In addition, unrestricted motion of the chains is not possible here, since they are anchored at the glycerol segments. It is, however, still possible to obtain small values for S_α as $\Delta\alpha$ tends toward 90° (cf Figure 8).

Chain isomerization is characterized by an averaging of the methylene segment orientation arising from rapid interconversion among

FIGURE 8

The chain reorientation order parameter, S_α, calculated as a function of the extent of chain fluctuation as measured by $\Delta\alpha$(-) assuming a constant distribution for angles less than $\Delta\alpha$, or α_o(---) assuming a normal distribution with a standard deviation of α_o.

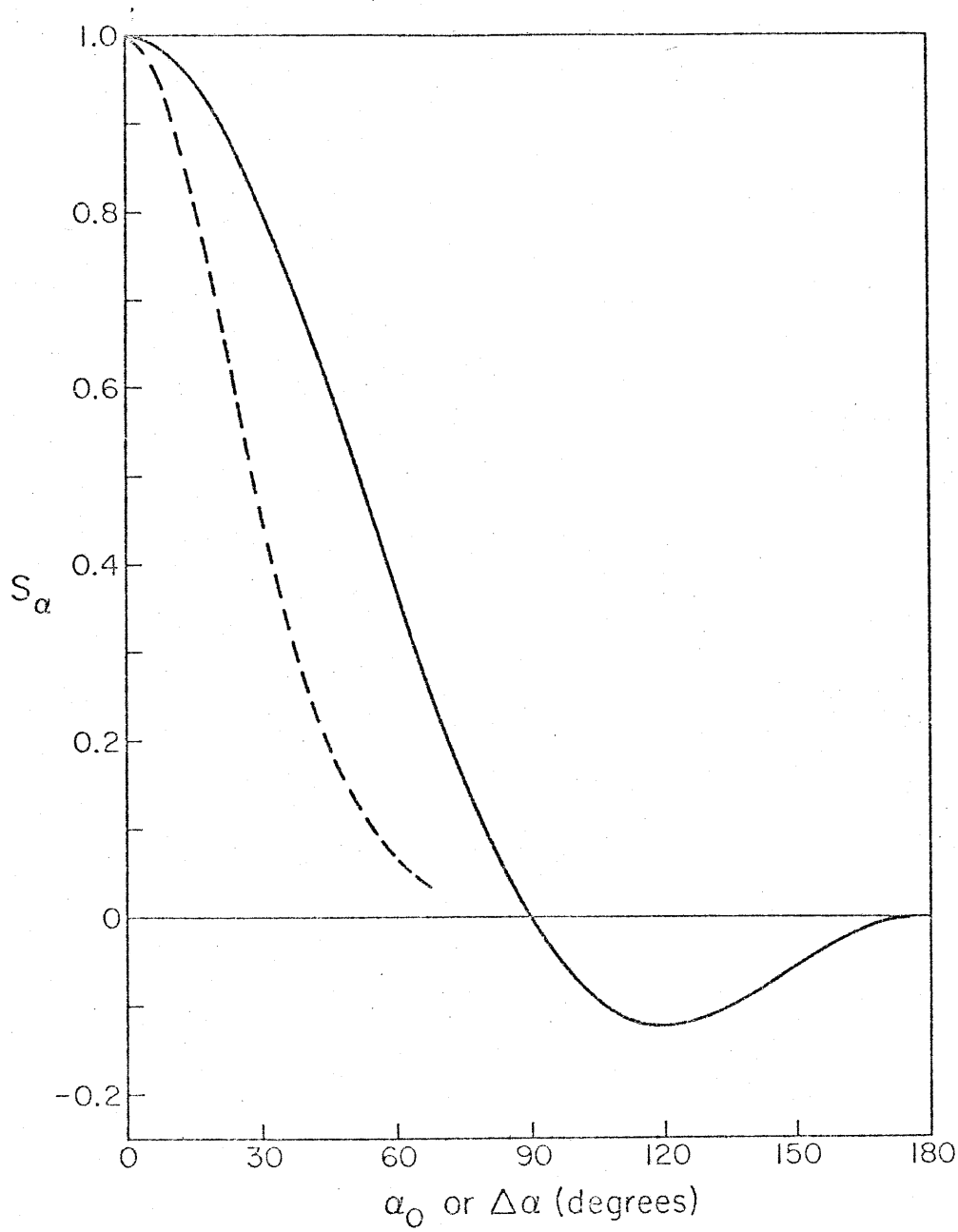
1.0
0.8
0.6
0.4
0.2
0
-0.2
S_α
0
30
60
90
120
150
180
α_o or $\Delta\alpha$ (degrees)

distinct conformers. There are three likely conformations in the model: trans, gauche + and gauche - (37). Because of the symmetry of saturated hydrocarbon chains, the two gauche populations must be equal and as a consequence the normalization condition is

$$\sum p(\gamma_i) = p_t + 2p_g = 1 \qquad \text{(III-21)}$$

The angle γ_i for a given conformer depends on the magnetic resonance experiment employed to probe the motion. The proton-proton dipolar interaction depends on the orientation of the geminal interproton vector, while the deuterium quadrupolar interaction is sensitive to the C—D bond orientation. A typical acyl chain nitroxide spin label (Figure 4) (14) contains an unpaired electron in a p-orbital which is normal to the methylene segment plane. ESR spectra depend on the average orientation of this p-orbital in the magnetic field. Values for γ_i and $3\cos^2\gamma_i - 1$ are summarized in Table 1 for each conformer and for each of the magnetic resonance experiments under consideration. These values yield the following intramolecular order parameters:

(i) $S_\gamma = -\frac{3}{8} p_t - \frac{1}{8}$ for the nuclear dipolar interaction

(ii) $S_\gamma = -\frac{1}{2} p_t$ for the deuterium quadrupolar interaction

(iii) $S_\gamma = \frac{9}{8} p_t - \frac{1}{8}$ for the acyl-chain nitroxide radical (III-22)

Seelig and Seelig (17) have pointed out that a segment in the

TABLE 1

The values of $(3\cos^2\gamma - 1)$ for each of the three orientations of a methylene segment and for each of the magnetic resonance experiments.

Experiment	Interaction Vector	Conformer					
		Trans		Gauche +		Gauche -	
		γ	$(3\cos^2\gamma - 1)$	γ	$(3\cos^2\gamma - 1)$	γ	$(3\cos^2\gamma - 1)$
^{1}H-NMR	H → H	90°	-1	60°	-¼	120°	-¼
^{2}H-NMR	C—D	90°	-1	90°	-1	35°26[a]	1
ESR	p-orbital	0°	2	60°	-¼	60°	-¼

[a]Perfect tetrahedral symmetry has been assumed. Correction to the actual bond angles amounts to less than 1% in all cases.

trans conformation may appear to be in a gauche conformation whenever there is a single gauche rotation at a segment farther up along the chain. For this reason, p_t as used here would provide a lower limit of the true probability of a segment being in a trans conformation. In the present analysis, however, single trans-gauche rotations in the upper part of the chain contribute to the chain-reorientation order parameter because the motion is likely to be on a timescale comparable to the chain reorientation timescale as a result of similar steric restrictions. The p_t value should therefore not be very different from the true value particularly in the upper portion of the chain. Moreover, the larger the value of p_t, the smaller the contribution from single trans-gauche rotations to S_α or S_γ would be.

The experimental order parameters, S^{HH}, S^{CD} and S^{esr}, may be compared directly using eq III-22, provided S_α is assumed to have the same value for all these experiments. For instance, one can readily show that $S^{esr} = -9/4\ S^{CD} - 1/8$. It has been customary to define a molecular order parameter, S_{mol}, for methylene segments, such that the angle β is taken between the director and the normal to the methylene plane. For the ESR spin label discussed here $S_{mol} = S^{esr}$. In general, however, the experimental order parameters are related to S_{mol} only through equations analogous to eq III-22. Note that the common transformation $S_{mol} = -2S^{CD}$ (17,19) is then only valid in the limit of $p_t \to 1$.

In all probability, S_α is not the same for S^{CD} and S^{esr}. This arises because the timescale of observation for an ESR experiment is much shorter than that for NMR, and as a consequence, the two techniques are likely to sample the chain reorientation motion differently.

In fact, ESR experiments measure an instantaneous distribution of chain orientations, even in oriented samples. As we will discuss later, this might be the origin of the spectral effects which McFarland and McConnell (38) and Birrell and Griffith (39) have attributed to bent chains.

In contrast the timescales of observation for the two NMR measurements are comparable, so the contribution to the respective order parameters from S_α should be the same. A comparison of S^{HH} and S^{CD} can then be used to get an estimate of p_t, which of course is the same. Experimental values of S^{CD} for the first 10 carbon segments are always quite similar; for the bilayer in the liquid crystalline phase, the average value is about -0.20 ± 0.01 (17,19). Thus about two-thirds of the methylene segments have S^{CD} values of this magnitude, the remaining third being closer to zero. The order parameter, S^{HH}, for a geminal proton pair was obtained by computer simulation of the early part of the free induction decay (22) assuming that the geminal dipolar interaction dominates. The simulation was also performed allowing for all interpair (both intrachain and interchain) dipolar interactions, but these latter contributions were found to be small, affecting S^{HH} no more than about 10% for a given $\Delta\beta$ (cf eq III-10). In these computer simulations the interproton vector within the geminal pair was allowed to fluctuate freely within a specified range of angles, $\pm \Delta\beta$. The fluctuation angle was then obtained by direct comparison of calculated and experimental free induction decays. A best fit was obtained for $\Delta\beta \sim 55^\circ \pm 5^\circ$ from which the order parameter was estimated to be $S^{HH} = -0.17 \pm 0.04$. The error partially reflects the uncertainty in

the interpair and interchain contributions. Since the ^{1}H-NMR order parameter is deduced from the early part of the free induction decay, it is an average value for those segments with the largest absolute value of the order parameter. This implies that the average S^{CD} and the S^{HH}, deduced this way, measure the same portion of the chain, and it should be valid to compare them. The order parameter S^{CD} is nearly equal to or larger than S^{HH}, which by eq III-22 indicates that p_t must be close to unity. We conclude that a major contribution to the reduction of the order parameter in these systems arises from chain reorientation . This is illustrated more clearly in Figure 9 which shows the range of p_t values that will satisfy either the condition that $S^{CD} = -0.20 \pm 0.01$ or the condition that $S^{HH} = -0.17 \pm 0.04$ for a given $\Delta\alpha$. The region of overlap (indicated by the hatched area in Figure 9) corresponds to the combinations of p_t and $\Delta\alpha$ values which will satisfy both conditions simultaneously. For the bilayer membrane in the liquid crystalline phase the ranges of p_t and $\Delta\alpha$ are therefore

$$\begin{aligned} 1 \geq p_t \geq 0.8 \qquad & \text{with} \quad -0.5 \leq S_\gamma^{CD} \leq -0.40 \\ & \text{or} \quad -0.5 \leq S_\gamma^{HH} \leq -0.43 \end{aligned}$$

$$60^\circ \geq \Delta\alpha \geq 50^\circ \qquad \text{with} \quad 0.38 \leq S_\alpha \leq 0.53 \qquad \text{(III-23)}$$

It is interesting to note that the deuterium order parameters measured for the lyotropic liquid crystalline phase of long chain fatty acids are about 50% larger than those obtained for the lipid bilayer (32), suggesting a more ordered phase in the former. Seelig and Nieder-

FIGURE 9

The range of values of P_t, the probability of a trans orientation, for given values of $\Delta\alpha$, the limit of the chain fluctuation, which yield (i) a deuterium order parameter $S^{CD} = -0.20 \pm 0.01$(---) or (ii) a proton order parameter $S^{HH} = -0.17 \pm 0.04$(—). The region of overlap (/////) corresponds to the combination of P_t and $\Delta\alpha$ values which yield both $S^{CD} = -0.20 \pm 0.01$ and $S^{HH} = -0.17 \pm 0.04$.

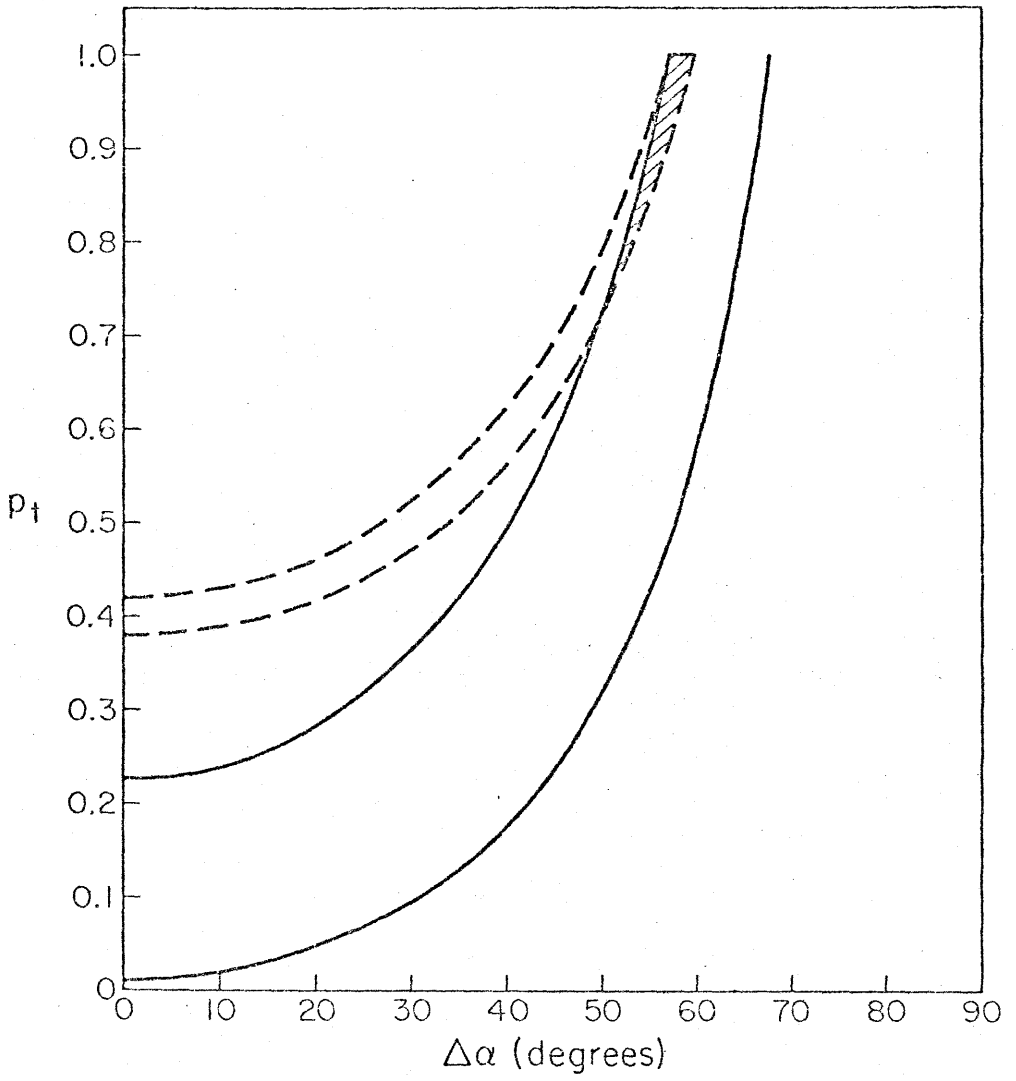
1.0
0.9
0.8
0.7
0.6
0.5
0.4
0.3
0.2
0.1
0
p_t
0
10
20
30
40
50
60
70
80
90
Δα (degrees)

berger (40) estimated a value for S_α of about 0.7 - 0.8, corresponding to a $\Delta\alpha$ of about 35°. The principal difference between the two systems is therefore a substantially smaller angular excursion of the chain in the case of the fatty acids, presumably because of a more regular packing of the acyl chains in their liquid crystalline phase.

5. Comparison of NMR and ESR Data

The choice of a constant distribution of angles α within the range of $\Delta\alpha$ (cf eq III-13), physically corresponds to freedom of movement of the chains within the specified restriction barriers. This is clearly an approximation, and angular distributions which more closely reflect the actual physical state of the bilayer could be employed, if the origin of chain reorientation were better understood. Note, however, that the choice of the distribution of α does not alter the basic conclusion, derived from Figure 9, that S_α must be in the range of 0.38 - 0.53, but merely reflects our view of <u>how</u> the chain reorientation motion leads to this value of S_α. As another illustration we consider the case of a normal distribution of chain reorientations about the director with a standard deviation given by the angle α_0. If we extend the angular range of α to include the whole domain, i.e., $0 \leq \alpha \leq \pi$, then the only quantity affecting the order parameter, S_α, is the standard deviation, α_0, and we can ascertain that value of α_0 which fits the observed S_α. With the distribution function written as

$$g(\alpha) = (\text{constant})\ e^{-\frac{1}{2}\left(\frac{\alpha}{\alpha_0}\right)^2} \qquad \text{(III-24)}$$

the S_α order parameter is given by

$$S_\alpha = \frac{1}{2} \frac{\int_0^\pi (3\cos^2\alpha - 1)\, e^{-\frac{1}{2}\left(\frac{\alpha}{\alpha_0}\right)^2} \sin\alpha \, d\alpha}{\int_0^\pi e^{-\frac{1}{2}\left(\frac{\alpha}{\alpha_0}\right)^2} \sin\alpha \, d\alpha} \qquad \text{(III-25)}$$

This expression requires numerical evaluation for each α_0. Results for this order parameter are plotted vs α_0 in Figure 8. Since S_α must fall in the range 0.38 - 0.53 to satisfy the ^{1}H- and ^{2}H-NMR order parameter data, it follows that the corresponding range of α_0 is 27-34°. These values of α_0 are naturally much smaller than the $\Delta\alpha$ values obtained with the constant distribution used above, because $\Delta\alpha$ is the upper limit of α, whereas α_0, in the normal distribution, corresponds approximately to the most probable value of α. To illustrate this point, we have plotted in Figure 10 both distribution functions for the appropriate value of $\Delta\alpha$ or α_0 which yield the observed experimental order parameters. A more meaningful comparison to make, perhaps, is that between the weighted distribution functions $g(\alpha)\sin\alpha$ (cf Figure 11), since it is a weighted distribution function which determines the composite ESR powder spectrum observed in the oriented spin label studies. In fact, it is those chains with instantaneous orientation close to the most probable orientation or the mean orientation which determine the gross features of the ESR spectrum. The shape of these weighted distribution functions clearly demonstrates that the most probable angle is nonzero, so that the ESR spectra can be interpreted in terms of permanently tilted chains (38,39,41). However, since the same spectral effects can arise from a statistical distribution of chains when the distribution

FIGURE 10

The distribution functions $g(\alpha)$ discussed in the text for a constant distribution within the angular range $0 \leq \alpha \leq 55^{\circ}$ (---) (i.e., $\Delta\alpha = 55^{\circ}$) and for a normal distribution with a standard deviation $\alpha_0 = 30^{\circ}$ (—). Both distribution functions yield an order parameter value $S_{\alpha} = 0.45$.

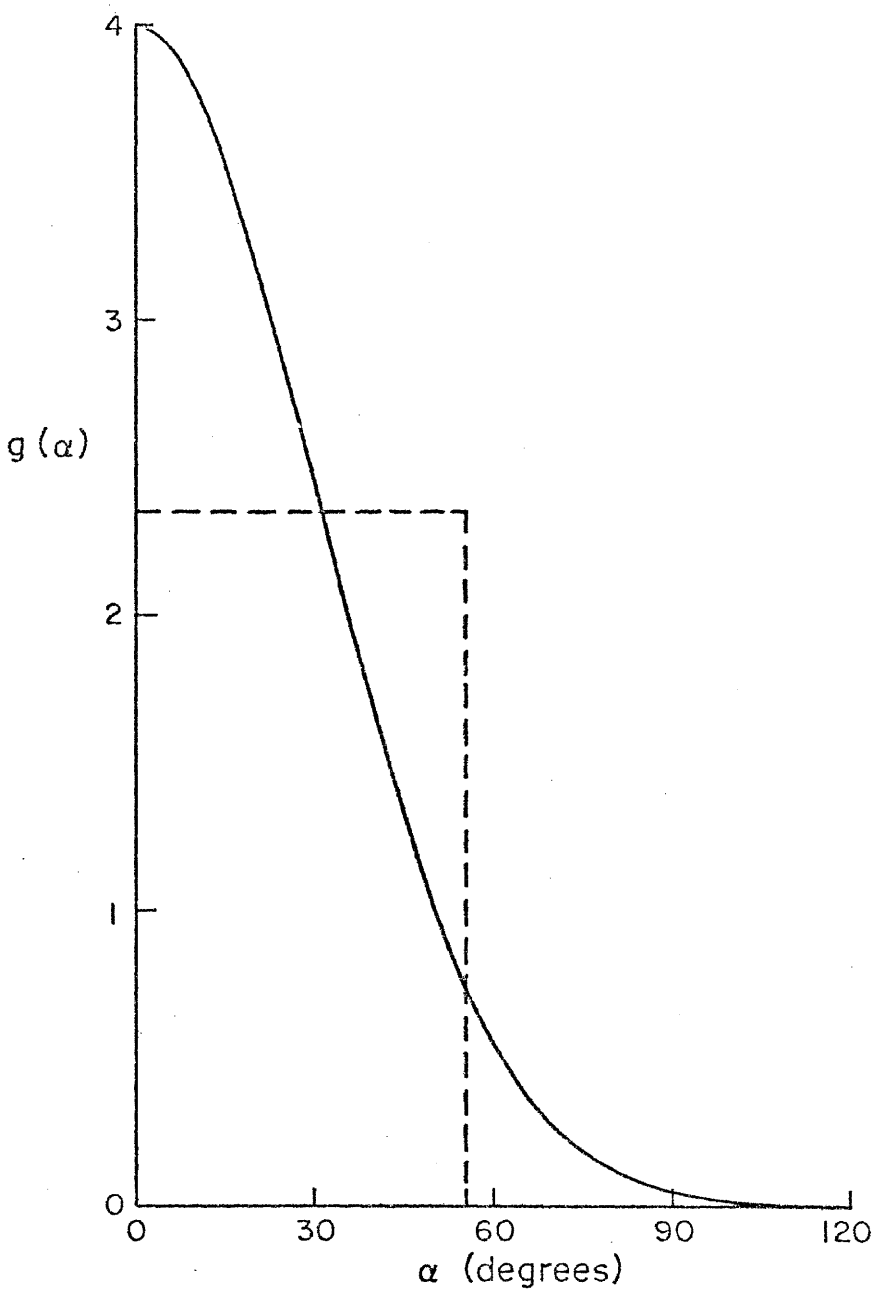
4
3
2
1
0
g (α)
0
30
60
90
120
α (degrees)

FIGURE 11

The normalized weighted distributions $g(\alpha)\sin\alpha$ for a constant distribution function $g(\alpha)$ with $\Delta\alpha = 55^{o}$ (---) and a normal distribution with $\alpha_{o} = 30^{o}$ (—). Both distribution functions yield an order parameter value $S_{\alpha} = 0.45$.

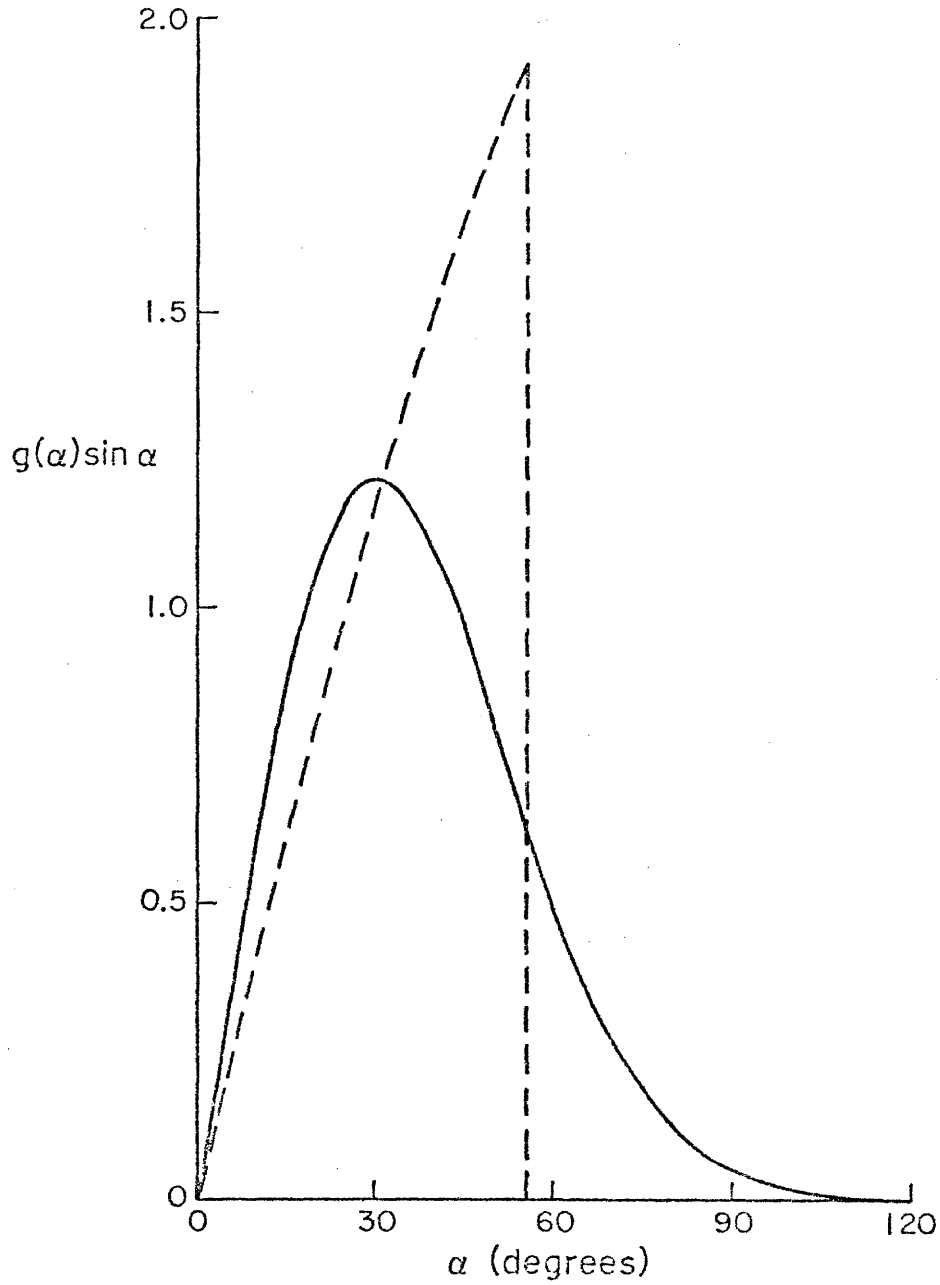
2.0
1.5
1.0
0.5
0
g(α)sin α
0
30
60
90
120
α (degrees)

is sampled on a short timescale, it is more correct, in our view, to interpret the tilt in a dynamic sense. Although our present conclusions based on NMR data are in substantial agreement with the ESR spin label results, the NMR method admittedly cannot distinguish between a normal distribution of chains about the director and a normal distribution about a permanently tilted orientation, provided that the chains rotate about the director in the latter case.

The present model does not explain the differences in the order parameter profiles along the chain observed between the S^{CD} and S^{esr} measurements (14,17). Apparently, these differences arise from the effect of the spin label on the packing density which in turn affects the profile of S_γ values (36).

6. Use of Relaxation Data to Assess Timescales

Although the order parameter provides a measure of the degree of motional restriction, the motional state of the bilayer system is only fully defined when both the motional distribution function and the timescales of the molecular motions are ascertained. In the previous section we proposed a motional model to account for the magnetic resonance order parameters. The purpose of the present and subsequent sections is to illustrate how the same motional model leads naturally to an interpretation of NMR relaxation measurements, which have previously been undertaken to elucidate the dynamic behavior of the system (21,23, 42,43,44). In particular, the present section is meant only to summarize some key data and results which pertain to the timescales for the molecular motions.

Proton and carbon-13 spin-lattice relaxation times of lipid bilayer membranes have been shown to increase with both increasing temperature and increasing frequency of irradiation (21,42). These findings can only be accounted for if the dipolar interactions responsible for the spin-lattice relaxation are modulated by at least two motions with correlation times, $\tau_{\parallel}$ and $\tau_{\perp}$, such that $(\omega_0\tau_{\parallel})^2 << 1$ and $(\omega_0\tau_{\perp})^2 >> 1$. Under these conditions, the spin-lattice relaxation rates may be approximated by (45)

$$\left(\frac{1}{T_1}\right) \simeq A\tau_{\parallel} + B\,\frac{1}{\omega_0^2\tau_{\parallel}} \qquad \text{(III-26)}$$

with the first term dominating the observed temperature dependence, and the second term responsible for the observed frequency dependence. On the basis of proton T_1 studies, Feigenson and Chan (21) have estimated the following ranges of correlation times for the liquid crystalline phase:

$$\tau_{\parallel} \simeq 10^{-9} - 2 \times 10^{-10}\ \text{s}$$

$$\tau_{\perp} \geq 10^{-7}\ \text{s} \qquad \text{(III-27)}$$

However, the origin of these timescales was not fully understood at that time. We suggest now that the faster timescale, $\tau_{\parallel}$, is associated with rotational isomerization whereas the slower timescale, $\tau_{\perp}$, reflects primarily the rate of chain reorientation. For the bilayer systems under consideration here, these timescales are sufficiently

different that expansion of the order parameter as presented in the previous sections is valid. A more detailed discussion of these timescales will be given later.

7. Interpretation of Homogeneous T_2's

The description of the order parameter presented in section 3 demonstrated that the first-order contributions to experimental spectra contain information about the degree of order in lipid systems. However, second-order effects were ignored, for example in reducing eq III-1 to III-2. Second-order effects give rise to relaxation, either spin-lattice or spin-spin relaxation which also affect the spectra. If the information on the spin-lattice and spin-spin relaxation times (T_1 and T_2) can be extracted, valuable information about timescales of motions can be obtained. This was illustrated briefly for T_1 in the previous section. Now we concentrate on the analysis of the spectral lineshape and its relationship to the spin-spin relaxation time T_2. Such analysis of magnetic resonance lineshapes usually reduces to the calculation of either the lineshape function, $F(\omega)$ or its Fourier transform, the free induction decay (FID), $G(t)$. We approach the problem by calculating the latter in general (Appendix II) and for the specific problem at hand in this section.

The theory developed in Appendix II (46) allows us to calculate the NMR free induction decays provided we can express the frequency fluctuations arising from modulation of the dipolar or quadrupolar interactions by molecular motion in terms of one or more random processes. In the following, we will show how this can be accomplished by consider-

ing in detail the model of chain motion of interest for a lipid system. First, however, we present an illustration of the method of Appendix II.

Consider the frequency fluctuations arising from modulations of the dipolar interaction between the pair of protons in a methylene group reorienting isotropically in space. We assume the angular motion to be a stationary, isotropically distributed, random process. Reorientation by Brownian motion is a process which satisfies these requirements. In this case the frequency fluctuations may be written (cf eq AII-3) as sum of a static and fluctuating term

$$\omega'(t) = \omega_0 \pm \omega(t) \tag{III-28}$$

in which the fluctuating component is given by (cf eq III-3)

$$\omega(t) = \Omega' \ (3\cos^2\theta(t) - 1) \tag{III-29}$$

where as before $\Omega' = 3/4(\gamma^2\hbar/r^3)$. Isotropic reorientation results in a mean of

$$\langle \omega(\tau) \rangle = 0 \tag{III-30}$$

and a variance of

$$\langle \omega(\tau)^2 \rangle = \frac{4}{5} \Omega'^2 \tag{III-31}$$

According to eqs AII-24 and AII-25, the FID is exponential with a time

constant of

$$\frac{1}{T_2} = \frac{4}{5}\,\Omega'^{2}\tau_c \qquad \text{(III-32)}$$

where τ_c is the correlation time of the random process $\omega(t)$. This result is well known (47) and the example is included here merely to demonstrate that the present theory leads to results which are compatible with previous treatments.

a. The lineshapes in oriented multilayers and liposomes.

We now consider the geminal pair of protons as part of a molecule undergoing the restricted motion in the motional model presented in section 3. To describe the motions in detail, we let $\theta(t)$, $\theta''(t)$ and θ' denote the polar angles which the magnetic field makes with respect to the interproton axis, the molecular axis, and the director, respectively (Figure 12). In addition, we let $\alpha(t)$ and $\phi(t)$, respectively, denote the polar and azimuthal angles of the motion of the molecular axis relative to the director; likewise $\gamma(t)$ and $\phi'(t)$ refer to the polar and azimuthal angles for the motion of the interspin axis relative to the molecular axis. Using the addition formula for spherical harmonics we can then write the frequency fluctuations in terms of the motion of the spin pair relative to the molecular axis, and that of the molecular axis relative to the magnetic field as

FIGURE 12

Illustration of the vectors and angles used in the motional model to calculate the lineshape in liposomes (see also Figure 6). a: Represents the motion of the interproton vector, $\vec{r}$, relative to the chain, $\vec{c}$. b: Represents the motion of the chain relative to the director, $\vec{d}$. The director is normal to the bilayer surface. H_0 is the direction of the applied magnetic field.

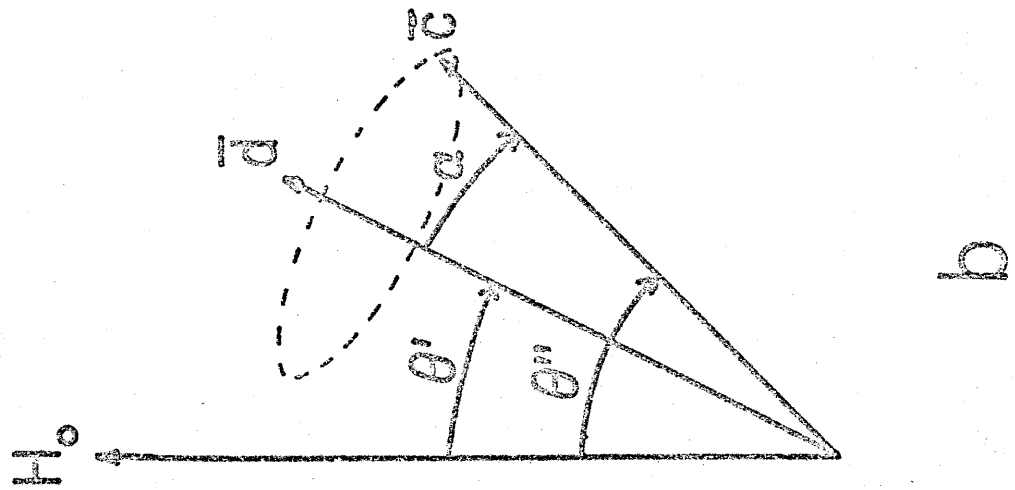

b

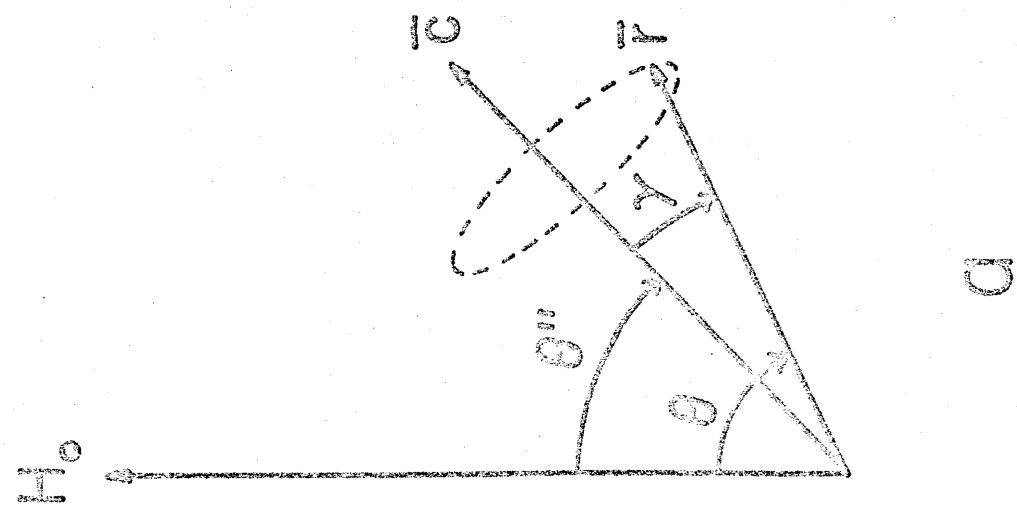

a

$$\omega(t) = \Omega'(3\cos^2\theta(t) - 1)$$

$$= \frac{1}{2}\Omega'(3\cos^2\theta''(t) - 1)\ (3\cos^2\gamma(t) - 1)$$

$$+ \frac{3}{2}\Omega'\ \sin^2\theta''(t)\ \sin^2\gamma(t)\ \cos 2\phi'(t)$$

$$+ \frac{3}{2}\Omega'\ \sin 2\theta''(t)\ \sin 2\gamma(t)\ \cos\phi'(t) \qquad \text{(III-33)}$$

Note that if we assume $\theta''(t)$, $\gamma(t)$ and $\phi'(t)$ to be independent, strictly stationary, strongly mixing, random processes (see Appendix II), then any polynomial expression of sines and cosines of the random processes will satisfy the same conditions. Also, the model implies that $\phi'(t)$ is uniform in the sense that

$$\text{(i)}\quad \text{Prob}\ \{\phi'(t) = x\} = \frac{1}{2\pi} \qquad \text{when } 0 \leq x \leq 2\pi \qquad \text{(III-34a)}$$

and

$$\text{(ii)}\ \text{Prob}\ \{\phi'(t + \tau) = x \text{ given } \phi'(t) = y\}$$
$$\text{depends only on } \tau \text{ and } (x-y) \qquad \text{(III-34b)}$$

As a consequence,

$$\left\langle \cos\phi'(t) \right\rangle = \left\langle \cos 2\phi'(t) \right\rangle = 0 \qquad \text{(III-35)}$$

and we see, using the independence of the random processes, that the mean of the total process is

$$\langle\omega(t)\rangle \equiv \bar{\omega} = \Omega' \left\langle 3\cos^2\theta''(t) - 1\right\rangle \left\langle \frac{3}{2}\cos^2\gamma(t) - \frac{1}{2}\right\rangle$$

$$= \Omega' S_\gamma \left\langle 3\cos^2\theta''(t) - 1\right\rangle \qquad \text{(III-36)}$$

where we define as in eq III-19

$$S_\gamma = \left\langle \frac{3}{2}\cos^2\gamma(t) - \frac{1}{2}\right\rangle \qquad \text{(III-37)}$$

The total correlation function (cf eq AII-9) of $\omega(t)$ is

$$R(\tau) = \langle\omega(t+\tau)\omega(\tau)\rangle - \bar{\omega}^2$$

$$= \Omega'^2 \left\langle (3\cos^2\theta''(t+\tau) - 1)(3\cos^2\theta''(t) - 1)\right\rangle \left\langle (\tfrac{3}{2}\cos^2\gamma(t+\tau) - \tfrac{1}{2})(\tfrac{3}{2}\cos^2\gamma(t) - \tfrac{1}{2})\right\rangle$$

$$+ \frac{9}{4}\Omega'^2 \left\langle \sin^2\theta''(t+\tau)\sin^2\theta''(t)\right\rangle \left\langle \sin^2\gamma(t+\tau)\sin^2\gamma(t)\right\rangle \left\langle (\cos 2\phi'(t+\tau)\cos 2\phi'(t)\right\rangle$$

$$+ \frac{9}{4}\Omega'^2 \left\langle \sin 2\theta''(t+\tau)\sin 2\theta''(t)\right\rangle \left\langle \sin 2\gamma(t+\tau)\sin 2\gamma(t)\right\rangle \left\langle \cos\phi'(t+\tau)\cos\phi(t)\right\rangle$$

$$- \Omega'^2 S_\gamma^2 \left\langle 3\cos^2\theta''(t) - 1\right\rangle^2 \qquad \text{(III-38)}$$

Because of the independence of the random processes there should be no cross terms in the correlation function. In particular, the first term in eq III-33 is independent of the other two because it contains no

functions of $\phi'(t)$. The second and third terms are uncorrelated because, under the present assumptions, $\cos\phi'(t)$ is uncorrelated with $\cos 2\phi'(t)$. This is readily shown, using eq III-34, since

$$\left\langle \cos\phi'(t+\tau)\cos 2\phi'(t) \right\rangle$$

$$= \frac{1}{2\pi} \int_0^{2\pi} \int_0^{2\pi} \cos x \cos 2y \text{ Prob } \{\phi'(t+\tau) = x \text{ given } \phi'(t) = y\} dy\, dx$$

$$= \frac{A}{2} \int_0^{2\pi} \cos y \cos 2y\, dy + \frac{B}{2\pi} \int_0^{2\pi} \sin y \cos 2y\, dy = 0 \qquad \text{(III-39)}$$

with

$$A = \int_0^{2\pi} \cos(x-y) \text{ Prob } \{\phi'(t+\tau) = x \text{ given } \phi'(t) = y\}\, d(x-y)$$

and

$$B = \int_0^{2\pi} \sin(x-y) \text{ Prob } \{\phi'(t+\tau) = x \text{ given } \phi'(t) = y\}\, d(x-y)$$

Defining the correlation fuctions

$$R''(\tau) \equiv \left\langle (3\cos^2\theta''(t+\tau) - 1)(3\cos^2\theta''(t) - 1) \right\rangle - \left\langle 3\cos^2\theta''(t) - 1 \right\rangle^2 \qquad \text{(III-40a)}$$

$$R_\gamma(\tau) \equiv \left\langle (\frac{3}{2}\cos^2\gamma(t+\tau) - \frac{1}{2})(\frac{3}{2}\cos^2\gamma(t) - \frac{1}{2}) \right\rangle - S_\gamma^2 \qquad \text{(III-40b)}$$

$$R_{\phi'}(\tau) \equiv \left\langle \cos\phi'(t+\tau)\cos\phi'(t) \right\rangle \qquad \text{(III-40c)}$$

$$R_{2\phi'}(\tau) \equiv \left\langle \cos 2\phi'(t+\tau)\cos 2\phi'(t) \right\rangle \qquad \text{(III-40d)}$$

and denoting their respective correlation times (cf eq AII-12) τ'', τ_γ, $\tau_{\phi'}$, and $\tau_{2\phi'}$, we find

$$R(\tau) = \Omega'^2 S_\gamma^2 R''(\tau) + \Omega'^2 \langle 3\cos^2\theta''(t) - 1\rangle^2 R_\gamma(\tau) + \Omega'^2 R''(\tau) R_\gamma(\tau)$$

$$+ \frac{9}{4}\Omega'^2 \langle \sin^2\theta''(t+\tau)\sin^2\theta''(t)\rangle \langle \sin^2\gamma(t+\tau)\sin^2\gamma(t)\rangle R_{2\phi'}(\tau)$$

$$+ \frac{9}{4}\Omega'^2 \langle \sin 2\theta''(t+\tau)\sin 2\theta''(t)\rangle \langle \sin 2\gamma(t+\tau)\sin 2\gamma(t)\rangle R_{\phi'}(\tau) \qquad \text{(III-41)}$$

We note that the first term in eq III-41 involves only the correlation function of the slowest process in the model, $\theta''(t)$, while the faster processes $\gamma(t)$ and $\phi'(t)$ contribute to the remaining terms. Accordingly, the first term dominates, and we can treat the contributions from the fast motions as a small error, $\varepsilon(\tau)$, and write

$$R(\tau) = (\Omega')^2 S_\gamma^2 R''(\tau) + \varepsilon(\tau) \qquad \text{(III-42)}$$

where $0 < \varepsilon(\tau) \leq 4\Omega'^2 R_\gamma(\tau) + \frac{9}{4}\Omega'^2 (R_{2\phi'}(\tau) + R_{\phi'}(\tau))$

With this result and that of eq III-36, application of the central limit theorem (Appendix II) gives the following FID for the proton pair

$$g(t) = \cos(\Omega' S_\gamma \langle 3\cos^2\theta''(t) - 1\rangle \cdot t)\, e^{-t/T_2} \qquad \text{(III-43a)}$$

and

$$\frac{1}{T_2} = \Omega'^2 S_\gamma^2 \,\mathrm{Var}(3\cos^2\theta''(t) - 1)\tau'' + E \qquad \text{(III-43b)}$$

where E represents the contribution to $1/T_2$ from the $\varepsilon(\tau)$ term, i.e.,

$$0 < E < 4\Omega'^2 \, \mathrm{Var}(\tfrac{3}{2}\cos^2\gamma(t) - \tfrac{1}{2})\tau_\gamma$$

$$+ \tfrac{9}{4}\Omega'^2(\mathrm{Var}(\cos\phi'(t))\tau_{\phi'} + \mathrm{Var}(\cos 2\phi'(t))\tau_{2\phi'}) \qquad \text{(III-44)}$$

Since the variances of $\cos\phi'(t)$ and $\cos 2\phi'(t)$ are both one half (eq III-34a), we may obtain the upper limit of E by replacing $\mathrm{Var}(\frac{3}{2}\cos^2\gamma(t) - \frac{1}{2})$ by its largest possible value, $\frac{9}{16}$, and replacing τ_γ, $\tau_{\phi'}$, and $\tau_{2\phi'}$ by the largest of the three and calling it τ_{fast}. This yields

$$0 < E << \tfrac{9}{2}\Omega'^2\tau_{fast} \qquad \text{(III-45)}$$

The relative error introduced in $1/T_2$ by neglecting E in eq III-43b is therefore less than $(9/2S_\gamma^2)(\tau_{fast}/\tau'')$ if $\mathrm{Var}(3\cos^2\theta'' - 1)$ may be taken to be of the order of unity. This error is small since $\tau_{fast} << \tau''$ (cf section 6).

It is instructive to consider the limit where the interspin axis is permanently coincident with the molecular axis. In this case we obtain the same result as eq III-43 except that S_γ is unity and the error term E is absent. Thus, to within a small error, the effects of the fast motions in the general case are to average the dipolar interaction onto the molecular axis, and to scale the dipolar interaction constant, Ω', to an effective interaction constant, $\Omega = S_\gamma\Omega'$. We may also consider the other limit where the intramolecular motion is fast and unrestricted. Here S_γ approaches zero and $1/T_2$ is given by the

error term and is small. The significance of these points is discussed further below.

To calculate the contribution from the molecular axis reorientation in $\theta''(t)$ to the FID, we now expand $(3\cos^2\theta''(t) - 1)$ in terms of θ', $\alpha(t)$, and $\phi(t)$. This expansion gives

$$\omega(t) = \Omega(3\cos^2\theta''(t) - 1)$$

$$= \frac{1}{2}\Omega(3\cos^2\theta' - 1)(3\cos^2\alpha(t) - 1)$$

$$+ \frac{3}{2}\Omega\sin^2\theta' \sin^2\alpha(t) \cos 2\phi(t)$$

$$+ \frac{3}{2}\Omega\sin 2\theta' \sin 2\alpha(t) \cos\phi(t) \qquad \text{(III-46)}$$

We again assume that $\alpha(t)$ and $\phi(t)$ are independent random processes, that they are also independent of $\gamma(t)$ and $\phi'(t)$, and that they satisfy the requirements of the central limit theorem. Since the random processes, $\alpha(t)$ and $\phi(t)$, both describe the molecular axis reorientation, they are expected to fluctuate on similar timescales. Therefore, no single term in eq III-46 will dominate. We proceed to find the means, variances, and correlation times for each of the processes involved in eq III-46. We assume that $\phi(t)$ is uniform in the sense of eqs III-34, so that

$$\langle\cos\phi(t)\rangle = \langle\cos 2\phi(t)\rangle = 0 \qquad \text{(III-47)}$$

$$\mathrm{Var}(\cos\phi(t)) = \mathrm{Var}(\cos 2\phi(t)) = \frac{1}{2} \qquad \text{(III-48)}$$

We define, as in eq III-19,

$$S_\alpha = \left\langle \frac{3}{2}\cos^2\alpha(t) - \frac{1}{2} \right\rangle \qquad \text{(III-49)}$$

as well as

$$\sigma_\alpha^2 \equiv \mathrm{Var}\left(\frac{3}{2}\cos^2\alpha(t) - \frac{1}{2}\right) \qquad \text{(III-50)}$$

$$\mu_\alpha \equiv \left\langle \sin 2\alpha(t) \right\rangle \qquad \text{(III-51)}$$

From these

$$\mathrm{Var}(\sin 2\alpha(t)) = \frac{8}{9}\left(1 + S_\alpha - 2\sigma_\alpha^2 - 2S_\alpha^2 - \frac{9}{8}\mu_\alpha^2\right) \qquad \text{(III-52)}$$

$$\left\langle \sin^2\alpha(t) \right\rangle = \frac{2}{3}\left(1 - S_\alpha\right) \qquad \text{(III-53)}$$

$$\mathrm{Var}(\sin^2\alpha(t)) = \frac{4}{9}\sigma_\alpha^2 \qquad \text{(III-54)}$$

From these results eq III-36 becomes

$$\overline{\omega} = \Omega S_\alpha(3\cos^2\theta' - 1) = \Omega' S_\gamma S_\alpha(3\cos^2\theta' - 1) \qquad \text{(III-55)}$$

By analogy with eqs III-40c and d we define the correlation functions $R_\phi(\tau)$ and $R_{2\phi}(\tau)$ and denote their correlation times as τ_ϕ and $\tau_{2\phi}$, respectively. The correlation functions $R_\alpha(\tau)$ and $R_{2\alpha}(\tau)$ are given by

$$R_\alpha(\tau) \equiv \left\langle \left(\frac{3}{2}\cos^2\alpha(t+\tau) - \frac{1}{2} - S_\alpha\right)\left(\frac{3}{2}\cos^2\alpha(t) - \frac{1}{2} - S_\alpha\right)\right\rangle \tag{III-56}$$

and

$$R_{2\phi} \equiv \left\langle (\sin 2\alpha(t+\tau) - \mu_\alpha)(\sin 2\alpha(t) - \mu_\alpha)\right\rangle \tag{III-57}$$

with correlation times τ_α and $\tau_{2\alpha}$. Also, it can be shown that

$$\left(\sin^2\alpha(t+\tau) - \frac{2}{3}(1-S_\alpha)\right)\left(\sin^2\alpha(t) - \frac{2}{3}(1-S_\alpha)\right) = \frac{4}{9}R_\alpha(\tau) \tag{III-58}$$

With these results, the correlation function of $\omega(\tau)$ is

$$\begin{aligned} R(\tau) = {} & \Omega^2(3\cos^2\theta' - 1)^2 R_\alpha(\tau) + \Omega^2(1 - S_\alpha)^2 \sin^4\theta' R_{2\phi}(\tau) \\ & + \Omega^2 \sin^4\theta' R_\alpha(\tau) R_{2\phi}(\tau) + \frac{9}{4}\Omega^2\mu_\alpha^2 \sin^2 2\theta' R_\phi(\tau) \\ & + \frac{9}{4}\Omega^2 \sin^2 2\theta' R_{2\alpha}(\tau) R_\phi(\tau) \end{aligned} \tag{III-59}$$

and we obtain the following expression for the FID

$$g(t) = \cos(\Omega S_\alpha(3\cos^2\theta' - 1)\cdot t)\, e^{-t/T_2} \tag{III-60a}$$

with

$$\frac{1}{T_2} = \Omega^2\sigma_\alpha^2(3\cos^2\theta' - 1)^2\tau_\alpha + \frac{1}{2}\Omega^2(1 - S_\alpha)^2\sin^4\theta'\tau_{2\phi}$$

$$+ \frac{9}{8}\Omega^2\mu_\alpha^2\sin^2 2\theta'\tau_\phi + \frac{1}{2}\Omega^2\sigma_\alpha^2\sin^4\theta'\tau_* \qquad \text{(III-60b)}$$

$$+ \Omega^2(1 + S_\alpha - 2\sigma_\alpha^2 - 2S_\alpha^2 - \frac{9}{8}\mu_\alpha^2)\sin^2 2\theta'\tau_{2*} + E$$

In the above, we have, as before

$$0 < E << \frac{9}{2}\Omega'^2\tau_{fast} \qquad \text{(III-61)}$$

and have defined the correlation times τ_* and τ_{2*} by

$$\tau_* = \frac{1}{R_\alpha(0)R_{2\phi}(0)}\int_0^\infty R_\alpha(\tau)R_{2\phi}(\tau)\,d\tau \qquad \text{(III-62)}$$

and

$$\tau_{2*} = \frac{1}{R_{2\alpha}(0)R_\phi(0)}\int_0^\infty R_{2\alpha}(\tau)R_\phi(\tau)\,d\tau \qquad \text{(III-63)}$$

The result of eq III-60 corresponds to a pair of lines in the frequency spectrum positioned at $\omega_0 \pm \Omega' S_\alpha S_\gamma(3\cos^2\theta' - 1)$ in agreement with eq III-16. However, eq III-60 also predicts that each line has a Lorentzian lineshape and a linewidth at half-maximum given by eq AII-26. The effect of motion is therefore to change the single-crystal spectrum, which is simply a pair of Lorentzian lines positioned at $\omega_0 \pm \Omega'(3\cos^2\theta' - 1)$ (Figure 7c) (Appendix I) (30), into a pair of Lorentzian

lines with their separation reduced by a factor $S = S_\alpha S_\gamma$, the order parameter, and with linewidths determined by the local molecular motions (eqs AII-26 and III-60).

We have described the FID and frequency spectrum resulting from a geminal pair of protons undergoing complex restricted motions appropriate to a fatty acid chain of a molecule in a bilayer membrane. However, we have ignored the fact that in many cases, including the latter, there are more than two interacting protons, but we will not discuss this complication in the present context. The problem is exceedingly complex and only a few attempts have been made to solve it (48,49,50).

The results of eq III-60 were developed to describe the FID from CH_2 groups, which are introduced selectively into perdeuterated fatty acid chains (51). Furthermore, the results are applicable to the deuterium NMR of a CD_2 segment in a fatty acid chain. Here, the fluctuations of the C—D bond modulate the quadrupolar interaction, and the FID is given by eq III-60 with the appropriate interaction constant, Ω' (eq III-8), and intramolecular order parameter S_γ (eq III-22). The same treatment can be extended to a rapidly rotating methyl group.

Most often, the samples used for NMR measurements are not the highly oriented samples, but rather liposomes in which there is an isotropic distribution of <u>director</u> orientations (Figure 5). The observed FID is therefore a superposition of the FID's arising from different director orientations. Thus

$$g_{powder}(t) = \frac{1}{2}\int_{-1}^{1} \cos(\Omega' S_\gamma S_\alpha (3\cos^2\theta' - 1)\cdot t)\; e^{-t/T_2(\cos\theta')}\; d(\cos\theta') \qquad \text{(III-64)}$$

with $1/T_2(\cos\theta')$ given by eq III-60b.

b. The lineshapes for vesicles

The model used in the previous example assumes that motion of the director is slow on the NMR timescale, and is therefore applicable to the large multilamellar aggregates. There are, however, many systems for which the molecular aggregate reorients isotropically, and with sufficient rate to contribute to the motional averaging. This is true for small bilayer vesicles and for nearly spherical lipoproteins. To describe the FID resulting from the geminal proton pair in such a system, we need to treat the polar angle between the director and the magnetic field, $\theta'(t)$, as a random process. We carry through all the assumptions of the molecular motions and include the assumption that $\theta'(t)$ is an isotropically distributed random process which satisfies the central limit theorem requirements and is independent of $\alpha(t)$, $\phi(t)$, $\gamma'(t)$ and $\phi'(t)$. The only necessary modification to the theory of the preceeding subsection is that eq III-46 must be revised to

$$\omega(t) = \frac{1}{2}\Omega(3\cos^2\theta'(t) - 1)\,(3\cos^2\alpha(t) - 1)$$

$$+ \frac{3}{2}\Omega\sin^2\theta'(t)\,\sin^2\alpha(t)\,\cos 2\phi(t)$$

$$+ \frac{3}{2}\Omega\sin 2\theta'(t)\,\sin 2\alpha(t)\,\cos\phi(t) \qquad \text{(III-65)}$$

Since $\theta'(t)$ is isotropic

$$\left\langle 3\cos^2\theta'(t) - 1\right\rangle = 0 \qquad \mathrm{Var}(3\cos^2\theta'(t) - 1) = \frac{4}{5} \tag{III-66a}$$

$$\left\langle \sin^2\theta'(t)\right\rangle = \frac{2}{3} \qquad \mathrm{Var}(\sin^2\theta'(t)) = \frac{4}{45} \tag{III-66b}$$

$$\left\langle \sin 2\theta'(t)\right\rangle = 0 \qquad \text{and } \mathrm{Var}(\sin 2\theta'(t)) = \frac{8}{15} \tag{III-66c}$$

The mean of the total process is then

$$\bar{\omega} = 0 \tag{III-67}$$

Thus the NMR signal becomes homogeneously broadened as a consequence of the isotropic motion. This is to be expected since the aggregate motion renders every director equivalent. In order to characterize the lineshape of the homogeneous line, we introduce the correlation functions

$$R_{\theta'}(\tau) \equiv \left\langle (3\cos^2\theta'(t+\tau) - 1)\ (3\cos^2\theta'(t) - 1)\right\rangle \tag{III-68}$$

and

$$R_{2\theta'}(\tau) \equiv \left\langle \sin 2\theta'(t+\tau)\ \sin 2\theta'(t)\right\rangle \tag{III-69}$$

Note that

$$\left\langle (\sin^2\theta'(t+\tau) - \tfrac{2}{3})\ (\sin^2\theta'(t) - \tfrac{2}{3})\right\rangle = \frac{1}{9} R_{\theta'}(\tau) \tag{III-70}$$

The total correlation function for the frequency fluctuations in this problem is

$$R(\tau) = \Omega^2 S_\alpha^2 R_{\theta'}(\tau) + \Omega^2 R_{\theta'}(\tau) R_\alpha(\tau) + \frac{4}{9}\Omega^2 (1 - S_\alpha)^2 R_{2\phi}(\tau)$$

$$+ \frac{1}{9}\Omega^2 (1 - S_\alpha)^2 R_{2\phi}(\tau) R_{\theta'}(\tau) + \frac{4}{9}\Omega^2 R_{2\phi}(\tau) R_\alpha(\tau)$$

$$+ \frac{1}{9}\Omega^2 R_{2\phi}(\tau) R_{\theta'}(\tau) R_\alpha(\tau) + \frac{9}{4}\Omega^2 \mu_\alpha^2 R_{2\theta'}(\tau) R_\phi(\tau)$$

$$+ \frac{9}{4}\Omega^2 R_{2\theta'}(\tau) R_\phi(\tau) R_{2\alpha}(\tau) \qquad \text{(III-71)}$$

This correlation function predicts the exponential FID

$$g(t) = e^{-t/T_2} \qquad \text{(III-72)}$$

and hence a homogeneous Lorentzian line with

$$\frac{1}{T_2} = \frac{1}{45}\Omega^2 \left(36 S_\alpha^2 \tau_{\theta'} + \sigma_\alpha^2 (36\tau_{3*} + 10\tau_* + 2\tau_\dagger)\right.$$

$$+ (1 - S_\alpha)^2 (10\tau_{2\phi} + 2\tau_{5*} + 27\mu_\alpha^2 \tau_{4*}$$

$$\left. + 24(1 + S_\alpha^2 - 2\sigma_\alpha^2 - 2S_\alpha^2 - \frac{9}{8}\mu_\alpha^2)\tau_{2\dagger}\right) + E \qquad \text{(III-73)}$$

Here, in addition to the correlation times previously defined, we have introduced

$$\tau_{\theta'} = \frac{1}{R_{\theta'}(0)} \int_0^\infty R_{\theta'}(\tau)\, d\tau \qquad \text{(III-74a)}$$

$$\tau_{3*} = \frac{1}{R_{\theta'}(0)R_{\alpha}(0)} \int_0^\infty R_{\theta'}(\tau)R_{\alpha}(\tau)\, d\tau \qquad \text{(III-74b)}$$

$$\tau_{4*} = \frac{1}{R_{2\theta'}(0)R_{\phi}(0)} \int_0^\infty R_{2\theta'}(\tau)R_{\phi}(\tau)\, d\tau \qquad \text{(III-74c)}$$

$$\tau_{5*} = \frac{1}{R_{\theta'}(0)R_{2\phi}(0)} \int_0^\infty R_{\theta'}(\tau)R_{2\phi}(\tau)\, d\tau \qquad \text{(III-74d)}$$

$$\tau_{+} = \frac{1}{R_{\theta'}(0)R_{\alpha}(0)R_{2\phi}(0)} \int_0^\infty R_{\theta'}(\tau)R_{\alpha}(\tau)R_{2\phi}(\tau)\, d\tau \qquad \text{(III-74e)}$$

$$\tau_{2+} = \frac{1}{R_{2\theta'}(0)R_{2\alpha}(0)R_{\phi}(0)} \int_0^\infty R_{2\theta'}(\tau)R_{2\alpha}(\tau)R_{\phi}(\tau)\, d\tau \qquad \text{(III-74f)}$$

Analysis of linewidths from small bilayer vesicles was first considered in terms of restricted motion by Seiter and Chan (22), who arrived at an expression similar to eq III-73. The principal result of their treatment and of eq III-73, is that the linewidth is determined by three effects: (i) averaging by vesicle tumbling, (ii) averaging by local chain motion (which in the present derivation is a complex motion), and (iii) the spin-lattice relaxation due to very fast motions. In the special case of lipid bilayer vesicles, we can simplify eq III-73 by making the following approximations for the correlation times: (1) since $\phi(t)$ and $\alpha(t)$ both are related to the molecular axis reorientation, we expect fluctuations in $(\frac{3}{2}\cos^2\alpha(t) - \frac{1}{2})$, $\sin^2\alpha(t)$, $\sin 2\alpha(t)$, and $\cos 2\phi(t)$ to exhibit nearly the same correlation times; (2) similarly, we expect fluctuations in $(3\cos^2\theta'(t) - 1)$, $\sin^2\theta'(t)$,

and $\sin 2\theta'(t)$ to have nearly the same correlation times, and (3) we expect the correlation time associated with $\cos 2\phi(t)$ to be about twice as fast as that for $\cos\phi(t)$. These approximations should introduce an error no greater than a factor of two in these correlation times. A summary of the correlation times, the random processes from which they originate, and the results of making the above approximations is presented in Table 2. Note that here we reintroduce the symbols of Seiter and Chan (22) by associating τ_V with τ_θ, and $\tau_\perp$ with τ_α, and assume that for the composite processes the correlation times may be obtained as if the correlation functions of the individual processes are exponential, e.g. $\tau_* = (1/\tau_\alpha + 1/\tau_\phi)^{-1}$. With these approximations eq III-73 simplifies to

$$\frac{1}{T_2} = \frac{4}{5}\Omega^2\left(S_\alpha^2\tau_V + \left(\frac{7}{6}\sigma_\alpha^2 + \frac{1}{3}(1-S_\alpha)^2 + \frac{3}{2}\mu_\alpha^2 + \frac{4}{9}(1+S_\alpha - 2\sigma_\alpha^2 - 2S_\alpha^2 - \frac{9}{8}\mu_\alpha^2)\right)\tau_\perp\right)$$

$$= \frac{4}{5}\Omega^2\left(S_\alpha^2\tau_V + \frac{1}{9}\left(\frac{5}{2}\sigma_\alpha^2 - 5S_\alpha^2 + 9\mu_\alpha^2 - 2S_\alpha + 7\right)\tau_\perp\right) \qquad \text{(III-75)}$$

The first term in eq III-75 is identical to the first term of the corresponding equation derived by Seiter and Chan, and represents that contribution to the linewidth arising from modulation by vesicle tumbling of the residual dipolar interaction not averaged by local motion. The remainder of eq III-75 corresponds to the last term of the Seiter-Chan formula, and represents the linewidth contribution from the local chain motion. Our derivation yields a more complex expression for this

TABLE 2

Correlation Times Associated with the Various Random Processes Resulting in Eq III-75 of the Text

Correlation Times	Random Processes	Approximation of Correlation Time for Lipid Bilayer Vesicles
$\tau_{\theta'}$	$3\cos^2\theta'(t) - 1, \sin^2\theta'(t)$	τ_V
$\tau_{2\theta'}$	$\sin 2\theta'(t)$	τ_V
τ_{α}	$\frac{3}{2}\cos^2\alpha(t) - \frac{1}{2}, \sin^2\alpha(t)$	$\tau_{\perp}$
$\tau_{2\alpha}$	$\sin 2\alpha(t)$	$\tau_{\perp}$
τ_{ϕ}	$\cos\phi(t)$	$2\tau_{\perp}$
$\tau_{2\phi}$	$\cos 2\phi(t)$	$\tau_{\perp}$
τ_{*}	$\sin^2\alpha(t)\cos 2\phi(t)$	$\frac{1}{2}\tau_{\perp}$
τ_{2*}	$\sin 2\alpha(t)\cos\phi(t)$	$\frac{2}{3}\tau_{\perp}$
τ_{3*}	$(3\cos^2\theta'(t) - 1)(\frac{3}{2}\cos^2\alpha(t) - \frac{1}{2})$	$\tau_{\perp}$
τ_{4*}	$\sin 2\theta'(t)\cos\phi(t)$	$2\tau_{\perp}$
τ_{5*}	$\sin^2\theta'(t)\cos 2\phi(t)$	$\tau_{\perp}$
$\tau_{\dagger}$	$\sin^2\theta'(t)\sin^2\alpha(t)\cos 2\phi(t)$	$\frac{1}{2}\tau_{\perp}$
$\tau_{2\dagger}$	$\sin 2\theta'(t)\sin 2\alpha(t)\cos\phi(t)$	$\frac{2}{3}\tau_{\perp}$

contribution because of the more detailed motional model. As a consequence this model predicts slightly broader resonance lines for vesicles than the Seiter-Chan model.

Interpretation of the linewidth in terms of eq III-75 is discussed further in the next section, where calculations using eq III-75 are compared with experimental data from the small vesicle system.

8. Interpretation of Vesicle Linewidths.

As indicated earlier, the effect of sonication is to produce vesicles which are small enough to permit the overall tumbling of the bilayer unit, and therefore the director, to contribute to averaging of the residual first order dipolar or quadrupolar interactions (22). If the vesicles are less than about 500 Å in diameter, their tumbling rate should be fast enough to satisfy the assumptions used in calculating the lineshape for vesicles (section 7b). Under these circumstances it was found that the linewidth becomes homogeneous (eq III-67) and is given by

$$\Delta\nu_H = \frac{1}{\pi T_2} = \frac{4}{5\pi}\left(\frac{3\gamma^2\hbar}{4r^3}\right)^2 (S_\gamma^{HH})^2 \{S_\alpha^2 \tau_e + \frac{1}{9}\left(\frac{5}{2}\sigma_\alpha^2 - 5S_\alpha^2 - 2S_\alpha + 9\mu_\alpha^2 + 7\right)\tau_\perp\} \qquad \text{(III-76)}$$

This is identical to eq III-75 except that these are the effective correlation times associated with modulation of the dipolar interactions. Thus, $(1/\tau_e) = (1/\tau_v) + (1/\tau_{1d})$ where $(1/\tau_v)$ is the rate of vesicle tumbling and $(1/\tau_{1d})$ is the rate of lateral diffusion of a

lipid molecule on the spherical vesicle surface. Since the director orientation is modulated by its translation along the curved surface, a rapid lateral diffusion may be important. The contribution to the linewidth from the spin-lattice relaxation is not included since $(1/T_2) >> (1/T_1)$ for anisotropic motion. Note further, that if chain reorientation relative to the director is absent, the second term in the linewidth expression of eq III-76 is identically zero and

$$\Delta\nu_H = \frac{4}{5\pi}\left(\frac{3\gamma^2\hbar}{4r^3}\right)^2 S_{HH}^2 \tau_e \qquad \text{(III-77)}$$

This expression is commonly employed in linewidth calculations for sonicated vesicles (52). We contend, however, that this approximation is not justified for the bilayer vesicle system, because of the substantial chain reorientation relative to the director found even in the multilayers (cf section 4).

Since the derivation resulting in eq III-76 is strictly valid only for isolated pairs of protons, eq III-76 does not account for interpair dipolar interactions in the fatty acid chain. However, the theory is exact for ^{2}H-NMR experiments where the linewidth is controlled by the modulation of the quadrupolar interaction. To calculate the deuterium linewidth it is only necessary to introduce into the treatment the appropriate interaction constant (eq III-8) and intramolecular order parameter (section 4). Thus,

$$\Delta\nu_D = \frac{9\pi}{20}\left(\frac{e^2qQ}{h}\right)^2 (S_\gamma^{CD})^2 \{S_\alpha^2 \tau_e + \frac{1}{9}\left(\frac{5}{2}\sigma_\alpha^2 - 5S_\alpha^2 - 2S_\alpha + 9\mu_\alpha^2 + 7\right)\tau_\perp\} \qquad \text{(III-78)}$$

We note that this linewidth expression reduces to that previously proposed by Stockton et al (19)

$$\Delta\nu_D = \frac{9}{20}\left(\frac{e^2qQ}{h}\right)^2 S_{CD}^2 \tau_V + \frac{1}{\pi T_1} \qquad \text{(III-79)}$$

only in the limit where chain reorientation and lateral diffusion are not important motions.

Equations III-76 and III-78 predict that the ratio of the calculated proton and deuterium linewidths is just the ratio of the interaction constants multiplied by the ratio of the intramolecular order parameters. On this basis one expects $(\Delta\nu_H/\Delta\nu_D) = 0.016\ (S_\gamma^{HH}/S_\gamma^{CD})$, which is about 0.016 since S_γ^{HH} and S_γ^{CD} are about equal (cf section 4). The observed proton linewidths are about 20-30 Hz at 220 MHz when the full methylene intensity is observed for the composite methylene signal (53) (Figure 13). This is true also for signals from the α-CH_2's adjacent to the carbonyls of the acyl chains, which might be expected to produce the broadest resonances. Corresponding deuterium linewidths (for the upper part of the chain at comparable temperatures) are about 550 ± 50 Hz (19). The observed linewidth ratio of 0.036 indicates that the proton linewidth of 20 Hz is indeed an upper limit of the true value. This is reasonable since the dispersion of chemical shifts for the protons along the chain, as well as spin-spin coupling, will tend to make the resonances appear broader. Extrapolation of linewidth data to zero field (45) yields a linewidth of 8 Hz, supporting this contention.

Stockton et al (19) have measured both deuterium linewidths of

FIGURE 13

Typical 220 MHz proton NMR spectrum of a sample of small sonicated vesicles of DPL at about 50°C. Assignments are as follows (cf. Figure 2):

a: CH group of glycerol

b: HOD

c: CH_2 groups of glycerol and the O-CH_2 group of the choline

d: $\overset{+}{N}$-CH_2 group of choline

e: $\overset{+}{N}$-$(CH_3)_3$ groups of choline

f: CH_2 in the α position to the acyl carbonyl

g: CH_2 in the β position to the acyl carbonyl

h: Composite methylene signal of the bulk of the acyl CH_2 groups

i: CH_3 groups of acyl chains.

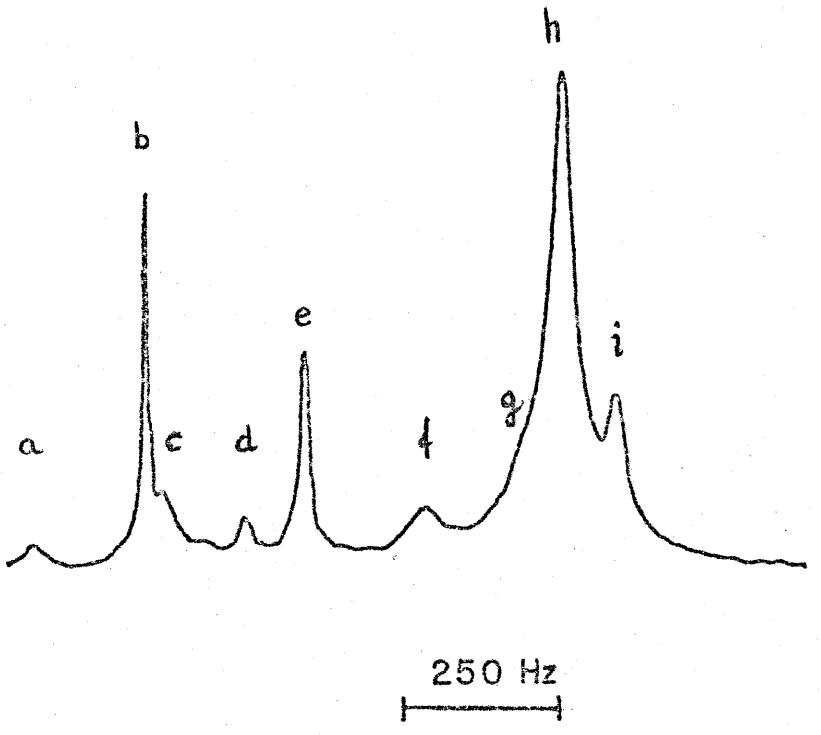
h
b
e
i
a
c
d
f
g
250 Hz

vesicles and order parameters in multilayers for the same lipid system as a function of the deuterium position along the chain. They found that vesicle linewidths for different positions vary linearly with the square of the multilayer order parameter measured for the same position in the chain, and argued on the basis of this correlation that there is no reduction of the order parameter upon sonication. Equation III-78 predicts this correlation if (i) there is no change in the intramolecular order parameter S_γ^{CD} upon sonication, or (ii) if the flexibility gradient changes proportionally along the chain. The important conclusion is that this correlation is independent of the value of S_α, or changes in it, since S_α applies to the whole chain.

If there is no structural perturbation of the lipid bilayer membrane upon sonication, then, on the basis of the order parameters measured for lecithin multilayers, we expect the homogeneous linewidths observed for small sonicated vesicles to be determined by the rate of vesicle tumbling, lateral diffusion of the lipid molecules, or some combination of the two motions. Although there have been numerous attempts to ascertain any vesicle proton linewidth dependence on solution viscosity (54,27,53,55), none, in fact, has been observed. This could mean that the effect of vesicle tumbling on the linewidth is small compared to the effect of lateral diffusion, i.e., $1/\tau_e \geq 1/\tau_{ld}$. This possibility is not supported by current estimates for the lateral diffusion coefficient of lipids in multilayers of 10^{-8} cm^2/sec (56). It is possible that this diffusion is in fact much faster in the vesicular bilayer. However, ^{31}P-NMR measurements (57) also have recently yielded estimates of 10^{-8} cm^2/sec for the lateral diffusion coefficient in

lecithin bilayer vesicles. For these reasons, we must conclude that proton and deuterium linewidths from small vesicles are controlled by modulation of the dipolar interaction by local motions, that is, the second term of eqs III-76 and III-78 dominates the total linewidth. Also, the ^{31}P-NMR studies of bilayer vesicles showed that the ^{31}P linewidths of the glycerol phosphate moiety in these systems exhibit a viscosity dependence (57), indicating that the chemical shift anisotropy mechanism contributing to these linewidths is modulated at least in part by overall tumbling of the bilayer unit. This important observation is to be contrasted with the lack of any detectable viscosity dependence in the proton spectrum.

If we use the model outlined in section 4, for which the distribution of chain reorientations relative to the director is uniform within an angular range of zero to $\Delta\alpha$ (eq III-13), we can rewrite eqs III-76 and III-78 as

$$\Delta\nu = C\{A(\Delta\alpha)\tau_e + B(\Delta\alpha)\tau_\perp\} \qquad \text{(III-80)}$$

where $A(\Delta\alpha) = S_\alpha^2 = \frac{1}{4}(\cos^2\Delta\alpha + 2\cos^3\Delta\alpha + \cos^4\Delta\alpha)$

and $B(\Delta\alpha) = \frac{1}{72}(92 + 55\cos\Delta\alpha - 24\cos^2\Delta\alpha - 85\cos^3\Delta\alpha - 38\cos^4\Delta\alpha)$

The constant C is either $\frac{4}{5\pi}\left(\frac{3\gamma^2\hbar}{4r^3}\right)^2(S^{HH})^2$ or $\frac{9\pi}{20}\left(\frac{e^2qQ}{h}\right)^2(S_\gamma^{CD})^2$, depending on whether eq III-80 refers to the proton or deuterium linewidth. The apparent lack of viscosity dependence implies that the second term dominates, and since τ_e is apparently dominated by τ_v we

expect

$$B(\Delta\alpha)\tau_{\perp} \geq A(\Delta\alpha)\tau_{v} \qquad \text{(III-81)}$$

The equality represents an upper limit for $A(\Delta\alpha)\tau_v$ since we expect that if 50% of the linewidth is viscosity dependent it would be detectable. Figure 14 shows the dependence of $\Delta\nu/C\ \tau_v = A(\Delta\alpha) + B(\Delta\alpha)\ \frac{\tau_\perp}{\tau_v}$ on $\Delta\alpha$ for various ratios of $\tau_\perp/\tau_v$. The solid lines refer to that part of the function where eq III-81 is applicable, that is, where there is little or no viscosity dependence. For a linewidth of 20-30 Hz and reasonable values for τ_v (5×10^{-6} to 5×10^{-7}) we see no viscosity dependence only if $\Delta\alpha > 70$ and if $\tau_\perp/\tau_v$ is small. The vesicle linewidth and its viscosity independence therefore indicate a significant reduction (by a factor of 2-3) in the order parameter. We point out that these arguments give an underestimate of $\Delta\alpha$ in part because the proton linewidth of eq III-76 is an underestimate of the true linewidth. The dipolar interaction due to the other protons on the chain would lead to further broadening of the signal. It would be interesting to carry out a similar analysis with the deuterium linewidths. Unfortunately, the viscosity dependence here is not known. When such data become available, the relative importance of vesicle tumbling and local motion in the motional averaging can then be ascertained more precisely.

In summary, the available NMR data on sonicated lipid systems at 50°C suggest that upon sonication (i) the order parameter is reduced by a factor of 2-3 to a value about -0.07 to -0.1, (ii) the order parameter is reduced primarily through S_α, thereby causing all the order

FIGURE 14

The function $A(\Delta\alpha) + B(\Delta\alpha)\frac{\tau_\perp}{\tau_v} = \frac{\Delta\nu}{C \cdot \tau_v}$ (Eq III-80) as a function of $\Delta\alpha$ and for a series of values of $\tau_\perp/\tau_v$. The solid portion of the curves corresponds to the combination of $\Delta\alpha$ and $\tau_\perp/\tau_v$ for which $B(\Delta\alpha)\tau_\perp \geq A(\Delta\alpha)\tau_v$, the region over which little or no viscosity dependence of the linewidth should be observed. The correlation time for vesicle tumbling, τ_v, is expected to be within the range indicated based on the following experimental findings: for a 220 Å diameter vesicle in aqueous suspension at 20°C the Stokes-Einstein relationship predicts $D_{20,w} = 1.9 \times 10^{-7}$ cm²/s. The measured value for fractionated egg yolk lecithin vesicles is $D_{20,w} = 1.9 \times 10^{-7}$ cm²/s. At 50°C, this value corresponds to a $D_{50,w} = 3.9 \times 10^{-7}$ cm²/s which leads to a tumbling correlation time of $\tau_{50°C} = \frac{2}{9}\frac{R^2}{D} \sim 10^{-6}$ s. The lateral diffusion correlation time is approximately $\tau_{ld} = \frac{R^2}{4D_{ld}} = 3 \times 10^{-5}$ s.

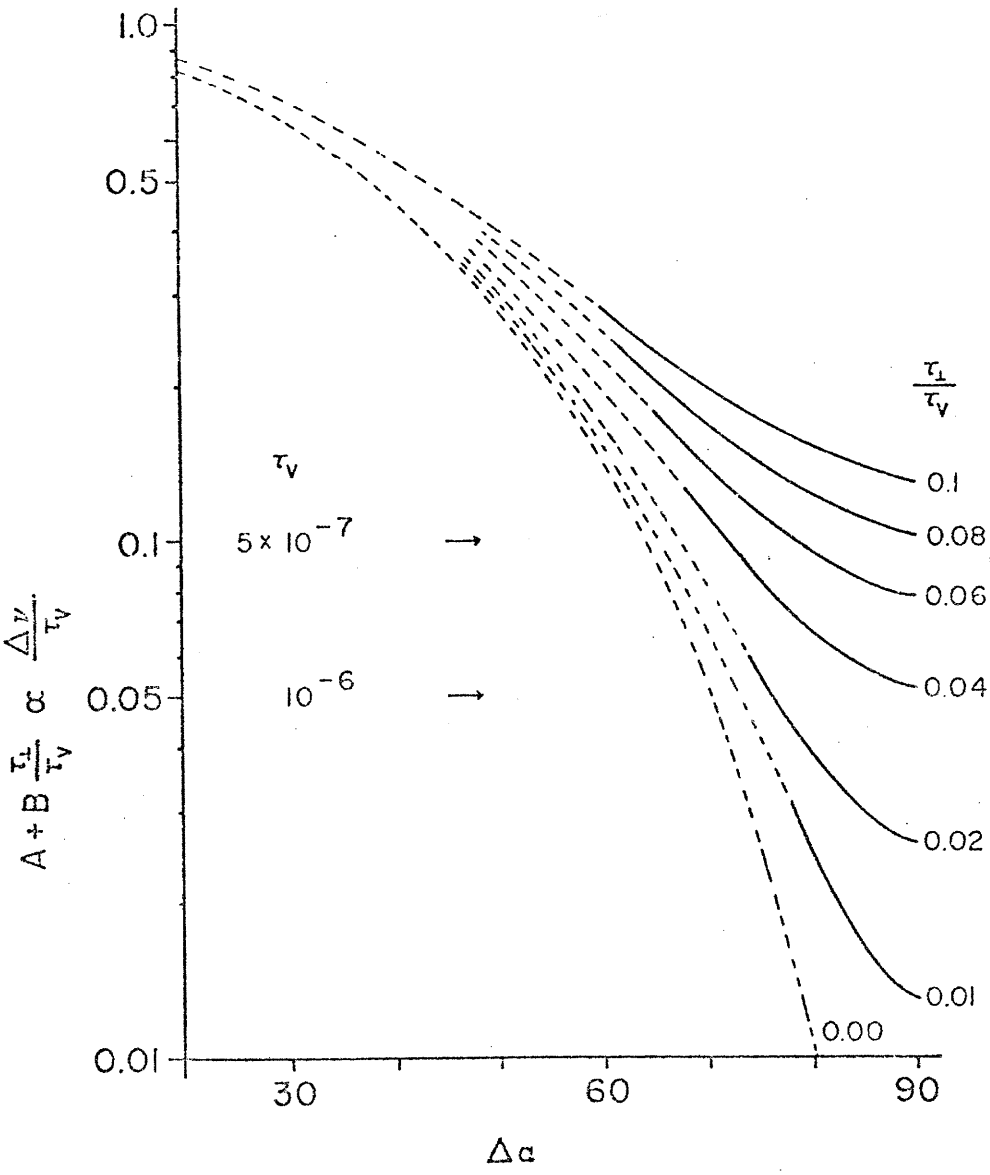
1.0
0.5
0.1
0.05
0.01
30
60
90
Δα
A + B τ⊥/τv ∝ Δν/τv
τv
5 × 10⁻⁷ →
10⁻⁶ →
τ⊥/τv
0.1
0.08
0.06
0.04
0.02
0.01
0.00

parameters along the chain to decrease by a near constant factor, and (iii) the correlation time $\tau_{\perp}$ for chain reorientation is decreased from $\sim 10^{-7}$ s to 10^{-8}-10^{-9} s.

9. Further Comments on the Motions.

The interpretation of the magnetic resonance data outlined in the previous sections supports the general picture of molecular motions suggested in the model of section 2. The purpose of this section is to elaborate on the details of the molecular motions in the model, and to describe the chain isomerization and reorientation in more detail.

It has been suggested by Träuble (58) that most trans-gauche rotations in the lipid chains occur as β-coupled pairs of trans-gauche ± rotations rather than as isolated events. The net result of the coupled rotation is the formation of a kink. The suggestion is based on the arguement that a kink is energetically favored over isolated trans-gauche rotations, because they produce less unfavorable interactions with neighboring chains. The notion of kinks is in accord with the finding that the entropy associated with melting of hydrocarbon chains from the gel to the liquid crystalline phase (see Chapter IV) is about one half of that for melting from a crystalline to an isotropic phase (9). The need to invoke kinks in the membrane system is a direct consequence of the anisotropy of the membrane bilayer.

Formation and subsequent disappearance of a kink in a chain is one mechanism whereby the dipolar interaction can be modulated (45,59). Examination of the molecular models also suggests that a kink may be displaced along the chain by a set of δ-coupled rotations around the

kink as illustrated in Figure 15. A kink may conveniently be denoted by $k_n^{\pm}$, where the subscript denotes the carbon atom closest to the acyl end of the chain, such that the first trans-gauche rotation in the kink occurs around the bond between carbon n and $n+1$, and the superscript denotes the sense of that bond rotation (37). The δ-coupled rotations then transform an even kink to another even kink but with opposite sense. That is, a kink diffusion corresponds to an interconversion among even or odd kinks with alternating sense, e.g.,

$$\cdots k_{n-4}^{+} \rightleftarrows k_{n-2}^{-} \rightleftarrows k_{n}^{+} \rightleftarrows k_{n+2}^{-} \rightleftarrows k_{n+4}^{+} \cdots$$

There are therefore, in effect, four subsets of kinks with interconversions among the subsets only possible either (i) through a totally eclipsed conformation, which is energetically very unfavorable, or (ii) by kink annihilation to form the all-trans chain followed by formation of a kink of a different sense or at a new position.

It is reasonable to argue that formation of a kink is most likely to occur at the terminal end of the chain, where there is the least steric hindrance. Once formed, the kink would diffuse along the chain, passing through each methylene segment many times as it undergoes a simple random-walk type motion. The lifetime of a kink is determined by the number of times the kink is reflected at each end of the chains before it ultimately is dissipated at the terminal end of the chain. In this diffusion process, the correlation time $\tau_{\parallel}$ is associated with the time duration between a kink leaving and returning to a given segment, in the meantime having undergone a random walk along the chain. Clearly

FIGURE 15

Schematic illustration of δ-coupled trans-gauche ± rotations around a kink leading to kink diffusion. The arrows indicate the sense of the rotations keeping the higher numbered carbon fixed, and the particular sequence illustrated corresponds to, from left to right,

$$\text{all-trans} \rightarrow k_1^+ \rightarrow k_3^- \rightarrow k_5^+.$$

The carbon atoms are numbered, and the pair of methylene segments which are oriented off-axis with respect to the chain are indicated by the rectangle around the carbon numbers. It is evident that this kink diffusion sequence will affect every methylene segment along the chain.

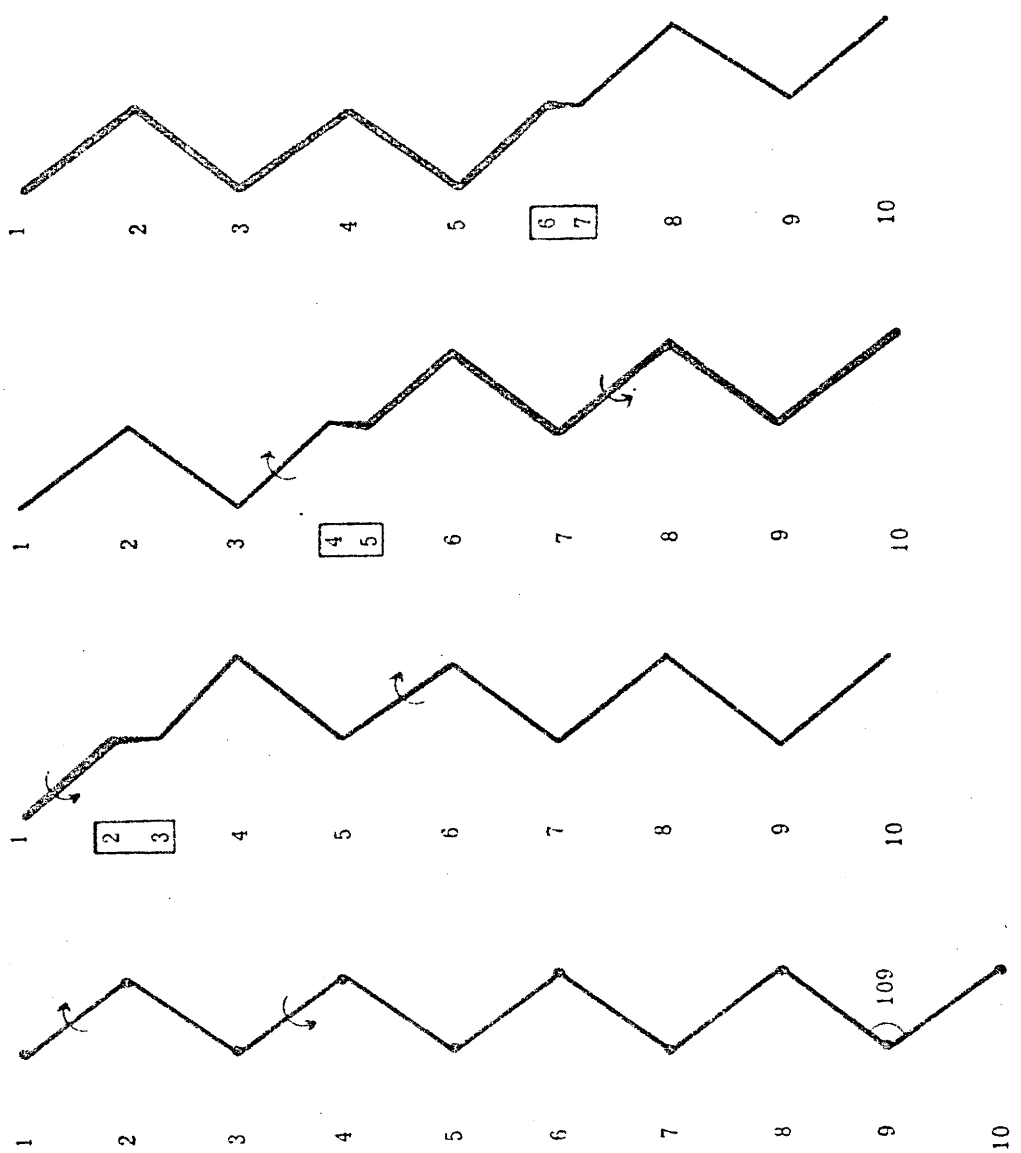
1
2
3
4
5
6
7
8
9
10
109

$\tau_{\parallel} \leq \tau_{lifetime}$. One might expect $\tau_{\parallel}$ to vary somewhat with the location of the methylene segment in the chain. In particular, $\tau_{\parallel}$ should be shorter the closer the segment is to that end of the chain which serves as the kink sink.

The value of $\tau_{\parallel}$ for the upper part of the chain may be estimated on the basis of simple one-dimensional diffusion theory as follows. Once a kink is formed, the jump rate, i.e., the rate at which the kink becomes displaced by one unit length l, is given by

$$\tau_{jump}^{-1} = Ae^{-\Delta E/RT} \qquad \text{(III-82)}$$

Here A is the frequency factor ($\sim 10^{14}$ s^{-1}) and ΔE, the activation energy for the δ-coupled rotation, which is estimated to be 3-4 kcal per mole of kinks (45). The jump time is then approximately 10^{-12} - 10^{-11} s. Since the mean square distance $\langle l^2 \rangle$ travelled in the time $\tau_{\parallel}$ is

$$\langle l^2 \rangle = 2 \frac{l^2}{\tau_{jump}} \cdot \tau_{\parallel} \qquad \text{(III-83)}$$

$\tau_{\parallel}$ may be estimated to be about 10^{-10} s, which is the order of magnitude inferred from the proton T_1 data.

For sonicated bilayer vesicles McLauglin et al (42) and Lee et al (43) have shown that the carbon-13 T_1's are slightly longer toward the tail end of the chain. The same observation has been noted for the proton T_1's (60). Proton and carbon-13 spin-lattice relaxation measurements of chain resonances in the vesicle system exhibit a temperature

and frequency dependence analogous to that found in unsonicated systems (45,61). The chain motions which dominate T_1 are therefore similar for the two bilayer systems. These findings, to be in accord with a smaller order parameter in this region of the bilayer (17,19,38), necessarily imply that $\tau_{||}$ is faster at the tail of the chain than in the upper portion of the chain. This is in agreement with the kink diffusion model described above. In fact, our preliminary computer simulations (62) of a one-dimensional random walk among a limited number of sites with a reflective barrier at one end (the head group) and a partially absorptive barrier at the other end (the methyl end) indicate that the kink diffusion model can account for a difference in T_1 along the chain. In these simulations, it was found that the autocorrelation functions decay exponentially at all positions along the chain. The decay constant for these autocorrelation functions is constant over a large region of the chain, slightly longer at the reflective barrier and much shorter (about half) at the partially absorptive barrier where kinks are formed and annihilated. The magnitude of the decay constants as well as the relative values along the chain were found to depend linearly on the ratio of the jump rate to the rate of formation of kinks. This ratio is not well established or easily modeled and is presently the major uncertainty in the modeling.

In the kink diffusion model the jump rate is assumed to be independent of the position along the chain, and it may be argued that it should also be independent of the chain length since ΔE of eq III- 82 is likely to be independent of chain length. This was verified indirectly by our findings (63) that the apparent activation energy (for

the T_1 process) does not vary with the chain length. However, in a longer chain the number of sites available to the kink is larger and $\tau_{\parallel}$ should be longer as a consequence. Indeed, the computer simulations (62) show that the decay time of the autocorrelation function increases with increasing chain length. The same trend is predicted from experimental data since the spin-lattice relaxation rate increases with increasing chain length (63).

If the slower correlation time $\tau_{\perp}$ for multilayers arises from fluctuations of the chain tilt with respect to the bilayer normal, then $\tau_{\perp}^{-1}$ measures the rate at which the chain traverses the angular range $\Delta\alpha$. In general, one expects $\Delta\alpha$ and $\tau_{\perp}$ to exhibit a complex dependence on the property of the bilayer, particularly since chain reorientation could be partly molecular and partly cooperative in its origin. If chain reorientation is principally molecular and controlled by rotational diffusion processes, then one expects the rate of chain reorientation to be inversely proportional to the amplitude of the angular fluctuation; that is, the larger $\Delta\alpha$, the larger $\tau_{\perp}$ is expected to be. On the contrary, if chain reorientation is principally cooperative, involving say several hundred lipid molecules, then one expects a distribution of correlation times with both a high and a low frequency cutoff. The former is expected to be controlled by the single molecule reorientation rate, while the latter should depend on the nature of the cooperative unit. The $\tau_{\perp}$ measured by T_1 (21; eq III-27) really reflects the most effective combination of timescales and amplitudes of the chain reorientation for the spin-lattice relaxation process. Thus if the size of the cooperative unit decreases, as is likely to happen

as the bilayer becomes less ordered, the effective correlation time is expected to decrease. This is in accord with the slightly shorter $\tau_{\perp}$ found for vesicles.

10. Conclusions

a. General

We have presented a motional model for the fatty acid chain in a bilayer membrane which involves rapid chain isomerization by kink diffusion and restricted axially symmetric chain fluctuations relative to the bilayer normal. In addition to these motions the model requires rapid diffusion about the long molecular axis. We have demonstrated that it is necessary to interpret the NMR order parameters observed for lipid bilayers in terms of chain reorientations in addition to isomerization of the chain. For a bilayer membrane in the liquid crystalline phase, the order parameter can be written as a product of two independent order parameters representing the two individual motions. We emphasize again that NMR experiments will always measure the product. This is in contrast to ESR spin label experiments, where the spectra are primarily sensitive to chain isomerization because of the short timescale of measurement. Understanding the inherent differences in these measurements enabled us to compare the state of chain motion deduced from the various techniques. It is clear that ESR measurements predict a permanently tilted chain because the chain reorientational motion is incompletely averaged.

Detailed analysis of the observed proton and deuterium order parameters indicates that the chain has considerable intramolecular

order ($p_t > 0.8$) except for the region at the tail of the chain. All told there is on the average less than one kink per chain in the upper portion of the chain. The high p_t value arrived at here is consistent with that derived by Hubbell and McConnell (14) on the basis of their spin label measurements, but the variation in p_t along the upper part of the chain must be small in accordance with the ^{2}H-NMR experiments of Seelig and coworkers (17). It thus appears that the observed proton and deuterium NMR order parameters arise to a large extent from significant fluctuations of the tilt of the chain as a unit about the bilayer normal, albeit on a rather long timescale (10^{-8} - 10^{-7} s). The amplitude of this chain reorientation about the bilayer normal ($\Delta\alpha \simeq 50^{\circ}$) is consistent with the extent of off-axis motion ($\Delta\beta \simeq 55^{\circ}$) previously deduced by Seiter and Chan (22) in their analysis of ^{1}H-NMR data.

The motional model was also shown to lend itself naturally to a simple interpretation of the nuclear magnetic relaxation measurements on lipid bilayer systems. In order to account for the temperature and frequency dependences of proton T_1 data, it is necessary to invoke two correlation times of quite different timescales. In the present work, we propose that the faster timescale $\tau_{\parallel}$ is to be attributed to the intramolecular isomerization of the hydrocarbon chain (kink diffusion), and the slower timescale $\tau_{\perp}$ to cooperative fluctuations in the tilt of the chains about the bilayer normal.

The effect of surface curvature on the packing of the lipid chains in vesicle systems is also found to be readily understood in terms of the proposed motional model. The earlier linewidth theory of Seiter and Chan (22) has been modified for this motional model and

extended to determination of deuterium linewidths of rapidly tumbling vesicles. Comparison of calculated deuterium linewidths with those recently reported by Stockton et al (19) leads to the conclusion that introducing a high curvature in the bilayer by sonication causes significant increases in the rate and amplitude of chain tilting without appreciable disruption of the intramolecular order.

It is likely that the model can be refined, particularly in the mathematical modeling of the motions. Thus, new data may lead to improvement in the choices of $g(\gamma)$ and $g(\alpha)$ or may suggest even more realistic interpretations of the isomerization and reorientation motion. Nevertheless, we are confident that the physics of the model is substantially correct and that these two essentially independent sets of motion occur at quite different rates. It is therefore reasonable to discuss further some of the implications the model has on our view of other molecular interactions in the membrane.

b. Correlation with other experiments

The conclusion that chain isomerization is not the only important motion in lipid bilayers is in agreement with data from x-ray diffraction studies (5). The electron density profile of the lipid bilayer in the gel phase shows a deep electron deficient trough at the center of the bilayer, which arises from the terminal methyl groups of the chain. When the bilayer is heated to the liquid crystalline phase, the previously sharp trough broadens and becomes shallow, which has been interpreted to mean that the methyl groups are localized over a larger range of the bilayer. This can be accounted for by chain reorientation or chain isomerization but the large p_t value suggests a

low probability of many simultaneous trans-gauche rotations in a given chain. Hence any delocalization effect due to chain isomerization should be fairly minimal.

Recent detailed interpretations of Raman spectra obtained from lipid bilayers (64,65) enabled these investigators to assess quantitatively the variations with temperature of both the intramolecular and the intermolecular order. These workers observed large changes in both quantities upon passing from the gel to the liquid crystalline phase. The intramolecular order determined for the liquid crystalline phase is compatible with a large p_t value, and the observed changes in the intermolecular order are consistent with increased chain reorientation above the phase transition temperature. Moreover, the Raman spectroscopic studies have shown that well above the transition temperature there are no detectable differences in intramolecular order between unsonicated and sonicated bilayer systems since the intensities of those Raman lines, which are proportional to the average number of extended all-trans chain segments, were found to be essentially identical for the two systems. This is compatible with the S_γ value being comparable for the two model membranes. In contrast, the Raman spectra show pronounced intensity differences in that region of the spectra which has been interpreted to measure intermolecular or interchain interactions. This reduction of intermolecular coupling of Raman active CH vibrations is compatible with a larger amplitude ($\Delta\alpha$) of chain reorientation in vesicles. The Raman data therefore support our present interpretation of the magnetic resonance data in terms of the larger amplitudes of chain reorientation with increasing surface curvature.

c. Implications for permeability

A possible correlation between kink diffusion and permeability of small molecules across lipid membranes has previously been suggested (58,59). It is therefore interesting to note that a kink diffusion process like the one described here would result in local density fluctuations in the bilayer. Moreover, these density fluctuations would be directed along the length of the chain and therefore across the phospholipid bilayer. It is readily seen how such a process might facilitate diffusion of small ionic and neutral solutes, e.g. H_2O across a membrane. It is even possible that in boundary regions between rigid and flexible lipid molecules, these density fluctuations actually become enhanced. The enhancement would occur because, on the timescale of kink diffusion in a fluid chain, a neighboring rigid chain would not be able to compensate for the shape and volume change associated with the kink. Since the density perturbation is highly localized, the percentage volume change per kink is large. However, if the neighboring chain is a fluid chain, i.e. it contains kinks, it may respond to the kink in the original chain even on the fast timescale of kink diffusion. The effect is that the density perturbation per kink becomes dispersed over a few chains and the percentage volume change per kink is smaller. The phenomenon might well explain why the permeability of certain ions, e.g. Na^+, exhibits a maximum at the phospholipid phase transition (66) where gel and liquid crystalline phases coexist. Similarly, unannealed vesicles (67) probably contain boundary regions where local density fluctuations are large enough to allow rapid permeation of ionic species. These ideas are readily extendable to lipid mixtures. For

example the enormous enhancement in permeability in lysolecithin/lecithin mixtures at temperatures below the transition temperature of the host lipid compared to the permeability at temperatures above this temperature (68) may be accounted for in this way.

d. Implications for lipid mixtures and protein-lipid interactions

The chain reorientation motion will only occur to a significant extent if there is cooperativity among neighboring lipids. If sufficiently different membrane components are in mutual contact, it is possible that the amount of chain reorientation is reduced. Since membrane fluidity is controlled in part by the amplitude of chain reorientation, the motion is biologically significant. The well-known condensation effect of cholesterol on phospholipid bilayers is readily understood in this context. A significant decrease in the angle of chain fluctuation can account for the increase in the order parameter observed when cholesterol is added. A more detailed account of this effect will be given in Chapter IV in the description of the phospholipid-cholesterol phase diagram.

A similar condensing effect might be expected if large protein molecules are embedded in the membrane. By virtue of their size and shape these proteins could easily modify the extent of chain reorientataion of phospholipid molecules in their immediate vicinity. The evidence for an annulus of motionally restricted lipid molecules around certain proteins (69) is in agreement with this concept. More importantly, however, the restricted chain reorientation would occur in several layers of lipids around the protein thereby generating an "order gradient." The extended region of order interacts with that of neigh-

boring proteins leading to lipid-mediated protein-protein interactions. This effect is expected to be most significant at high protein to lipid ratios, where protein-induced condensations of phospholipids can produce effects similar to those observed at high concentrations of cholesterol. The domains of condensed lipids which are formed are distinguished from those lipids far removed from the protein molecules by their motional state. However, the boundary monolayer of lipids which has been inferred from spin label measurements (69) comprises only a small fraction of the condensed lipids. Protein-lipid interactions of this type are not specific but can nevertheless modify the overall motional properties of the membrane. Since membrane fluidity affects the activity of a specific membrane protein, this activity may not depend on the type of neighboring proteins provided the total protein to lipid ratio is high thus ensuring the presence of a condensed lipid domain. In our judgment, modifications of chain reorientation amplitudes represent the most effective way of controlling membrane fluidity over an extensive surface domain.

The terms "fluidity" and "liquid-like" have often been used in describing the motional state of membranes. We point out that, in general, it is the extent of correlation of intermolecular interactions which determines whether a condensed phase is ordered or "liquid-like." To be sure, the conformational states of the component molecules can change upon transition from an ordered to a disordered state, but the intramolecular effect is a consequence rather than a cause of reduced correlation among molecules. For this reason an operational definition of a liquid state is a condensed state which cannot sustain shear

forces. Therefore, the order parameter S_{α} is a better indicator of membrane fluidity than S_{γ}.

References

1. E. Gorter and F. Grendel, J. Exptl. Med., 41, 439 (1925).
2. H. Davson and J.F. Danielli, in "The Permeability of Natural Membranes" (2nd ed.), London, Cambridge University Press, 1952.
3. D. Chapman, Biol. Membranes, 1, 125 (1968).
4. A. Tardieu, V. Luzzati and F.C. Reman, J. Mol. Biol., 75, 711 (1973).
5. M.H.F. Wilkins, A.E. Blaurock and D.M. Engelman, Nature (London) New Biology, 230, 72 (1971).
6. M.J. Janiak, D.M. Small and G.G. Shipley, Biochemistry, 15, 4575 (1976).
7. B.D. Ladbrooke and D. Chapman, Chem. Phys. Lipids, 3, 304 (1969).
8. H.J. Hinz and J.M. Sturtevant, J. Biol. Chem., 247, 6071 (1972).
9. D. Chapman, R.W. Williams and B.D. Ladbrooke, Chem. Phys. Lipids, 1, 445 (1967).
10. D. Chapman, Ann. N.Y. Acad. Sci., 195, 179 (1972).
11. H. Wennerström and G. Lindblom, Quarterly Review Biophysics, in press (1977).
12. G.J.T. Tiddy in "Nuclear Magnetic Resonance" (Specialists Report), R. K. Harris, ed., Vol. 4, 233 (1975).
13. D. Chapman and N.J. Salsbury, Progr. Surf. Sci., 3, 121 (1970).
14. W.L. Hubbell and H.M. McConnell, J. Am. Chem. Soc., 93, 314 (1971).
15. J. Seelig, J. Am. Chem. Soc., 92, 3881 (1970).
16. P. Jost, A.S. Waggoner and O.H. Griffith in "Structure and Function of Biological Membranes", L. Rothfield, ed., New York, N.Y., Academic Press, 1971.

17. A. Seelig and J. Seelig, Biochemistry, 13, 4839 (1974).

18. H. Schindler and J. Seelig, Biochemistry, 14, 2283 (1975).

19. G.W. Stockton, C.F. Polnaszek, A.P. Tulloch, F. Hasan and I.C.P. Smith, Biochemistry, 15, 954 (1976).

20. J. Seelig and W. Niederberger, Biochemistry, 13, 1585 (1974).

21. G.W. Feigenson and S.I. Chan, J. Am. Chem. Soc., 96, 1312 (1974).

22. C.H.A. Seiter and S.I. Chan, J. Am. Chem. Soc., 95, 7541 (1973).

23. A.F. Horwitz, W.J. Morsley and M.P. Klein, Proc. Nat. Acad. Sci. (U.S.), 69, 590 (1972).

24. M.A. Hemminga and H.J.C. Berendsen, J. Magn. Reson., 8, 133 (1972).

25. K.J. Longmuir and F.W. Dahlquist, Proc. Nat. Acad. Sci. (U.S.), 73, 2716 (1976).

26. M.P.N. Gent, I.M. Armitage and J.H. Prestegaard, in press (1976).

27. M.P. Sheetz and S.I. Chan, Biochemistry, 11, 4573 (1972).

28. J. Urbina and J.S. Waugh, Proc. Nat. Acad. Sci. (U.S.), 71, 5062 (1974).

29. A.C. McLaughlin, P.R. Cullis, J.A. Berden and R.E. Richards, J. Magn. Reson., 20, 146 (1975).

30. A. Abragam, in "The Principles of Nuclear Magnetism", Oxford University Press, 1961 .

31. J. Seelig and A. Seelig, Biochem. Biophys. Res. Commun., 57, 406 (1974).

32. W. Niederberger and J. Seelig, Ber. Bunsenges. Phys. Chem., 78, 947 (1974).

33. S. Marčelja, J. Chem. Phys., 60, 3599 (1974).

34. S. Marčelja, Biochim. Biophys. Acta, 367, 165 (1974).

35. M.B. Jackson, Biochemistry, 15, 2555 (1976).

36. L. Scott, J. Magn. Reson., in press (1977).

37. P.S. Flory, in "Statistical Mechanics of Chain Molecules", Interscience Publishers, 1969, p. 13.

38. B.G. McFarland and H.M. McConnell, Proc. Nat. Acad. Sci. (U.S.), 68, 1274 (1971).

39. G.B. Birrell and O.H. Griffith, Arch. Biochem. Biophys., 172, 455 (1976).

40. J. Seelig and W. Niederberger, J. Am. Chem. Soc., 96, 2069 (1974).

41. B.J. Gaffney and H.M. McConnell, J. Magn. Reson., 16, 1 (1974).

42. A.C. McLaughlin, F.Podo and J.K. Blaise, Biochim. Biophys. Acta, 330, 109 (1973).

43. A.G. Lee, N.J.M. Birdsall and J.C. Metcalfe, Chem. Britt., 9, 116 (1973).

44. A.G. Lee, N.J.M. Birdsall and J.C. Metcalfe, in "Methods in Membrane Biology", E.D. Korn, ed., Vol. 2, Plenum Press, 1974.

45. P.A. Kroon, M. Kainosho and S.I. Chan, Biochim. Biophys. Acta, 433, 282 (1976).

46. P.S. Hagan, N.O. Petersen and S.I. Chan, J. Magn. Reson., submitted for publication (1977).

47. R. Kubo and K. Tomita, J. Phys. Soc. Japan, 9, 888 (1954).

48. P.S. Hagan, N.O. Petersen and S.I. Chan, J. Magn. Reson., in preparation (1977).

49. M. Bloom, in preparation (1977).

50. M. Bloom, J. Magn. Reson., in press (1977).

51. M. Bloom, VIIth International Conference on Magnetic Resonance in

Biological Systems, St. Jovite, Canada (1976).

52. M. Bloom, E.E. Burnell, M.I. Valic and G. Weeks, Chem. Phys. Lipids, 14, 107 (1975).

53. D. Lichtenberg, N.O. Petersen, J.L. Girardet, M. Kainosho, P.A. Kroon, C.H.A. Seiter, G.W. Feigenson and S.I. Chan, Biochim. Biophys. Acta, 382, 10 (1975).

54. A.F. Horwitz, D. Michaelson and M.P. Klein, Biochim. Biophys. Acta, 298, 1 (1975).

55. M. Bloom, personal communication (1976).

56. M. Edidin, Annu. Rev. Biophys. Bioengineer., 3, 179 (1974).

57. P.R. Cullis, FEBS Letters, 70, 223 (1976).

58. H. Träuble, J. Membr. Biol., 4, 193 (1971).

59. R. Kimmich and A. Peters, J. Magn. Reson., 19, 144 (1975).

60. J.L. Girardet and S.I. Chan, unpublished results (1974).

61. P.E. Godici and F.R. Landsberger, Biochemistry, 14, 3927 (1975).

62. P.K.L. Yu, N.O. Petersen and S.I. Chan, unpublished results (1976).

63. M. Kainosho, P.A. Kroon, R. Lawaczeck, N.O. Petersen and S.I. Chan, Chem. Phys. Lipids, submitted for publication (1977).

64. R. Mendelsohn, S. Sunder and H.J. Bernstein, Biochim. Biophys. Acta, 419, 563 (1976).

65. B.P. Gaber and W.L. Peticolas, Biochim. Biophys. Acta, submitted for publication (1976).

66. P. Papahadjopoulos, K. Jacobson, S. Nir and T. Isac, Biochim. Biophys. Acta, 323, 659 (1973).

67. R. Lawaczeck, M. Kainosho and S.I. Chan, Biochim. Biophys. Acta, 443, 313 (1976).

68. Y.K. Lee and S.I. Chan, Biochemistry, 16, 1303 (1977).

69. P. Jost, O.H. Griffith, R.A. Capaldi and G. Vanderkooi, Biochim. Biophys. Acta, 311, 141 (1973).

IV. STUDIES OF THE EFFECTS OF LIPID COMPOSITION IN MIXTURES OF LIPIDS ON THE THERMAL TRANSITIONS OF THE BILAYER SYSTEM. DETERMINATION OF PHASE DIAGRAMS FOR MULTICOMPONENT SYSTEMS.

1. Introduction

It has been known for some time that phospholipid-water mixtures exhibit complex phase diagrams (1,2). At low hydration levels (less than 25% water by weight) there is evidence for cubic, hexagonal, lamellar and isotropic phases, depending on the temperature and water content (2) (Figure 16). In well-hydrated preparations ($\sim$ 25% water by weight) the lipids exist in a lamellar phase at most temperatures. It is the fully hydrated lamellar phase in equilibrium with excess water ($\sim$ 40% by weight) which is of interest biologically, and which is found (1,2,3) to exhibit several lyotropic mesophases depending on temperature. At low temperatures, the phospholipids are in a semi-crystalline lamellar phase with very little motion of the hydrocarbon chains. At higher temperatures the systems exhibit a thermally induced endothermic order-disorder transition into a liquid crystalline lamellar phase, termed the Chapman transition (4). In addition to the Chapman transition, phosphatidylcholines (lecithins) undergo a pretransition a few degrees below the Chapman transition temperature (T_c) (1,5). There have been several proposals for the nature of the three phases in lecithins. The low temperature phase is an $L_{\beta'}$ phase [1] with the hydrocar-

[1] The nomenclature adopted to describe the lyotropic mesomorphism is that of Luzzati and coworkers (2). Here the capital letter refers to the geometry of the phase; L: 2-dimensional lamellar, P: 3-dimensional lamellar, H: Hexagonal, C: cubic. The Greek subscript refers to the state of the hydrocarbon chain in the phase; α: motionally disordered, β: extended chains normal to the bilayer surface, β': extended chains oriented at an angle relative to the bilayer normal (Figure 16).

FIGURE 16

Schematic representation of some of the phases formed by mixtures of phospholipids and water. The nomenclature is that of Luzzati and coworkers (2) (see also the footnote on the preceeding page).

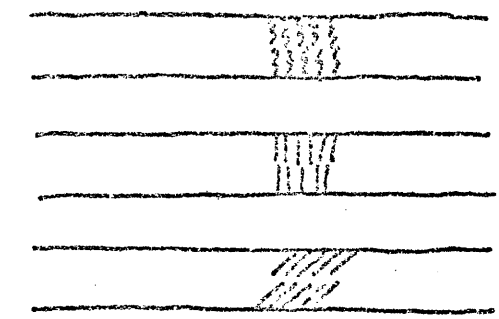

L_α

L_β

$L_{\beta'}$

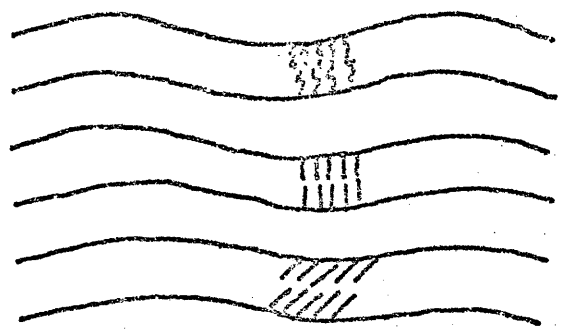

P_α

P_β

$P_{\beta'}$

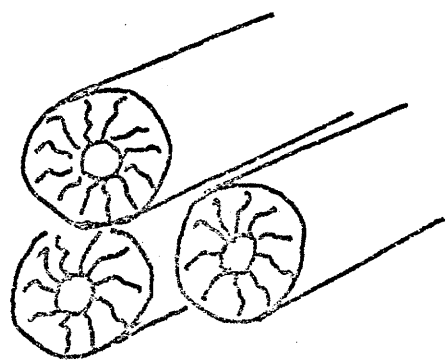

H

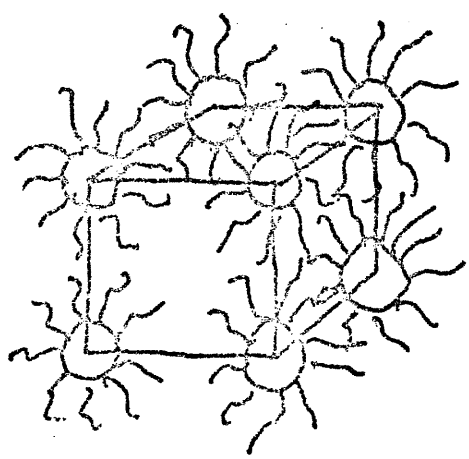

C

bon chains rotationally disordered and at a 30^{o} angle relative to the bilayer normal. The liquid crystalline phase at high temperatures is an L_{α} phase, to which the motional model presented in Chapter III pertains. Rand et al (6) have suggested that the pretransition at T_p is between an $L_{\beta'}$ and an L_{β} phase. However, Janiak et al (7) interpreted the x-ray data in terms of a transition from the $L_{\beta'}$ to a $P_{\beta'}$ phase. The latter interpretation of the x-ray data is supported by Freeze-Etch Electron Microscopy (8) where ripples are observed when samples are rapidly frozen from a temperature intermediate between T_p and T_c.

Thermal transitions in the fully hydrated lamellar system have been studied carefully since the phase behavior reflects the intermolecular interactions. Mathematical models for phase transitions are better understood in two than in three dimensions, so studies of thermal transitions in mono- and bilayer systems may lead to improvements in the modeling (9). Several statistical mechanical models have been proposed to account for the thermal transition at T_c (10,11,12, 13). The most successful of these to date is that of Marčelja (13) which is based on a self-consistent mean field theory (14) using an intermolecular potential proportional to $(3\cos^2\eta - 1)$. (The angle η is between the long axes of two lipid chains). This theory is capable of predicting the transition temperature and the order parameter profile for the hydrocarbon chain. However, it seems necessary to include short range (hard sphere) interactions in this model since Monte Carlo calculations (15) demonstrate that the order parameter profile is very sensitive to packing density. None of these models, however, take into account the effect of a change in chain orientation during a transition

from a β' to an α phase.

Thermal phase transitions have been observed at physiologically relevant temperatures for several natural membranes, particularly in cholesterol-free lipid extracts (16,17,18,19, 20). It is important to establish whether such transitions are important in vivo and to understand how they occur, since changes in the motional state of the lipids would alter the function or activity of the membrane as a whole. Although an abrupt transition could be detrimental, a gradual transition might serve to modulate membrane function or activity. In vivo, control of lipid mobility is achieved by varying the membrane composition rather than the temperature. The thermal transition temperature for bilayers prepared from M. Ladlawii lipid extracts depends on the medium on which the organism is grown. This adaptive feature suggests that as the lipid composition is changed, membrane fluidity is altered. It is, therefore, important to elucidate the motional states of lipids in mixed lipid systems.

To gain some insight into molecular interactions in mixed lipid systems we have chosen to study in detail their phase diagrams. Much of the data will only be interpreted qualitatively but allows us to interpret the motional state of mixtures of phospholipids and cholesterol.

First, as an introduction to the techniques, we present transition data for some binary phospholipid-water systems followed by a series of ternary phospholipid "A"-phospholipid "B"-water systems as well as the quaternary system of DML, DPL, DSL, and H_2O. All experiments were performed in excess water, most at about 50% by weight water.

Thus, all the phases illustrated in the diagrams are in equilibrium with free water as a phase, which is often excluded for simplicity. Finally, we show results for some annealing experiments (21,22) on phospholipid-cholesterol mixtures which lead us to propose a new phospholipid-cholesterol phase diagram.

2. Results

a. Binary phospholipid-water systems.

A convenient technique for studying thermal transitions in hydrated phospholipid multilayers is Differential Thermal Analysis (DTA). In these measurements the temperature difference between the sample and a reference is monitored as a function of the reference temperature. The reference sample, in these experiments either water or a 1:1 ethylene glycol-water mixture, is chosen to match the heat capacity of the sample as closely as possible and should have no thermal transitions in the interesting temperature range. When the sample undergoes an endothermic thermal transition, its temperature remains constant while the reference temperature continually changes. The temperature differential increases in magnitude during an enthalpic transition for which it is defined to be negative. Figure 17 illustrates the thermal phase transitions for four saturated lecithins (DLL, DML, DPL and DSL). The smaller pretransition is clearly seen in all cases but for the DLL. All samples containing DLL were prepared in a 1:1 (v/v) mixture of H_2O and ethylene glycol to supress the ice-water transition DTA thermograms of DPL, DML and DSL in this solvent are indistinguishable from those in neat water, but the absence of the pretransition in DLL could be a

FIGURE 17

Traces of DTA heating curves for the four common lecithins in excess water. The sample with DLL also contained ethylene glycol (50% by volume) to supress the free water transition. All the transitions are endothermic.

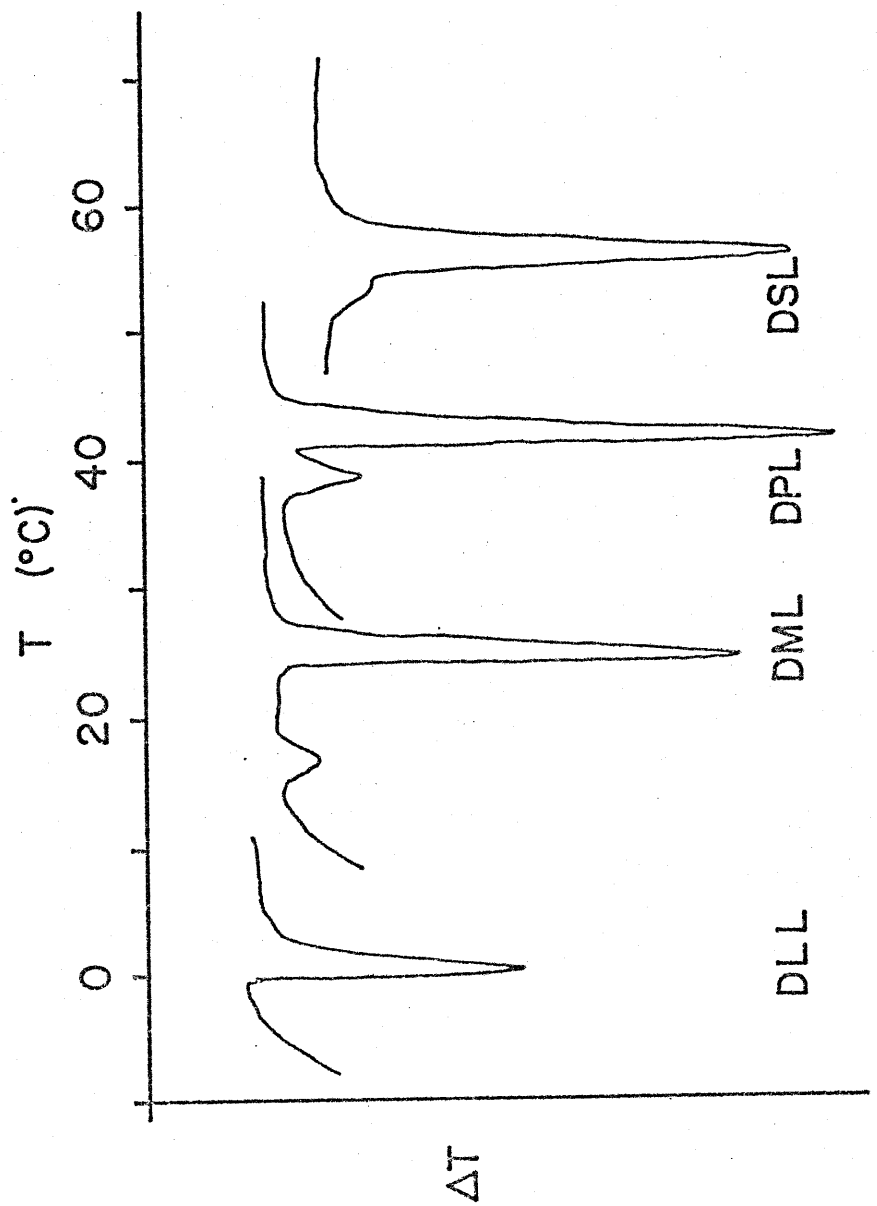
T (°C)
0
20
40
60
ΔT
DLL
DML
DPL
DSL

result of the ethylene glycol.

Although DTA is not as sensitive as Differential Scanning Calorimetry (DSC) it is much more convenient, particularly for measuring a large number of samples, and shows good correspondence with DSC (1). The transition data obtained from Figure 17 are listed in Table 3.

Observations by Vaughan and Keough (23) that the pretransition only occurs for lecithins suggest that structure of the headgroup influences this transition. The DTA results of Figure 18 suggest that the stereochemistry of the headgroup (D, L, or DL) is not important, whereas the configuration is, as seen for the symmetric lipid, β-DPL, for which both T_p and T_c are much lower. Similarly, when the fatty acid chains are perdeuterated, both transition temperatures are lowered by about 4-5°C as seen in Figure 19 for DPL-d_{62} and DSL-d_{70} (24). The transition data for these lipids are all included in Table 3.

DTA measurements require only small sample volumes which must be quite concentrated so the technique is not suitable for measuring thermal transitions in vesicles. It is possible to obtain thermograms of 2% weight/volume lipid to water suspensions (Figure 20) but these are so concentrated that the results may not reflect the properties of small bilayer vesicles. Nonetheless, a broadening of the main transition, concomittant with a decrease in the pretransition intensity, seems to take place. Note, however, that the position of the peak of the transition has not changed significantly.

A more sensitive technique for studying the transition behavior of vesicles at low concentrations is found through absorbance measurements. This is illustrated in Figure 21 for a 2% solution of vesicles

TABLE 3

Transition Temperatures (T_c) and Pretransition Temperatures (T_p) for a Series of Lecithins

Lipid	T_p (°C)			T_c (°C)		
	Onset	Peak	End	Onset	Peak	End
L-α-DLL[1]	-	-	-	-1	0	3
L-α-DML	14	17	18	22	23	25
L-α-DPL	36	37	39	42	43	45
L-α-DSL	52	54	-	55	56	58
D-α-DPL	36	39	-	42	43	45
DL-α-DPL	36	38	39	42	43	45
β-DPL	20	23	25	36	37	39
L-α-DPL-d_{62}	32	34	36	36	37	39
L-α-DSL-d_{70}	48	-	-	49	50	53

[1]Measured in the presence of ethylene glycol, added to suppress the ice-water transition.

FIGURE 18

Traces of DTA heating curves for DL-α-DPL, D-α-DPL and β-DPL in excess water. All the transitions are endothermic.

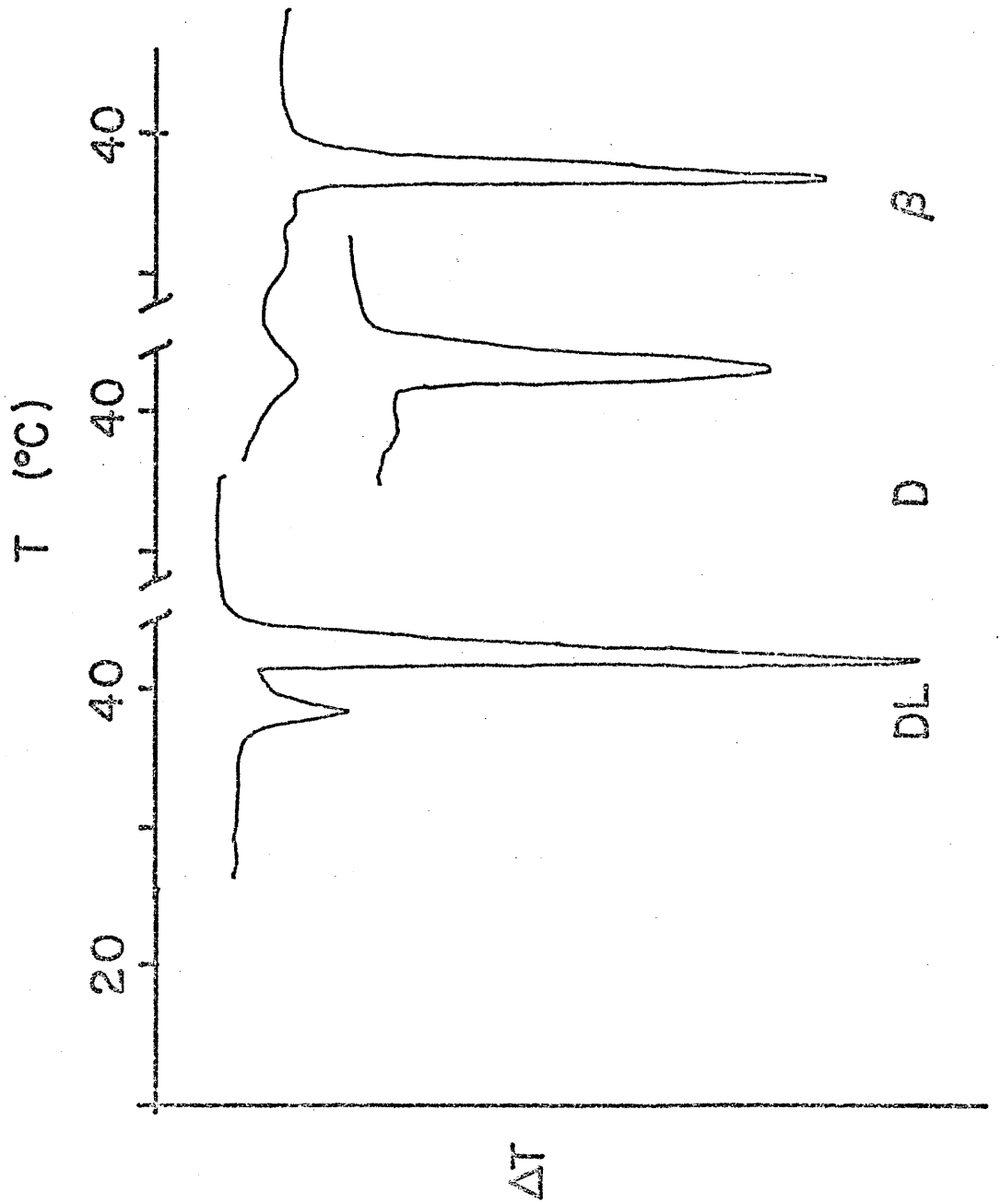
T (°C)
40
40
40
20
ΔT
DL
D
B

FIGURE 19

Traces of DTA heating curves for a: L-α-DPL, b: L-α-DPL-d_{62}, c: L-α-DSL and d: L-α-DSL-d_{70} in excess water. All the transitions are endothermic. The arrows indicate the peak of pretransition in each trace (24).

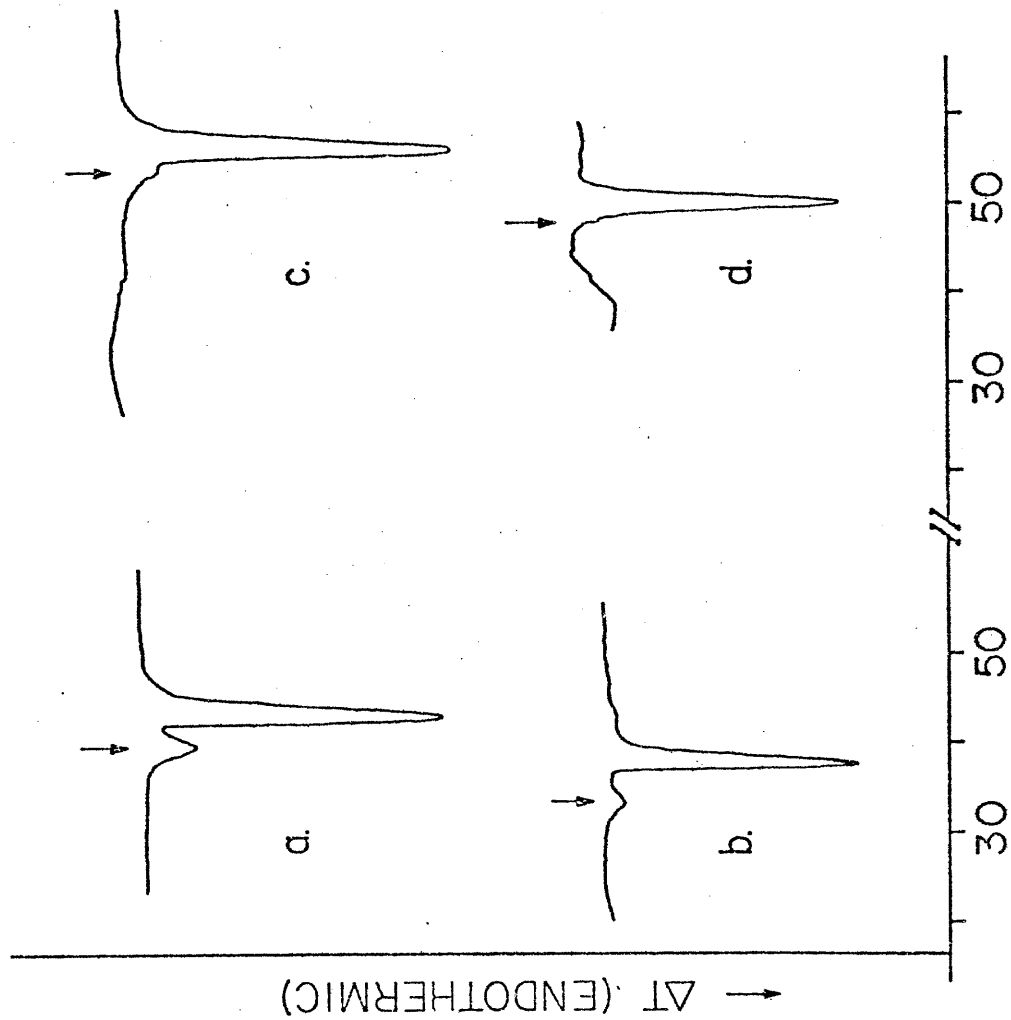

Fig 3

FIGURE 20

Trace of a DTA heating curve for 20% weight/volume DPL in water. The sample was sonicated 15 min. The transition(s) is endothermic.

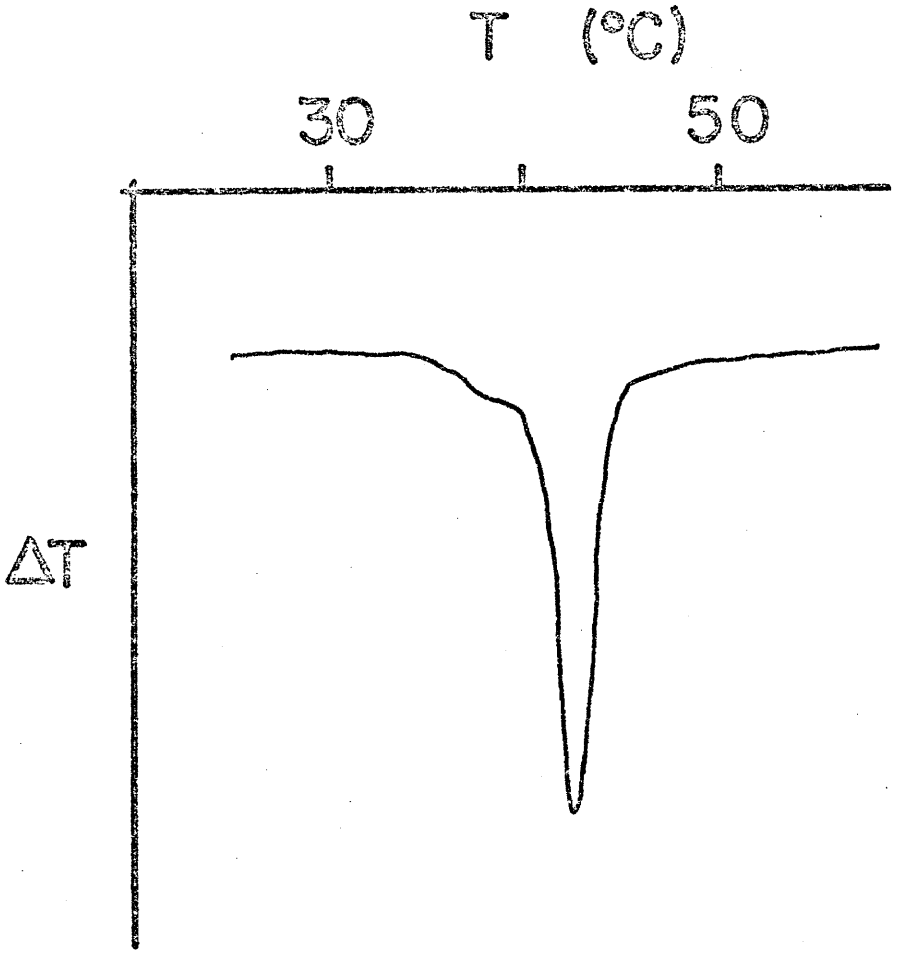
T (°C)
30
50
ΔT

FIGURE 21

Temperature dependence of the optical density for 2% by weight, sonicated vesicle suspensions. x for L-α-DPL, o for L-α-DPL-d_{62}.

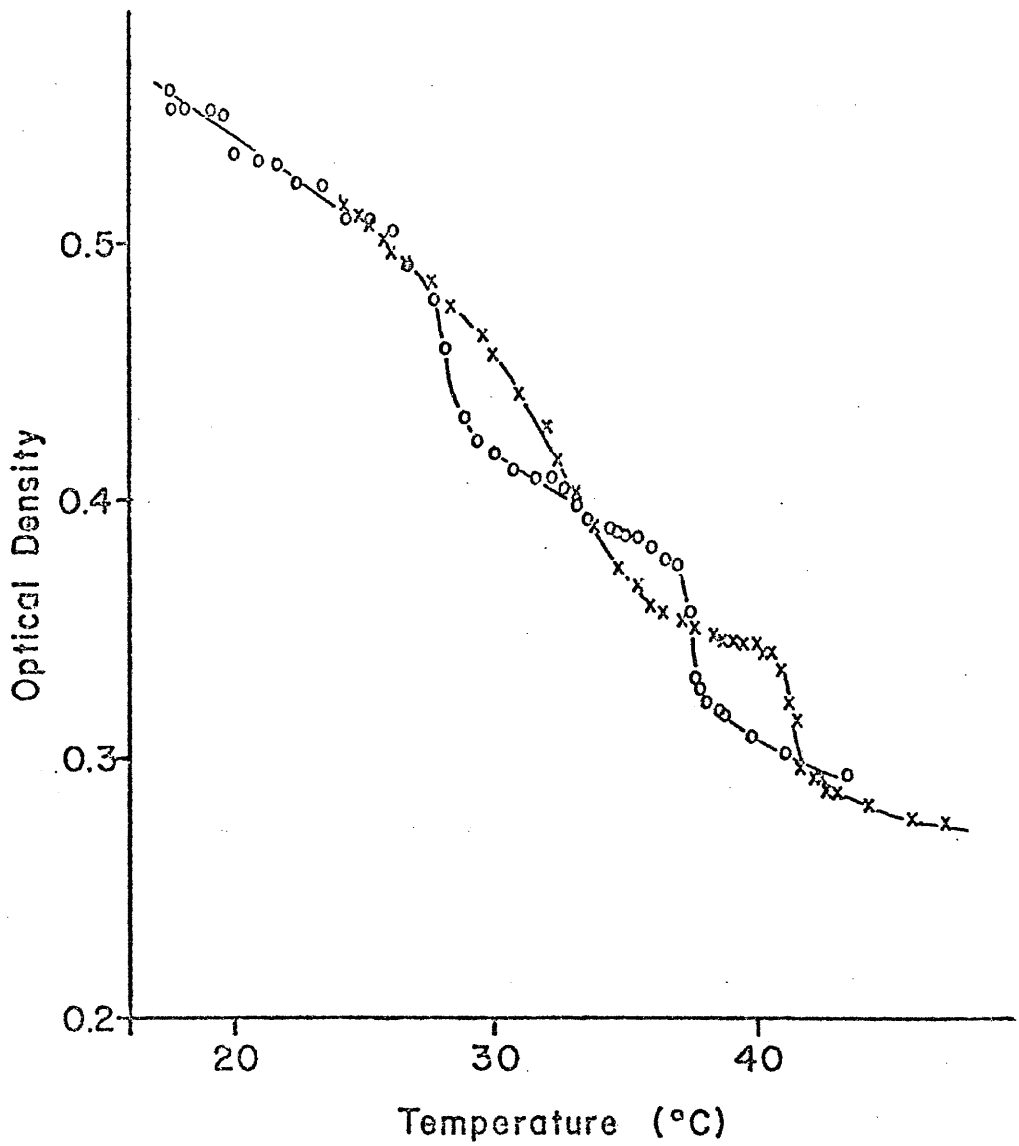

Fig. 2

prepared from DPL and from DPL-d_{62}. The causes of the absorbance changes are the subject matter of Chapter V. Note that there are in fact indications for the presence of a pretransition in the vesicle system.

b. Mixtures of phospholipids.

DTA measurements may provide information about the progress of the transition with change in temperature. This is particularly true for mixtures of lipids where the width of the transition is a measure of how ideally the solutions behave (25). In pure lipid systems, the transition width is in part determined by experimental factors such as heating rate, but in mixed lipid systems these effects are usually negligible.

To illustrate the types of differential thermograms obtained, we show in Figure 22 the four DTA measurements on equimolar mixtures of DSL with (a) DSL-d_{70}, (b) DPL, (c) DML and (d) DLL. For mixtures (a) and (b), the transitions are symmetrical, with a single peak occurring at temperatures half way between the melting temperatures of the pure components. For the (c) and (d) mixtures, however, there are two broadened transitions, which have been termed biphasic or montectic transitions (4,26,27,28). They are believed to reflect incomplete mixing of the components in the gel phase.

In order to summarize the data on the many mixtures studied, we have chosen to present them in experimental phase diagrams, in which we plot the onset, peak and end temperatures, as illustrated in Figure 22 by the arrows. For the fairly broad transitions observed in most of the mixtures, the onset of the transition upon cooling coincided with

FIGURE 22

Traces of DTA heating curves for four equimolar mixtures of DSL with a: DSL-d_{70}, b: DPL, c: DML and d: DLL. All transitions are endothermic. The arrows indicate the onset, peak and end of the transition for the DSL-DPL mixture.

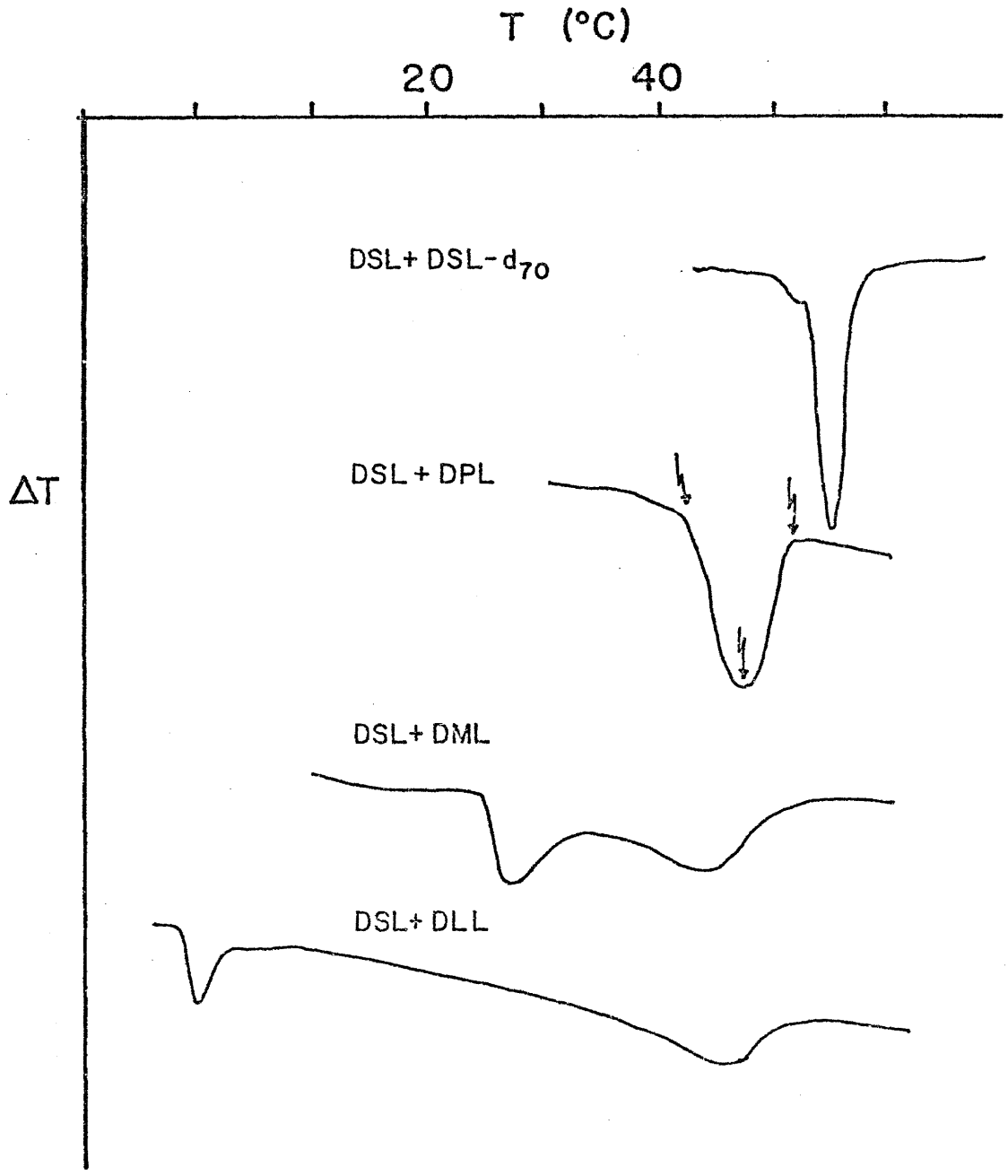
T (°C)
20
40
ΔT
DSL+ DSL-d_{70}
DSL + DPL
DSL+ DML
DSL+ DLL

the end of the transition upon heating within about 1-2°C. All the data presented are from heating curves.

Experimental phase diagrams for mixtures of DPL and DSL with their perdeutero acyl analogs, DPL-d_{62} and DSL-d_{70} respectively, are shown in Figure 23. The data (24) show only a slightly broader transition for the mixtures than for the pure components. At all compositions studied, there is evidence for a pretransition.

Phase diagrams for lecithin mixtures depend on the difference in acyl chain length as well as the difference between the transition temperatures of the pure components. DSL and DPL whose chains differ by two methylene groups have transition temperatures 12°C apart. Mixtures of these lipids exhibit single, but broadened, transitions and the pretransition is seen for all compositions (Figure 24). A similar phase diagram is observed for DPL and DML mixtures (Figure 25). If the difference in transition temperatures of the pure lipid constituents is increased further, as for DLL and DML, the single transition is only observed for a limited range of compositions with large amounts of DML (Figure 26). With excess DLL, biphasic transitions are observed. Also the pretransition is only observed at high DML concentrations.

If the difference in chain length between the lipid constituents is increased to four methylenes, as with DML-DSL mixtures (Figure 27) and DLL-DPL mixtures (Figure 28) there are extended composition ranges where biphasic melting is observed. At large concentrations of either constituent the transitions appear broad but with a single asymmetric peak. In the case of the DML-DSL mixtures, the pretransition is observed only at high DML concentrations. For the mixture of DLL and

FIGURE 23

Experimental phase diagram for DPL with DPL-d_{62} and DSL with DSL-d_{70} (24) in excess water.

o peak of the main transition

x peak of the pretransition

- onset and end of the main transition

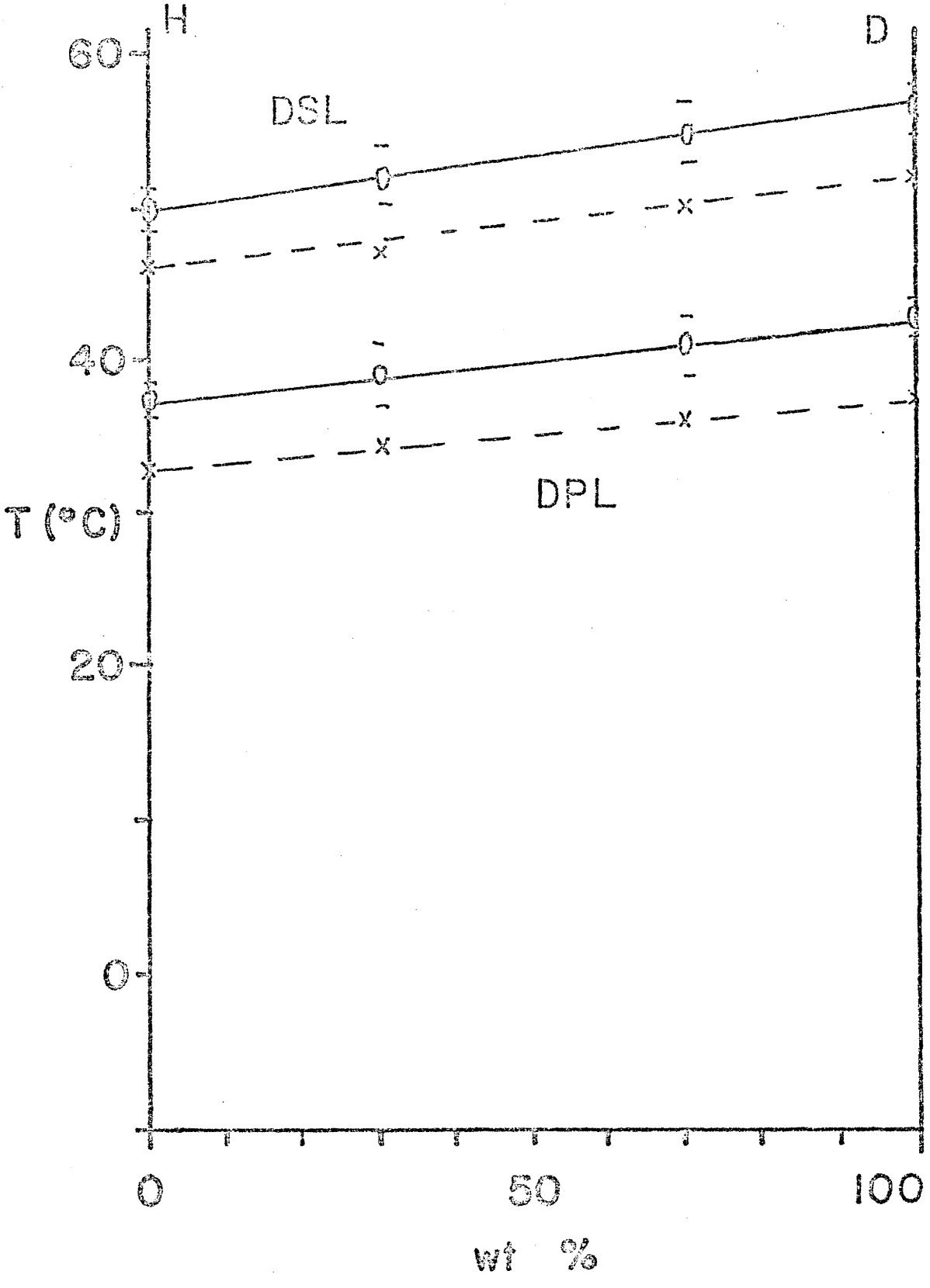
H
D
60
40
20
0
DSL
DPL
T (°C)
0
50
100
wt %

FIGURE 24

Experimental phase diagram for DPL with DSL in excess water.

o peak of the main transition

x peak of the pretransition

- onset and end of the main transition

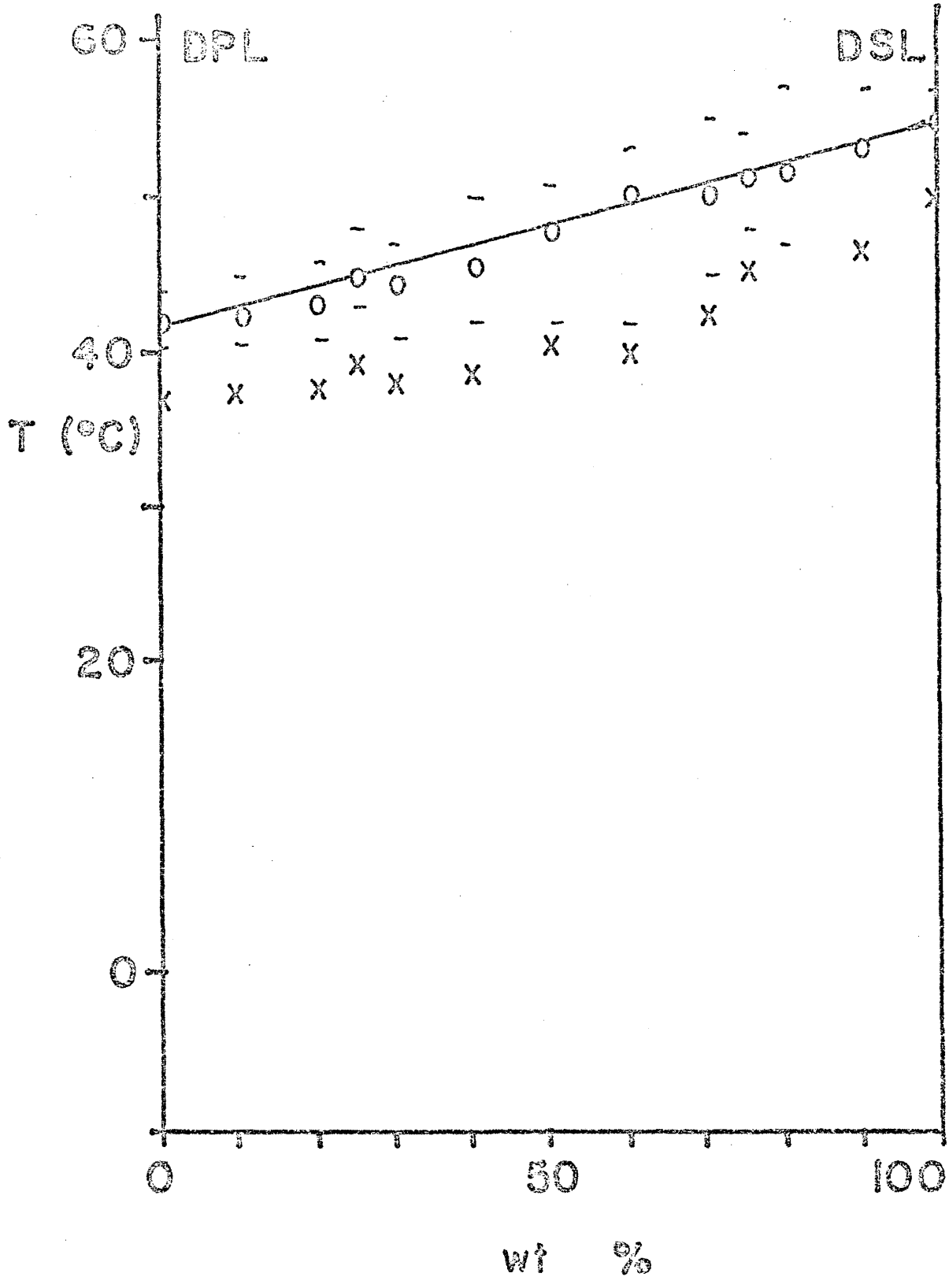
60
40
20
0
T (°C)
DPL
DSL
0
50
100
wt %

FIGURE 25

Experimental phase diagram for DML with DPL in excess water.

o peak of the main transition

x peak of the pretransition

- onset and end of the main transition

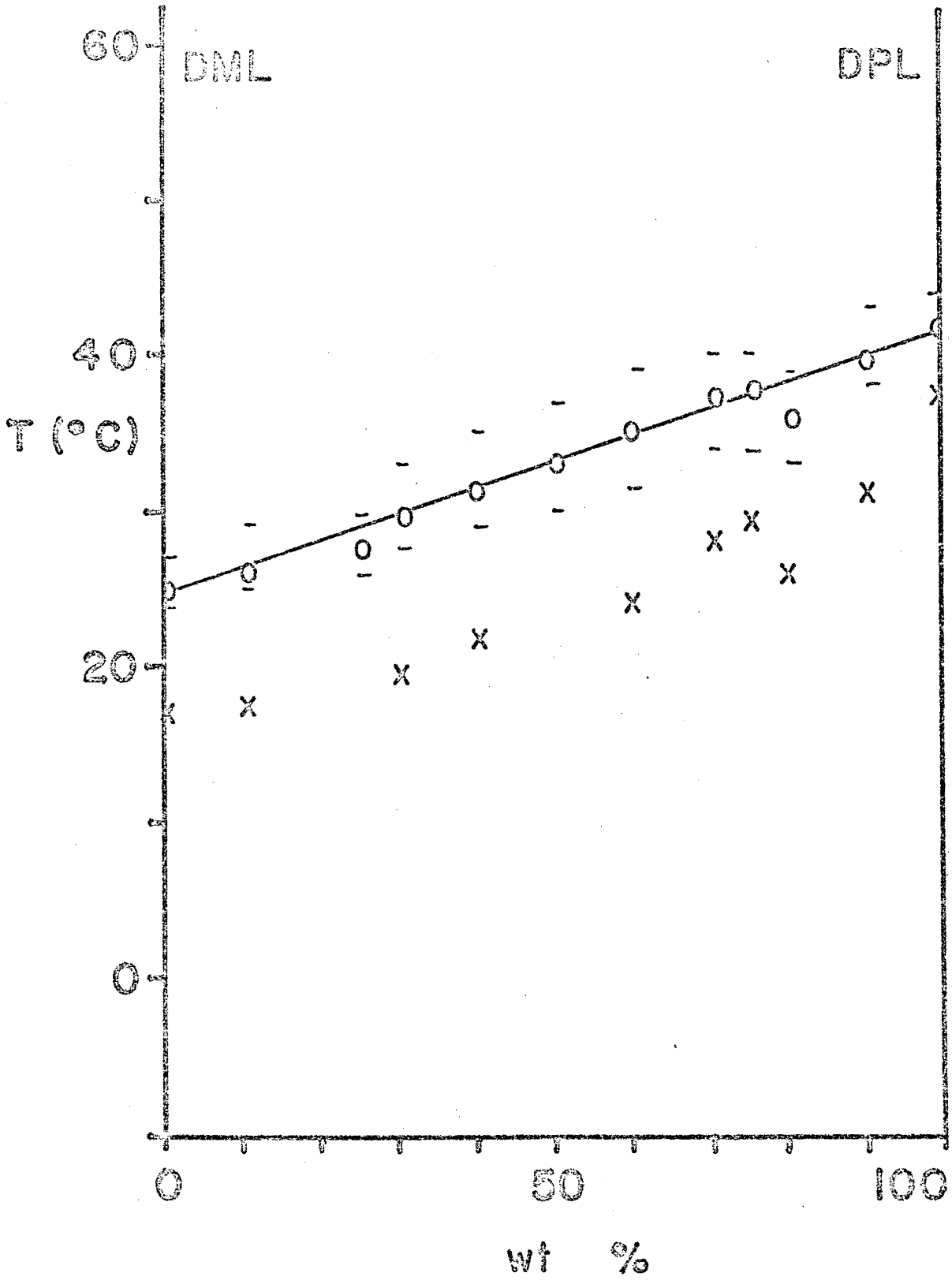
60
40
20
0
DML
DPL
T (°C)
0
50
100
wt %

FIGURE 26

Experimental phase diagram for DLL with DML in excess water.

o peak of the main transition

x peak of the pretransition

- onset and end of the transitions

All samples contained ethylene glycol in the water.

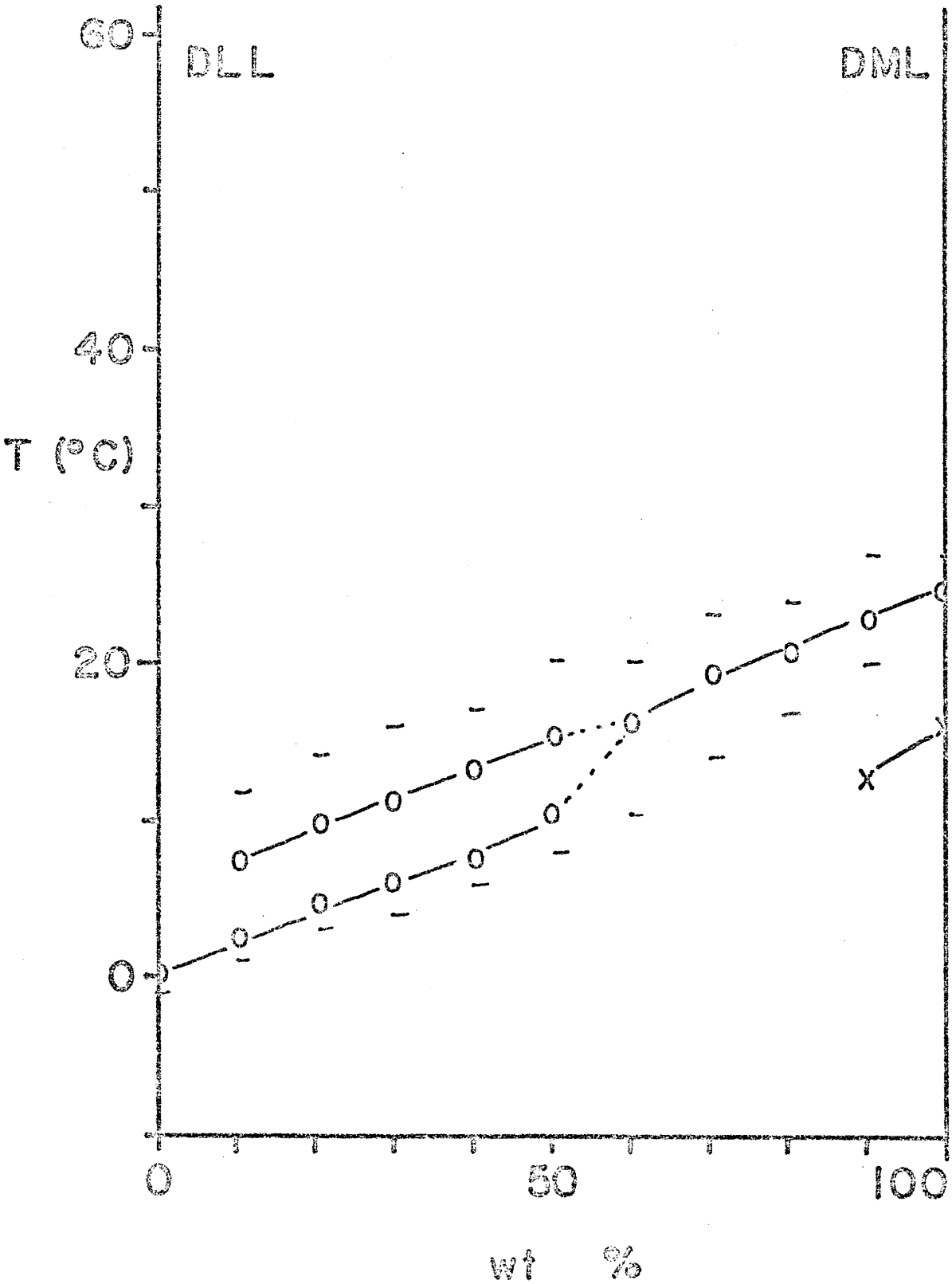
60
40
20
0
T (°C)
DLL
DML
0
50
100
wt %

FIGURE 27

Experimental phase diagram for DML with DSL in excess water.

o peak of the main transitions

x peak of the pretransition

- onset and end of the main transitions

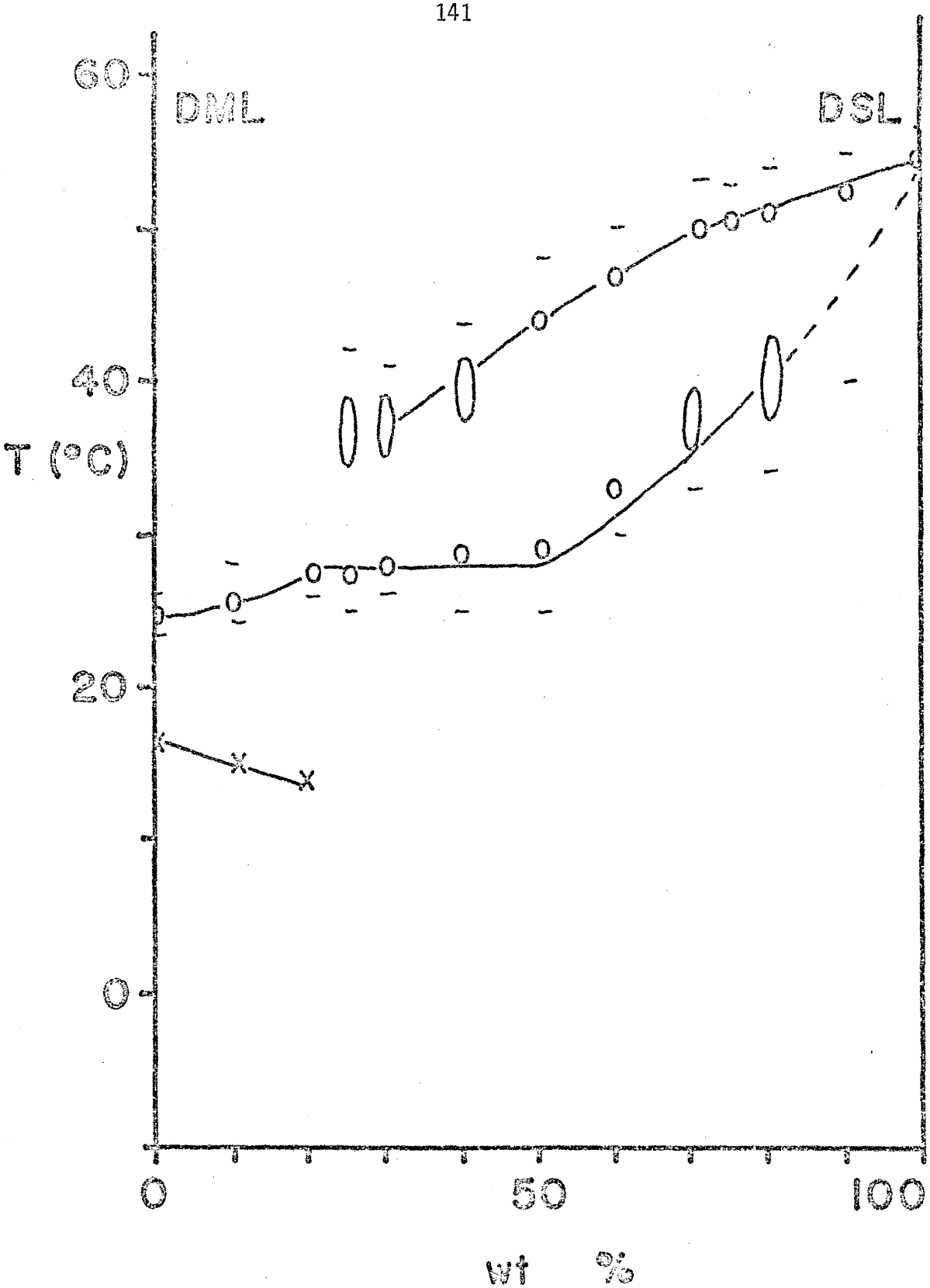
60
40
20
0
T (°C)
DML
DSL
0
50
100
wt %

FIGURE 28

Experimental phase diagram for DLL with DPL in excess water.

o peak of the main transitions

- onset and end of the main transitions

All samples contained ethylene glycol in the water.

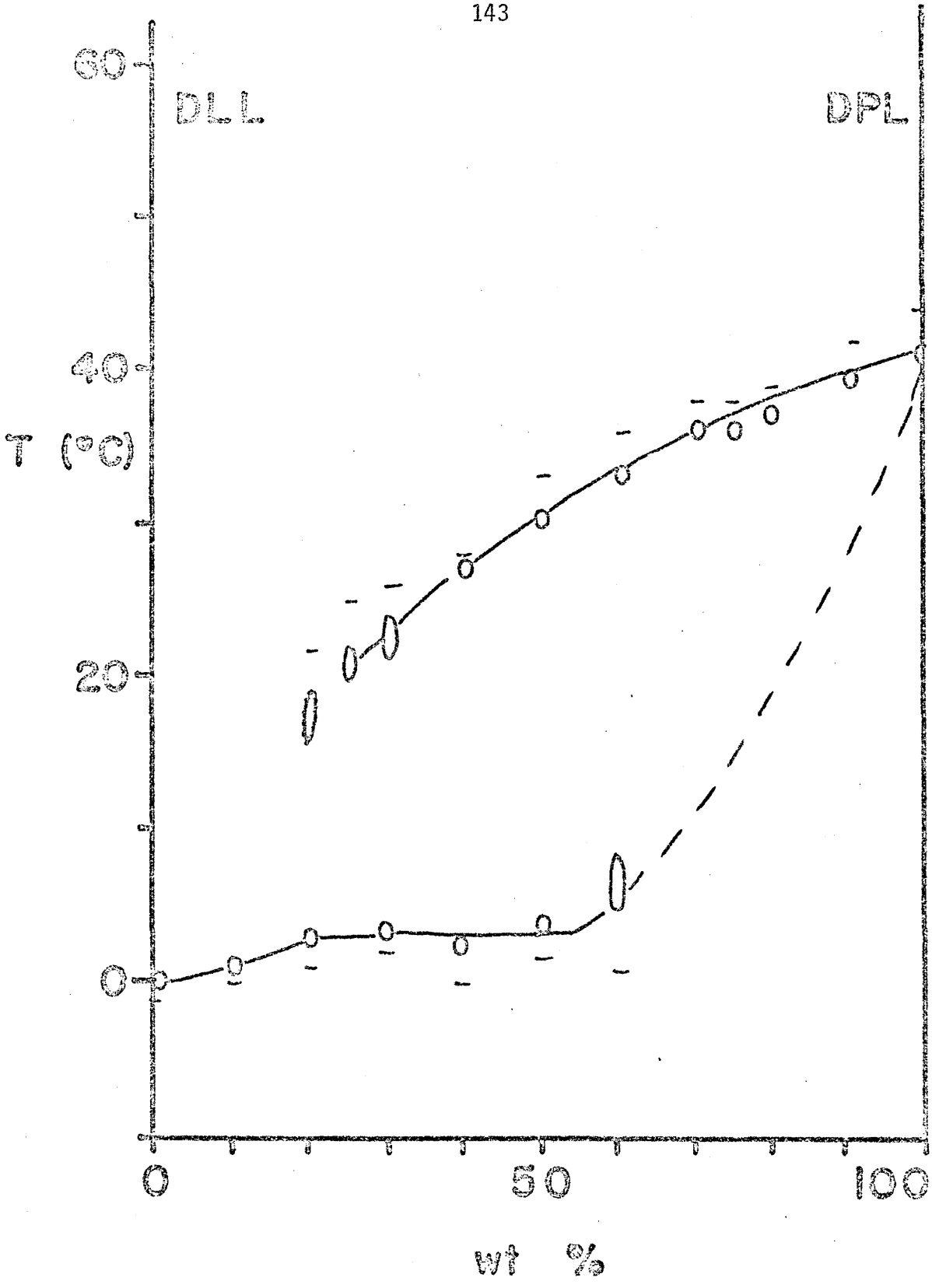
60
40
20
0
T (°C)
DLL
DPL
0
50
100
wt %

DSL there is evidence for biphasic transitions at all compositions (Figure 29).

The effect on the transition of an equimolar mixture of two phospholipids when adding the third phospholipid is shown for the quaternary system: DML-DPL-DSL-H_2O in Figures 30,31 and 32. There are certain composition ranges for which biphasic transitions are detected, and others for which the pretransition exists. These data, along with those of Figures 24,25 and 27 can be used to construct part of the quaternary phase diagram, which will be presented in a subsequent section.

c. Phospholipid-cholesterol mixtures.

Numerous techniques have been employed in an attempt to elucidate the nature of phospholipid-cholesterol interactions (4,28,29,30, 31, 32,33), through which part of the phase diagram has been obtained. Molecular interpretation of some phases are still in doubt, so we have sought evidence for a phase boundary by measuring the temperature at which annealing takes place.

The annealing process in small sonicated vesicles was characterized in detail by Lawaczeck et al (21) for pure lipid systems and a few well-behaved mixed systems (21,22). They found that vesicles prepared and kept at temperatures lower than the thermal transition temperature were fully permeable to ionic species. However, even a relatively short exposure to temperatures above the thermal transition abolished this permeability completely. The interpretation of these results is that crystal defects present in the gel structure are annealed out as the bilayer melts to the liquid crystalline phase. In these studies

FIGURE 29

Experimental phase diagrams for DLL with DSL in excess water.

o peak of the main transitions

- onset and end of the main transitions

All samples contained ethylene glycol in the water.

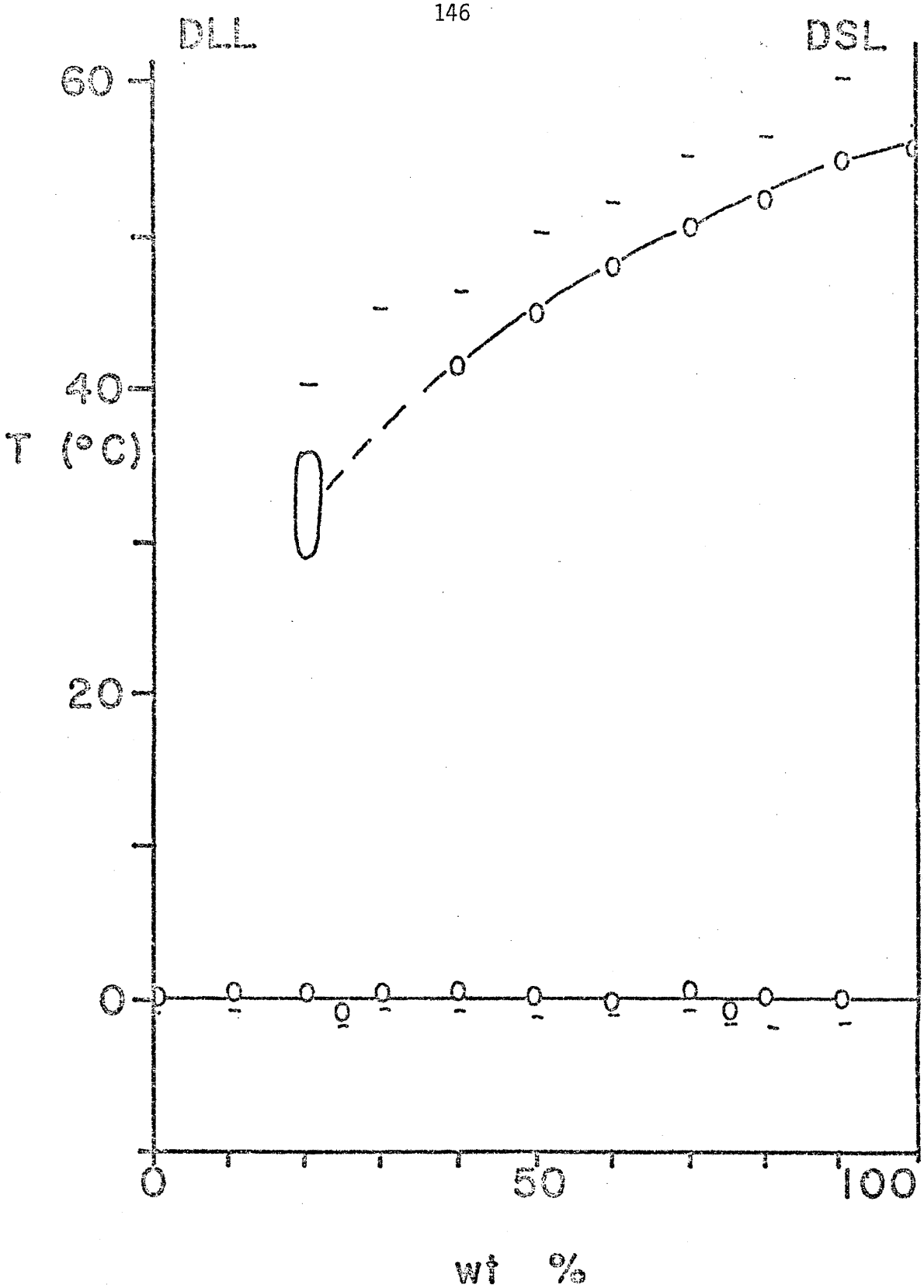
DLL
DSL
60
40
20
0
T (°C)
0
50
100
wt %

FIGURE 30

Experimental phase diagram for an equimolar mixture of DML and DSL with DPL in excess water.

o peak of the main transitions

x peak of the pretransition

- onset and end of the main transitions

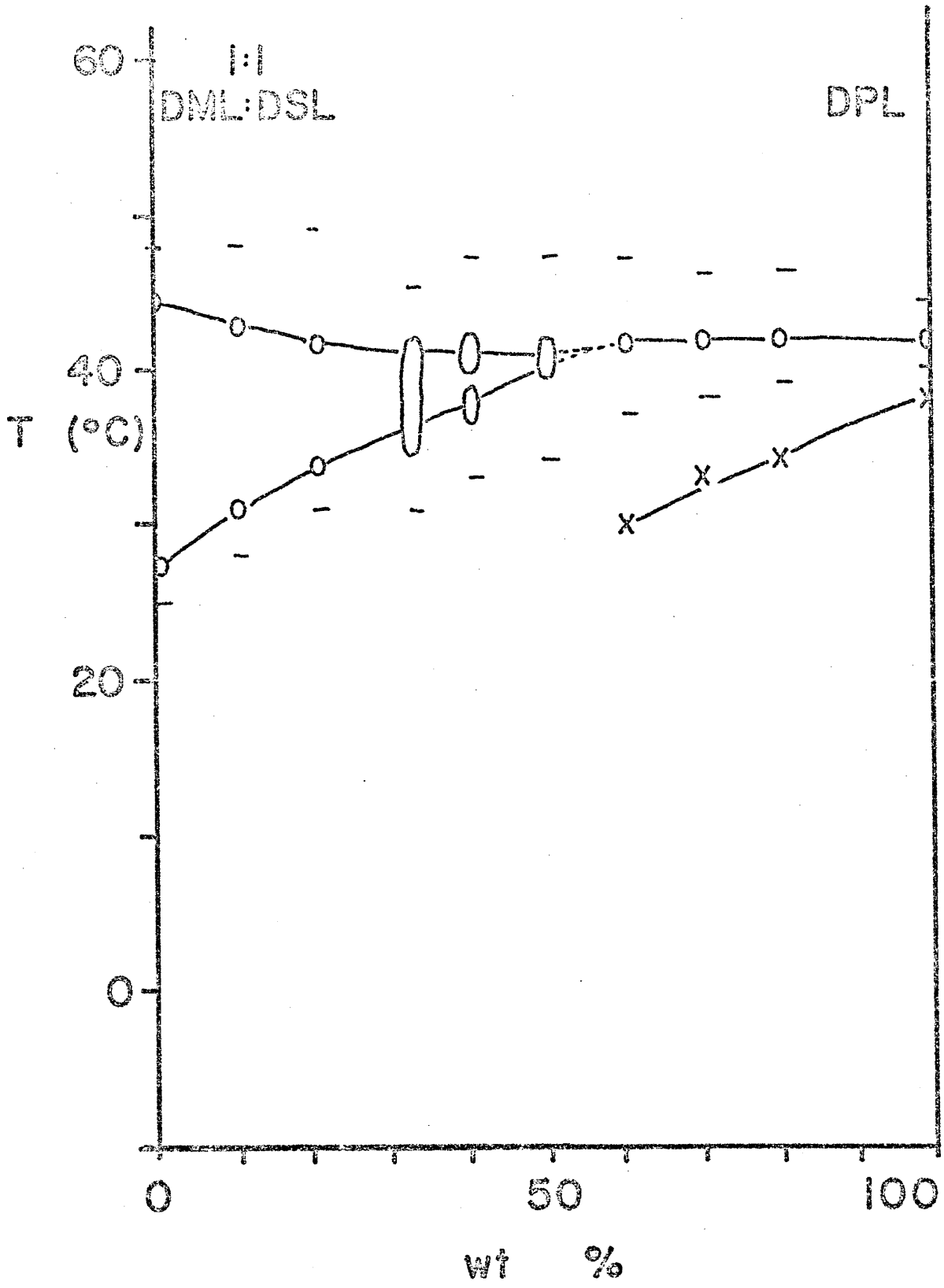
60
40
20
0
T (°C)
1:1
DML:DSL
DPL
0
50
100
Wt %

FIGURE 31

Experimental phase diagram for an equimolar mixture of DPL and DSL with DML in excess water.

o peak of the main transitions

x peak of the pretransition

- onset and end of the main transitions

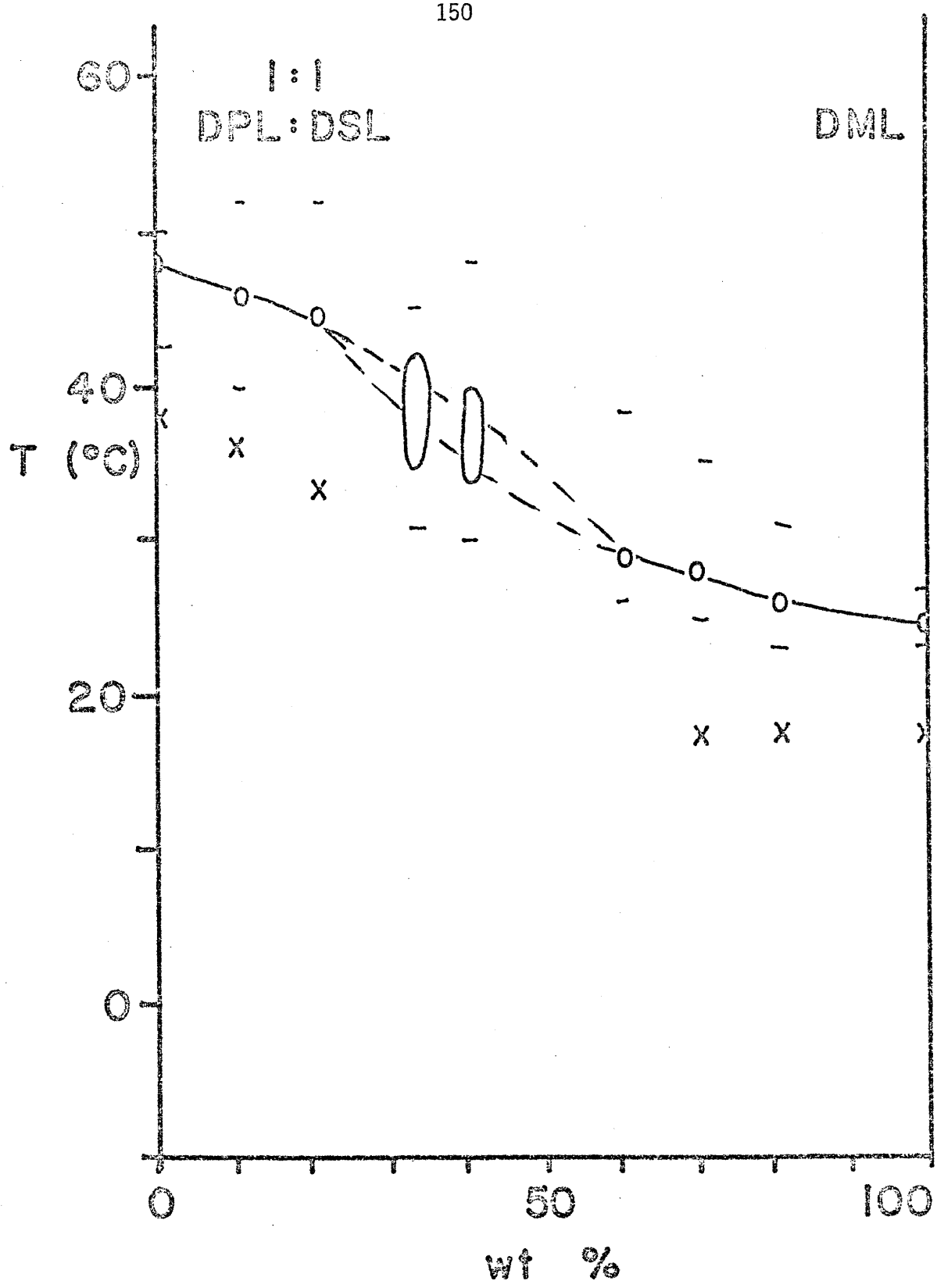
1:1
DPL:DSL
DML
60
40
20
0
T (°C)
0
50
100
wt %

FIGURE 32

Experimental phase diagram for an equimolar mixture of DML and DPL with DSL in excess water.

o peak of the main transitions

x peak of the pretransitions

- onset and end of the main transitions

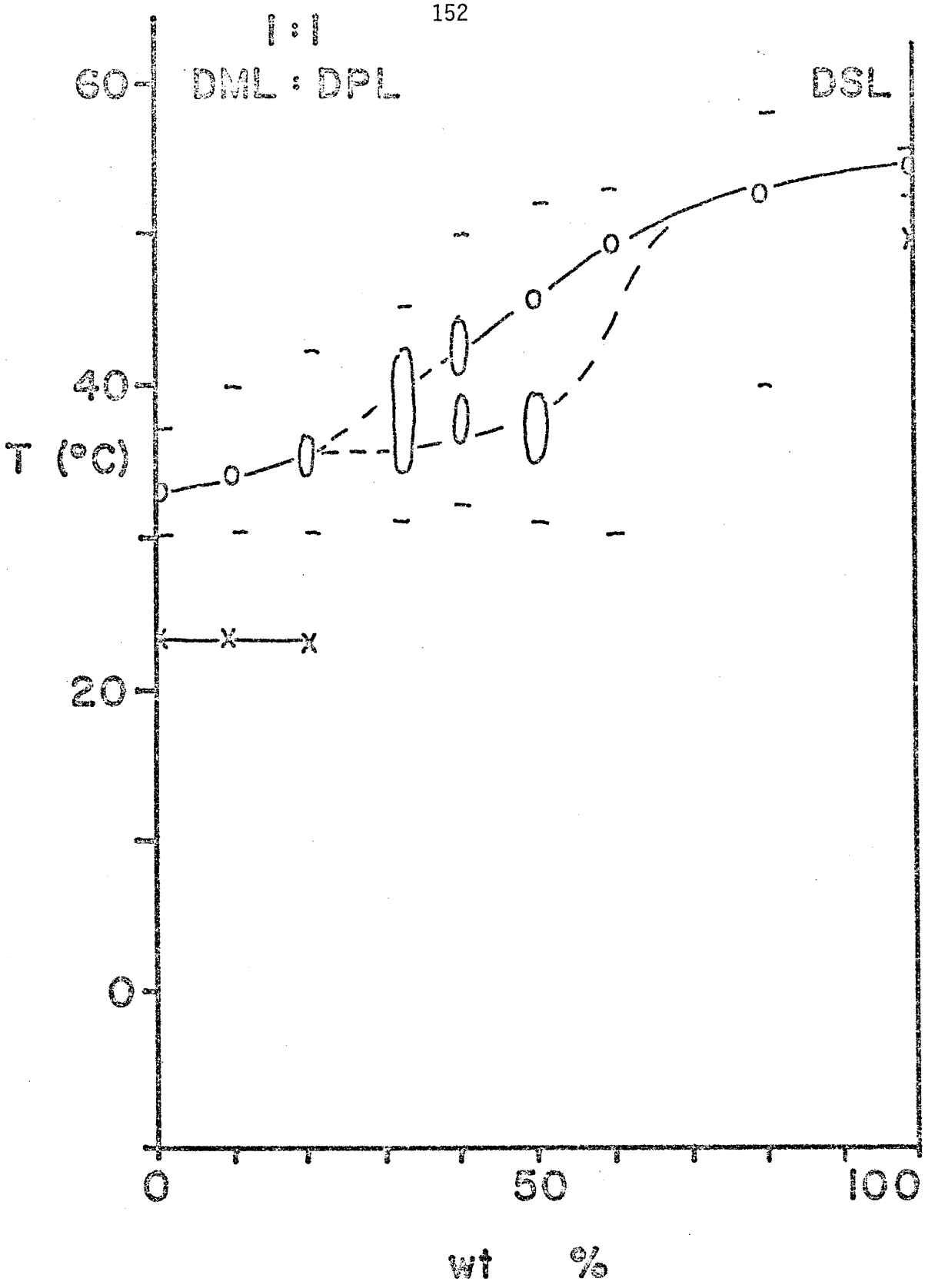
1 : 1
DML : DPL
DSL
60
40
20
0
T (°C)
0
50
100
wt %

the points during the transition at which the annealing starts and ends were not established. If the transition is broad it is particularly important to determine this relationship. Figure 33 shows biphasic DTA melting curves for three DML-DSL mixtures along with the temperature range over which annealing takes place. The data imply that onset of annealing occurs during the early part of the last transition. There are probably lattice defects in both gel phases but complete annealing can occur only when the highest melting phase starts to melt thereby defining the annealing temperature. The 1:3 mixture appears to anneal at a temperature higher than expected. The DTA measurements are performed without di- of trivalent salts whereas the annealing experiments require trivalent shift reagents, which for sharp transitions have the effect of increasing T_c by 1-5°C depending on the lipid (34, 35, 36). It appears that annealing occurs when a substantial amount of mobility is present in the bilayer. The annealing temperature therefore is an indicator of the minimum motional freedom necessary to repair lattice defects.

The annealing temperatures determined for DPL-cholesterol mixtures are shown in Figure 34 and those for DSL-cholesterol mixtures in Figure 35. For mixtures containing less than 75 mole % DPL or 80 mole % DSL it is impossible to prepare samples which are not annealed. As indicated in Figure 3, the highest temperature attained during sonication, and therefore an upper limit for the annealing temperature, is about 23°C in these preparations. This upper limit is indicated in Figures 34 and 35 by the open-ended symbols in this composition range.

FIGURE 33

Traces of DTA heating curves for three mixtures of DML and DSL in the molar proportions indicated. The hatched areas indicate the temperature ranges over which annealing takes place for vesicles prepared with the same proportions of DML and DSL but in 5 mM $La(NO_3)_3$.

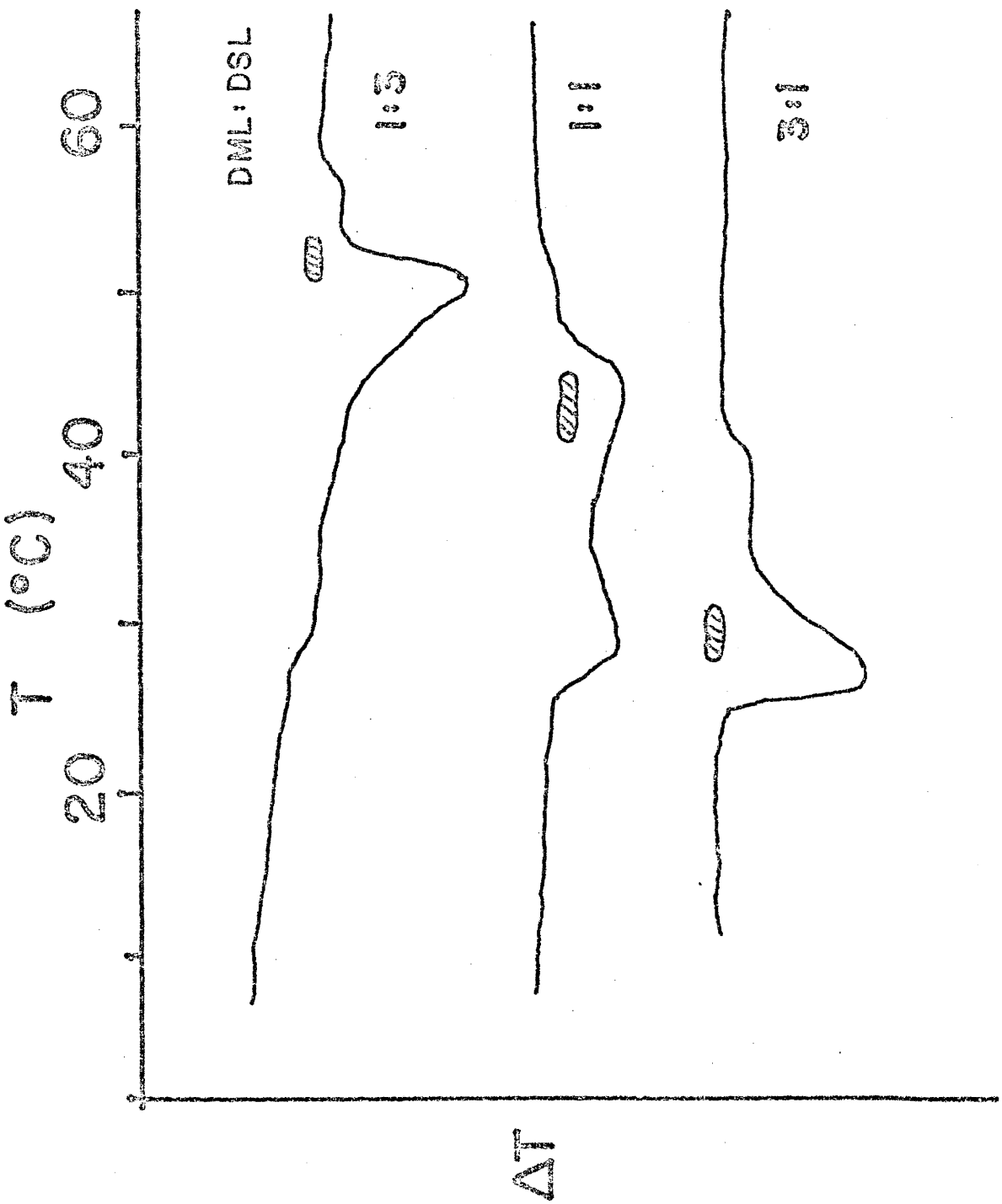
T (°C)
20
40
60
DML: DSL
1:3
1:1
3:1
ΔT

FIGURE 34

The temperatures (o) at which annealing occurs for DPL vesicles prepared with various amounts of cholesterol. At cholesterol concentrations higher than about 25 mole %, the vesicles are annealed during preparation at a temperature below 23°C.

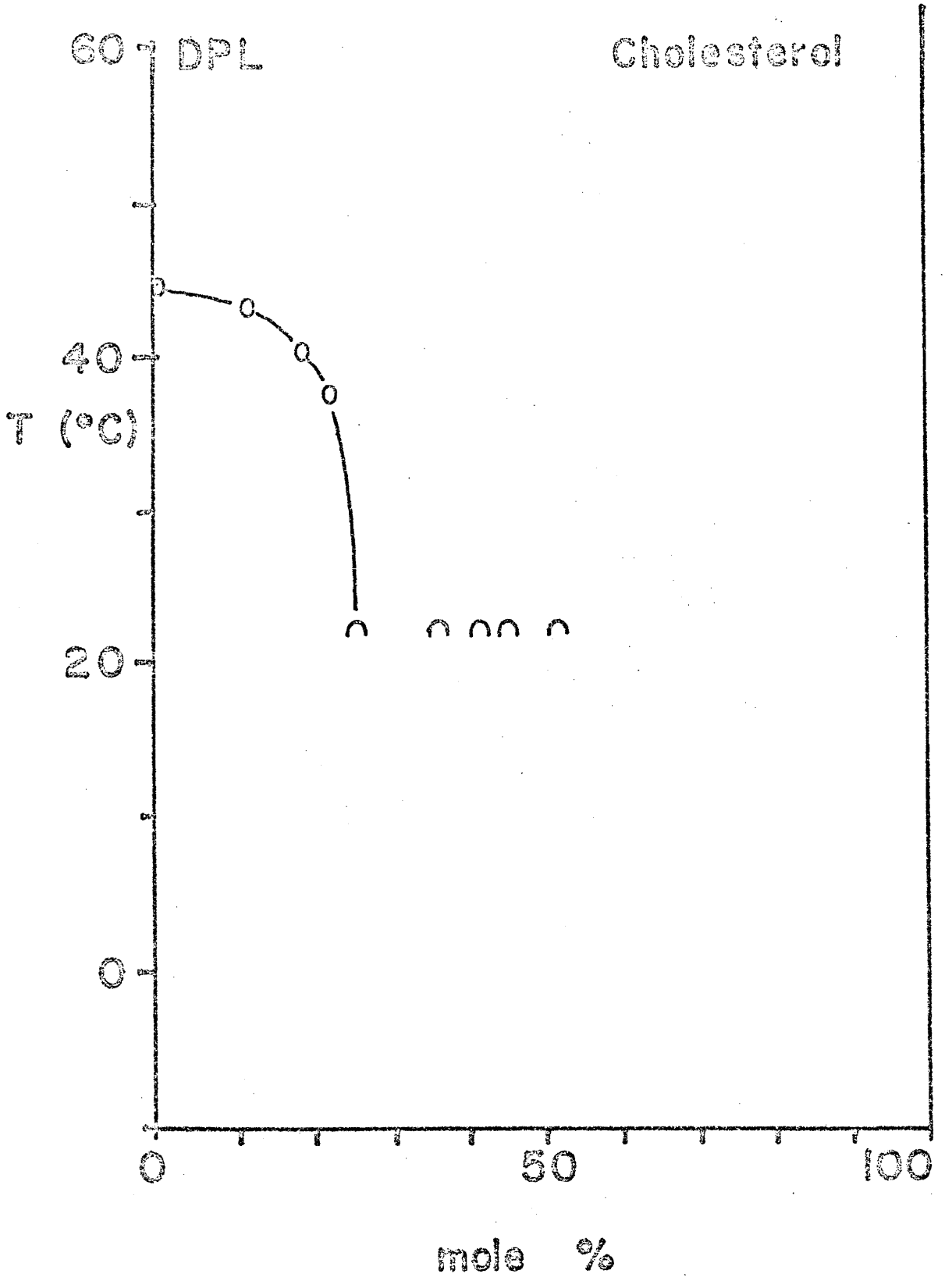
60
40
20
0
T (°C)
DPL
Cholesterol
0
50
100
mole %

FIGURE 35

The temperatures (o) at which annealing occurs for DSL vesicles prepared with various amounts of cholesterol. At cholesterol concentrations higher than about 20 mole %, the vesicles are annealed during preparation at a temperature below 23°C.

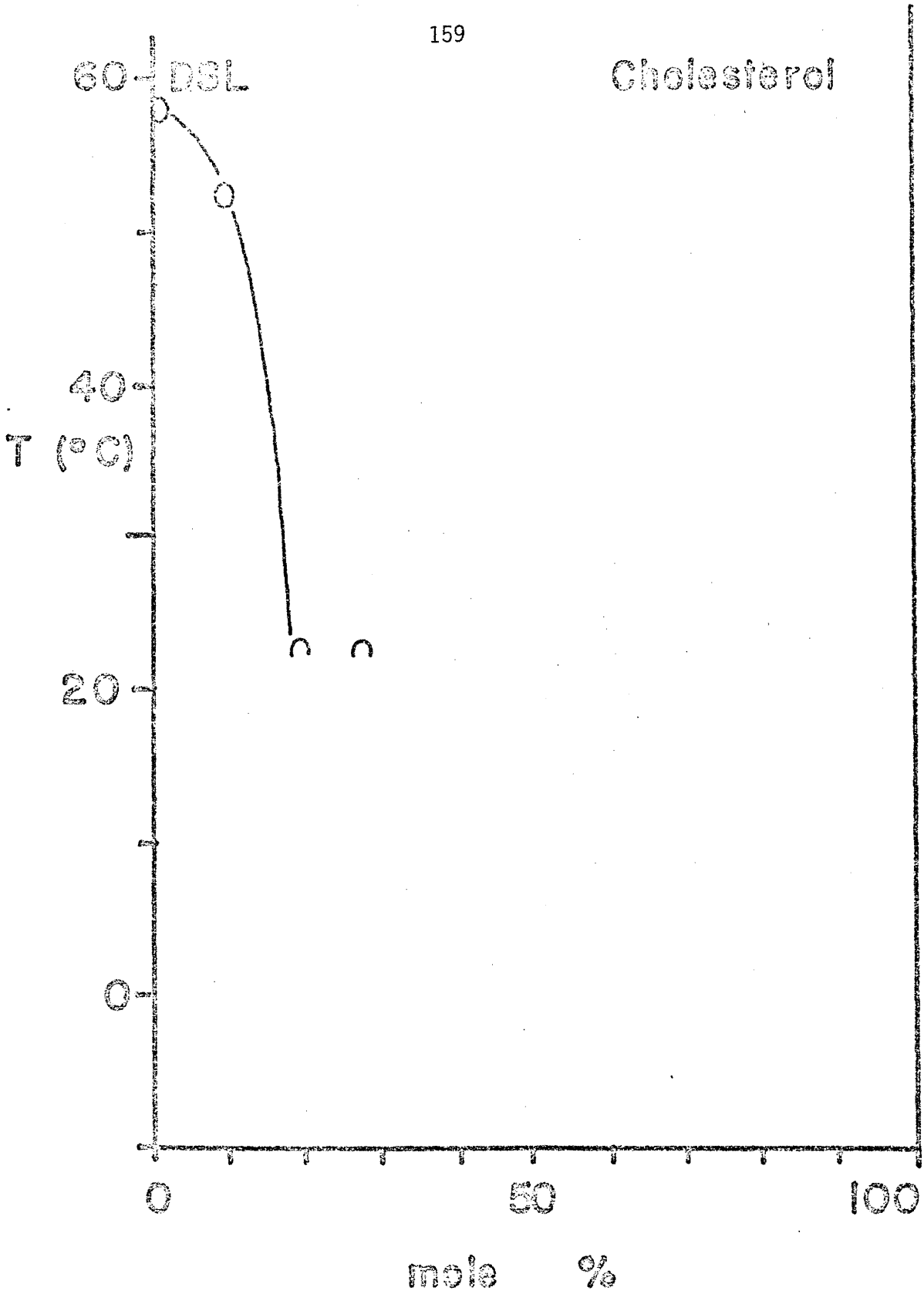
DSL
Cholesterol
60
40
20
0
T (°C)
0
50
100
mole %

3. Discussion

a. Binary phospholipid-water systems.

The thermal transitions of the pure phospholipid-water systems presented here are typical of lecithins, showing both a pretransition and a main transition (Figure 17). It is interesting to note that the stereochemistry at the glycerol C-2 appears to have no effect on the ability of the phospholipid to form an $L_{\beta'}$ phase. This implies that the $L_{\beta'}$ phase is sufficiently flexible to allow equally good packing of the two steroisomers. However, if substitution at the glycerol is changed from a 1,2-acyl (α-DPL) to a 1,3-acyl (β-DPL), the intermolecular interactions are slightly weaker and the transition temperature is lowered by 5°C. This is probably a result of a slightly larger interchain distance in the β-DPL molecule. It is actually not known whether β-DPL is in a β or β' phase, and although the DTA (Figure 18) suggests a pretransition at about 23°C, the data do not shed light on the nature of the gel phases. Currently, x-ray measurements on this system are being performed to establish this point (A.E. Blaurock, R.C. Gamble and N.O. Petersen, unpublished).

The intermolecular forces are also weakened slightly by perdeuteration of the fatty acyl chains, resulting in a 4-5°C decrease in the transition temperature without affecting the nature of the phases. A pretransition is still observed.

The thermogram of the vesicle solution (Figure 20) suggests a slight broadening of the transition with a lower onset temperature and a much diminished and broadened pretransition. It is not clear how representative of small bilayer vesicles a 20% sonicated solution is.

We have shown that the ^{1}H-NMR spectra for the liquid crystalline phase of 27% and 1% suspensions are identical (37), but the concentrated vesicle suspension should approach a close packing of vesicles with a relatively small amount of water between them which could affect the transition behavior. The absorbance data (Figure 21) show that there are significant changes in optical density at temperatures close to T_p, implying that there is a pretransition in the vesicle bilayers. In Chapter V we provide evidence that the absorbance changes are intimately associated with a pretransition which behaves like that in multilamellar systems.

b. Mixtures of phospholipids.

The degree of miscibility of two phospholipid components, A and B, in a membrane depends on the intermolecular interactions between the lipids. An ideal, or perfect, solution is defined (40):

> "as one in which the fugacity of each constituent is proportional to the mole fraction of that constituent . . . at every pressure and every temperature"

Inasmuch as the fugacity, f, is a measure of the "escaping tendency" (40) of a constituent, this definition of an ideal solution by Lewis and Randall demands that the interactions of A with A, B with B, and A with B, are all identical. The proportionality constant in the above definition is the fugacity of the pure liquid constituent, f^o, at the same pressure and temperature. Clearly then, for an ideal binary solution Raoult's Law for each component i.e.

$$f_A = f_A^o X_A$$

$$f_B = f_B^o X_B \qquad \text{(IV-1)}$$

must be obeyed over the entire range of compositions. Here X_A and X_B are the mole fractions of A and B, respectively.

Seltz (25) extended this concept to ideal solid solutions and required that eq IV-1 be obeyed with the fugacities and mole fractions referenced to the solid rather than the liquid states. The change in fugacity of component A with temperature, $\partial \ln f_A / \partial T$, is related to the ideal heat of vaporization of A, $H_A^* - \bar{H}_A$, by (41)

$$\frac{\partial \ln f_A}{\partial T} = \frac{H^* - \bar{H}_A}{RT^2} \qquad \text{(IV-2)}$$

Seltz (25) used these thermodynamic relations with the requirement that the fugacity of a component in the liquid equal that in the solid at equilibrium, to calculate the equilibrium compositions of the liquid and solid solutions during a transition. These calculations were applied by von Dreele (42) and Lee (43) to binary lipid systems using heats of melting and transition temperatures of pure components as determined by Hinz and Sturtevant (5).

The theory of Seltz (25) predicts that the transition in ideal mixtures will broaden with increased differences in heats of fusion and transition temperatures between the components. If we assume the entropy changes associated with the transitions for DPL and DPL-d_{62} are identical, the heat of fusion of DPL-d_{62} can be calculated from that for DPL using their transition temperatures (24) by

$$\Delta H_A = \Delta H_B \times \frac{T_A}{T_B} = 9.7 \times \frac{310}{315} \text{ kcal/mole} = 9.55 \text{ kcal/mole} \qquad \text{(IV-3)}$$

The very small ΔH difference (0.15 kcal/mole) and the small change in transition temperature suggest that ideal mixtures of DPL and DPL-d_{62} should exhibit a small broadening of the transition in accord with experimental observations (Figure 23). Identical arguments hold for the DSL-DSL-d_{70} mixtures. In both sets of mixtures the considerations also apply to the pretransition.

Calculations by von Dreele (42) and Lee (43) suggest that broadening of the transition in mixtures of DML with DPL and DPL with DSL, can be accounted for fully by the ΔH and T_c differences between the lipids. This is supported further by a calculation (courtesy of P.H. von Dreele) of the DSC melting curve for an equimolar DML-DPL mixture. The calculation compares favorably with experimental DTA data for a 1:1 (w/w) mixture of these lipids (Figure 36). We conclude that in mixtures of DPL with DPL-d_{62}, DSL with DSL-d_{70}, DML with DPL, and DPL with DSL, the L_α, L_β and $L_{\beta'}$ phases all behave as <u>ideal solutions</u> as defined thermodynamically by Lewis and Randall (40) and Seltz (25). Thus Raoult's law is obeyed at all compositions. On this basis, the phase diagrams for these four mixtures can be schematically represented as illustrated in Figure 37, in analogy with standard vapor-liquid phase diagrams. There is a two phase region within the lens representing, in this case, temperatures and compositions at which liquid is in equilibrium with solid. The compositions and proportions of the liquid and solid phases in equilibrium at any given temperature are given by the horizontal tie line at that temperature (Figure 37). The pretransitions are not included for the sake of clarity.

In mixtures of DLL with DML, the systems appear to behave ideally

FIGURE 36

Comparison of a calculated DSC curve and an experimental DTA curve for an equimolar mixture of DML and DPL in excess water. The calculated curve (—) is obtained assuming an ideal mixture of the lipids in all phases (42,43).

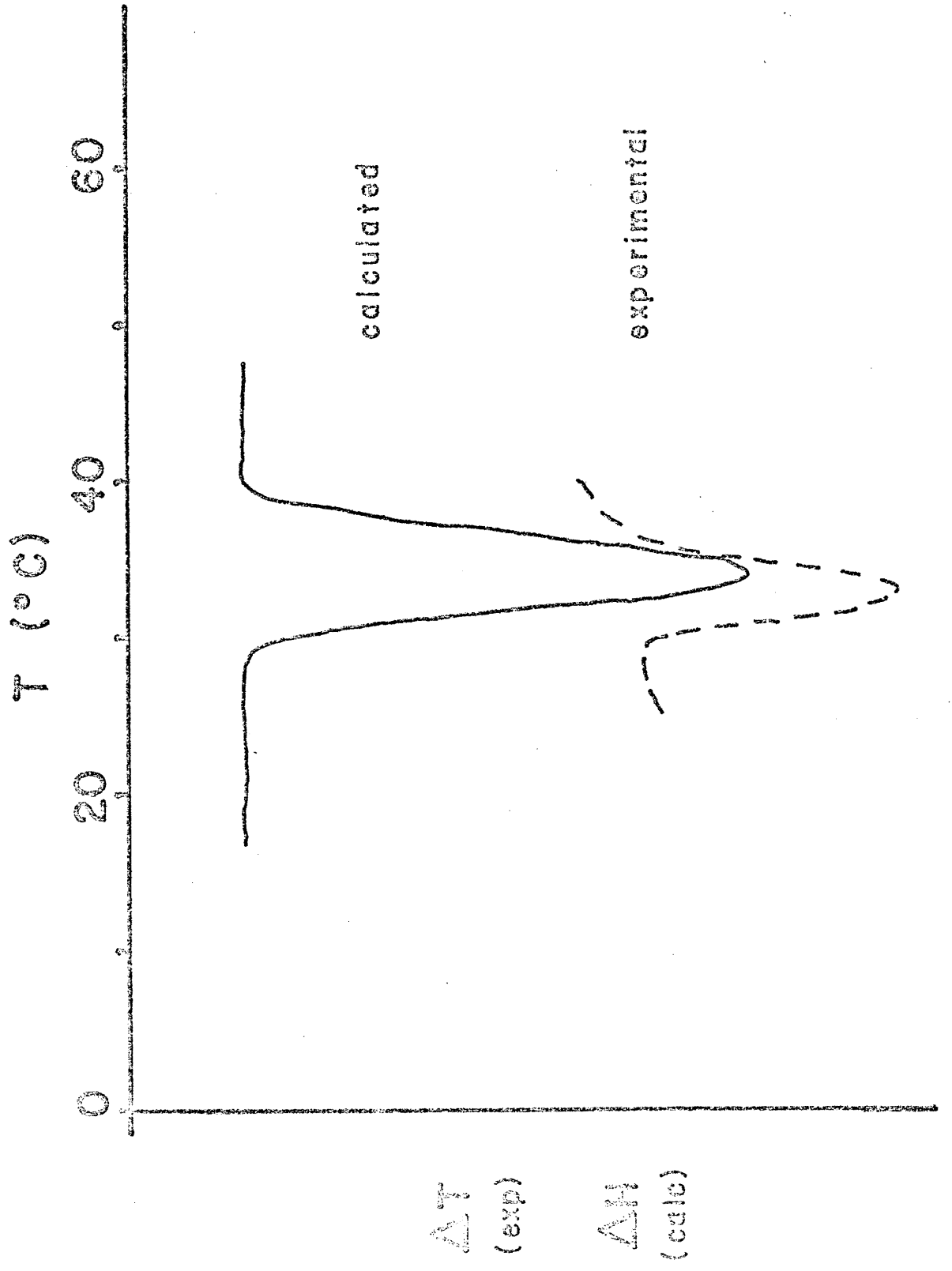
T (°C)
0
20
40
60
calculated
experimental
ΔT (exp)
ΔH (calc)

FIGURE 37

The idealized phase diagrams for the phospholipids which form ideal mixtures in all phases and at all compositions. The phase diagrams only represent the main transition. The high temperature phase is an L_α phase, the low temperature phase an L_β or an $L_{\beta'}$ phase. There are 2 phases in equilibrium in the region inside the lens. The relative amounts and their composition are determined by a tie line as illustrated in the DML-DPL diagram.

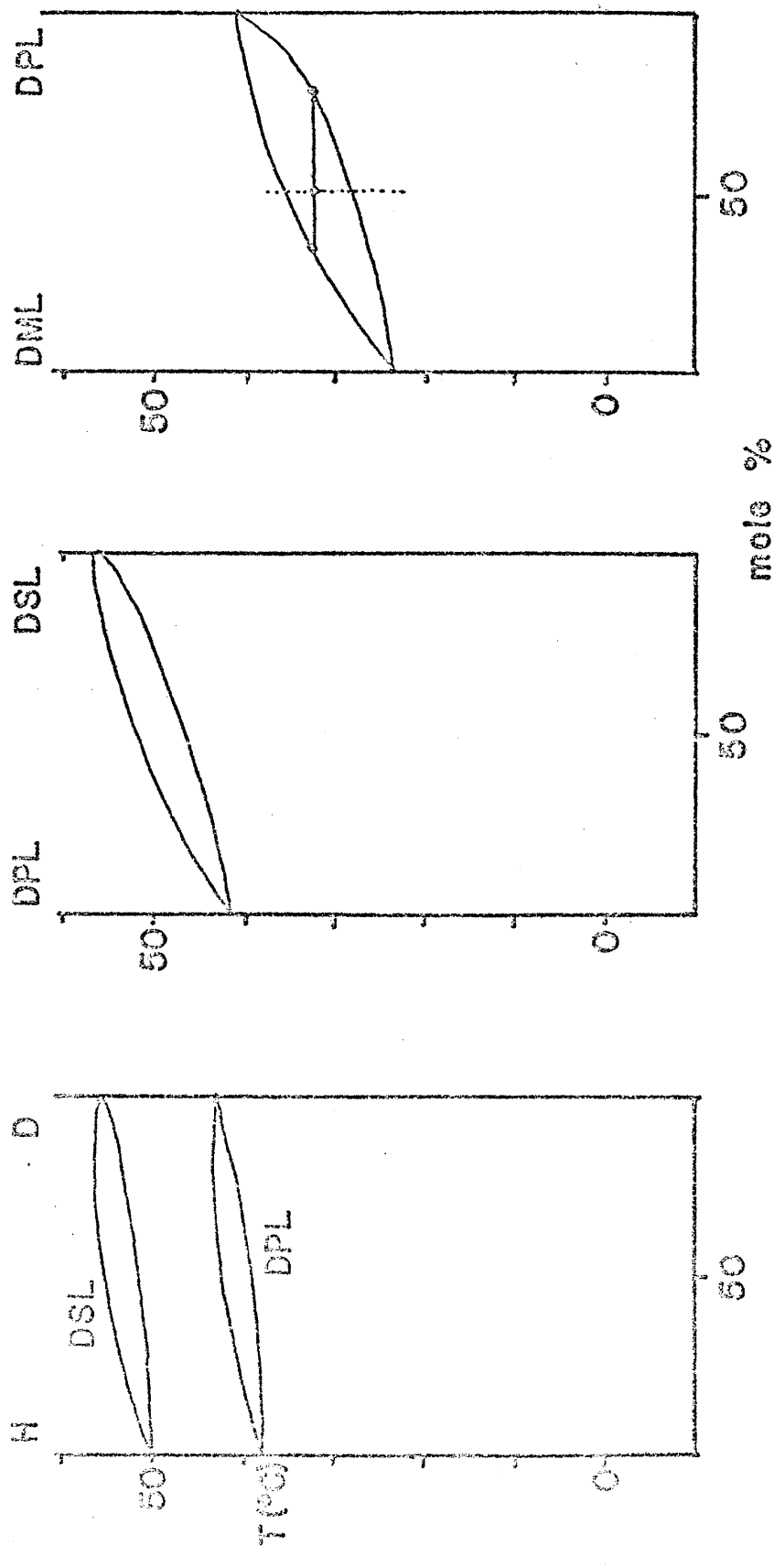
DPL
DML
50
0
50
DSL
DPL
50
0
50
mole %
H
D
DSL
DPL
50
T(°C)
0
50

at low DLL concentrations, while at low DML concentrations the transitions exhibit biphasic behavior. The nature of the transition curves at low DLL concentrations suggests that DLL and DML form a regular solution, at least in the gel phases, which obeys Henry's and Raoult's laws up to about 30 mole % DLL. At higher DLL concentrations there appears to be immiscibility in the gel phases, but there is miscibility in the L_α phase. It is possible that Henry's and Raoult's laws may also be obeyed for solid phases containing very high DLL concentrations.

Both von Dreele (42) and Lee (43) found that Seltz's theory (25) could not account for transition curves for mixtures of DML with DSL (Figure 27). This is true partly because the transitions are far too broad, and partly because the transition curves predicted by this theory for ideal solutions cannot be biphasic. However, there is reasonable agreement between the compositions predicted and measured for the liquid crystalline phase along the fluidus line, suggesting that the L_α phase in these mixtures still behaves as a nearly ideal solution. Similar results are observed for mixtures of DLL with DPL (Figure 28) and DLL with DSL (Figure 29). We may conclude that the L_α phases of all the phospholipid mixtures investigated are thermodynamically ideal solutions in which complete miscibility of all components occurs.

The L_β or $L_{\beta'}$ phases of all mixtures of DML-DSL, DLL-DPL, and DLL-DSL are non-ideal solutions. A pretransition is observed whenever there appears to be miscibility in the gel phase. Since the data suggest immiscibility for some compositions, we propose the schematic phase diagrams presented in Figure 38 for these three mixtures. A more detailed illustration of these phase diagrams is provide in Figure

FIGURE 38

Proposed idealized phase diagrams for phospholipids which form ideal mixtures only in the high temperature L_α phase. Only the main transition is represented. At low temperatures DML-DSL and DLL-DPL mixtures exhibit partial miscibility whereas DLL-DSL mixtures are totally immiscible.

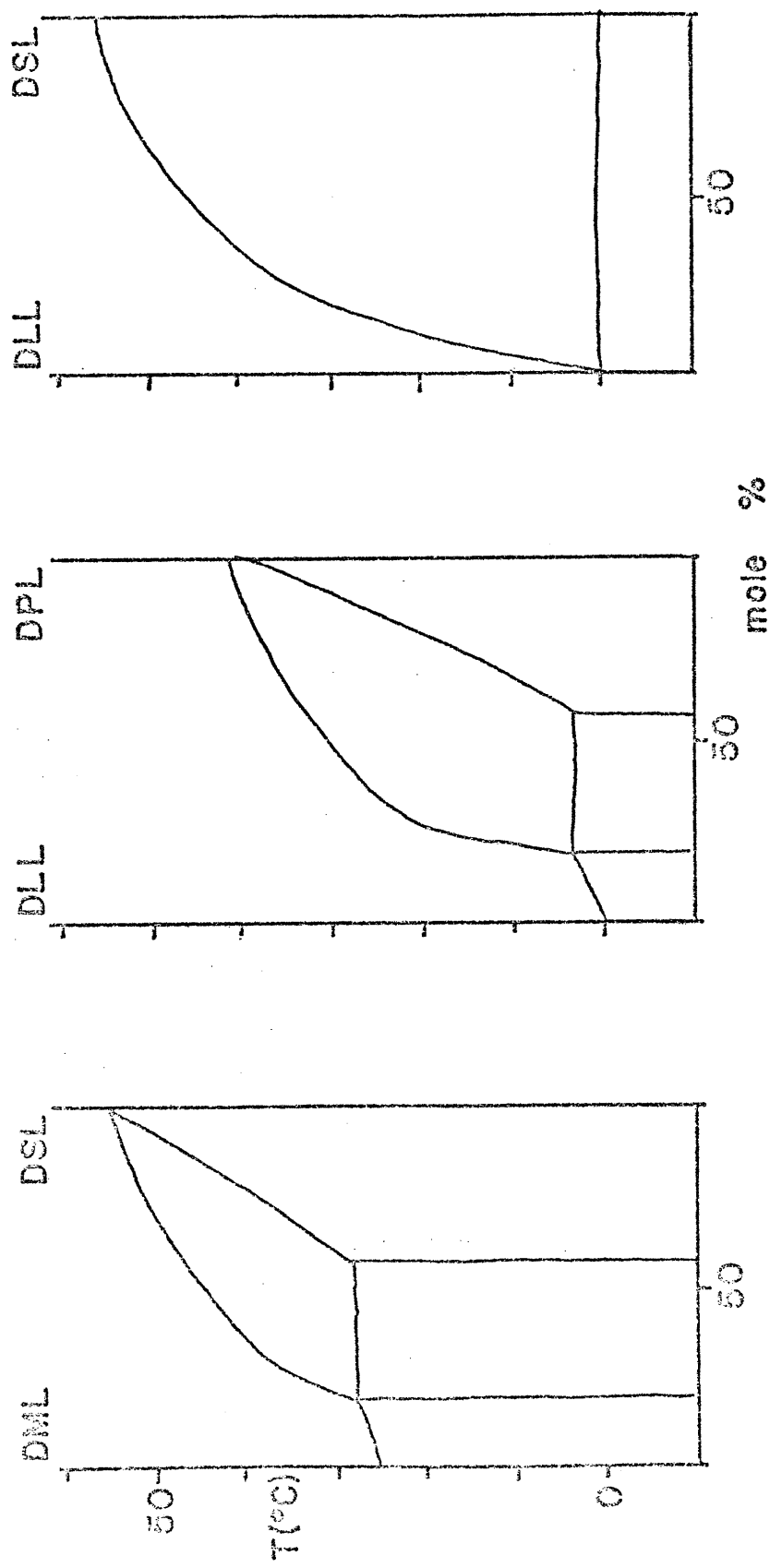
DSL
DLL
50
DPL
DLL
50
% mole
DSL
DML
50
T(°C)
0
50

39 for DML-DSL mixtures. A brief account of the phase changes with temperature at three compositions follows.

A mixture of 90% DSL and 10% DML at a temperature below ∿ 44°C exists as a homogeneous L_β (or possibly $L_{\beta'}$) phase in equilibrium with excess water. Upon heating above 44°C, a small amount of the L_β phase melts to form a homogeneous L_α phase with a composition of about 50% DSL. As the temperature is raised, the L_α phase changes in composition towards an increasing amount of DSL. Simultaneously, the L_β phase gets richer in DSL with the proportion of L_α and L_β phases dictated by horizontal tie lines. When the temperature reaches about 50°C the L_α phase contains 90% DSL and is the only phase left in equilibrium with excess water.

For mixtures containing 30% DSL kept at temperatures below 25°C two solutions with ∿ 20% DSL and ∿ 60% DSL, respectively, are in equilibrium. Depending on the exact temperature, either may be in the L_β or $L_{\beta'}$ form. As the temperature reaches 25°C, the component richest in DML melts over a fairly narrow temperature range, the width of which is supressed in Figures 38 and 39 to facilitate presentation of the phase diagrams. As the temperature is raised further, the component richest in DSL melts continually into the L_α phase and both the L_α and L_β phases are enriched in DSL. When the temperature reaches ∿ 33°C, all the lipid is in a single L_α phase with a composition of 30% DSL and 70% DML in equilibrium with excess water.

With only 10% DSL and at temperatures below ∿ 15°C, there is a single $L_{\beta'}$ phase in equilibrium with excess water. As the temperature is raised, this undergoes a transition at ∿ 15°C into the L_β phase

FIGURE 39

Detailed idealized phase diagram for the DML-DSL system in excess water. The phases are designated in accord with the definitions of Luzzati (2) and Figure 16. A detailed description of the diagram may be found in the text.

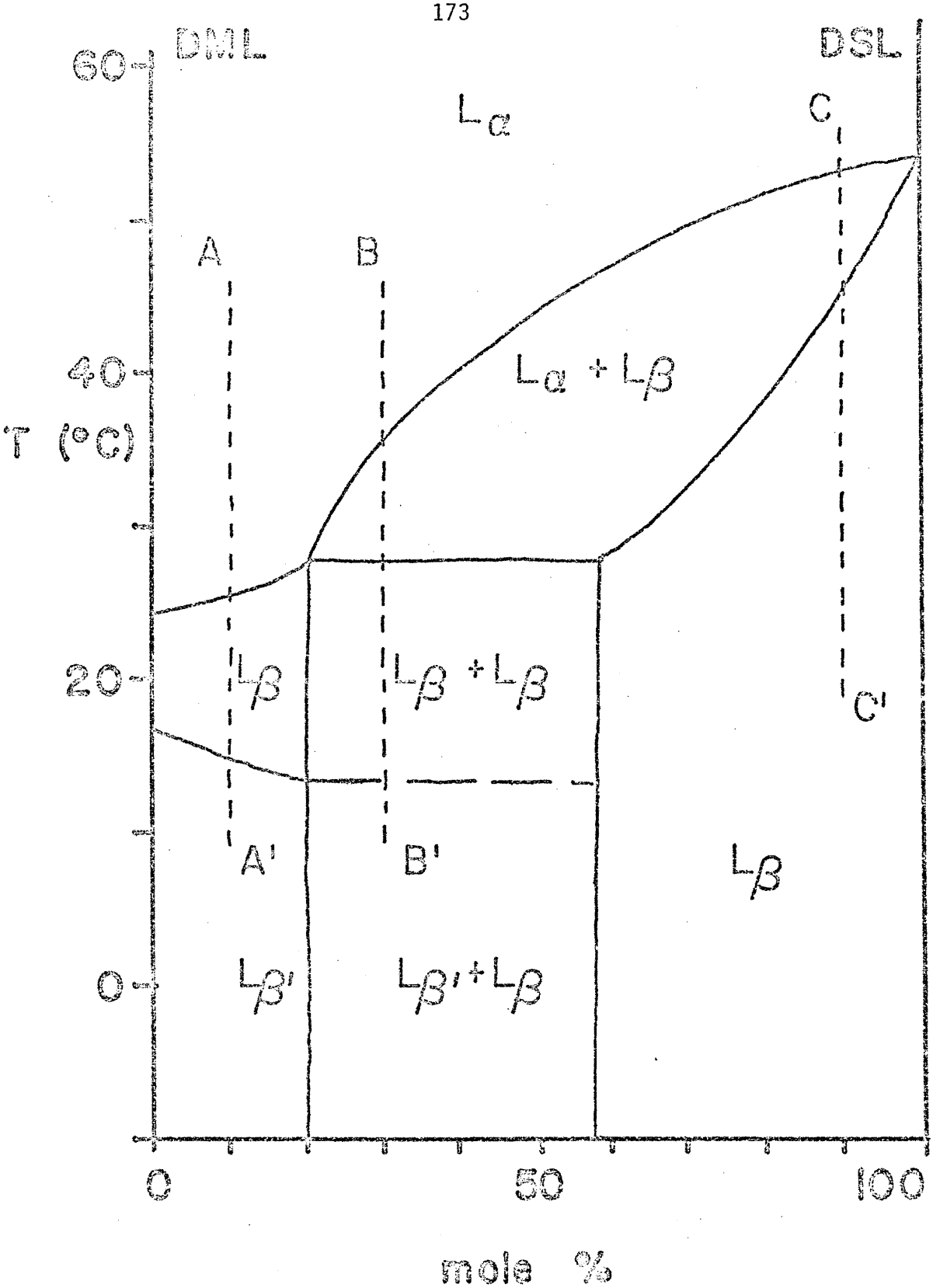
DML
DSL
60
40
20
0
T (°C)
L_α
C
A
B
$L_\alpha + L_\beta$
L_β
$L_\beta + L_\beta$
C'
A'
B'
L_β
$L_{\beta'}$
$L_{\beta'} + L_\beta$
0
50
100
mole %

which in turn melts into the L_α phase at 24°C.

The other phase diagrams of Figure 38 may be interpreted similarly, except that DLL and DSL are completely immiscible. The data of Figures 30, 31 and 32 may be interpreted in the same fashion. If one combines these data with those of Figures 24,25 and 27, it is possible to construct a ternary phase diagram for a fixed excess H_2O concentration, as shown in Figure 40. In this diagram, the pretransition is not included for simplicity of representation. In the composition region indicated by the hatched area in the basal triangle, 3 phases coexist at low temperatures (< 25°C): H_2O plus two L_β phases. The compositions of these L_β phases are given by horizontal tie lines. These tie lines are probably parallel to the DML-DSL composition plane at low DPL concentrations, but could in principle have any orientation as long as they connect two points on the curved vertical surface. At some temperature above 25°C, an L_α phase forms in equilibrium with an L_β phase and excess H_2O, but since the orientations of the tie lines are unknown, the compositions and proportions cannot be specified. At compositions other than those described above, there are only two phases : H_2O and either an L_β, $L_{\beta'}$ or L_α phase depending on the temperature.

It is easy to visualize how a large number of lipid components can mix to produce a biological membrane with a broad transition as in fact is observed (16,17,18,19,20). Likewise, the transition is sensitive to composition, and it is reasonable to conclude that the transition behavior, and therefore the motional state of lipids in real membranes, is modulated by changes in composition.

FIGURE 40

Proposed idealized phase diagram for DML-DPL-DSL mixtures in excess water. The hatched area corresponds to the compositions for which two lamellar phases coexist. The actual compositions of these two phases are determined by tie lines between two points on the curved line, but the orientations of the tie lines are unknown.

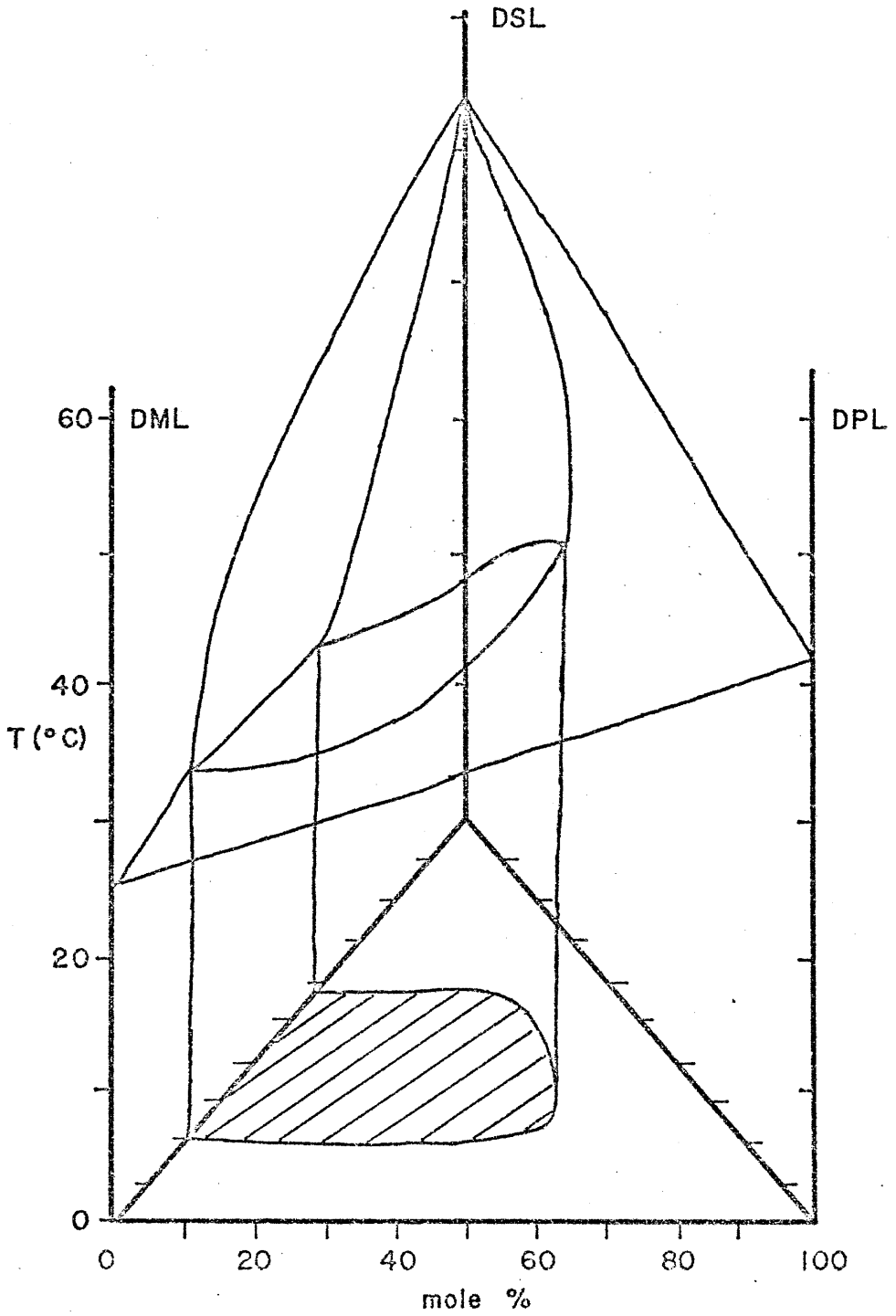
DSL
DML
DPL
60
40
20
0
T (°C)
0
20
40
60
80
100
mole %

c. Phospholipids and cholesterol.

The data obtained for DML-DSL mixtures indicate that annealing occurs at the onset of melting of the L_β phase, which is richest in DSL. We conclude that the crystalline defects in a given phase are annealed when a sufficient amount of the L_α phase is formed. Presumably, only a small fraction of L_α phase is needed because melting is likely to occur in the defect areas first. Membrane fluidization at the transition entails not only increased chain mobility but also the onset of rotational diffusion (38) and enhancement of the rate of lateral diffusion (44). Moreover, when the bilayer melts, phospholipid flip-flop occurs more readily leading to annealing (22). We therefore submit that phase boundaries measured by annealing techniques designate the temperatures and compositions at which rotational and lateral diffusion are significantly enhanced.

Our data on annealing of phospholipid-cholesterol mixtures (Figures 34 and 35) will be utilized in conjunction with previously published data (4,22,28-33, 50-71) to establish a phase diagram for lecithin-cholesterol mixtures in excess water. Most data relevant to phase equilibria in lecithin-cholesterol mixtures were obtained with liposome preparations, but some, including our annealing data, pertain to vesicle preparations. Phase diagrams for the two preparations are likely to differ for a number of reasons. (i) The lateral surface pressure for flat bilayers in a liposome preparation is smaller than that for a curved bilayer in a vesicle (45). The excess pressure of $\sim$ 2 atm in the latter is balanced by a hydrostatic pressure across the bilayer. Since pressure is an important thermodynamic parameter which strongly

affects the transition behavior (9,13,14), the phase equilibria in curved bilayers would differ from those in flat bilayers. (ii) The larger chain fluctuations in the L_α phase (cf Chapter III) suggest that the intermolecular interactions are weaker in vesicle bilayers, which could easily alter the miscibility of components. Indeed, there are differences between the transition curves observed for equimolar mixtures of DML and DSL in liposomes and in vesicles (46). (iii) The vesicle bilayers are asymmetric, so their outer monolayer often has a different composition from that in the inner monolayer (47). The two monolayers could be in different phase equilibria for a given total composition, although they must be in equilibrium with each other. (iv) The motional state and the molecular packing interactions of the two vesicle monolayers are different (48) so their phase diagrams could be different. Thus care must be exercised when data are interpreted since phase boundaries may vary significantly between vesicle and liposome bilayers.

Bourgès and coworkers (50) measured the ternary phase diagram of egg yolk lecithin (EYL), cholesterol and H_2O at 25°C (Figure 41a). Ladbrooke et al (28), using these data along with their own DSC and x-ray results for DPL, cholesterol and water, proposed the ternary phase diagram illustrated in Figure 41b. The biologically most interesting regions of the phase diagram are regions IV and VI where there is always excess water. It is important to note that the lecithin-cholesterol diagram elucidated in excess water is independent of the amount of excess, since it always refers to the liquid crystalline phase depicted at the border of regions III and IV.

FIGURE 41

Traces of previously established or proposed ternary phase diagrams for lecithin-cholesterol-water mixtures.

a: EYL-cholesterol-water at 25^{o}C (50).

b: DPL-cholesterol-water (28)

The phase regions are discussed in the text.

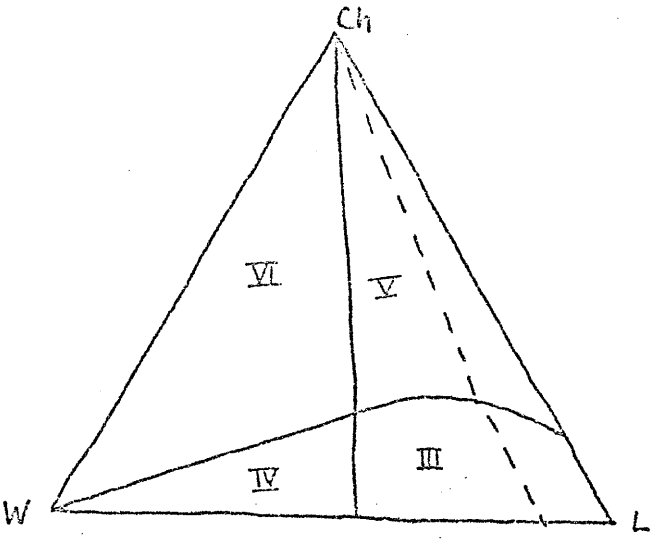

a

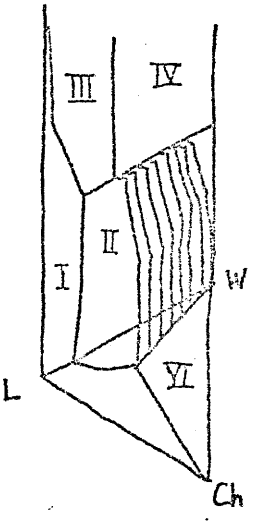

b

Since Ladbrooke et al (28) proposed the phase diagram in Figure 41b, many data have suggested an additional phase boundary for DPL-cholesterol-water mixtures at 20-25°C with about 33 mole % cholesterol (20 wt %) (30,52,53,55,57). For example, ESR measurements (30,57) of cholesterol spin-label derivatives show that a rotational motion is present at more than 33 mole % but not below 33 mole %. DSC measurements (55) clearly show a loss of a thermally induced transition at more than 33 mole % cholesterol. Engelman and Rothman (52,53) interpreted their x-ray data in terms of a lateral separation of a phase with a 2:1 stoichiometry of DPL to cholesterol, which was proposed to be in equilibrium with a pure DPL $L_{\beta'}$ phase. Engelman and Rothman's description (52) of their data is at odds with the x-ray data presented by Inoko et al (51) which show no evidence for a lateral phase separation. Furthermore, the magnetic resonance data at 25°C (30,56,57) suggest that, with increasing cholesterol concentration, there is a gradual change in the orientation of spin-labelled cholesterol derivatives without any fast rotational motion up to about 25-30 mole % cholesterol. With more than 33 mole % cholesterol the rotational motion is rapid on the ESR timescale of measurement. The DSC data (28,32,54, 55) show no evidence for heat absorption at lower temperatures, as expected if the proportion of two phases changes while the temperature increases. Since the annealing experiments presented here also suggest that the phase boundary is one at which rotational and lateral mobility sets in, we propose the phase diagram shown in Figure 42 for the DPL-cholesterol lamellar phase in excess water. The phase boundary lines are shown for liposomes rather than vesicles and consequently differ

FIGURE 42

Proposed DPL-cholesterol phase diagram diagram for liposomes in excess water. The details of the phase diagram are discussed in the text.

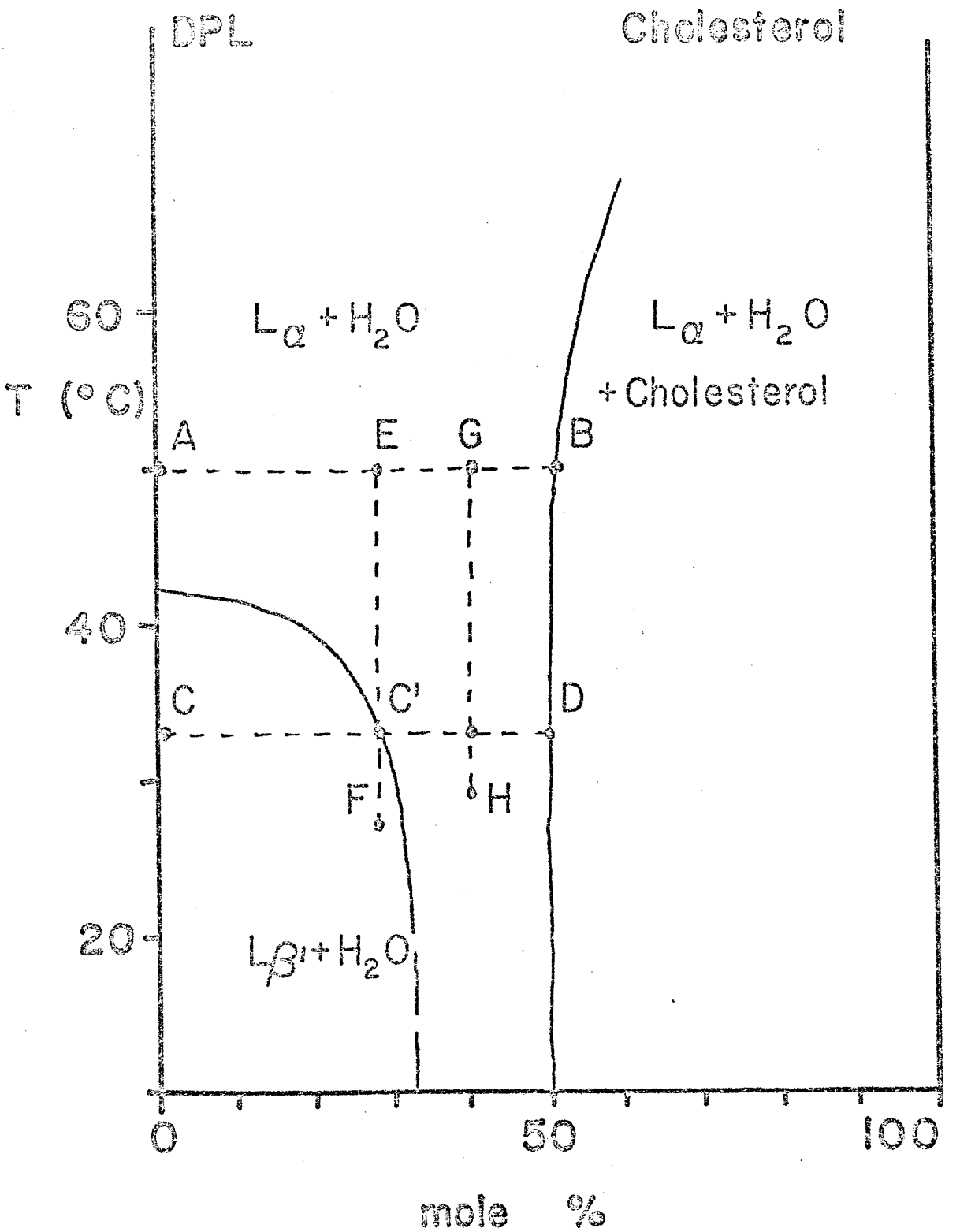
DPL
Cholesterol
60
40
20
T (°C)
$L\alpha + H_2O$
$L\alpha + H_2O$
+ Cholesterol
A
E
G
B
C
C'
D
F
H
$L\beta' + H_2O$
0
50
100
mole %

from the data in Figure 28. Note that the phase diagram shown is in excess water, so that the composition of the L_α phase is given by the points on the phase boundary between regions III and IV in Figure 41a. Thus as cholesterol is added to DPL at high temperatures, the hydration decreases from 45% to 35% by weight. However, at low temperatures, the hydration increases from about 25% to 35% upon addition of cholesterol to DPL (4,28). The two lines, AB and CC' are actually in different planes whereas the C'D line is in the same plane as the AB line. The complete ternary phase diagram is shown in Figure 43, in which we have ignored the phases at low hydration levels.

The following description will make use of the common labelling scheme for Figures 41,42 and 43. Region I: This represents a single $L_{\beta'}$ phase with a composition determined by the proportion of the components. The angle of tilt of the phospholipid hydrocarbon chains decreases as the cholesterol concentration increases. Regions I' and V': Very low hydration levels yield numerous poorly characterized phases (2, 28, 50). Region II: This is a two phase region with pure H_2O in equilibrium with an $L_{\beta'}$ phase, which has a composition defined by the vertical plane containing the line CC'. The lamellar phase is equivalent to the $L_{\beta'}$ phase in Region I. Region III: A single L_α phase with a composition defined by the component proportions. Region IV: The two phase region consisting of pure H_2O in equilibrium with an L_α phase with composition determined by a point in the vertical plane containing the points A, B, C" and D. This is the biologically most interesting phase region. Region V: A two phase region with pure cholesterol crystals in equilibrium with an L_α phase from Region III.

FIGURE 43

Proposed ternary phase diagram for the DPL-cholesterol-water system. The details of the various phases are discussed in the text.

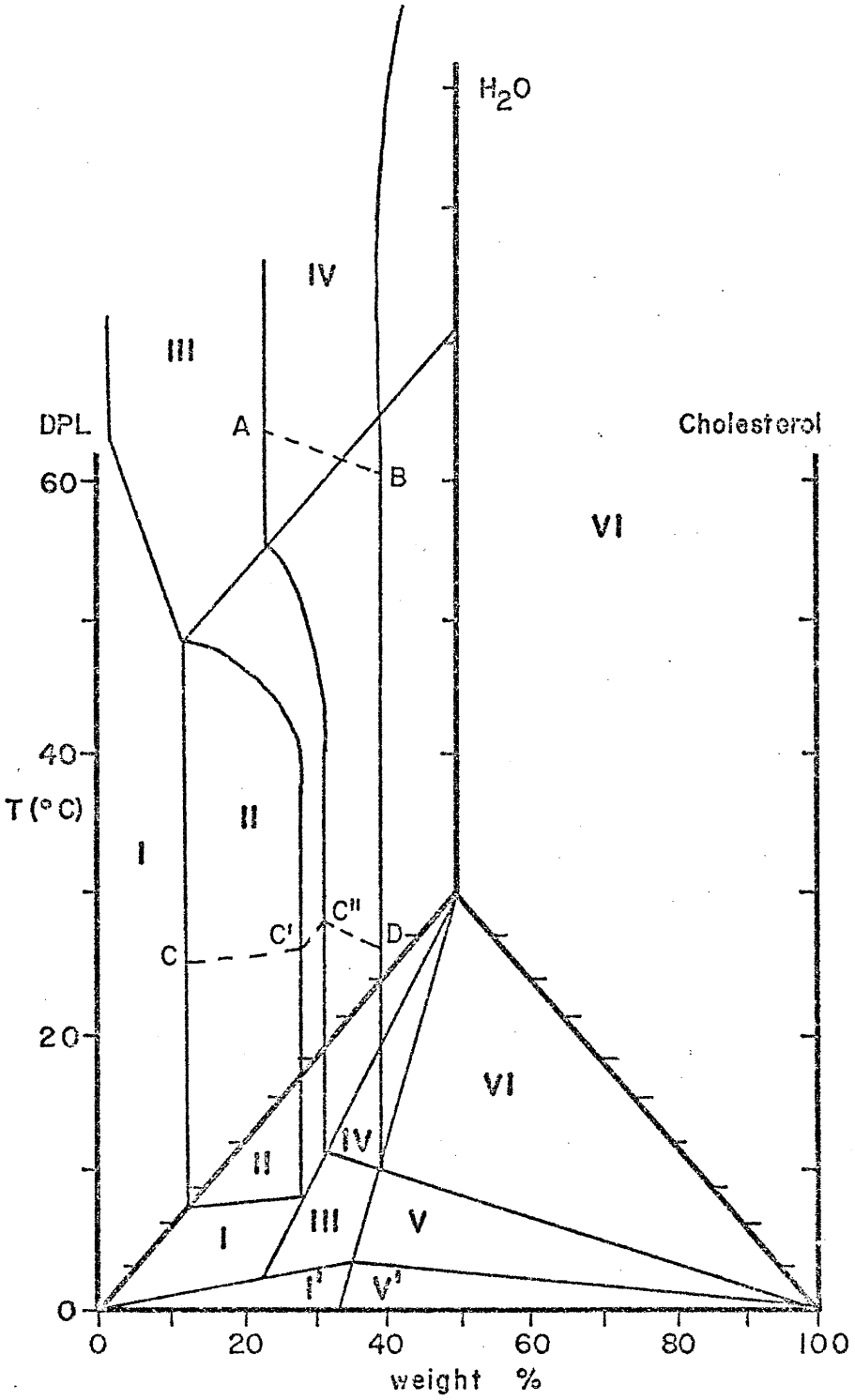
H2O
IV
III
DPL
A
B
Cholesterol
60
VI
40
T (°C)
II
I
C''
C'
C
D
20
VI
IV
II
III
V
I
I'
V'
0
0
20
40
60
80
100
weight %

Region VI: A three phase region consisting of pure H_2O, pure crystalline cholesterol and an L_α phase with a composition defined by a triple point composition. The triple points are on the line defined by the points B and D.

Phase diagrams indicate the phase boundaries but provide little or no information about the state of motion within a given phase region. We, therefore, turn to a motional description of the phases encountered along the lines AB, CD, EF and GH in Figure 42. We apply the motional model developed in Chapter III to the liquid crystalline phase characterized by rotational and lateral diffusion. We assume excess water in all cases.

(i) The A-B line: At A, pure lecithin is in an L_α phase with the order parameter $S_\alpha \sim 0.5$. When cholesterol is added, the chain fluctuation amplitude decreases continuously and S_α increases (32,62,63,72). At B, the bilayer is saturated with cholesterol and a pure cholesterol crystalline phase appears. Concomitant with the order parameter changes, there is an increase in bilayer thickness and a decrease in water content (29).

(ii) The C-D line: At point C, the pure lecithin is in an $L_{\beta'}$ phase.[1] The angle of tilt is about 30° (2,6,7). When cholesterol is added we propose that a single $L_{\beta'}$ phase is formed with a smaller tilt angle (57). As more cholesterol is added, the tilt angle approaches zero and a gradual transformation into an L_β phase is achieved.

---

[1]We have ignored the consideration of the pretransition in this phase diagram, since there are no data on the effect of cholesterol on the pretransition.

In addition the lamellar phase takes up water (2) and some changes in the lamellar repeat distance are observed (28). It appears that with less than 7.5 mole % cholesterol, the increase in bilayer thickness due to a decreasing tilt angle more than compensates for the decrease in interlamellar spacing resulting from the water uptake, so the lamellar repeat distance increases. With more than 7.5 mole %, the incremental bilayer thickening is smaller than the reduction in interlamellar spacing, thereby decreasing the total lamellar repeat distance. At C' the L_α phase at C" (Figure 43) appears. The amount depends on the degree of hydration and is determined by the C'-C" tie line (Figure 43). In the C"-D range, the amplitude of the chain fluctuation is steadily reduced corresponding to the changes along the AB line. At the lower temperature (C"-D vs E-B) the order parameter is expected to be larger.

(iii) The E-F line: Upon cooling a sample containing less than 33 mole % cholesterol, the S_α order parameter increases gradually until, at point C", the L_β, phase at C' is formed. Further cooling has little effect.

(iv) The G-H line: As along the E-C" line, the chain fluctuations are gradually retarded and reduced, as seen in the line width increase in ^{1}H-NMR measurements (61).

(v) The B-D line: This line represents the triple point composition as a function of temperature. The line is shown as curved above point B since the solubility of cholesterol in the lamellar phase is expected to increase at higher temperatures. It is perhaps unfortunate that so many studies have been performed at 50 mole % cholesterol (33, 56,58,59,60,66 ,70) since this is at the border of cholesterol satura-

tion, and no cooperative transitions are expected or observed. It should be noted that Raman measurements (33,70) suggest that the extent of chain isomerization also decreases as the temperature is lowered from B to D. At low temperatures it is possible that the phase is most properly termed an L_β phase.

We noted earlier that the phase boundaries for vesicles and liposomes are expected to be different. The data in Figure 34 indicate that 25 rather than 33 mole % cholesterol is needed to generate the L_α phase which anneals vesicles. It is likely that the difference in position of the phase boundary is exaggerated as a consequence of an asymmetric distribution of cholesterol in the two halves of the vesicle bilayer. For small vesicles without cholesterol, the fraction of the lecithin in the outer monolayer is about 0.7. When cholesterol is added, the fraction of the lecithin in the outer monolayer approaches 0.5 (73). The conclusion is that there is proportionally more cholesterol in the outer monolayer than in the inner monolayer. Thus when the total cholesterol concentration is at 25 mole %, the concentration in the outer monolayer may exceed 33 mole %. The outer monolayer would then be in an L_α phase which should completely anneal the vesicles. One may rationalize the asymmetric distribution of cholesterol by its wedge shape which is better accommodated in the outer monolayer. For thicker membranes, the bilayer asymmetry would be enhanced, which might explain why the DSL-cholesterol vesicles anneal completely at a lower total cholesterol concentration.

d. Conclusions.

We have seen how our motional model for lipid components in the

bilayer membrane can give new insight into the nature of the lipid-lipid interactions for mixtures of lecithins and cholesterol. Although the descriptions of the motional states in these mixtures are still rather qualitative, they aid us in understanding the basic intermolecular interactions in the membrane. We have emphasized the importance of the anisotropy of the fluid membrane. The fact that we can easily describe the anisotropy in the membrane by the S_{α} parameter, may, in fact, be the most important aspect of our motional picture.

In a cell membrane the lipid composition is somewhat more complex than in the mixtures studied here. Nonetheless, we may begin to understand the role of various lipid components through a description of molecular interactions and motions in model systems. In general terms, the phospholipid composition in a cell membrane probably is controlled so that small fluctuations in composition or temperature will not result in large changes in membrane structure or motional state. Yet, it should be noted that the present discussion deals with a lamellar phase presumed to be at a thermodynamic equilibrium. The cell membrane, however, is a system at steady state. The motional state of the membrane components could therefore vary locally, for example around protein components or in highly curved regions of the cell membrane.

References

1. D. Chapman, Biol. Membranes, 1, 125 (1968).
2. A. Tardieu, V. Luzzati and F.C. Reman, J. Mol. Biol., 75, 711 (1973).
3. B.D. Ladbrooke and D. Chapman, Chem. Phys. Lipids, 3, 304 (1969).
4. M.C. Phillips, Prog. Surf. Sci., 5, 139 (1972).
5. H.J. Hinz and J.M. Sturtevant, J. Biol. Chem., 247, 6071 (1972).
6. R.P. Rand, D. Chapman and K. Larsson, Biophys. J., 15, 1117 (1975).
7. M.J. Janiak, D.M. Small and G.G. Shipley, Biochemistry, 15, 4575 (1976).
8. T. Gulik-Krzywicki, Biochim. Biophys. Acta, 415, 1 (1975).
9. D.S. Cannell, private comunications (1977).
10. J.F. Nagle, Proc. Nat. Acad. Sci. (U.S.), 70, 3443 (1973).
11. J.F. Nagle, J. Chem Phys., 58, 252 (1973).
12. M.B. Jackson, Biochemistry, 15, 2555 (1976).
13. S. Marčelja, J. Chem. Phys., 60, 3599 (1974).
14. S. Marčelja, Biochim. Biophys. Acta, 367, 165 (1974).
15. L. Scott, J. Magn. Reson.,in press (1977).
16. J.M. Steim, M.E. Tourtellote, J.C. Reinert, R.N. McElhaney and R.L. Rader, Proc. Nat. Acad. Sci. (U.S.), 63, 104 (1969).
17. J.F. Blazylet and J.M. Steim, Biochim. Biophys. Acta, 266, 737 (1972).
18. J.C. Reinert and J.M. Steim, Science, 168, 1580 (1970).
19. D.L. Melchior, H.J. Morowitz, J.M. Sturtevant and T.Y. Tsong, Biochim. Biophys. Acta, 219, 114 (1970).
20. D. Chapman and J. Urbina, FEBS Letters, 12, 169 (1971).

21. R. Lawaczeck, M. Kainosho, J.L. Girardet and S.I. Chan, Nature, 256, 584 (1975).

22. R. Lawaczeck, M. Kainosho and S.I. Chan, Biochim. Biophys. Acta, 443, 313 (1976).

23. D.J. Vaughan and K.M. Keough, FEBS Letters, 47, 158 (1974).

24. N.O. Petersen, P.A. Kroon, M. Kainosho and S.I. Chan, Chem. Phys. Lipids, 14, 343 (1975).

25. H. Seltz, J. Am. Chem. Soc., 56, 307 (1934).

26. M.C. Phillips, B.D. Ladbrooke and D. Chapman, Biochim. Biophys. Acta, 196, 35 (1970).

27. P.H.J.Th. Ververgaert, A.J. Verkleij, P.R. Elbers and L.L.M. van Deenen, Biochim. Biophys. Acta, 311, 320 (1973).

28. B.D. Ladbrooke, R.M. Williams and D. Chapman, Biochim. Biophys. Acta, 150, 333 (1968).

29. H. Lecuyer and D.G. Dervichian, J. Mol. Biol., 45, 39 (1969).

30. J.C. Hsia, H. Schneider and I.C.P. Smith, Can. J. Biochem., 49, 614 (1971).

31. A. Darke, E.G. Finer, A.G. Flook and M.C. Phillips, J. Mol. Biol., 63, 265 (1975).

32. E. Oldfield and D. Chapman, FEBS Letters, 23, 285 (1972).

33. J.L. Lippert and W.L. Peticolas, Proc. Nat. Acad. Sci. (U.S.), 68, 1572 (1971).

34. H. Träuble and H. Eibl, Proc. Nat. Acad. Sci. (U.S.), 71, 214 (1974).

35. K. Jacobson, D. Papahadjopoulos, Biochemistry, 14, 152 (1975).

36. A.J. Verkleij, B. DeKruyff, P.H.J.Th. Ververgaert, J.F. Tocanne

and L.L.M. van Deenen, Biochim. Biophys. Acta, 339, 432 (1974).

37. D. Lichtenberg, N.O. Petersen, J.L. Girardet, M. Kainosho, P.A. Kroon, C.H.A. Seiter, G.W. Feigenson and S.I. Chan, Biochim. Biophys. Acta, 382, 10 (1975).

38. A.C. McLaughlin, P.R. Cullis, J.A. Berden and R.E. Richards, J. Magn. Reson., 20, 146 (1975).

39. R.Bar-Adon and H. Gilboa, VIIth International Conference on Magnetic Resonance in Biological Systems, St. Jovite, Canada, (1976).

40. G.N. Lewis and M. Randall, revised by K.S. Pitzer and L. Brewer, in "Thermodynamics" 2nd Ed., McGraw-Hill Book Co., 1965, p. 225.

41. ibid, p. 156 and p. 204.

42. P.H. von Dreele, J. Am. Chem. Soc., submitted for publication (1976).

43. A.G. Lee, Biochim. Biophys. Acta, 413, 11 (1975).

44. P.R. Cullis, FEBS Letters, 70, 273 (1976).

45. M. Sheetz and S.I. Chan, Biochemistry, 11, 4573 (1972).

46. P.H. von Dreele and S.I. Chan, Proc. Nat. Acad. Sci. (U.S.), submitted for publication (1976).

47. D.M. Michaelson, A.F. Horwitz and M.P. Klein, Biochemistry, 12, 2637 (1973).

48. A. Chrzeszczyk, A. Wishnia and C.S. Springer, Jr., A.C.S. Symposium, 34, 483 (1976).

49. B.P. Gaber and W.L. Peticolas, Biochim. Biophys. Acta, submitted for publication (1976).

50. H. Bourgès, D.M. Small and D.G. Dervichian, Biochim. Biophys. Acta, 137, 157 (1967).

51. Y. Inoko, T. Yamguchi, K. Furuya and T. Mitsui, Biochim. Biophys.

Acta, 413, 24 (1975).

52. D.M. Engelman and J.E. Rothman, J. Biol. Chem., 247, 3694 (1972).

53. J.E. Rothman and D.M. Engelman, Nature (London) New Biology, 237, 42, (1972).

54. B. DeKruyff, R.A. Demel, A.J. Slotboom, L.L.M. van Deenen and A. F. Rosenthal, Biochim. Biophys. Acta, 307, 1 (1973).

55. H.J. Hinz and J.M. Sturtevant, J. Biol. Chem., 247, 3697 (1972).

56. M.A. Hemminga and H.J.C. Berendsen, J.Magn. Reson., 8, 133 (1972).

57. J.M. Boggs and J.C. Hsia, Biochim. Biophys. Acta, 290, 32 (1972).

58. E. Sackman and H. Träuble, J. Am. Chem. Soc., 94, 4482 (1972).

59. E. Sackman and H. Träuble, J. Am. Chem. Soc., 94, 4492 (1972).

60. H. Träuble and E. Sackman, J. Am. Chem. Soc., 94, 4499 (1972).

61. P.A. Kroon, M. Kainosho and S.I. Chan, Nature, 256, 582 (1975).

62. G.W. Stockton, C.F. Polnaszek, A.P. Tulloch, F. Hasan and I.C.P. Smith, Biochemistry, 15, 954 (1976).

63. G.W. Stockton, C.F. Polnaszek, L.C. Leitch, A.P. Tulloch and I.C. P. Smith, Biochem. Biophys. Res. Commun., 60, 884 (1974).

64. A. Darke, E.G. Finer, A.G. Flook and M.C. Phillips, FEBS Letters, 18, 326 (1971).

65. M.C. Phillips and E.G. Finer, Biochim. Biophys. Acta, 356, 199 (1974).

66. J. Ulmius, H. Wennerström, G. Lindblom and G. Arvidson, Biochim. Biophys. Acta, 389, 197 (1975).

67. M.C. Phillips, H. Hauser and F. Paltauf, Chem. Phys. Lipids, 8, 127 (1972).

68. M.P.N. Gent and J.H. Prestergaard, Biochemistry, 13, 4027 (1974).

69. S.M. Johnson, Biochim. Biophys. Acta, 307, 27 (1973).

70. R. Mendelsohn, Biochim. Biophys. Acta, 290, 15 (1972).

71. E.J. Shimshick and H.M. McConnell, Biochemistry, 12, 2351 (1973).

72. I.C.P. Smith, private communication, VIIth International Conference on Magnetic Resonance in Biological Systems, St. Jovite, Canada, (1976).

73. N.O. Petersen, unpublished results (1976).

V. STUDIES OF INTERMEMBRANE INTERACTIONS IN SMALL BILAYER VESICLES. THE EFFECTS OF CHANGING SURFACE PROPERTIES BY THERMAL TRANSITIONS OR BY ADSORPTION OF DIVALENT CATIONS ON THE AGGREGATION OF VESICLES.

1. Introduction

Small phospholipid bilayer vesicles are studied extensively as a model membrane system for a number of reasons. They are excellent for permeation studies because they provide a single-walled partition between two aqueous solutions. They can be prepared in sizes equivalent to those of vesicles found *in vivo*, for example presynaptic vesicles (1). Reconstituted protein-lipid bilayer systems as well as isolated membrane fragments are conveniently prepared in the form of nearly spherical, small vesicles (2). Furthermore, since vesicles tend to undergo vesicle-vesicle fusion (3) they are excellent systems in which to study the membrane fusion process. It is possible that appropriately prepared vesicles may be used to introduce, through vesicle fusion with the cell membrane, selected components into specific cell membranes. Analogously, it is likely that chemical agents contained within the vesicle can be injected into selected cells through a fusion process. Details of how the fusion process occurs and how it may be controlled and targeted to certain cells *in vitro* or *in vivo* are not yet established.

In model systems, it has been shown (4,5,6) that the presence of fatty acid or lysolecithin components in the vesicle bilayer tend to enhance the rate of vesicle-vesicle fusion in certain cases. Similarly, surface active agents, specifically alamethicin, have been found to accelerate the fusion process when present on the external bilayer sur-

face (7). The effect of these agents may be twofold. First, they may modify the surface properties of the bilayer, allowing vesicle-vesicle contact for a long enough period of time for fusion to occur. Second, they may destabilize the bilayer structure, such that fusion becomes more favorable.

One conclusion arrived at in Chapters III and IV is that the phospholipid bilayer constituting small vesicles is structurally and dynamically different from that of liposomes. The NMR data, when interpreted in terms of the motional model discussed in Chapter III, indicate that the vesicle bilayer allows greater chain fluctuations and at a faster rate. The phase transition data for mixed phospholipids (8) and phospholipid-cholesterol mixtures (Chapter IV) suggest that the phase equilibria are different in the two bilayer systems, reflecting (i) a larger lateral surface pressure (9), (ii) weaker intermolecular interactions (8) and (iii) an asymmetric distribution of components between the two monolayers (10,11) for the vesicles. For these reasons, much of the thermodynamic data obtained for liposomes (Chapter IV) is not directly relevant to the vesicle bilayer stability, so that it is necessary to study the vesicle bilayer system itself. The results of Figure 20 demonstrate that the DTA technique is not sensitive enough for measurements on dilute vesicle systems. In contrast, measurement of turbidity changes with temperature can be performed on quite dilute samples (Figure 21) and are indeed sensitive to changes in the bilayer phase (11,12,13). Since light scattering or turbidity measurements are also ideally suited for measuring changes in the state of aggregation of colloids (14,15,16a), we felt that a careful study of turbidity

as a function of temperature and time could yield valuable information on the nature of thermal phase transitions as well as the state of aggregation in the vesicle system. Through such measurements, we can assess the relative influence of aggregation and fusion on vesicle stability. Thus, we can learn to control and manipulate the rate of fusion by changing vesicle aggregation and bilayer stability.

In this chapter we present absorbance data measured for vesicle suspensions as a function of temperature, time and ionic composition. We discuss first the origin of changes in absorbance at the thermal phase transitions and present evidence for the existence of a pretransition in vesicles. Next, we interpret time dependent absorbance changes in terms of classical colloidal theory pertaining to the interaction of two spherical particles. This interpretation allows us to describe the state of aggregation of a vesicle suspension through the processes of flocculation and coagulation.

2. Analysis of Absorbance Measurements

For a non-absorbing system the turbidity, τ, is defined for a 1 cm path length by (17a)

$$\tau = -\ln\left(\frac{I}{I_0}\right) = 2.303 \log\left(\frac{I}{I_0}\right) = 2.303\ A \qquad \text{(V-1)}$$

and is a measure of the integrated intensity of light scattered at all angles. Here I_0 is the incident intensity, I is the intensity of the transmitted light and A is the measured absorbance. The turbidity is often rewritten as

$$\tau = -\ln\left(1 - \frac{I_o - I}{I_o}\right) = -\ln(1 - x)$$

$$= x + \frac{1}{2}x^2 + \frac{1}{3}x^3 + \frac{1}{4}x^4 + \ldots \qquad \text{(V-2)}$$

where $x = \frac{I_o - I}{I_o} < 1$. Clearly, if $x \ll 1$, the turbidity simply is

$$\tau = x = \frac{I_o - I}{I_o} \qquad \text{(V-3)}$$

If x is greater than $\sim$0.2, the higher order terms in the expansion in eq V-2 contribute significantly (> 10%). In practice then, the approximation in eq V-3 is not valid for absorbance values greater than 0.1 cm^{-1}. For lipid vesicle suspensions and colloidal suspensions in general, the turbidity is usually larger than 0.2 cm^{-1} and eq V-3 is not applicable. Accordingly, interpretation of the turbidity under these conditions is not straightforward. However, as we shall show, turbidity ratios may provide a measure of changes in the light scattering properties of these systems.

The intensity difference, $I_o - I$, is the integrated intensity of light scattered at all angles, and thus (17a)

$$I_o - I = \int_0^{\pi} 2\pi r^2 i_\theta \sin\theta d\theta \qquad \text{(V-4)}$$

where i_θ is the intensity of light scattered at the angle θ when observed at a distance r from the sample. The intensity of light scattered by small particles in solution is given by

$$i_\theta = I_o \frac{2\pi^2 Mc\ \tilde{n}_o^2 (\partial\tilde{n}/\partial c)^2 (1 + \cos^2\theta)}{N\lambda^4 r^2} \qquad (V\text{-}5)$$

where M is the molecular weight and c, the concentration (in g/cm^3) of the scattering particles, $\tilde{n}_o$ the refractive index of the solvent, $\partial\tilde{n}/\partial c$ the specific refractive index increment, N, Avogadro's number and λ the wavelength of light employed. Equation V-5 is applicable for an unpolarized light source. It is customary (17b) to express the scattered light intensity in terms of the Rayleigh ratio $r^2 i_\theta / I_o$, or

$$R_\theta = r^2 i_\theta / I_o (1 + \cos^2\theta) \qquad (V\text{-}6)$$

For particles with dimensions much smaller than the wavelength, where eq V-5 is valid, the ratio in eq V-6 is independent of the angle θ and is often written as

$$R_o = \frac{2\pi^2 Mc\ \tilde{n}_o^2 (\partial\tilde{n}/\partial c)^2}{N\lambda^4} \qquad (V\text{-}7)$$

which corresponds to the so-called limit of Rayleigh scattering.

If the particle dimension is larger than about $\lambda/20$, but less than $\lambda/2$, the intensity of the light scattered at a given angle is attenuated by interference of light scattered from different points within the particle. This is the Rayleigh-Gans limit of scattering, provided the refractive index difference between solute and solvent is small. The attenuation of intensity at a given angle is corrected for by the introduction of a particle scattering function, $P(\theta)$, defined

by the relation (16b,17c)

$$R_\theta = R_o\, P(\theta) \tag{V-8}$$

where R_θ is given by eq V-6, R_o is given by eq V-7, with i_θ in eq V-6 being

$$i_\theta = I_o \frac{2\pi^2 Mc\, \tilde{n}_o^{\,2} (\partial\tilde{n}/\partial c)^2 (1 + \cos^2\theta)}{N\lambda^4 r^2} \cdot P(\theta) \tag{V-9}$$

The particle scattering function is a purely geometric correction factor and in principle can be calculated for any particle with n scattering points by (17d)

$$P(\theta) = \frac{1}{n^2} \sum_{i=1}^{n} \sum_{j=1}^{n} \frac{\sin\mu r_{ij}}{\mu r_{ij}} \tag{V-10}$$

where r_{ij} is the separation of points i and j, and $\mu = 4\pi\sin(\theta/2)/\lambda$.

For bilayer vesicles, the particle scattering function has been calculated assuming a homogeneous bilayer (12,13) as well as an anisotropic bilayer (22,24). For turbidity experiments, the integrated intensity will depend on the integrated particle scattering function. By eq V-4

$$I_o - I = \int_0^{\pi} 2\pi r^2 i_\theta \sin\theta d\theta$$

$$= \int_0^{\pi} 2\pi I_o R_\theta (1 + \cos^2\theta)\sin\theta d\theta$$

$$= 2\pi I_o R_o \int_0^{\pi} P(\theta)(1 + \cos^2\theta)\sin\theta d\theta$$

$$= \frac{16\pi}{3} I_o R_o Q \qquad \text{(V-11)}$$

where Q is the particle dissipation factor defined by (16c)

$$Q \equiv \frac{3}{8} \int_0^{\pi} P(\theta)(1 + \cos^2\theta) \sin\theta d\theta \qquad \text{(V-12)}$$

Hence, the turbidity can be written as

$$\tau = -\ln (1 - \frac{16\pi}{3} R_o Q) \qquad \text{(V-13)}$$

which for small values of the turbidity gives

$$\tau \simeq \frac{16}{3} R_o Q = \tau_o Q \qquad \text{(V-14)}$$

The approximation in eq V-14 is not, however, adequate if the absorbance (eq V-1) is greater than 0.1 cm^{-1}. Although the particle dissipation factor is occasionally defined by the relation $\tau = \tau_o Q$ (16c), it must be noted that the Q so defined bears no relation to that in eq V-12 unless τ is small. Equation V-14 also illustrates that the rela-

tion (17a)

$$\tau = \frac{16}{3} R_\theta \tag{V-15}$$

is only valid in the Rayleigh scattering limit, for which Q = 1 and $R_\theta = R_o$, and for small τ. It is therefore not realistic to expect that the turbidity measured for vesicle suspensions will obey V-15 or even V-14. Further, a ratio of turbidity measurements at different temperatures of times does not necessarily represent the corresponding ratios of the R_θ values or the R_oQ values. It is possible, however, to obtain the quantity R_oQ from a turbidity measurement by eq V-13. Thus by eq V-2 and eq V-13, the ratio of turbidities, τ_2/τ_1, at two temperatures, say, will be

$$\frac{\tau_2}{\tau_1} = \frac{x_2}{x_1}\left\{1 + \frac{1}{2}(x_2 - x_1) + \frac{1}{12}(4x_2^2 - x_1^2 - 3x_2x_1)\right.$$

$$\left. + \frac{1}{12}(6x_2^3 - 4x_2^2x_1 - x_2x_1^2 - x_1^3) + \ldots\right\} \tag{V-16}$$

where $x_i = 16\pi R_{oi}Q_i/3$. If the turbidities are close, then the error in the approximation

$$\frac{\tau_2}{\tau_1} = \frac{x_2}{x_1} = \frac{R_{o2}Q_2}{R_{o1}Q_1} \tag{V-17}$$

is small. Figure 44 illustrates the calculated value of the turbidity ratio τ_2/τ_1 as a function of x_1 for a series of x_2/x_1 values. The difference between the ratios is the correction from the higher order

FIGURE 44

The turbidity ratio τ_2/τ_1 as a function of x_1 (= I_1-I_o/I_o) given by eq V-16 for selected values of the ratio x_2/x_1 (indicated by the curves). The X illustrates that for a measured τ_2/τ_1 of 0.75 with x_1 = 0.85, the ratio x_2/x_1 is 0.85. These particular numbers refer to the experimental data found by Yi and MacDonald (12) (cf discussion section).

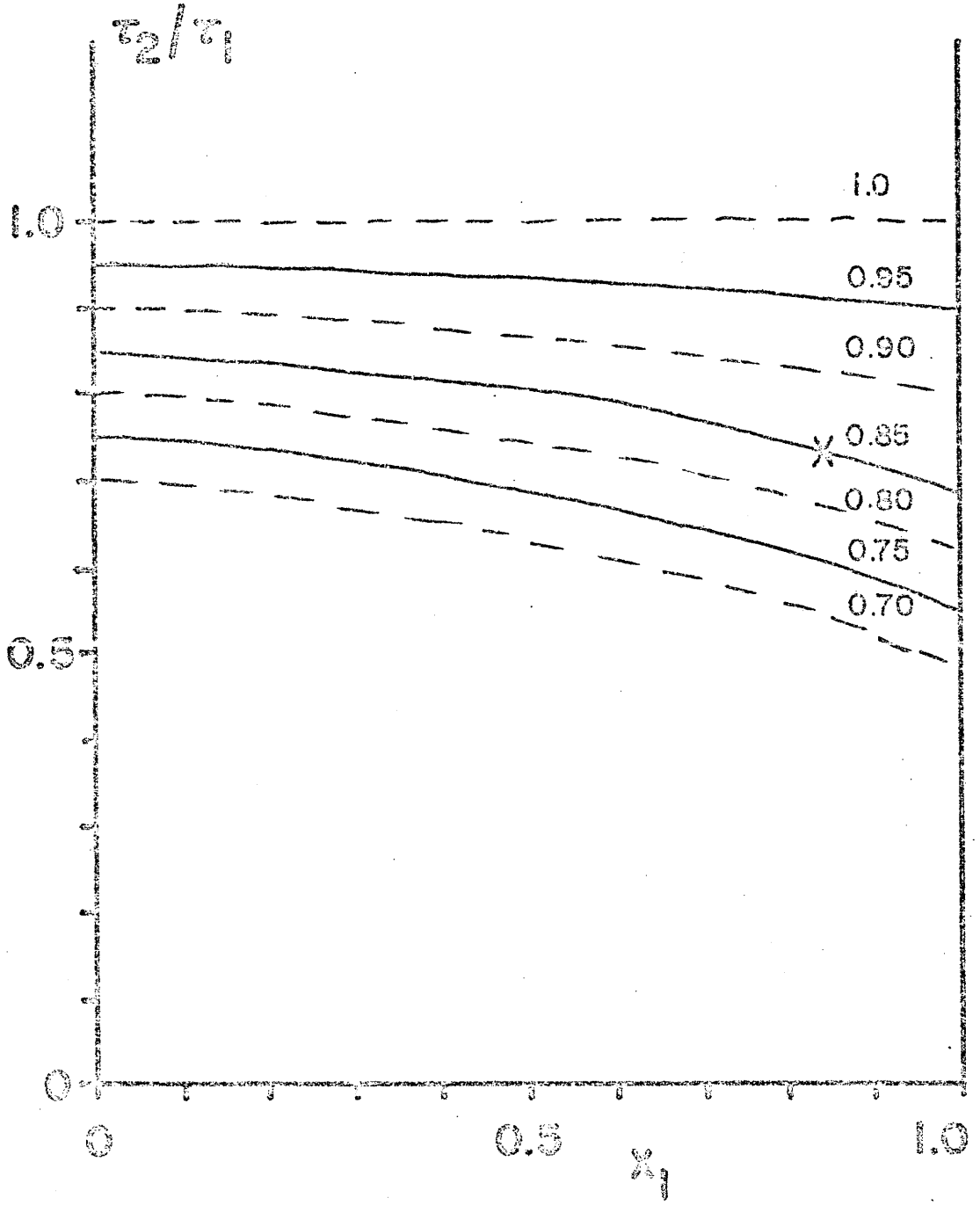
τ2/τ1
1.0
0.95
0.90
0.85
0.80
0.75
0.70
1.0
0.5
0
0
0.5
1.0
x1

terms in eq V-16, which, for a typical absorbance measurement of about 0.5 cm^{-1}, amounts to about 10 - 20%.

3. Results

In the following experiments, the absorbance, A, was measured as a function of temperature and time for a series of preparations of lipids in different salt solutions. These measurements were partly prompted by the findings (12) that light scattering and turbidity measurements are indeed sensitive to phase transitions in DPL vesicles in salt-free solutions, and partly by the desire to explore the aggregation properties of bilayer vesicles under various circumstances. In our studies we have measured the melting curves for liposomes and vesicles in $Ca(NO_3)_2$ and for vesicles in $La(NO_3)_3$, $NaNO_3$ and salt-free solutions. We have found evidence for a pretransition in these systems and have studied the hysteresis of this transition for liposomes and vesicles. The time dependence of the absorbance was monitored for vesicles, and has provided insight into the aggregation states of the vesicles as a function of salt and temperature.

a. Melting curves.

(i) Multilayers. The absorbance of a dilute liposome suspension (0.06% by weight DPL in 40 mM $Ca(NO_3)_2$) is shown in Figure 45 as a function of temperature. The heating curve (curve a) exhibits two abrupt decreases in absorbance, the larger of which occurs at 44°C and the smaller at about 37°C. The cooling curve (curve b) shows the change associated with the thermal phase transition at 44°C in the DPL bilayer but the absence of an absorbance change at the pretransition

FIGURE 45

Traces of the absorbance changes with temperature for

a: heating of 0.06% by weight DPL liposomes in 40 mM $Ca(NO_3)_2$;

b: cooling of the sample heated in (a);

c: heating of 2% by weight DPL vesicles in 40 mM $Ca(NO_3)_2$.

The inset illustrates how the extrapolated turbidities at the transition are obtained. The ratio of τ_2 to τ_1 is used to determine R (eq V-18).

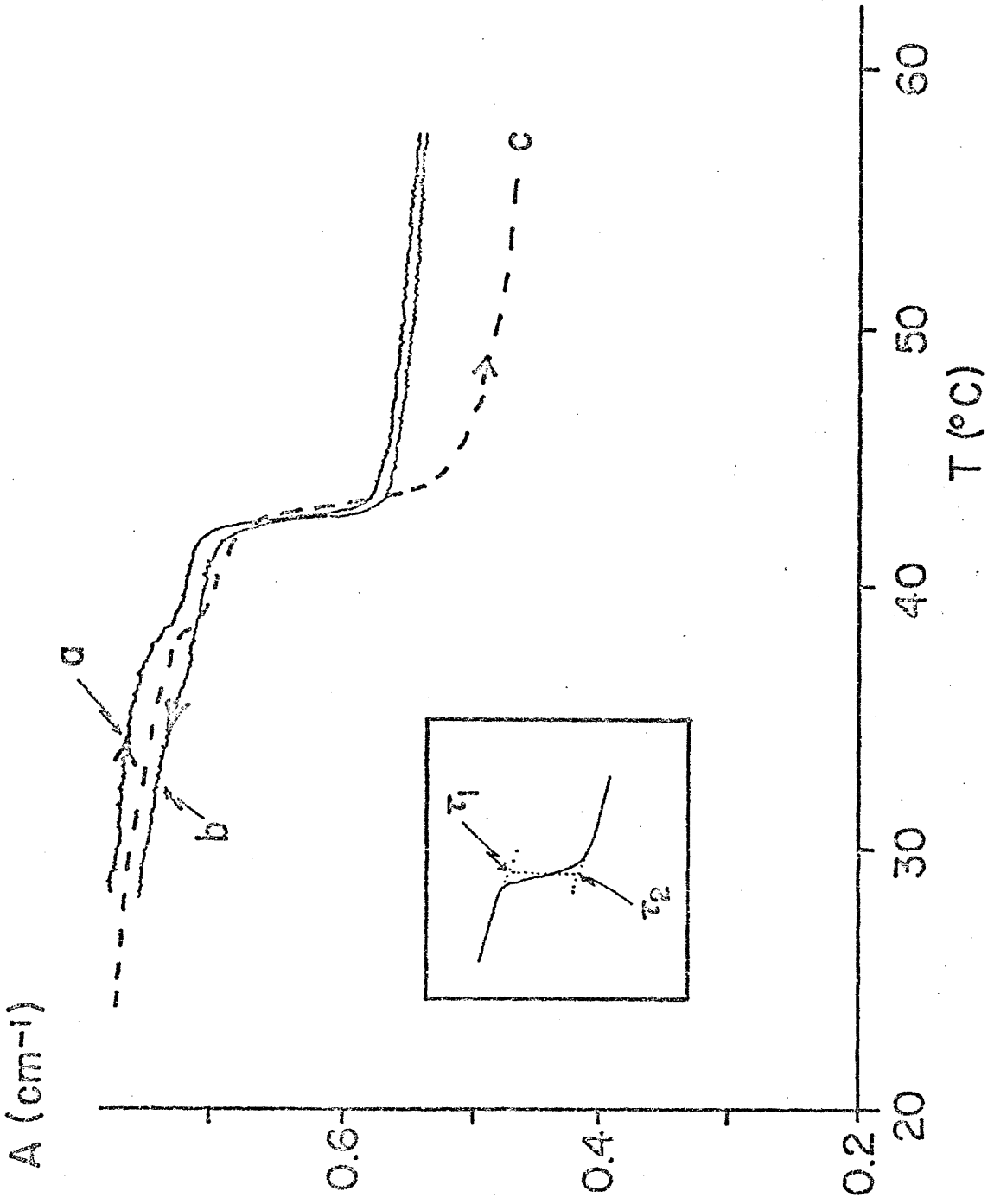
A (cm⁻¹)
0.6
0.4
0.2
20
30
40
50
60
T (°C)
a
b
c
τ1
τ2

temperature is apparent. The presence of calcium ions causes the phase transition temperature to be a few degrees higher (18,19,20) than the 41-42°C usually observed (Chapter IV)

Numerous attempts to measure the melting curve for dilute salt-free, unsonicated lipid dispersions failed because of instability of the suspension. There was a large drift in the turbidity while the suspension settled.

In order to describe the absorbance transition curves quantitatively, it is convenient to define the following ratios

$$R_{main} \equiv \tau(T_c + \Delta T)/\tau(T_c - \Delta T)$$

$$R_{pre} \equiv \tau(T_p + \Delta T)/\tau(T_p - \Delta T) \quad \text{and}$$

$$R_{total} \equiv \tau(T_c + 10^{\circ}C)/\tau(T_c - 10^{\circ}C) \qquad \text{(V-18)}$$

where, as before (Chapter IV), T_c and T_p are the temperatures at which the Chapman and the pretransition, respectively, take place. ΔT is a small increment of temperature greater than the transition width. In practice, R_{main} or R_{pre} is obtained as the ratio (τ_2/τ_1) where τ_2 and τ_1 are the extrapolated values of the turbidity at T_c (or T_p) (Figure 45, inset). The values obtained for these parameters from the curves in Figure 45 are listed in Table 4.

(ii) Sonicated vesicles in $Ca(NO_3)_2$. The equivalent melting curve for a week old, sonicated suspension of small DPL vesicles in 40 mM $Ca(NO_3)_2$ is included in Figure 45 (curve c). In this curve the

TABLE 4

Turbidity Ratios Defined by Eq V-18 for

Several Preparations of Lecithin Suspensions

Sample	R_{main}	R_{pre}	R_{total}
Unsonicated DML liposomes in $Ca(NO_3)_2$	0.73	-	-
Unsonicated DPL liposomes in $Ca(NO_3)_2$	0.82	0.97	0.70
Unsonicated DSL liposomes in $Ca(NO_3)_2$	0.89	-	-
Sonicated DPL vesicles in $Ca(NO_3)_2$	0.72	0.96	0.63
Sonicated DPL vesicles in $La(NO_3)_3$	0.72	1.00	0.70
Sonicated DPL vesicles in ^2H_2O (t = 0)	0.76	0.52	0.36
Sonicated DPL vesicles in ^2H_2O (t = 48 hrs)	0.75	0.37	0.27

transition occurs over a slightly broader temperature range and the change in absorbance through the transition is proportionally larger. It is evident from Table 4 that the R_{main} and R_{total} values are significantly smaller for the vesicle system, whereas R_{pre} is not much different.

(iii) Sonicated vesicles in $La(NO_3)_3$. Preparations of sonicated DPL vesicles in 20 mM $La(NO_3)_3$ solutions exhibit absorbance changes with temperature which are comparable to those of vesicles in 40 mM $Ca(NO_3)_2$. There is, however, no detectable absorbance change at the pretransition temperature for these samples in $La(NO_3)_3$.

(iv) Sonicated vesicles in neat ^2H_2O. Figure 46 shows the heating (a,b) and cooling (a',b') curves for sonicated DPL vesicles in ^2H_2O immediately (10 min) after preparation (a,a') and 48 hours later (b,b'). The R_{main} , R_{pre} and R_{total} values for the two heating curves are also listed in Table 4. It is evident that R_{pre} and R_{total} are much smaller than those for the sonicated vesicles in $Ca(NO_3)_2$ whereas R_{main} is about the same. The cooling curves once again show no absorbance changes at the pretransition. This was characteristic of all the cooling curves measured, independent of the nature of the sample. However, the absorbance change could be observed upon reheating under certain conditions.

b. The hysteresis of the pretransition.

The cooling curves of Figures 45 and 46 suggest that there is a hysteresis in the pretransition. It is possible to maintain the sample temperature at 28°C or higher for several hours without observing any increase in the sample absorbance. However, if the temperature is

FIGURE 46

Absorbance changes as a function of temperature for 2% by weight DPL vesicles in $^{2}H_{2}O$. a and b are heating curves, a' and b' the corresponding cooling curves. a and a' were obtained 10 min after preparation whereas b and b' were measured 48 hrs later for the same sample kept in the meantime at room temperature.

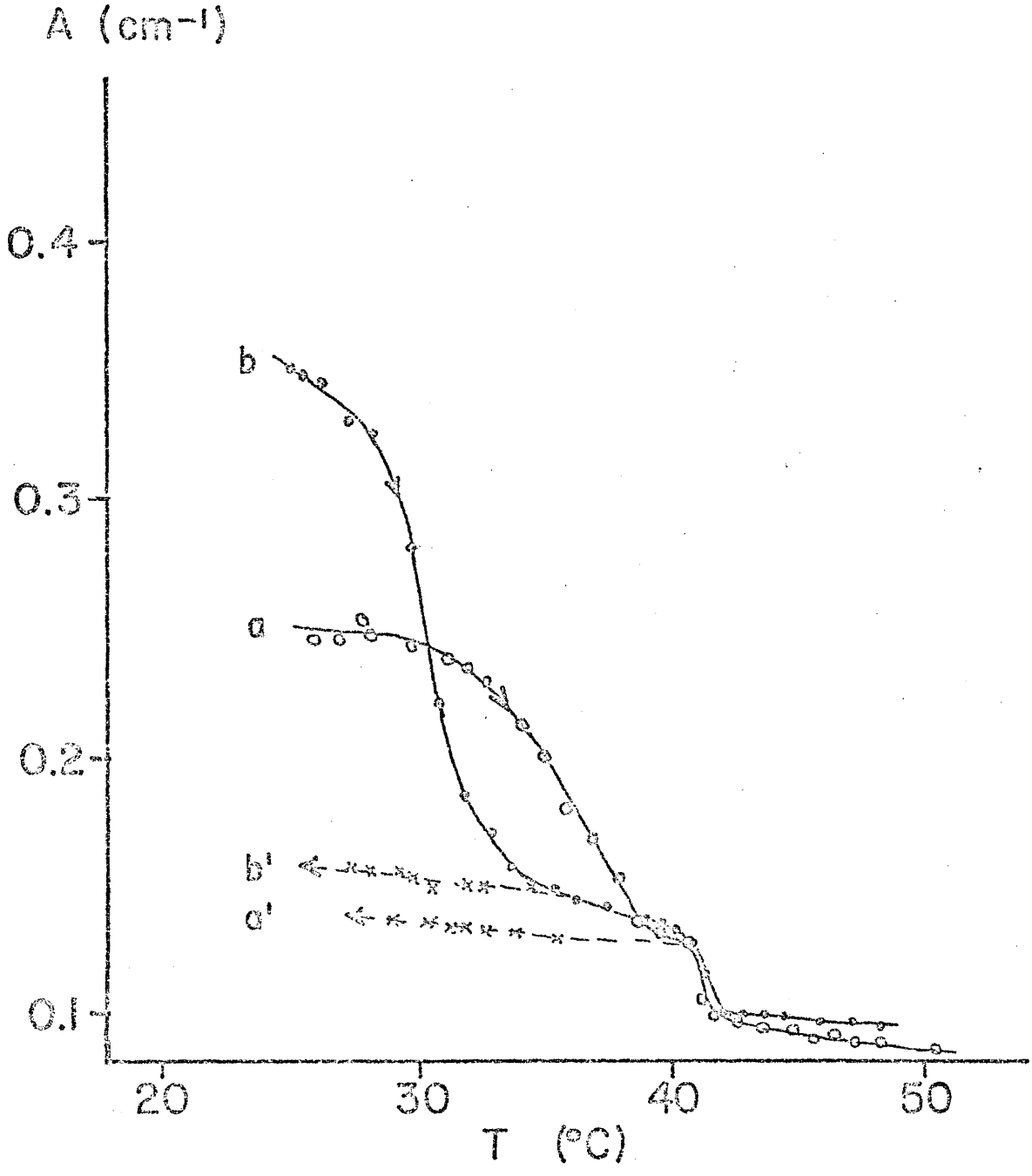
A (cm⁻¹)
0.4
0.3
0.2
0.1
b
a
b'
a'
20
30
40
50
T (°C)

maintained at 25°C, the absorbance increases slowly and reaches 50, 75 and 100% of its original value in about 10, 20 and 60 minutes, respectively. After 60 min the absorbance continues to increase but at a slower rate. At lower temperatures the absorbance reaches its original value faster.

The hysteresis effect and the time course of recovery of sample absorbance for a dilute vesicle suspension can be correlated with the hysteresis observed in differential thermal analysis for the pretransition in liposomal preparations. This hysteresis is characterized by the observation that, following a heating and cooling cycle, the pretransition will not reappear in the subsequent DTA heating curve unless the sample has been cooled to a temperature lower than about 8-10°C below the pretransition temperature. Furthermore, at 10-12°C below the pretransition temperature, the DTA pretransition reappears at a slow rate and recovers fully after about an hour. At lower temperatures the recovery is substantially faster.

Qualitatively, the DTA hysteresis effects observed in pure lipid systems and ideally mixed lipid systems are identical. A particularly well documented example of the hystersis and the recovery is illustrated in Figure 47 for a 1:1 mixture of DPL and DPL-d_{62}. In the sequence of thermograms b to h, the sample is cooled to different temperatures below the pretransition, and after one minute, is reheated. In the sequence h to l, the sample is cooled to 23°C and left from 1 to 90 minutes at that temperature (± 1°C). The percentage recovery of the pretransition as a function of time kept at 23°C (shown in the graph of Figure 46) was calculated from the peak height of the thermograms

FIGURE 47

Illustration of the pretransition hysteresis.
A. The sequence of DTA heating curves labelled b through h, illustrates that there is no evidence for recurrence of the pretransiton till the sample is cooled to $\sim 10^{\circ}$ below the pretransition temperature. Lowest temperature is in (b) $31^{\circ}C$, (c) $30^{\circ}C$, (d) $29^{\circ}C$, (e) $28^{\circ}C$, (f) $27^{\circ}C$, (g) $25^{\circ}C$, and (h) $23^{\circ}C$. The sequence from h to l illustrates the time rate of recovery of the pretransition when the sample is kept at $23^{\circ}C$ for (h) 1 min, (i) 2 min, (j) 5 min, (k) 10 min and (l) 80 min.
B. The recovery curve obtained from these scans.

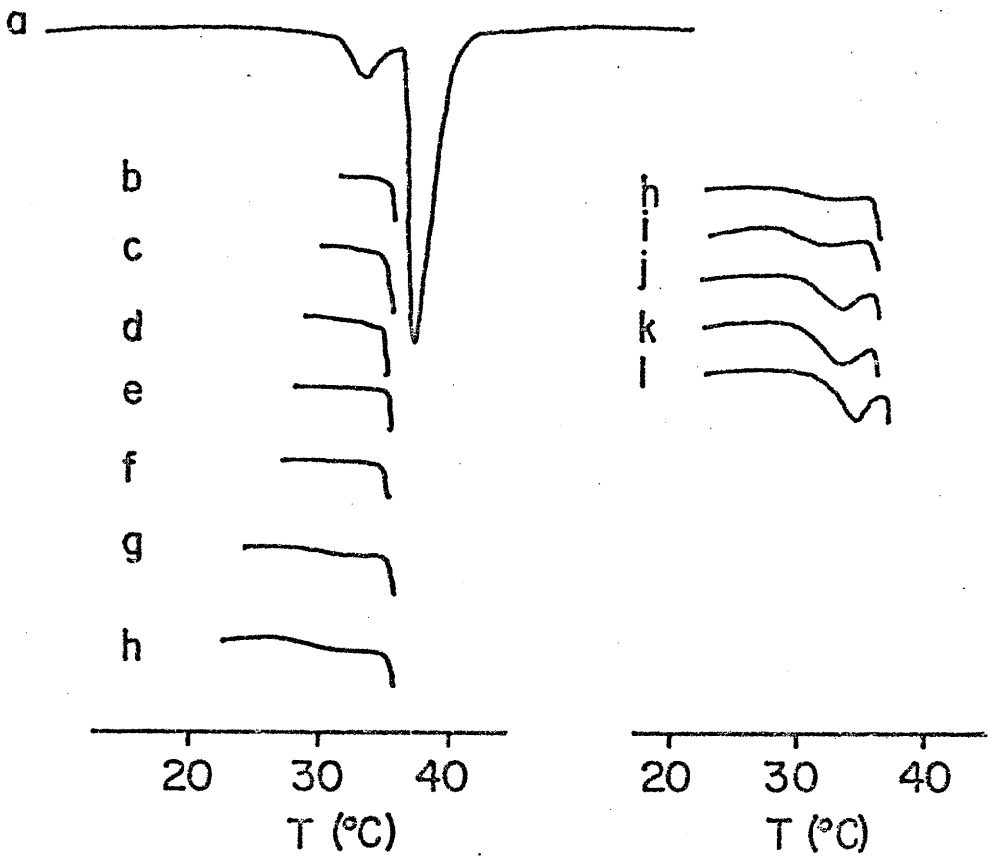
a
b
c
d
e
f
g
h
20
30
40
T (°C)
h
i
j
k
l
20
30
40
T (°C)

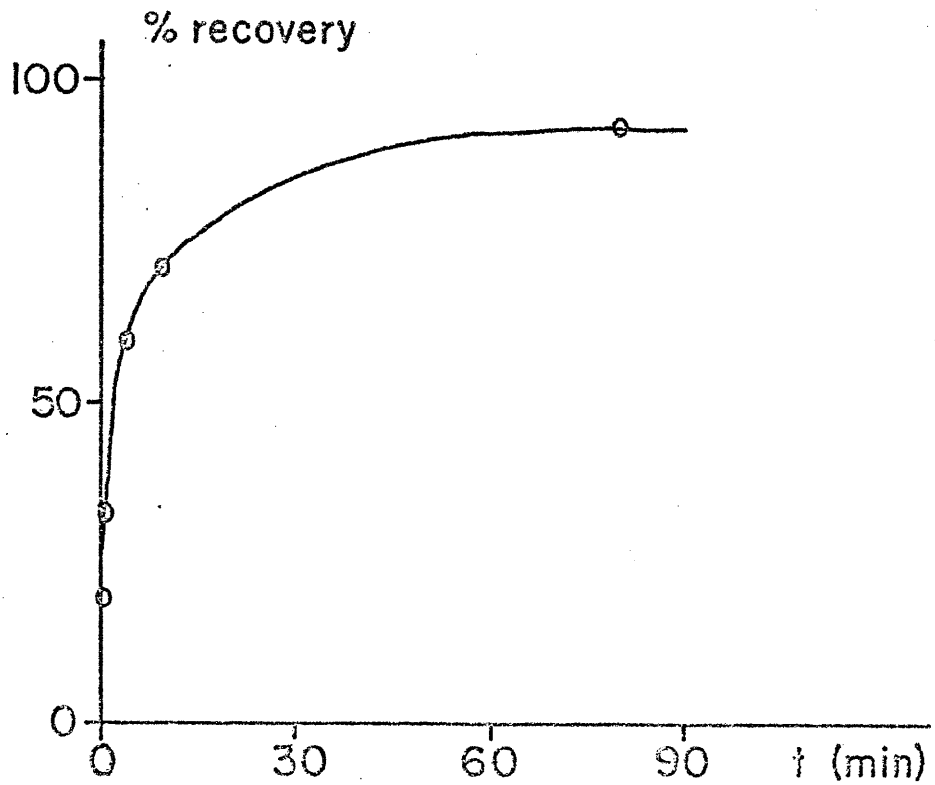
% recovery
100
50
0
0
30
60
90
t (min)

labelled h to l relative to that of a. The main transition did not change significantly in these runs, so the pretransition signal height was normalized to the main transition signal height.

Figure 47 illustrates that when a liposome sample is heated through the transition and cooled to 23°C, the intensity of the DTA pretransition on subsequent heating increases with the length of time the sample is kept at 23°C. However, the intensity never exceeds that observed in the first DTA heating curve for samples prepared well in advance of the measurement. Similarly, when a liposome sample is heated and cooled to about 23°C, the absorbance of the sample at 23°C slowly increases and reaches but seldom exceeds the absorbance value observed for the sample at 23°C prior to the heating-cooling cycle. In contrast, the absorbance at 23°C for a vesicle sample which has been subjected to a similar heating-cooling cycle increases steadily. These observations will be presented in detail in the following subsection.

c. Time dependent absorbance changes for vesicle suspensions.

(i) DPL vesicles in neat ^2H_2O. The effect on the heating curve of keeping a suspension of small DPL vesicles in ^2H_2O at 23°C for 48 hours is seen in Figure 46. At each temperature, the absorbance increases with time but to varying extents. We follow the absorbance changes at several temperatures by measuring the entire heating curve at selected times. In order to characterize these absorbance changes we define the ratio of the turbidity at time zero to that at time t for a given temperature, T, by

$$r_T(\tau) = \tau(0)/\tau(t) \qquad \text{(V-19)}$$

We also find R_{main}, R_{pre} and R_{total} for the melting curve at each time. For the curves in Figure 46 we find $r_{25} = 0.69$ and $r_{50} = 0.95$ after the sample has been kept 48 hours at room temperature. Clearly, the absorbance change over this period of time is much larger at 25°C than at 50°C. This is a characteristic trait of the absorbance for vesicles in salt-free solutions or in monovalent salt solutions (see below).

(ii) DPL vesicles in monovalent salts. Samples prepared with $NaNO_3$ or NaCl exhibit absorbance changes similar to those observed for samples without salts. Because the absorbance in these systems is usually rather large and difficult to quantify, very few heating curves were measured.

Vesicles prepared in neat ^2H_2O exhibit an absorbance increase when a monovalent salt solution is added at room temperature. Moreover, the increase is greater the higher the salt concentration. However, if the samples are heated to a temperature above the transition temperature, the salt-dependent absorbance increase almost disappears. The "salting-out" phenomenon is even more pronounced for vesicles prepared with purified DPL. In these systems, a turbid flocculate actually separates at room temperature a few hours after addition of NaCl. The flocculate disperses spontaneously (without shaking or stirring) at temperatures above about 40°C, but when cooled to room temperature, the flocculate reappears within several minutes. This dispersion-flocculation cycle was observed while heating and cooling the sample for several weeks. The effect of NaCl concentration on the amount of flocculate in a 1% by weight DPL suspension is shown in Figure 48. The flocculate appears at the surface in these ^2H_2O solutions because the lipid

FIGURE 48

Illustration of the salting-out effect of DPL vesicles in NaCl solutions in $^{2}H_{2}O$ at 23°C. The turbid area at the top of the tubes is separated flocculates.

Sample 10-11: 0.00 M NaCl

10-12: 0.01 M NaCl

10-13: 0.05 M NaCl

10-14: 0.10 M NaCl

10-15: 0.20 M NaCl

10-16: 0.80 M NaCl

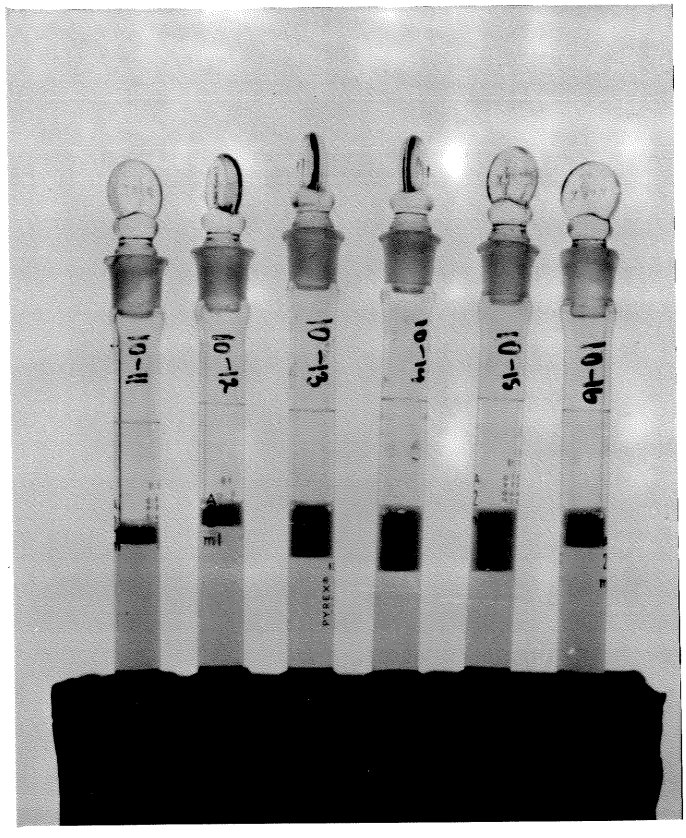
11-10
12-09
13-08
14-07
15-06
16-05

density is intermediate between the densities of heavy and light water.

(iii) DPL vesicles in $Ca(NO_3)_2$. When the heating curve is measured at selected times over a 200 hour period for a sample of DPL vesicles sonicated in 40 mM $Ca(NO_3)_2$ kept at 23°C, R_{main}, R_{pre} and R_{total} remain constant while r_{25} and r_{50} decrease steadily (Figure 49A). Both decrease at the same rate indicating that the phenomena responsible for the absorbance increases are not sensitive to temperature, in contrast to DPL in neat ^2H_2O.

We repeated the above experiments for several solutions with 1%, 2% and 5% by weight DPL. As illustrated in Figure 49B, there appears to be no concentration dependence of the relative absorbance changes, r_{25} and r_{50}. Nevertheless, the early part of the absorbance change is compatible with second order aggregation kinetics and suggests

$$A + A \rightarrow A_2 \qquad \text{(V-20)}$$

provided the absorbance increments are linearly proportional to the concentration of A_2. To elucidate the kinetics, it is necessary to extend these studies to a greater concentration range and to obtain more accurate light scattering data with better time resolution.

The rate of change of absorbance for DPL vesicles is also sensitive to the sample preparation and handling. A sample which was cooled slowly after the sonication step rather than being brought to room temperature immediately, as was usually done, showed a slower increase in absorbance (Figure 49B) when the sample was subjected to repeated heating-cooling cycles. This slower change in r_{25} and r_{50} may in part

FIGURE 49

A: Time dependence of the turbidity ratios defined in eqs V-18 and V-19 for 2% by weight DPL vesicles.

B: r_{25} (filled symbols and x) and r_{50} (open symbols and +) defined in V-19 for various samples of DPL in 40 mM $Ca(NO_3)_2$.

▽, ▼	1% by weight vesicles
o, ●	2% by weight vesicles
△, ▲	5% by weight vesicles
□, ■	1% by weight vesicles cooled slowly after sonication
◇, ◆	2% by weight vesicles kept at 55°C between melting curve measurements
+, x	0.06% by weight liposomes

The samples were kept at 23°C between the melting curve measurements except for the one case noted (◇, ◆).

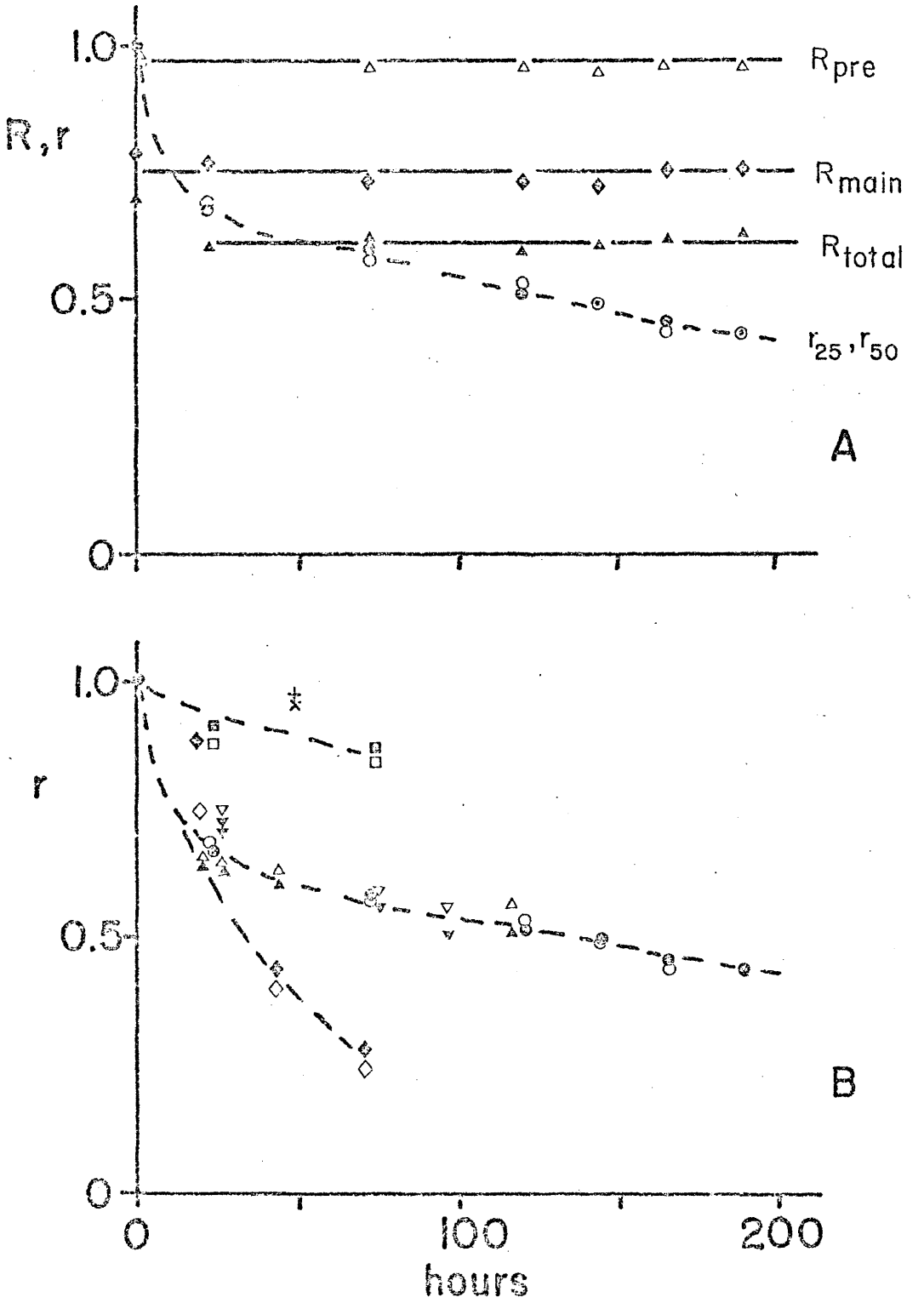
1.0
0.5
0
R, r
R_{pre}
R_{main}
R_{total}
r_{25}, r_{50}
A
1.0
0.5
0
r
B
0
100
200
hours

reflect the higher initial absorbance due to slow cooling. Also, a sample kept at 55°C between the transition curve measurements shows a greater rate of absorbance change and has an unusually large R_{main} value of 0.84. Qualitatively, it appears that the absorbance increases more rapidly if a sample is cycled through the transition many times, but this correlation is not yet fully documented.

(iv) DPL liposomes. In contrast to the steady absorbance increases observed in vesicles the time dependent absorbance changes for liposomes in $Ca(NO_3)_2$ are quite small (Figure 49B). Because liposome suspensions in salt-free preparations are unstable the particles settle, causing the absorbance to decrease.

d. Time dependent changes in the shape of vesicle melting curves.

Figure 50 shows selected melting curves measured at various intervals after sonication, for one sample of DPL in 40 mM $Ca(NO_3)_2$. The first heating curve (a) measured shortly after preparation exhibits a sharp rise in absorbance just below the main transition temperature (compare Figure 45). Upon immediate cooling and reheating the melting curve assumes the shape of b, which it maintains on subsequent heating-cooling cycles. If the sample is kept at room temperature for about a day, a' is observed in the first heating curve only. However, when it is allowed to sit another day or more at room temperature the first heating curves are always shaped like a".

The exact shape of the melting curves in similar experiments depends on the sample preparation but curve a (Figure 50) is representative of DPL vesicles in $Ca(NO_3)_2$ or $La(NO_3)_3$. On occasion similar effects are seen in salt-free solutions.

FIGURE 50

Selected absorbance melting curves for a sample of 2% by weight DPL vesicles in 40 mM $Ca(NO_3)_2$ kept for 1, 23 and 144 hours. Curves a, a' and a" are the first heating curves obtained at the time indicated whereas curves b and b" are the heating curves obtained immediately after cooling again.

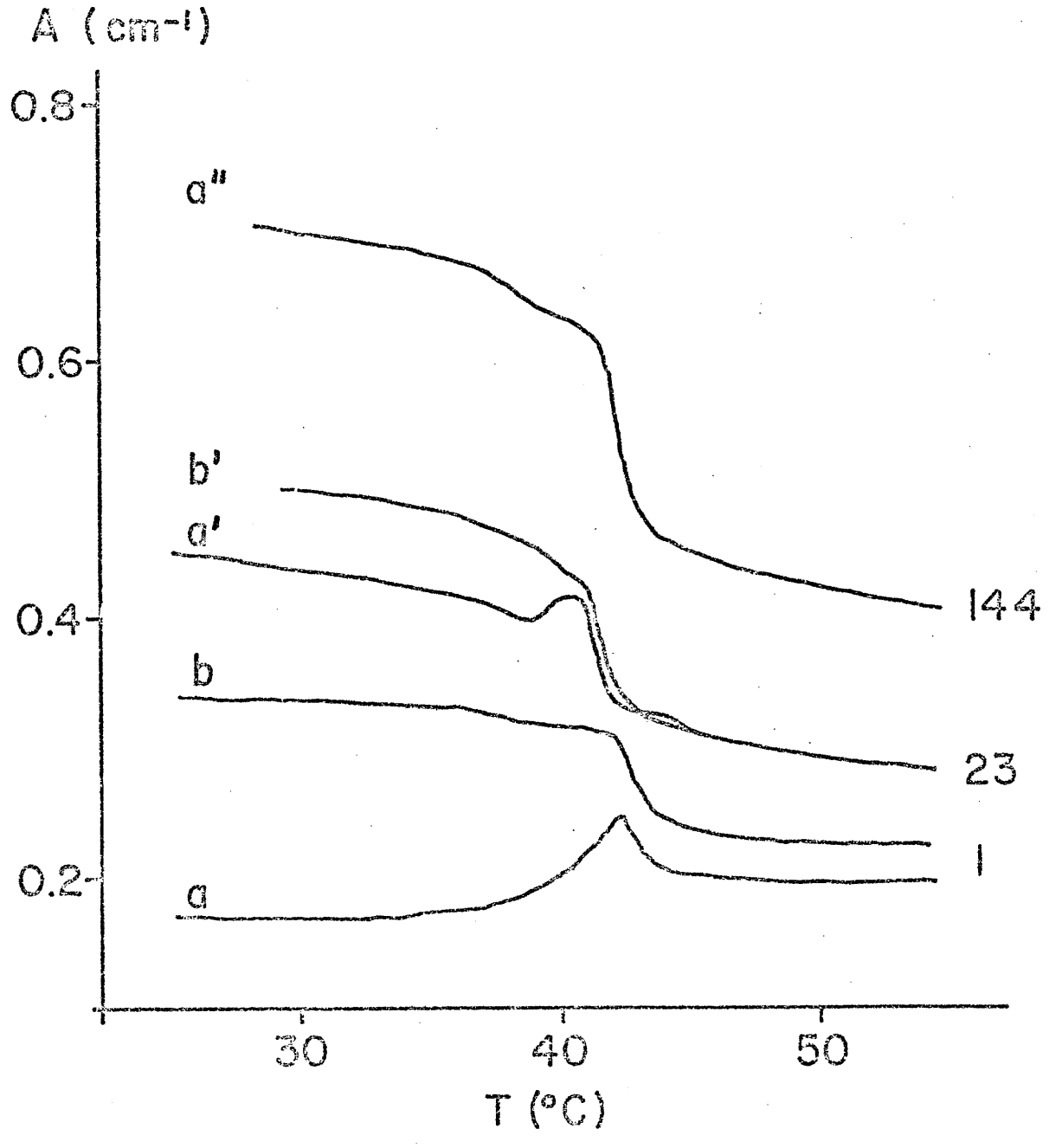
A (cm⁻¹)
0.8
0.6
0.4
0.2
a"
b'
a'
b
a
144
23
1
30
40
50
T (°C)

4. Discussion

a. Origin of absorbance changes at the main transition.

Yi and MacDonald (12) measured the refractive index, $\tilde{n}$, and the refractive index increment, $\partial\tilde{n}/\partial c$, for DPL dispersions as a function of temperature and found that both quantities decreased significantly at the thermal transition of the lipid bilayer. They demonstrated that the refractive index change, and the corresponding change in $\partial\tilde{n}/\partial c$, were quantitatively[1] accounted for by a partial molar volume change, $\Delta\bar{V}$, of the lipid. Their measured ratio of $\partial\tilde{n}/\partial c$ at 42°C to that at 40°C of 0.934 yields (eq V-7) the ratio of R_o's at these temperatures

$$\frac{R_o(42^oC)}{R_o(40^oC)} = (0.934)^2 = 0.872 \qquad (V\text{-}21)$$

If the particle scattering function is unity (Rayleigh scattering limit) or if there is no difference between the particle scattering functions at the two temperatures, then the intensity ratio of light scattered at any angle should be 0.872. However, Yi and MacDonald measured the intensity ratio for a 90° scattering angle to be 0.75, and claimed that the ratio of the particle scattering functions at the two temperatures is

$$P(90)_{42^oC}/P(90)_{40^oC} = 0.860 \qquad (V\text{-}22)$$

---

[1] Yi and MacDonald used a $\Delta\bar{V}$ of 1.4% to account for a 4.8% change in $\partial\tilde{n}/\partial c$. More recent dilatometry data suggest that $\Delta\bar{V}$ of 2.3%, when used in their model, accounts fully for the 6.6% change in $\partial\tilde{n}/\partial c$ actually observed between 40 and 42°C in their measurements.

These workers also demonstrated that the decrease in the particle scattering function upon melting was not a result of the vesicle size change, but rather due to a reduction in polarizability anisotropy.

The effect of an anisotropic polarizability of the hydrocarbon chain on the particle scattering function for small vesicles was first estimated by Tinker (22). He demonstrated that the particle scattering function at 90° is

$$P(90) = \frac{k}{15}(6\alpha_z^2 - 2\alpha_{xy}\alpha_z + 11\alpha_{xy}^2) \qquad \text{(V-23)}$$

where k is a proportionality constant and α_z and α_{xy} are the polarizabilities of hydrocarbon chain segments along and perpendicular to the molecular symmetry axis.

We now show that a ratio of about 0.86 in eq V-22 is, in fact, to be expected from the motional state of the vesicle bilayer inferred from the nuclear magnetic resonance experiments in Chapter III. To demonstrate this, we calculate the particle scattering function according to eq V-23 for the bilayer at temperatures below and above the transition temperature and evaluate the ratio

$$\frac{P(90)_{42^\circ C}}{P(90)_{40^\circ C}} = \frac{(6\alpha_z^2 - 2\alpha_{xy}^2\alpha_z + 11\alpha_{xy})_{42^\circ C}}{(6\alpha_z^2 - 2\alpha_{xy}^2\alpha_z + 11\alpha_{xy})_{40^\circ C}} \qquad \text{(V-24)}$$

For the bilayer at 40°C we assume that the hydrocarbon chain is normal to the bilayer surface and in an all-trans conformation. In this case, α_z and α_{xy}, respectively, are given by the molecular polarizabilities $\alpha_{\parallel}$ and $\alpha_{\perp}$ of a methylene group parallel and perpendicular to the normal to

the plane spanned by the CH_2 group. Numerical values for $\alpha_{\parallel}$ and $\alpha_{\perp}$ have been calculated, assuming the methylene group to be a cylindrically symmetric scattering element, by Ohki and Fukuda (23) to be

$$\alpha_{\parallel} = 5.72 \times 10^{-24} \text{ cm}^3$$
$$\alpha_{\perp} = 2.96 \times 10^{-24} \text{ cm}^3 \qquad \text{(V-25)}$$

Accordingly, the denominator of eq V-24 is

$$(6\alpha_{\parallel} - 2\alpha_{\perp}\alpha_{\parallel} + 11\alpha_{\perp}^2) = 258.83 \times 10^{-48} \text{ cm}^6 \qquad \text{(V-26)}$$

At temperatures above the phase transition temperature, we assume the motional state proposed in Chapter III; that is the hydrocarbon chain undergoes rapid isomerization through kink diffusion as well as much slower reorientation about a director normal to the bilayer. As a result of rapid isomerization of the chain, the effective polarizabilities parallel and perpendicular to the instantaneous chain direction are (12)

$$\alpha_{z'} = \alpha_{\parallel} p_t + (\tfrac{1}{4}\alpha_{\parallel} + \tfrac{3}{4}\alpha_{\perp})p_g$$

$$\alpha_{x'y'} = \alpha_{\perp} p_t + \tfrac{1}{2}(\tfrac{3}{4}\alpha_{\parallel} + \tfrac{3}{4}\alpha_{\perp})\, p_g \qquad \text{(V-27)}$$

where p_t and p_g give the probabilities of a methylene segment being in a trans or gauche conformation respectively. For a major portion of the chain $p_t \geq 0.8$, thus

$$5.31 \leq \alpha_{z'} \times 10^{24}\ \text{cm}^{-3} \leq 5.72$$
$$3.17 \leq \alpha_{x'y'} \times 10^{24}\ \text{cm}^{-3} \leq 2.96 \qquad \text{(V-28)}$$

In the absence of motions other than chain isomerization, then, we would have $\alpha_z = \alpha_{z'}$, $\alpha_{xy} = \alpha_{x'y'}$ so

$$(6\alpha_{z'} - 2\alpha_{x'y'}\alpha_{z'} + 11\alpha_{x'y'}) \geq 246.15 \times 10^{-48}\ \text{cm}^6 \qquad \text{(V-29)}$$

and a $P(90)_{42^\circ C}/P(90)_{40^\circ C}$ greater than 0.95, which is clearly too high in comparison with the experimental value (eq V-22). However, if the chains reorient about the bilayer normal then we have

$$\alpha_z = \alpha_{x'y'} + (\alpha_{z'} - \alpha_{x'y'}) \quad \cos^2\psi$$
$$\alpha_{xy} = \frac{1}{2}(\alpha_{x'y'} + \alpha_{z'}) - (\alpha_{z'} - \alpha_{x'y'}) \quad \cos^2\psi \quad) \qquad \text{(V-30)}$$

where ψ is the instantaneous angle of deflection of the chain relative to the director and the triangular brackets are used to denote the ensemble average over the distribution of angles $g(\psi)$. If in the motional model we assume a constant distribution in chain fluctuation within the range $0 \leq \psi \leq \Delta\psi$, then the nuclear magnetic resonance order parameter measurements suggest $\Delta\psi \leq 60^\circ$ for vesicles. In this limit, the particle scattering function is not very sensitive to the exact value of $\Delta\psi$ and we find find

$$226.2 \leq (6\alpha_z - 2\alpha_{xy}\,\alpha_z + 11\alpha_{xy}) \times 10^{48}\ \text{cm}^{-6} \leq 229.0 \qquad \text{(V-31)}$$

and $$0.87 \leq P(90)_{42^\circ C}/P(90)_{40^\circ C} \leq 0.89 \qquad \text{(V-32)}$$

a result which is in reasonable agreement with the experimental ratio.

Yi and MacDonald (12) also claimed their measured turbidity ratio of 0.75 reflected the intensity, and therefore the particle scattering function, ratio. The correspondence between the experimental ratios is, however, purely coincidental. Their absorbance at 42°C gives an x_1 value of 0.84 and from V-17 and Figure 44, we predict

$$\frac{R_o(42^o)Q_{42^oC}}{R_o(40^o)Q_{40^oC}} = 0.85 \qquad \text{(V-33)}$$

and hence a particle dissipation factor ratio of

$$Q_{42^oC}/Q_{40^oC} = 0.97 \qquad \text{(V-34)}$$

since by eq V-21, $R_o(42^o)/R_o(40^o) = 0.872$. Thus, the particle dissipation factor is not very sensitive to changes in anisotropy in the bilayer vesicle upon melting.

Pecora and Aragón have generalized the calculation of the particle scattering function for vesicles composed of anisotropic bilayers (24). The multilamellar structure of a liposome may be approximated by a large vesicle with a thick bilayer. In this limit, Pecora and Aragón's results predict that there is a negligible contribution to the particle scattering function from the anisotropy of the bilayer. Consequently, the particle dissipation factor for liposome suspensions should be insensitive to the anisotropy changes upon melting.

The turbidity ratio, R_{main}, for unsonicated dispersions in 40 mM $Ca(NO_3)_2$ is 0.82 when measured at an absorbance of 0.7. From eq V-17

and Figure 44, we then obtain

$$\frac{R_o(42^o)}{R_o(40^o)} \quad \frac{Q_{42^oC}}{Q_{40^oC}} = 0.89 \qquad \text{(V-35)}$$

But we expect Q_{42^oC}/Q_{40^oC} to approach unity for the liposome, so the turbidity ratio measures only the volume change associated with the transition. The different turbidity ratios for liposome preparations of DML,DPL and DSL (Table 4) therefore suggest that the volume change associated with the thermal transition in $Ca(NO_3)_2$ solutions follows the relation

$$\Delta\bar{V}_{DSL} > \Delta\bar{V}_{DPL} > \Delta\bar{V}_{DML}$$

If all turbidity changes observed with liposomal samples indeed are only due to density changes, then the measurable R_{pre} suggest that there is a small change in $\Delta\bar{V}$ of the bilayer, presumably by uptake of water, at the pretransition.

b. The pretransition in bilayer vesicles.

All heating curves show a decrease in absorbance at a temperature near the pretransition temperature (Chapter IV). For vesicles prepared in $Ca(NO_3)_2$, the change is quite small ($R_{pre} \sim 0.95$) and comparable to the change observed in the liposome system ($R_{pre} = 0.97$) (Figure 45 and 46). It is likely that this absorbance decrease corresponds to the small partial molar volume increase associated with the pretransition (21). Independent of its origin, the absorbance change along with the time course of its hysteresis provides strong evidence

that vesicle bilayers undergo a transition comparable to the pretransition observed with DTA techniques for liposomes (Chapter IV).

It is interesting to speculate on the meaning of the pretransition in a spherical bilayer. According to Luzzati's nomenclature, an L phase corresponds to a two-dimensional lamellar lattice while a P phase represents a three-dimensional lamellar lattice, possibly with ripples (Figure 16). For vesicles, the liquid crystalline phase should be referred to as a P_α phase.

Preliminary x-ray diffraction experiments have been performed in collaboration with Dr. A.E. Blaurock on vesicle samples in $Ca(NO_3)_2$. The low-angle diffraction pattern obtained for a vesicle suspension at 25°C is compatible with pairs of flat bilayers with a center-to-center separation of about 60 Å. The width of the high angle 4.2 Å diffraction indicates that the flat surfaces measure about 90-100 Å. Above the transition all evidence for pairs of bilayers disappears and the diffraction is compatible with spherical bilayer vesicles (25). The data suggest that at temperatures below the transition temperature the vesicle consists of numerous flat membrane facets each about 90 Å across corresponding to an L phase. This picture is in agreement with that proposed for unannealed vesicles (26) except that in the annealed vesicle the inside-outside lipid distribution is at an equilibrium. These preliminary x-ray data imply a transition between the two structures illustrated in Figure 51. We are currently investigating the temperature dependence of the x-ray diffraction patterns to ascertain whether the transition shown in Figure 51 occurs at the pretransition or the main transition.

FIGURE 51

Schematic representation of the possible change in bilayer structure upon heating through the transitions. Below the pretransition the x-ray evidence suggest pairs of flat bilayer facets. Above the main transition, the vesicles are spherical (25).

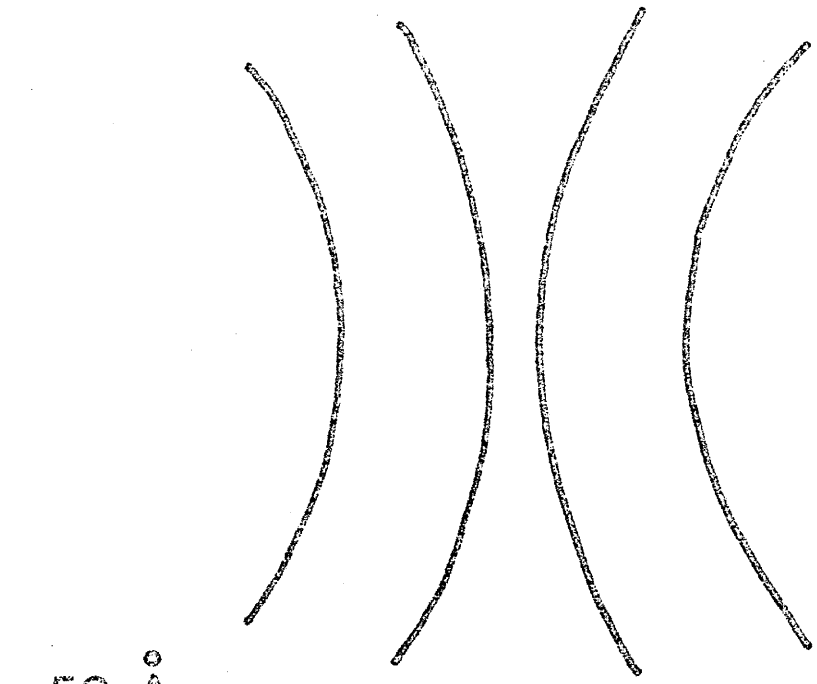

$T > T_c$

50 Å

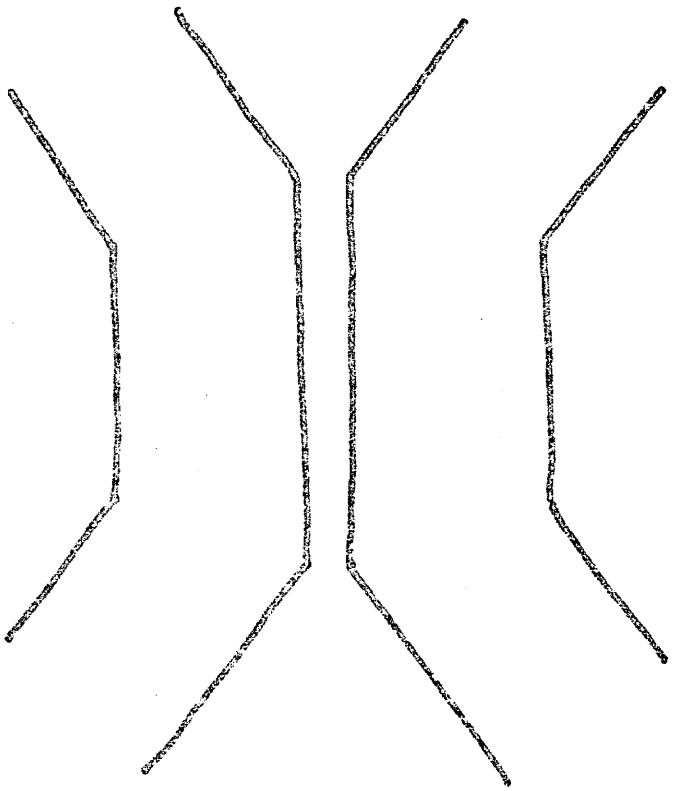

$T < T_p$

Since the pretransitions in vesicles and liposomes are quite similar, it is likely that the same structural changes occur here in both systems. Rand et al (27) have proposed that the phase change at the pretransition in liposomes is from an $L_{\beta'}$ to an L_{β} phase. This transition is possible in a vesicle if the facets still exist above the pretransition. In this case the transitions in the vesicle bilayer may be expressed as

$$L_{\beta'} \underset{T_p}{\overset{\rightarrow}{\leftarrow}} L_{\beta} \underset{T_c}{\overset{\rightarrow}{\leftarrow}} P_{\alpha}$$

On the other hand, Janiak et al (28) have suggested that the pretransition in liposomes is between an $L_{\beta'}$ and a $P_{\beta'}$ phase. If this hypothesis is extended to vesicles, then the facets in the vesicles are expected to disappear at the pretransition rather than at T_c, so

$$L_{\beta'} \underset{T_p}{\overset{\rightarrow}{\leftarrow}} P_{\beta'} \underset{T_c}{\overset{\rightarrow}{\leftarrow}} P_{\alpha}$$

It should be possible to distinguish between these two possibilities by x-ray difraction simply by noting the temperature at which the facets disappear.

The absorbance changes observed at the pretransition temperature in heating curves for vesicles in salt-free solutions are much greater than those seen for vesicles or liposomes in $Ca(NO_3)_2$. Its origin is not only the partial molar volume change but, since it is time dependent, presumably includes effects of an aggregation phenomenon.

c. States of aggregation of vesicle suspensions.

Yi and MacDonald (12) and Chong and Colbow (29) observed large temperature reversible absorbance changes at the pretransition and attributed these to a cooperative aggregation-dispersion process. The latter workers only discussed the dispersion, which they described as irreversible, since they did not consider the hysteresis effects in the pretransition. The time dependent absorbance changes observed here support the proposal that aggregation plays an important role in the vesicle system.

Since vesicles typically are 200-500 Å in diameter, they form a lyophobic colloid. Interactions among particles in a colloid have been studied extensively resulting in a general theory (30), the results of which are summarized in Appendix III. Examples of the results for two equally large spherical particles are illustrated in Figure 52. The major features to note about the curves in Figure 52 are: (i) a deep minimum (the primary minimum) in the energy interactions at small separations, (ii) an energy barrier with a maximum at intermediate separations, (iii) a shallow minimum (the secondary minimum) in the interaction energy at separations comparable to the particle radius. The exact positions and magnitudes of these extrema depend on the particle size and surface charge and the electrolyte composition and concentration.

Theoretical calculations of curves similar to those shown in Figure 52 have been performed assuming different surface potentials for the particle and using different electrolyte concentrations and charges (30,31). These calculations suggest the following trends. (i) If the

FIGURE 52

The total energy of interaction (—) between two identical spheres with radius a and with center-to-center separations R, as a function of the separation parameter $s = \frac{R}{a}$. The curve is drawn to scale from Kruyt (Figure 24, p. 276) (30). The dotted line (---) represents a possible shift in the interaction energy curve as a result of the phase change at the pretransition.

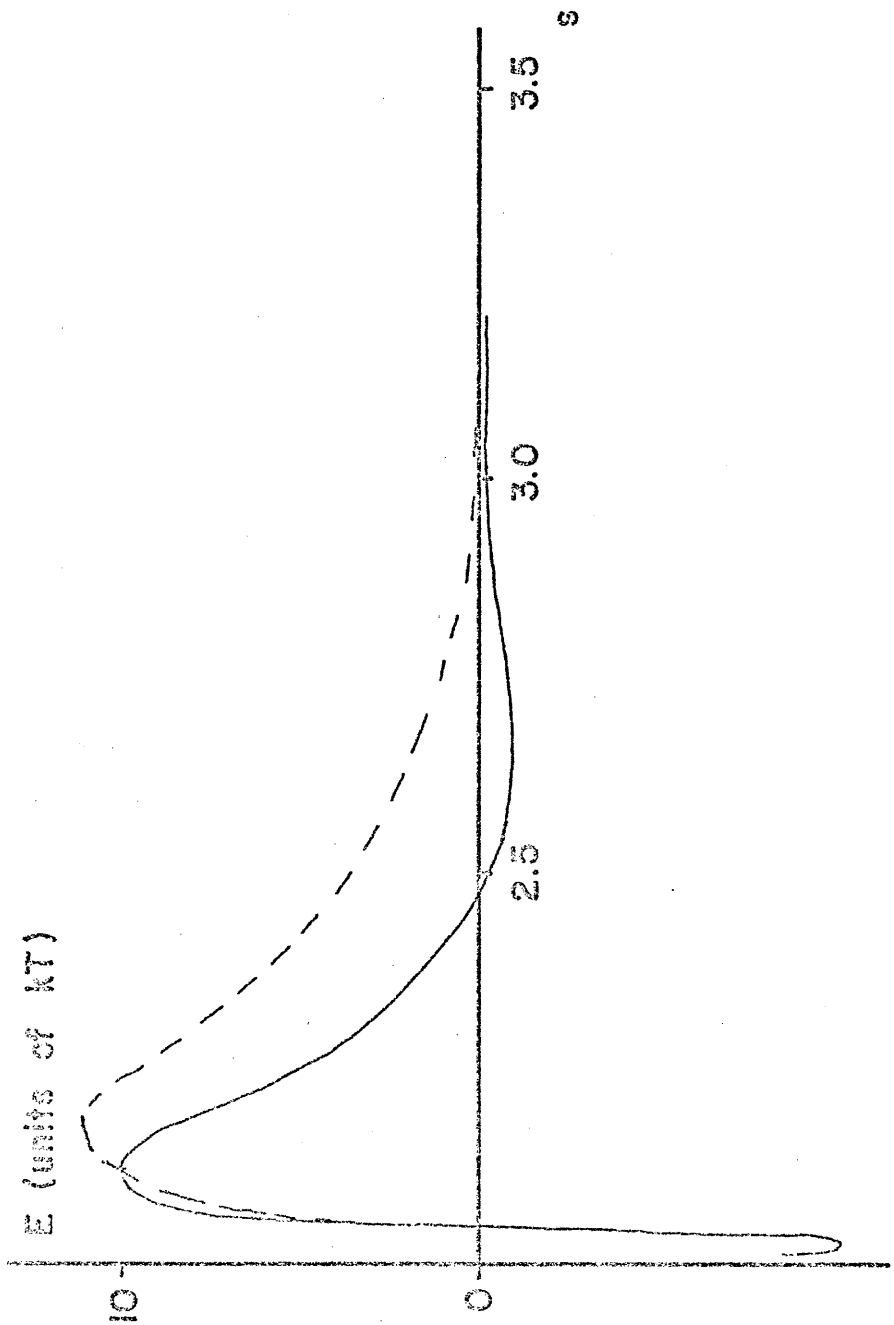
E (units of kT)
10
0
2.5
3.0
3.5
s

surface potential of the particle is increased, the maximum rises and the secondary minimum becomes less pronounced. (ii) If either the electrolyte concentration or charge is decreased, the Debye length of the Gouy-Chapman double layer increases. Qualitatively, this produces the same effects on the curves as an increased surface potential. (iii) The position and depth of the primary minimum is rather insensitive to changes in surface properties or electrolyte composition. (iv) The secondary minimum is quite shallow unless the maximum approaches kT and the particle radius is about 10^{-6} - 10^{-5} cm.

The results of the theoretical calculations indicate that intervesicular interactions may result in both close, practically irreversible contacts and distant, loose associations. We adopt the terms coagulation and flocculation, respectively (32) to describe the processes leading to these states, and propose that a colloidal suspension of vesicles may exist in any of the states illustrated in Figure 53: isolated, coagulated, flocculated, aggregated and fused. The time dependent absorbance changes reported here then reflect gradual changes from one state to another

Isolated vesicles are probably only found in dilute samples just after sonication. It should be possible to favor the isolated state by increasing the vesicle surface potential or decreasing the ionic strength. Indeed, vesicles with fatty acid impurities (3,4) or in low salt solutions are stabilized.

Flocculates of vesicles are formed through the long-range interactions (50-100 Å) associated with the secondary minimum. No conclusive evidence for a purely flocculated state exists. In fact, since

FIGURE 53

Schematic representation of possible aggregation states of vesicles in suspension.

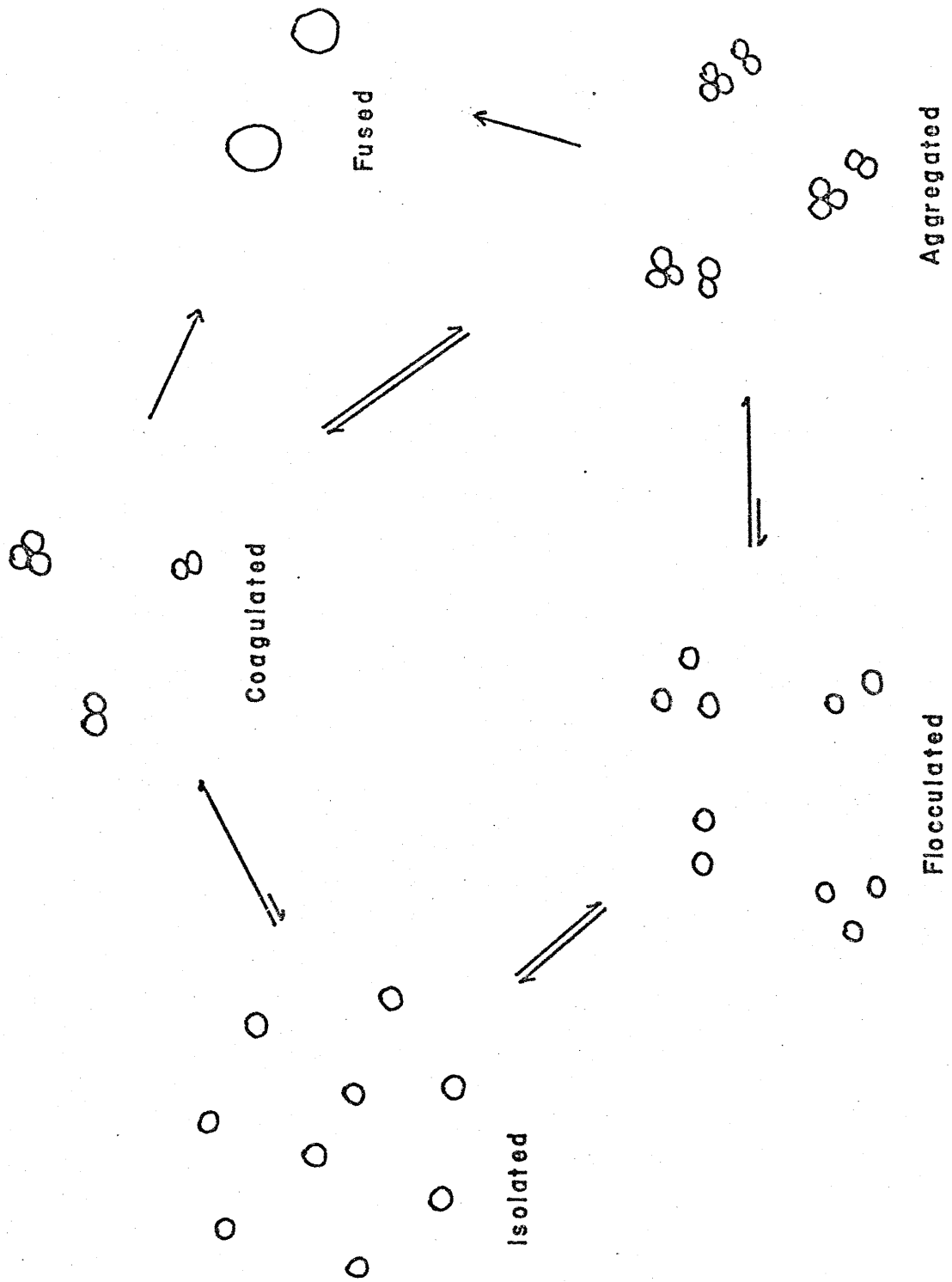
Fused
Aggregated
Coagulated
Flocculated
Isolated

the secondary minimum is not very deep unless the particles are large and the energy maximum is low, it is difficult to see how flocculation can occur without coagulation.

The predominant intervesicular interactions forming coagulates are at short distances (5-10 Å), at the primary energy minimum. These are strong interactions so a coagulate is not easily disrupted while flocculates are easily dispersed.

Since coagulates are larger than individual vesicles, the secondary minimum is deeper. Under favorable circumstances, coagulated vesicles will flocculate to form aggregates. Aggregates may also arise by coagulation of flocculated vesicles but the means of formation depends on which is the rate-determining process for the particular experimental conditions.

The fused vesicles differ from the initially produced vesicles only by their size. They can arise only if there is close contact between the vesicle surfaces as suggested by the model for fusion illustrated in Figure 54. Therefore, a prerequisite for fusion is a formation of coagulates or aggregates.

It is well known (14,15) that the light scattering intensity increases when colloidal particles coagulate. Consequently, turbidity measurements reflect the progress of aggregation, and is sensitive to both flocculation and coagulation. In the following we will discuss our experimental data in this context.

d. Changes in aggregation states.

(i) Vesicles in salt-free solutions. The large absorbance decrease observed at the pretransition while heating these systems (Fig-

FIGURE 54

Hypothetical model of vesicle-vesicle fusion. Note that close contact between the surfaces is a prerequisite for fusion.

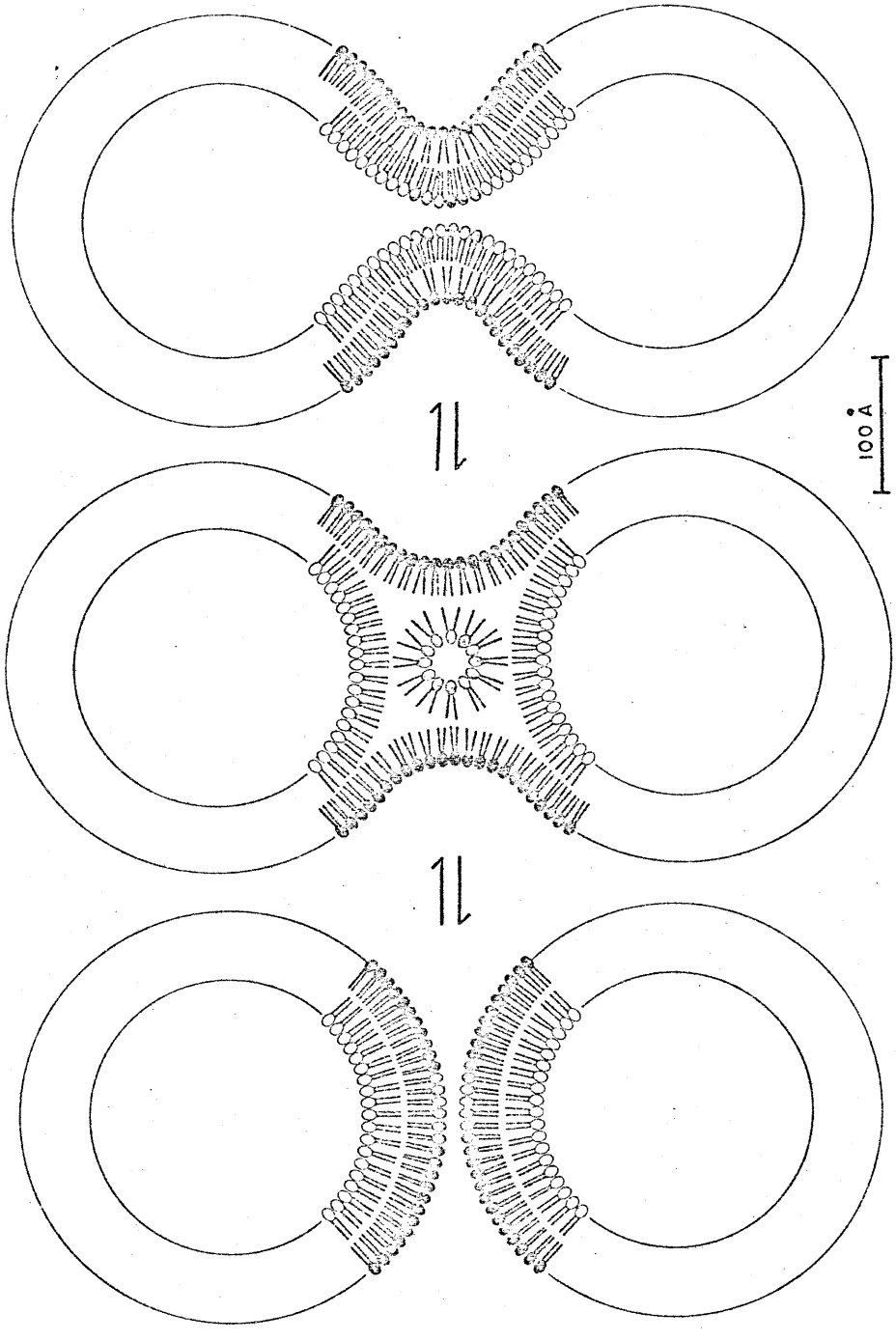
100 Å

ure 46a) cannot be accounted for solely by structural changes in the bilayer. Some reversible aggregation phenomenon must contribute to this temperature effect. Since a 10°C temperature rise will not significantly affect the intervesicular interactions, the state of aggregation must also be sensitive to the bilayer phase transition in the temperature range. Coagulates are not easily disrupted by changes in the nature of the colloidal particles whereas flocculates are very sensitive to surface properties. Therefore, we conclude that it is dispersion of flocculates which contributes to the absorbance decrease at the pretransition.

On cooling, the absorbance increase, and therefore flocculation, follows the time course of the pretransition hysteresis (Figures 46 and 47). Since flocculation and dispersion are so intimately connected with the pretransition phase change it must introduce a surface potential change. This may result from the altered motional state of the zwitterionic lipid headgroup (33). An alternative explanation is that intervesicular interactions are sensitive to the presence of facets, which then disappear at temperatures above T_p.

The long term irreversible absorbance increases seen by comparing curves a' and b' in Figure 46 indicate that a slow coagulation occurs.

(ii) Vesicles in $Ca(NO_3)_2$ solutions. In $Ca(NO_3)_2$ solutions there is no evidence for vesicle flocculation. The slow decrease in the turbidity ratios shown in Figure 49B represents coagulation. Since the divalent Ca^{++} ions bind to the vesicle surface (18,19,20), the Stern layer potential (Appendix III) is altered, abolishing the

secondary minimum in Figure 52, associated with flocculation. Although the surface potential is higher, coagulation still occurs because of a shielding by the electrolyte double layer formed in the high ionic strength medium. Similar effects are observed with $La(NO_3)_3$ at comparable ionic strength, and are expected for all strongly binding cations.

(iii) Vesicles in monvalent salt solutions. In solutions with NaCl and $NaNO_3$, a combination of the aggregation processes observed in salt-free solutions and with $Ca(NO_3)_2$ is seen. As with no salt, the flocculates (Figure 48) disperse readily on heating, but the total absorbance for equivalent DPL concentrations is greater at all temperatures, suggesting more coagulation. Because of weak monvalent cation binding the surface potential is not greatly affected. However, the Debye length (Appendix III) decreases with electrolyte concentration, enhancing the aggregation.

e. Fusion.

Studies performed in this laboratory (Y. Lee, M. Chan and S.I. Chan, unpublished) show that for samples with $Ca(NO_3)_2$ there is no fusion when they are kept for as long as 14 days at temperatures between 23 and 60°C. These findings support our conclusion that the steady absorbance change observed in these systems at room temperature is due to coagulation rather than fusion. However, Figure 50 illustrates that during the first 48 hours, cycling through the transition causes a net rise in absorbance (Figure 50, curves a and b). Fusion has been found in some cases (4,5) to be faster at temperatures around the transition temperature, and we attribute the abrupt absorbance in-

crease in the first heating curves to a fusion process. Increased coagulation at room temperature predisposes the system to fusion upon heating. The origin for fusion in these experiments is then the repeated cycling in temperature.

f. Conclusions.

By considering the colloidal nature of vesicle suspensions, we may begin to understand how to control the fusion process. We can ensure that coagulation is rate-determining, thereby inhibiting fusion. On the other hand, if coagulation is accelerated, the rate of the fusion process, as it is depicted in Figure 54, depends on the bilayer stability rather than its surface properties. Certain compounds such as lysolecithin could destabilize the bilayer. These concepts are currently being tested in this laboratory (Y.K. Lee, M. Chan, K. Eigenberg and S.I. Chan, private communication).

References

1. H.A. Lester, Sci. American, 236, 107 (1977).
2. E.L. Racker, in "Cell Membranes, Biochemistry, Cell Biology and Pathology", H.P. Publishing Co., 1975, Chapter 14.
3. C. Taupin and H.M. McConnell, Mitochondria/Biomembranes, 9th Fed. Eur. Biochem. Soc. Symp., 28, 219 (1972).
4. J.H. Prestegaard and B. Fellmeth, Biochemistry, 13, 1122 (1974).
5. H.L. Kantor and J.H. Prestegaard, Biochemistry, 14, 1790 (1975).
6. Y.K. Lee and S.I. Chan, in preparation (1977).
7. A.L.Y. Lau and S.I. Chan, Biochemistry, 13, 4942 (1974).
8. P.H. von Dreele and S.I. Chan, Proc. Nat. Acad. Sci. (U.S.), submitted for publication (1976).
9. M. Sheetz and S.I. Chan, Biochemistry, 11, 4573 (1972).
10. D.M. Michaelson, A.F.Horwitz and M.P. Klein, Biochemistry, 12, 2637 (1973).
11. P. Overath and H. Träuble, J. Am. Chem. Soc., 94, 4482 (1972).
12. P.N. Yi and R.C. MacDonald, Chem. Phys. Lipids, 11, 114 (1973).
13. M.B. Abrahamson, Biochim. Biophys. Acta, 225, 167 (1971).
14. G. Oster, J. Colloid Sci, 2, 291 (1947).
15. A. Lips and E. Willis, Trans. Faraday Soc., 69, 1226 (1973).
16a. H.G. Elias, in "Light Scattering from Polymer Solutions", H.B. Huglin (ed.), Academic Press, London - New York, 1972, Chapter 9.
b. P. Kratochvil, ibid, Chapter 7.
c. P. Kratochvil, ibid, Chapter 7, p.376.
17a. C. Tanford, in "Physical Chemistry of Macromolecules", S. Wiley

and Sons, Inc., New York, 1961, p.288

b. ibid, p. 287.

c. ibid, p. 298.

d. ibid, p. 302.

18. H. Träuble and H. Eibl, Proc. Nat. Acad. Sci. (U.S.), 71, 214 (1974).

19. K. Jacobson and D. Papahadjopoulos, Biochemistry, 14, 152 (1975).

20. A.J. Verkleij, B. De Kruyff, P.H.J.Th. Ververgaert, J.F. Tocanne and L.L.M. van Deenen, Biochim. Biophys. Acta, 339, 432 (1974).

21. J.F. Nagle, Proc. Nat. Acad. Sci. (U.S.), 70, 3443 (1973).

22. D.O. Tinker, Chem. Phys. Lipids, 8, 230 (1972).

23. S. Ohki and N. Fukuda, J. Theoret. Biol., 15, 362 (1967).

24. R. Pecora and S.R. Aragón, Chem. Phys. Lipids, 13, 1 (1974).

25. N. Webb, private communication, (1975).

26. R. Lawaczeck, M. Kainosho and S.I. Chan, Biochim. Biophys. Acta, 443, 313 (1976).

27. R.P. Rand, D. Chapman and K. Larsson, Biophys. J., 15, 1117 (1975).

28. M.J. Janiak, D.M. Small and G.G. Shipley, Biochemistry, 15, 4575 (1976).

29. C.S. Chong and K. Colbow, Biochim. Biophys. Acta, 436, 260 (1976).

30. M.K. Kruyt, Ed., in "Colloid Science" Vol. 1, Elsevier Publishing Co., Amsterdam, 1952.

31. E.J.W. Verwey and J.Th.G. Overbeek, in "Theory of the Stability of Lyophobic Colloids", Elsevier Publishing Co., Amsterdam, 1952.

32. M.J. Vold and R.D. Vold, in "Colloid Chemistry", Van Nostrand Reinhold Company, New York, 1964.

33. A.C. McLaughlin, P.R. Cullis, J.A. Berden and R.E. Richards, J. Magn. Reson., 20, 146 (1975).

VI. SUMMARY

Our objective in this work was to improve our understanding of intermolecular interactions in cell membranes. We focused on the study of lipid-lipid interactions in phospholipid bilayers, expecting to be able to extrapolate conclusions derived here to *in vivo* membrane systems.

In order to develop a description of interlipid interactions, we sought to understand their effects on the state of motion of the lipids in a liquid crystalline bilayer. It was therefore important to have a coherent description of the lipid motion compatible with available data. To do this, we have modeled the hydrocarbon chain motion on chain isomerization and reorientation as well as rotation about its long axis. The model was conceived to explain magnetic resonance data but was also found to be consistent with experimental data from x-ray diffraction, light scattering and Raman spectroscopy. No previously proposed models have been this successful.

An important aspect of the motional model presented here is the description of the lipid bilayer as an anisotropic fluid. The degree of reorientation was used as a measure of membrane anisotropy, which allowed us to explain the condensing effect of cholesterol and to predict a similar effect for membrane proteins.

Application of the model to vesicles confirmed that lipids in a curved bilayer are in a different motional state. However, this bilayer exhibits the same thermally induced phase transitions found in liposomes, as demonstrated by our light scattering experiments. These

also showed that the pretransition causes surface potential changes, which severely affect the state of vesicle aggregation. Time dependent absorbance changes with different salts supported the colloidal nature of the intervesicular interactions and suggested means of controlling fusion.

We also investigated the phase behavior of mixed phospholipids, and found evidence for ideal lipid-lipid interactions in the liquid crystalline phase of all mixtures. However, some lipids exhibit immiscibility in the gel phase. Conclusions derived from model bilayers in a liquid crystalline phase should be applicable to the complex mixtures found in natural membranes.

APPENDIX I. EXAMPLES OF SECOND RANK TENSOR INTERACTIONS IN MAGNETIC RESONANCE.

A good illustration of the effects which give rise to anisotropy in the incompletely averaged magnetic resonance experiments can be obtained by considering the nuclear dipolar interactions between two identical spins with I = 1/2. The Hamiltonian for the spin pair is given by (1,2)

$$\hat{H} = \hat{H}_Z + \hat{H}_D$$

$$= -\vec{\mu}_1 \cdot \vec{H} - \vec{\mu}_2 \cdot \vec{H} + \frac{\vec{\mu}_1 \cdot \vec{\mu}_2}{r^3} - 3\,\frac{(\vec{\mu}_1 \cdot \vec{r}_{12})(\vec{r}_{12} \cdot \vec{\mu}_2)}{r^5} \qquad \text{(AI-1)}$$

where $\vec{\mu}_i$ is the magnetic moment of nucleus i, $\vec{H}$ is the applied magnetic field and $\vec{r}$ is the internuclear vector. $\hat{H}_Z$ is the total Zeeman Hamiltonian and $\hat{H}_D$ is the total dipolar Hamiltonian. Other contributions such as chemical shift anisotropy have been ignored. The dipolar Hamiltonian may be rewritten in terms of the spin angular momenta which are quantized along the magnetic field and

$$\hat{H}_D = \frac{\gamma^2 \hbar^2}{r_{12}^3}\left(\vec{I}_1 \cdot \vec{I}_2 - \frac{3(\vec{I}_1 \cdot \vec{r}_{12})(\vec{r}_{12} \cdot \vec{I}_2)}{r_{12}^2}\right)$$

$$= \frac{\gamma^2 \hbar^2}{r_{12}^3}\, \vec{I}_1 \cdot \underline{\underline{D}} \cdot \vec{I}_2 \qquad \text{(AI-2)}$$

where $\underline{\underline{D}}$ is a symmetric tensor with a trace of zero. The quantities I_1, I_2 and $\underline{\underline{D}}$ are all referred to coordinate systems chosen so that the

z-axes are along the direction of the applied field. In spherical polar coordinates, the polar angle between the applied field H_0 and the inter-spin vector $\vec{r}$, is θ, and the corresponding azimuthal angle is ϕ. In this notation the dipolar interaction tensor is

$$\underset{\sim}{D} = \begin{pmatrix} 1 - 3\sin^2\theta\cos^2\phi & -3\sin^2\theta\sin\phi\cos\phi & -3\sin\theta\cos\theta\cos\phi \\ -3\sin^2\theta\sin\phi\cos\phi & 1 - 3\sin^2\theta\sin^2\phi & -3\sin\theta\cos\theta\sin\phi \\ -3\sin\theta\cos\theta\cos\phi & -3\sin\theta\cos\theta\sin\phi & 1 - 3\cos^2\theta \end{pmatrix} \tag{AI-3}$$

With this form of $\underset{\sim}{D}$ eq AI-2 can be expanded into a linear combination of the spherical harmonic functions $Y_2^m(\theta,\phi)$. To first order, only the terms with $Y_2^0(\theta,\phi)$ are important in determining the perturbation of the dipolar interaction on the Zeeman interaction. These first order terms are given by

$$\hat{H}_D = \frac{\gamma^2\hbar}{r_{12}^3}\{I_{1z}I_{2z} - \frac{1}{4}(I_{1+}I_{2-} + I_{1-}I_{2+})\}(1 - 3\cos^2\theta) \tag{AI-4}$$

Because the two spins are identical, the Zeeman energy levels of the two spin states $(\alpha_1\beta_2)$ and $(\beta_1\alpha_2)$ are degenerate. The proper choice of basis functions for the evaluation of the perturbation by the dipolar interaction is thus a linear combination of these spin states with $\psi_{T_0} = 1/\sqrt{2}\,(\alpha_1\beta_2 + \beta_1\alpha_2)$ and $\psi_{S_0} = 1/\sqrt{2}\,(\alpha_1\beta_2 - \beta_1\alpha_2)$. The energies of the four spin states then can be calculated as

$$E_{\psi+1} = \gamma\hbar H_o + \frac{1}{4}\frac{\gamma^2\hbar^2}{r_{12}^3}(1 - 3\cos^2\theta)$$

$$E_{\psi s_o} = 0$$

$$E_{\psi T_o} = 0 - \frac{1}{2}\frac{\gamma^2\hbar^2}{r_{12}^3}(1 - 3\cos^2\theta)$$

$$E_{\psi-1} = +\gamma\hbar H_o + \frac{1}{4}\frac{\gamma^2\hbar^2}{r_{12}^3}(1 - 3\cos^2\theta) \qquad \text{(AI-5)}$$

The transition in the absence of a dipolar interaction would correspond to a resonance frequency of

$$\omega_o = E_I/\hbar = \gamma H_o \qquad \text{(AI-6)}$$

The effect of the dipolar interactions is simply to split the resonance into two with frequencies

$$\omega_1 = \omega_o - \frac{3}{4}\frac{\gamma^2\hbar}{r_{12}^3}(1 - 3\cos^2\theta)$$

and $$\omega_2 = \omega_o + \frac{3}{4}\frac{\gamma^2\hbar}{r_{12}^3}(1 - 3\cos^2\theta) \qquad \text{(AI-7)}$$

Note that the pair of resonance lines are symmetrically displaced about ω_o, as they must be because the trace of the dipolar Hamiltonian is zero. In addition, the separation of the pair of lines, $\Delta\omega$, is

$$\Delta\omega = \frac{3}{2}\frac{\gamma^2\hbar}{r_{12}^3}(1 - 3\cos^2\theta) \qquad \text{(AI-8)}$$

which depends only on the magnitude and orientation of the internuclear vector relative to the direction of the applied field. The $\Delta\omega$ is independent of the magnitude of the applied field.

Comparable calculations may be used to show that for a nucleus with a quadrupolar moment, the resonance will be split into a pair of lines with a separation given by

$$Q = \frac{1}{2}\left(\frac{e^2qQ}{\hbar}\right)(1 - 3\cos^2\theta) \qquad \text{(AI-9)}$$

where Q is the quadrupolar moment of the nucleus, e is the charge of the electron and the quantity eq is a measure of the electric potential at the nucleus due to an electric field gradient around the nucleus. In AI-9 it is assumed that the field is axially symmetric at the nucleus and θ is the polar angle of the symmetry axis relative to H_0. It turns out to be a good approximation for a deuterium atom in a carbon-deuterium bond, and in this case the symmetry axis coincides with the carbon-deuterium bond vector.

Chemical shift anisotropy (1) in nuclear magnetic resonance arises from a variation in the effective magnetic field at the nucleus with orientation of the molecule. This orientation dependence comes from differences in the shielding by the electrons along the principal molecular axes. The shielding effect is accounted for by rewriting the Zeeman Hamiltonian as

$$\hat{H}_Z = -\vec{\mu}\,(\underset{\simeq}{1} - \underset{\simeq}{\sigma})\cdot\vec{H} \qquad \text{(AI-10)}$$

where $\underset{\simeq}{\sigma}$ is the chemical shift tensor. It is important to note that the trace of $\underset{\simeq}{\sigma}$ is not zero, but gives the chemical shift value for the spin when the molecule is moving isotropically.

The electronic Zeeman interaction in the ESR experiment is determined by the total angular momentum which contains contributions from spin and orbital angular momenta. The orbital angular momentum is induced by the applied magnetic field, and, depending on which electronic orbital the unpaired electron is in, the orbital angular momentum may be anisotropic. This is the case for the nitroxide spin label (Figure 4) and the electronic Zeeman interaction is written

$$\hat{H}_Z^e = -\beta\vec{S}\cdot\underset{\simeq}{g}\cdot\vec{H} \qquad \text{(AI-11)}$$

where β is the Bohr magneton ($= e\hbar/2m_e c$), $\vec{S}$ the spin angular momentum and $\underset{\simeq}{g}$ the tensor describing the anisotropy in the angular momentum. For the nitroxide spin label, $\underset{\simeq}{g}$ is nearly diagonal in the coordinate system included in Figure 4, and can be written

$$\underset{\simeq}{g} = \begin{pmatrix} g_x & 0 & 0 \\ 0 & g_y & 0 \\ 0 & 0 & g_z \end{pmatrix} \qquad \text{(AI-12)}$$

The effective g-value which determines the resonance frequency for a

given orientation of the unpaired electron orbital at a polar angle θ and azimuthal angle ϕ then is

$$g_{eff} = g_x \sin^2\theta\cos^2\phi + g_y \sin^2\theta\sin^2\phi + g_z \cos^2\theta \qquad \text{(AI-13)}$$

The electron-nuclear hyperfine interaction (1,3) is also characterized by an anisotropic tensor, $\underline{\underline{A}}$, which is analogous to the dipolar tensor and is given by

$$\hat{H} = \vec{I} \cdot \underline{\underline{A}} \cdot \vec{S} \qquad \text{(AI-14)}$$

References

1. C.P. Schlichter in "Principles of Magnetic Resonance", Harper and Row Publishers, New York, 1963.
2. A. Abragam, in "The Principles of Nuclear Magnetism", Oxford University Press, Oxford, 1961.
3. J.E. Wertz and J.R. Bolton in "Electron Spin Resonance", McGraw-Hill Book Co., New York, 1972.

APPENDIX II. CALCULATIONS OF NMR FREE INDUCTION DECAYS.

The FID is the Fourier transform of the lineshape function (1); that is

$$G(t) = \frac{1}{\sqrt{2\pi}} \int_{-\infty}^{\infty} F(\omega') e^{i\omega' t} \, d\omega' \qquad \text{(AII-1)}$$

In the case where the spin-lattice relaxation is dominated by fast motions and the FID is controlled by much slower motions ($\frac{1}{T_2} >> \frac{1}{T_1}$) the FID can be calculated by (2,3)

$$G(t) = \left\langle e^{i\int_0^t \omega'(t')dt'} \right\rangle \qquad \text{(AII-2)}$$

When the fluctuations in $\omega'(t')$ are caused by dipolar interactions among two spins, the lineshape is symmetric about the Larmor precession frequency, ω_0 , and the normalized FID can be written as

$$G(t) = \frac{1}{2} \left\langle e^{i\int_0^t (\omega_0+\omega(t'))dt'} + e^{i\int_0^t (\omega_0-\omega(t'))dt'} \right\rangle$$

$$= e^{i\omega_0 t} \left\langle \cos \int_0^t \omega(t') \, dt' \right\rangle \qquad \text{(AII-3)}$$

The signal is generally phase detected relative to the Larmor frequency and the observed FID is the real part of

$$g(t) = \left\langle e^{i\Phi(t)} \right\rangle \qquad \text{(AII-4a)}$$

where

$$\Phi(t) = \int_0^t \omega(t')dt' \qquad \text{(AII-4b)}$$

This expression of the FID is mathematically equivalent to

$$g(t) = \int_{-\infty}^{\infty} e^{ix} \text{ Prob } (x < \Phi(t) < x + dx) \qquad \text{(AII-5)}$$

where Prob $(x < \Phi(t) < x + dx)$ is the probability that the random variable $\Phi(t)$ falls within the interval $(x,x + dx)$. Clearly, if the probability distribution of $\Phi(t)$ is known, the FID can be calculated. The problem is therefore reduced to one of finding this probability distribution.

It is not usually possible to calculate the exact probability distribution of $\Phi(t)$ for all times but in a wide range of physically interesting cases, we can obtain the asymptotic distribution for sufficiently long times by applying a central limit theorem (2,5) which can be stated as follows:

> If $p(t)$ is a function which denotes a strictly stationary, strongly mixing, random process, whose correlation function, $R_p(t)$, exists and possesses its first two moments , then the random process, $\psi(t)$, defined by
>
> $$\psi(t) = \frac{1}{\sqrt{t}} \int_0^t (p(t') - \bar{p})\, dt' \qquad \text{(AII-6)}$$
>
> has a probability distribution which is asymptotic to the normal (Gaussian) distribution with mean equal to zero and variance
>
> $$\left\langle \psi(t)^2 \right\rangle = 2\int_0^{\infty} R_p(\tau)\, d\tau \quad . \qquad \text{(AII-7)}$$

A random process, $p(t)$, is stationary if and only if

$$\text{Prob}\,(p(t_1) = x_1,\ p(t_2) = x_2, \ldots,\ p(t_n) = x_n)$$

$$= \text{Prob}\,(p(t_1 + \tau) = x_1,\ p(t_2 + \tau) = x_2 \ldots,\ p(t_n + \tau) = x_n) \qquad \text{(AII-8)}$$

for all n; $t_1, t_2, \ldots, t_n$; $x_1, x_2, \ldots, x_n$; and τ (4,6). This essentially says that all probabilities connected with the random process, p(t), must remain unchanged under arbitrary translations in time. In particular, this implies that the probability that p(t) is any given value, x, is independent of time, and that the correlation function of p(t), defined by

$$R_p(t,\tau) \equiv \left\langle (p(t+\tau) - \bar{p})\ (p(t) - \bar{p}) \right\rangle = \left\langle p(t+\tau)p(t) \right\rangle - \bar{p}^{2} \qquad \text{(AII-9)}$$

is a function of τ only, and accordingly we have written it as $R_p(\tau)$. For a strictly stationary random process to be strongly mixing requires that for any $\tau > 0$, for $A(\tau)$ being any combination of events of p(t) occurring before t = 0, and for $B(\tau)$ being any combination of events of p(t) occurring after $t = \tau$, we have

$$|\text{Prob}(A(\tau) \text{ and } B(\tau)) - \text{Prob}(A(\tau))\ \text{Prob}(B(\tau))| \leq \alpha(\tau) \qquad \text{(AII-10)}$$

where $\alpha(\tau)$ is some decreasing function of τ whose integral converges (4,5). The minimum $\alpha(\tau)$ which satisfies eq AII-10, $\alpha^*(\tau)$, is a measure of the strongest interdependence of events separated in time by at least τ. We therefore define the mixing time

$$\tau_{mix} = \int_0^\infty \alpha^*(\tau)d\tau \qquad \text{(AII-11)}$$

as the timescale over which the process becomes independent of its past. Finally, we note that in order for the correlation function, $R_p(\tau)$, to exist the random process must have a finite mean and variance. The correlation time of the process is given by (6)

$$\tau_c = \frac{1}{R_p(0)} \int_0^\infty R_p(\tau)d\tau \qquad \text{(AII-12)}$$

where $R_p(0) = \mathrm{Var}(p(t))$. When the correlation function decays exponentially with time, such as occurs for Brownian motion and many other diffusive processes, the decay constant is the correlation time (1).

In order to compute the FID, we now express the frequency fluctuations, $\omega(\tau)$, as a linear combination of a finite number of uncorrelated, strictly stationary, strongly mixing, random processes, $p_j(t)$; that is,

$$g(t) = e^{i\int_0^t (\sum_j A_j p_j(t'))\, dt'} \qquad \text{(AII-13)}$$

The random processes, $p_j(t)$, are uncorrelated if

$$(p_j(t+\tau) - \bar{p}_j)\,(p_k(t) - \bar{p}_k) = \begin{cases} 0 & \text{for } j \neq k \\ R_{p_j}(\tau) & \text{for } j = k \end{cases} \qquad \text{(AII-14)}$$

where $R_{p_j}(\tau)$ is the correlation function of the random process, $p_j(\tau)$, and we assume they all satisfy the requirements mentioned earlier. The

corresponding correlation times are defined by eq AII-12 and denoted by τ_j. Note that, in particular, if the p_j's are all independent of one another, they are also uncorrelated. If we define the total random process P(t) as

$$P(t) \equiv \sum_j A_j p_j(t) \tag{AII-15}$$

it is immediately obvious that P(t) is also a strictly stationary, strongly mixing, random process with mean

$$\bar{P} = \langle P(t) \rangle = \sum_j A_j \overline{p_j(t)} \tag{AII-16}$$

and variance

$$\text{Var}\,(P(t)) = \sum_j A_j^2 \,\text{Var}(p_j(t)) \tag{AII-17}$$

The latter follows since the correlation function can be written as

$$R_p(\tau) = \langle (P(t+\tau) - \bar{P})\,(P(t) - \bar{P}) \rangle = \sum_j A_j^2 R_{p_j}(\tau) \tag{AII-18}$$

From this result we can define a correlation time for the overall process, P(t), which is

$$\tau_c = \frac{1}{R_p(0)} \int_0^\infty \sum_j A_j^2 R_{p_j}(\tau) d\tau = \frac{\sum_j A_j^2 \tau_j \,\text{Var}(p_j)}{\sum_j A_j^2 \,\text{Var}(p_j)} \tag{AII-19}$$

We see that P(t) satisfies all the requirements of the central limit

theorem, and therefore the random process

$$\psi(t) = \frac{1}{\sqrt{t}} (\Phi(t) - \bar{P}t) \tag{AII-20}$$

with

$$\Phi(t) = \int_0^t P(t')dt' = \int_0^t (\sum_j A_j p_j(t'))dt' \tag{AII-21}$$

is asymptotically normally distributed with a mean of zero, and with a variance of

$$V = 2 \sum A_j^2 \, \mathrm{Var}(p_j)\tau_j \tag{AII-22}$$

This is a very important and useful result, since it allows one to calculate the entire asymptotic probability distribution function using only the means, variances, and correlation times of the component processes.

With a probability distribution of $\psi(t)$ which is asymptotically Gaussian, it is an easy matter to find the asymptotic FID. According to eq AII-5,

$$g(t) = e^{i\bar{P}t} \int_0^\infty e^{ix} \, \mathrm{Prob}(\Phi(t) - \bar{P}t \in [x, x + dx])$$

$$= e^{i\bar{P}t} \int_0^\infty e^{iu\sqrt{t}} \, \mathrm{Prob}\left(\frac{\Phi(t) - \bar{P}t}{\sqrt{t}} \in [u, u + du]\right)$$

$$= \frac{e^{i\bar{P}t}}{\sqrt{2\pi V}} \int_{-\infty}^\infty e^{iu\sqrt{t} - u^2/2V} du$$

$$= e^{i\bar{P}t}\, e^{-Vt/2} \qquad \text{(AII-23)}$$

To complete the calculation, we take the real part

$$g(t) = \cos(\bar{P}t)\, e^{-Vt/2} \qquad \text{(AII-24)}$$

This result predicts that the envelope of the FID is asymptotically exponential with a time constant, T_2, given by

$$\frac{1}{T_2} = \frac{V}{2} = \sum_j A_j^2\, \mathrm{Var}(p_j)\tau_j \qquad \text{(AII-25)}$$

Eq AII-24 also predicts a frequency spectrum consisting of a pair of Lorentzian lines, each with a width at half-maximum of

$$\Delta\nu = \frac{1}{\pi T_2} \qquad \text{(AII-26)}$$

symmetrically displaced from the Larmor precession frequency by an amount $\bar{P}$.

We have therefore demonstrated that the FID function will be asymptotically exponential whenever the frequency fluctuations can be written as a finite linear combination of uncorrelated, strictly stationary, strongly mixing, random processes. Since these results are only asymptotically valid, we will briefly discuss some of the limitations of this approach.

The applicability of the central limit theorem is determined by

the relative timescales of the fluctuations of the motions and the experimental measurements. As the origin of this limitation is the asymptotic nature of the convergence to a normal distribution, the experimental observation must be made at sufficiently long times to ensure this convergence.

To place the problem in more quantitative terms we now consider the rate of the asymptotic convergence of $\psi(t)$ in eq AII-6 to a normally distributed variable. The usual rule-of-thumb (7,8) is that it takes a sum of 6-12 independent random variables, a_m's, before this sum converges to a normally distributed variable, provided the probability distribution of the a_m's is nearly symmetric and well behaved. In other words, the variable

$$\psi' = \frac{1}{\sqrt{N}} \sum_{m=1}^{N} (a_m - \bar{a}_m) \qquad \text{(AII-27)}$$

is often adequately normally distributed when N is about 6-12, and N needs seldom be more than 30-100 in general. The random process, $\psi(t)$, in the central limit theorem may be written as a sum of variables, each of which is the average of the random process, p(t), over a time interval τ_{mix}, namely

$$\psi(t) = \frac{1}{\sqrt{t}} \int_0^t (p(t') - \bar{p})dt'$$

$$= \frac{1}{\sqrt{t}} \sum_{m=1}^{t/\tau_{mix}} \int_{(m-1)\tau_{mix}}^{m\tau_{mix}} (p(t') - \bar{p})dt' \qquad \text{(AII-28)}$$

Since τ_{mix}, the mixing time defined by eq AII-11, provides a measure of

the rate at which the values of the random process become independent of one another, $\psi(t)$ can be approximated as a sum of independent random variables. It follows that for $\psi(t)$ to be adequately normally distributed, t/τ_{mix} must be about 6-12. Unfortunately τ_{mix} is not an easily accessible quantity, but for most physically reasonable processes we expect that τ_{mix} is quite well approximated by the correlation time, τ_c, which is measurable in many cases. Thus, as a rule-of-thumb, $\psi(t)$ should be adequately normally distributed when t/τ_c is about 6-12 or at most 30-100. It should be noted that for the general process, $P(t)$, which is a composite of many processes, $p_j(t)$, it is the slowest of the component processes, $p_j(t)$, which determines the rate at which the overall process, $\psi(t)$ (Eq AII-20), converges asymptotically to a normally distributed variable and hence governs the approach of the FID to exponential decay.

We have shown that if the probability distribution is asymptotically normal, the the FID is asymptotically exponential. We would like to be able to conclude the reverse; that is, if the FID is exponential then $\psi(t)$ is normally distributed. However, this is not true in general.

References

1. A. Abragam, "The Principles of Nuclear Magnetism", Oxford University Press, Oxford, 1961.
2. R. Kubo and K. Tomita, J. Phys. Soc. Japan, 9, 888 (1954).
3. P.W. Anderson, J. Phys. Soc. Japan, 9, 316 (1954).
4. I.A. Ibragimov, in "Theory of Probability and its Application", Vol. 7, p. 349 (1962).
5. M. Rosenblatt, Proc. Nat. Acad. Sci. (U.S.), 42, 43 (1956).
6. R.L. Stratonovich, in "Topics in the Theory of Random Noise", Vol. 1, Chapter 2, Gordon and Breach, Science Publ. N.Y., London, 1967.
7. L. Breiman, in "Probability and Stochastic Processes: With a View Toward Application", Chapter 4, Houghton Miflin Co., Boston, 1969.
8. H.D. Brank, in "An Introduction to Mathematical Statistics", Chapter 9, Ginn and Co., 1960.

APPENDIX III. SUMMARY OF COLLOID THEORY

The theory of stability of lyophobic colloids was developed principally by Derjaguin and Landau and by Verwey and Overbeek around 1940. Excellent summaries of their theory are provided by Shaw (1) and Vold and Vold (2). More detailed treatments are presented by Verwey and Overbeek (3) and Kruyt (4). The basis for colloid theory is the consideration of attractive London-van der Waals forces and repulsive electrostatic forces. The theory was developed first for two infinitely large flat charged surfaces and later adapted to spherical surfaces by appropriate approximations and modifications.

Let us consider the repulsive forces involved. There is an electric potential, ψ, associated with any charged surface, which is a function of the space coordinates employed. It is possible to apply the Poisson equation and obtain the charge at any point in space by

$$\nabla^2\psi = -\frac{4\pi\rho}{\varepsilon} \qquad \text{(AIII-1)}$$

where ε is the dielectric constant of the medium and ρ is the space charge density. The gradient of charge formed by the distribution of electrolytes in solution is also influenced by Boltzman's equation. These effects are best described by the Poisson-Boltzman equation

$$\nabla^2\psi = \frac{8\pi n\nu e}{\varepsilon}\sinh(\nu e\psi/kT) \qquad \text{(AIII-2)}$$

Eq AIII-2 can be solved explicitly for the boundary conditions of an

infinite flat surface, which leads to the concept of the flat diffuse double layer, a region of particularly high ion concentration close to the charged surface. The thickness of the diffuse double layer depends on the surface charge and the nature of the electrolyte. In the limit of small values for the surface potential, eq AIII-2 becomes

$$\nabla^2\psi = \frac{8\pi n\nu^2 e^2}{\varepsilon kT}\psi = \kappa^2\psi \qquad \text{(AIII-3)}$$

so, the electric potential falls off exponentially and reaches 1/e of its original value when $x = 1/\kappa$. x is the Debye length and is a measure of the double layer thickness. This is the simplest case and in general the solution is somewhat more complicated (3).

For spherical systems the same approximation of small values of ψ must be made for eq AIII-2 to be solvable, in which case the problem reduces to that of electrolytes in solution described by the Debye-Hückel theory (5). The solution to eq AIII-3 for the potential at a distance r from the center of a charged spherical surface of radius a is

$$\psi = \psi_a \cdot \frac{a}{r} e^{\kappa(a-r)} \qquad \text{(AIII-4)}$$

where ψ_a is the potential on the surface.

For colloids the assumption of a small ψ is not realistic and numerical integration to solve equation AIII-2 has been performed to extend the region of ψ for which the theory is applicable. A further limitation of eq AIII-4 is the assumption that $\kappa a \ll 1$, which is also

unrealistic for most colloids.

In practice, it is found that application of the exact derivations for two interacting flat double layers is accurate enough to account for most observed aggregation phenomena in true colloids. The solution to this particular problem is a repulsive energy of interaction between the two plates given by

$$V_R = \frac{64nkT}{\kappa} \gamma^2 e^{-2\kappa d} \qquad \text{(AIII-5)}$$

where

$$\gamma = \frac{e^{\nu e\psi_a/2kT} - 1}{e^{\nu e\psi_a/2kT} + 1} \qquad \text{(AIII-6)}$$

Another assumption implied by these expressions is that the ions in solutions are point charges. Since they are not, Stern introduced a modification of the Verwey-Overbeek theory, allowing for the actual ionic size. This correction takes into account that only a limited number of ions can be accommodated in the proximity of the surface. A further modification allows some counter ions to be adsorbed tightly to the surface, causing a potential drop across this so-called Stern layer. Therefore, the surface potential ψ_a should be replaced by the Stern layer potential, ψ_δ. This quantity is not experimentally accessible, but it is usually assumed that the shear plane of the colloid-solvent interface is at the Stern layer. Therefore the ζ potential, which is measured by electrokinetic studies, is often substituted for ψ_a in evaluating V_R.

Next we consider the attractive forces between two charged surfaces. These London-van der Waal forces contain contributions from (i) ion-ion interactions, (ii) ion-induced dipole interactions, (iii) dipole-dipole interactions, (iv) dipole-induced dipole interactions, (v) dispersion interactions, and (vi) overlap interactions. Of these (i) has an r^{-1} dependence and is of importance only when opposite charges are involved. (ii)-(v) all have r^{-6} dependences and of them it can be shown (4) that the London dispersion interactions (v) dominate in most cases. (vi) is only important at very close ranges where electron clouds can overlap. It has an r^{-9} - r^{-12} dependence. In the range where it is important, the previously determined V_R needs modification to include Born repulsion but neither overlap interactions nor Born repulsion will be taken into account at this point. Born repulsion will dominate at very close separations so that the total interaction energy will increase as $r \to 0$.

The London dispersion interactions between two plates or two spheres have been calculated by De Boer (6) and Hamaker (7). They added the interactions of one atom in one surface with all atoms in the other, and then integrated over all atoms in the first surface. The result for two plane surfaces of thickness δ and separation d is

$$V_A = - \frac{A}{48\pi} \left(\frac{1}{d^2} + \frac{1}{(d + \delta)^2} - \frac{2}{(d + \delta/2)^2} \right) \qquad \text{(AIII-7)}$$

The constant $A = \pi^2 q^2 \beta$, with q equal to the number of atoms per cm^3 and $\beta \simeq -1.62 \times 10^{-6} \alpha\chi$; α is the polarizability of the atom and χ is the diamagnetic susceptibility. Similarly, for two spheres of radius a,

whose centers are separated by R, they found an attractive potential

$$V_A = -\frac{A}{6}\left(\frac{2a^2}{R^2 - 4a^2} + \frac{2a^2}{R^2} + \ln\frac{R^2 - 4a^2}{R^2}\right) \qquad \text{(AIII-8)}$$

Defining the parameter s = R/a, eq AIII-8 is rewritten as

$$V_A = -\frac{A}{6}\left(\frac{2}{s^2 - 4} + \frac{2}{s^2} + \ln\frac{s^2 - 4}{s^2}\right) \qquad \text{(AIII-9)}$$

For close approaches, i.e., when d is small (compared to δ) or R approaches 2a, we obtain

$$V_A = -\frac{A}{48\pi d^2} \qquad \text{(AIII-10)}$$

and

$$V_A = -\frac{A}{12}\left(\frac{a}{R - 2a}\right) \qquad \text{(AIII-11)}$$

for flat plates and spheres, respectively.

Combining the repulsive potential of eq AIII-6 with the attractive potential of eq AIII-10 or AIII-11 the total energy profile can be calculated. The total potential depends on the same factors as V_R and V_A: electrolyte concentration and valency, surface potential, surface charge density, and molecular polarizability and susceptibility. The detailed effects of each of these factors on the overall potential energy are illustrated by Verwey and Overbeek (3) and reproduced by Kruyt (4). A typical curve for two identical spheres is shown in

Figure 52.

The following features are of particular interest to our discussion of vesicles. (i) There is a maximum in the energy. (ii) The height of the energy maximum is influenced among other things by the electrolyte concentration and valency (through κ) and by the Stern layer potential, ψ_δ. The energy barrier increases as κ decreases or as ψ_δ increases. (iii) The distance at which the maximum occurs is also influenced by κ and ψ_δ. The distance increases as both κ and ψ_δ decrease. (iv) There is a close range, deep energy minimum called the primary minimum. (v) There is a long-range, shallow energy minimum called the secondary minimum. (vi) The secondary energy minimum is only of importance when the particles are larger than about 10^{-6} cm and then only if the energy maximum is comparable to kT.

References

1. D.J. Shaw, in "Introduction to Colloid and Surface Chemistry" (2nd ed.), Butterworths, London, 1970.
2. M.J. Vold and R.D. Vold, in "Colloid Chemistry", Van Nostrand Reinhold Company, New York, 1964.
3. E.J.W. Verwey and J.Th.G. Overbeek, in "Theory of the Stability of Lyophobic Colloids", Elsevier Publishing Co., Amsterdam, 1948.
4. M.R. Kruyt, (ed.), "Colloid Science", Vol. 1, Elsevier Publishing Co., 1952.
5. W.J. Moore, in "Physical Chemistry" (4th ed.), Prentice-Hall, Inc., Englewood Cliffs, N.J., 1972, p. 449 and following.
6. J.H. De Boer, Trans. Faraday Soc., 32, 21 (1936).
7. M.C. Hamaker, Physica, 4, 1058 (1937).